CSIC
CONSEJO SUPERIOR DE INVESTIGACIONES CIENTÍFICAS
INSTITUTO EDUARDO TORROJA

UAM
UNIVERSIDAD AUTONOMA DE MADRID

HIGH STRENGTH STAINLESS STEEL PROTECTION CAPACITY FOR PRESTRESSED CONCRETE STRUCTURES

HITHAM MAHMOUD AMIN HASSAN

DOCTORAL THESIS

Madrid 2013

Supervisors (CSIC): **Mª CRUZ ALONSO ALONSO**
MERCEDES SÁNCHEZ MORENO
Tutor (UAM): **CONCEPCIÓN ALONSO FUENTE**

For my dear parents and
brothers who always support
me and stay by my side
along my way

ACKNOWLEDGMENTS

I would like to express my utmost gratitude and sincere appreciation to Prof. Mª Cruz Alonso Alonso and Dr. Mercedes Sánchez Moreno. I am greatly indebted to them for their valuable guidance, suggestion and encouragement throughout all phases of my research work. I am truly fortunate to have had the opportunity to work on a novel topic with a group of such talented and sincere individuals, who allowed me to carve my own path for this research. Prof. Mª Cruz Alonso Alonso and Dr. Mercedes Sánchez Moreno: I thank you for pushing me to strive for excellence.

I am also grateful acknowledge to the financial assistance provided by the Spanish MICINN for the financial support given to the research projects and for the FPI grant, also I would like to thank INOXFIL for the material supplying.

I deeply appreciate Prof. X. Ramón Nóvoa and all the member of the group ENCOMAT for their valuable advice and helpful support in my research during my short stay in the Escola de Enxeñaría Industrial, University of Vigo-Spain.

I wish also to express my profound gratitude to Prof. Luca Bertolini for his valuable generous assistance, valuable suggestions, and his kind hospitality during my short stay in Dipartimento di Chimica, Materiali ed Ingegneria Chimica "G. Natta" Politecnico di Milano-Italy.

This work would not have been possible without the assistance, support and collaboration of many people, so I would like to seize the opportunity to thank them these few lines. I want to express my deep appreciation to all my colleagues of

Eduardo Torroja Institute for their constant encouragement and support during my work, it would have been much more difficult without them.

I would like to show my gratitude to those with whom I have shared unforgettable moments, which have made this way more enjoyable. I would like to acknowledge Virtudes Flor-Laguna not only for helping me with experimental setups and equipment operations, but also for her style in handling and organization. Thanks also Javier Recio for never hesitating to sit down with me and talk about research and life, and also for nice comments about the Arabic people. Thanks Eva Mazarío for your encouragement and help during the hard first two years, thanks for being my company in DEA, and the congresses. Thanks José Luis García and Cristina Rodríguez for your kind reception in the first day for me in the institute and for helping me with the Spanish translation during my grant. I would like to thank you Alvaro for making me able to make jokes in Spanish with asking with is the meaning of "Telón". And I would like to thank Eduardo, Carlos, Virginia and Nuria for the unforgettable moments during the breakfast, and also Fran, Fidel, Filipe for the incredible Fridays afternoons.

I would like also to thank my dear Galician friends who make me feel like an Egyptian with "morriña" to Galicia. Thanks David, Bea guitian, Bea Puga, Ricardo, Ana, Marina, Andrea, Lorena.

Furthermore, I want to thank Andrea Della Pergola, Franco Traisci, Federica Lollini, Elena Redaelli, Matteo Gastaldi, Maddalena Carsana for their encouragement and support during my short stay in Dipartimento di Chimica, Materiali ed Ingegneria

Chimica "G. Natta" –Italy. Also I would like to express my deep appreciate to Cristina Ungurescu for her encouragement and telling me that I have to do the thesis well and that I am able to make it. Thanks all my dear Egyptian friends for supporting me in good and hard moments. Thanks Moied, Haitham, Waleed, Idress, Youssef, Ihab, Adel, Dr. Yasser El Said, Dr. Tag, Fouad, and Ihab Youssef.

Finally and most importantly, I would like to thank my dear parents, Mahmoud Amin and Aida Youssef, and my lovely brothers, Nosa, Fawzia, Hassan, and Mohammed, for their unending love and encouragement. The great support and sacrifices you make have taught me the values of continuous and uninterrupted tender. Thanks my dears and let me dedicate this work to you.

SUMMARY

Reinforced concrete is a composite material in which reinforcing steel bars have been integrated to improve the relatively low tensile strength of concrete. Besides, concrete is a porous material wherein the solid phases are in chemical equilibrium with an aqueous phase produced during the cement hydration process. The high alkalinity of the aqueous phase in contact with the steel reinforcement induces the formation of a stable passive film which protects the embedded steels from the surrounding environment. However, the penetration of aggressive ions such as chloride through the concrete pores can lead to destabilize the passive film and to initiate a localized attack, and consequently, induces the loss of durable properties of concrete.

Prestressed concrete is a type of reinforced concrete in which the embedded steel is permanently stressed during its service life. Consequently, high strength steels with special mechanical performance are used as prestressed steels. Prestressed structures are more sensitive to corrosion process because the prestressing steel can suffer corrosion problems when subjected to a mechanical load in aggressive environments. The prestressing steel corrosion is the main cause of deterioration of the concrete structures incorporating such material. Nowadays, the application of High Strength Stainless Steel (HSSS) in prestressed concrete stands out as a promising alternative solution to improve the durability of these structures.

Summary

HSSS are produced by a cold drawn deformation process which increases the tensile strength of the parent stainless steel. This process aims to reduce the cross section of the parent steels by stretching the steel wires, passing through a hole with lower diameter than the original diameter of the wire. HSSS are normally obtained by applying 50-80% cold drawing degree.

Cold drawn HSSS have already been used as cables for bridges and towers in contact with atmosphere. In this case, the maximum strength required not exceeded $\sigma_{Max} \cong 1400$ MPa and HSSS were tensioned to 40% of its maximum load. However, in prestressed concrete structures, a higher maximum strength is required ($\sigma_{Max} \cong 1700$MPa) and HSSS must withstand loads in service up to 70-80% of its maximum load. Furthermore, in prestressed concrete structures, HSSS will be in direct contact with concrete, or in ducts filled with grout. Consequently, the practical experience of HSSS cables in contact with atmosphere is not directly applicable to the circumstances of the application of HSSS in prestressed concrete.

Early researches to evaluate the corrosion behaviour of HSSS in contact with concrete were performed on austenitic HSSS. Although the results have shown a high resistance to corrosion for these SS, even in highly aggressive conditions, it has been confirmed that during the production of austenitic HSSS by a cold drawn deformation process a possible transformation of austenite phase to martensite can take place. This change in the austenitic HSSS microstructure affects their susceptibility to pitting corrosion and increases the risk of hydrogen embrittlement.

The high cost of austenitic HSSS due to its high Ni content and the risk of formation of martensite phase during the cold drawn process lead to the introduction of duplex HSSS for prestressed structures as new alternative solution. However, the lack of knowledge of the corrosion behaviour of duplex HSSS when they are embedded in concrete or cement-based alkaline environments is one of the main reasons that limit the employ of duplex HSSS in prestressed concrete.

In literature, most of the published studies have been concentrated in conventional stainless steels in alkaline media, and it has been concluded that the passive layer formation and its electrochemical response against the chloride action depend primarily on the stainless steel chemical composition and on the exposure environment (alkalinity, chloride content, etc.). On the other side, few studies are available to highlight the corrosion behaviour and the electrochemical response of HSSS in alkaline media in presence and in absence of aggressive agents as chloride ion.

The present thesis focuses on evaluating the electrochemical response and the protective capacity of duplex HSSS against the action of chloride when exposed to an alkaline environment such as concrete.

The specific objectives of present thesis are:

1. Study passivation processes of duplex high strength stainless steels (HSSS) in alkaline environments and evaluate the electrochemical response of the passive film in presence of chloride at different exposure conditions.

2. Evaluation of depassivation processes of duplex HSSS and determination of the critical concentration of chloride required to initiate active pits on the steel surface at different conditions.
3. The pitting corrosion propagation in extreme exposure conditions, high temperature and high concentration of chloride.

Two duplex stainless steels with different chemical composition have been studied: 2304 (0.1 wt% Mo) and 2205 (3.7 wt% Mo). For each case, both parent (Ø = 9 mm) and cold-drawn (Ø = 4 mm) steels have been considered. The influence of the composition and the microstructure in the passivation and depassivation process of high strength duplex stainless steels in alkaline environment with and without chlorides has been investigated. Furthermore, the influence of the alkalinity of the exposure medium has also been considered.

The electrochemical tests have been carried out in various types of electrolytes to simulate different exposure conditions:

1. Saturated $Ca(OH)_2$ solutions with different concentrations of KOH to obtain alkaline solutions of pH 12.5 and 13.5, which simulate the alkaline aqueous phase of concrete. Different concentrations of chlorides in form of sodium chloride (NaCl) were added to the alkaline solutions in order to study the behaviour of the passive layer in aggressive conditions at different temperatures (from 25 to 50 °C), the changes induced in the passive film due to

the presence of chloride, the critical chloride concentration and the propagation of the pit.

2. Chloride penetration tests and chloride mixed-in mortars have been used to determine the critical chloride concentration of duplex stainless steels embedded in mortar.

To study the electrochemical response of the duplex HSSS, different electrochemical techniques have been used:

I. *Cyclic Voltammetry* was used to study the different redox processes that take place in the passive film formed on the stainless steel surface in alkaline media without and with chloride.

II. *Potentiostatic pulse*: in the case of the passivation study, potentiostatic pulse tests were used to evaluate the behaviour of the passive layer at different potentials in the passivity and the transpassivity domains.

However, in depassivation tests, potentiostatic tests in the transpassivity region were performed by applying a constant potential until the onset of pitting corrosion, both in alkaline solutions and in mortar.

III. *Periodic measurements of corrosion potential, polarization resistance and electrochemical impedance spectroscopy at different immersion times in alkaline media* in order to study the evolution of the electrochemical response of duplex HSSS in alkaline medium in absence and in presence of chloride, which can help to understand the mechanism of the electrochemical passivation and depassivation processes.

Regarding the passivation of duplex HSSS in alkaline media without chloride, the more relevant results indicate that:

- The electrochemical behaviour of duplex HSSS is affected by the conditions in which the passive layer is generated. The SS chemical composition and microstructure and the exposure media are relevant parameters that control the passivation process and the electrochemical response of SS in both alkaline media and mortar.
- Increasing the alkalinity of the surrounding media induces the formation of a more conductive passive film with lower oxidation degree of the iron oxides components.
- Ageing of the passive film in alkaline media induces the enrichment of stable oxides with high oxidation degree, and thereby, the reactivity of the passive film decreases. In addition, the expected enrichment in Cr^{III}-oxides in the passive layer with ageing improves the protection capacity of the layer.
- The presence of Mo during the formation of the passive layer affects both the passive film composition and its electrochemical response (probably associated with changes in the composition and ratio of iron and chromium oxides). Furthermore, the Mo behaviour in the film appears to be affected by the pH of the surrounding media.

Regarding the influence of the presence of chloride in the electrochemical behaviour of duplex HSSS, both 2304 and 2205 stainless steels show high corrosion resistance against the localized attack caused by chloride. The results in the presence of chloride show the following:

- The presence of a chloride concentration less than the critical chloride threshold significantly affects the oxidation processes occurring in the passive layer. An increase in the corrosion current density is registered with the presence of chloride, which probably related to the oxidation of $Cr(OH)_3$ species present in the outermost part of the passive film, and the formation of dissolved chromate, which could be enhanced by the presence of chloride in the interface. The dissolved chromate is expected to inhibit the breakdown of the passive film hindering the formation of active pits on the duplex SS surface. However, the oxidation process to chromate decreases the thickness of the passive layer, and as a consequence, the passive film becomes more susceptible to pitting corrosion in presence of higher concentration of chloride. The impedance measurements have confirmed the reduction of the resistance of the passive layer with the increase of the chloride concentration (Cl^- < CCT) at the passive film/electrolyte interface, where a tendency to a less capacitive behaviour at low frequency limit has been observed with the chloride content increasing.
- The alkalinity of the medium has a significant influence on the critical chloride concentration of duplex HSSS which increases with the increase of the pH of the surrounding media. Although this behaviour seems inconsistent with the results of passivation in chloride free alkaline media, which indicated the formation of more conductive passive films in more alkaline media, it can be explained by the fact that, in more alkaline solutions, the media becomes less aggressive due to the diminution of $[Cl^-]/[OH^-]$ ratio in the passive film/electrolyte interface.

- Concerning the influence of the Mo content in the electrochemical response of duplex HSSS in presence of chloride ion, duplex HSSS with higher Mo content exhibits higher resistance against pitting corrosion in aggressive environments both at room and at elevated temperatures. Furthermore, the critical concentration of chloride for duplex stainless steel with high Mo content is about one order of magnitude higher than those without Mo.
- Cold drawn duplex HSSS are more resistant to chloride depassivation process in comparison with parent duplex stainless steels, which in turn confirms the role of the stainless steel microstructure and surface roughness in the electrochemical behaviour of stainless steels.
- The critical chloride concentration depends on the methodology applied for its determination. The potentiostatic determination leads to higher values compared to the potentiodynamic tests. This is probably related to the nature of the passive layer formed during potentiodynamic and potentiostatic tests.
- Regarding the determination of the critical chloride concentration of duplex stainless steels in mortar, determined by chloride penetration potentiostatic test, the critical chloride concentrations for 2304 duplex stainless steels (DSS) varies from 3.06 ± 0.5 % total Cl^- (with respect to the cement weight) for cold drawn (CD) DSS to 2.3 ± 0.2 % total Cl^- for parent duplex stainless steel. Concerning 2205 HSSS, no detection of active pits has been observed during chloride penetration test, however, in some cases, a general superficial attack has been noticed, which was intensified after exposure to atmosphere, which probably related to the effect of the duration of the polarization test.

On the other hand, relatively lower critical chloride concentration for 2304 CD-DSS (from 1.8 ± 0.2 to 2.1 ± 0.2 % total Cl^-) have been potentiostatically measured in chloride mixed-in mortar.

- Pitting propagation results of duplex HSSS in alkaline media at high temperatures indicate that, duplex HSSS with higher Mo content shows more elevated critical pitting temperature (CPT). Furthermore, increasing the alkalinity of the medium increases the CPT of the steels.
- The evolution of the pitting corrosion electrochemical charge confirms that pitting corrosion risk and propagation in case of parent DSS, exposed to extreme conditions, is higher than cold drawn duplex SS, which in turn confirms the positive effect of cold drawn deformation process on the electrochemical behaviour of duplex stainless steels, which can be related to the absence of generation of martensitic phases in duplex cold drawn HSSS surface and the formation of more refined grain size and less surface roughness. This observation is considered as an advantage that can characterize the cold drawn duplex HSSS in comparison with cold drawn austenitic HSSS.

RESUMEN

El hormigón armado es un material compuesto en el que un recubrimiento de hormigón protege a una armadura de acero embebida que mejora las propiedades mecánicas del conjunto. El hormigón es un material poroso en el que las fases sólidas se encuentran en equilibrio químico con la fase acuosa contenida en la estructura porosa. La elevada alcalinidad de esta fase acuosa en contacto con la armadura favorece la formación de una película pasiva sobre la misma protegiéndola del medio. Sin embargo, la penetración de agresivos a través de los poros del hormigón, como el cloruro, puede llevar a la desestabilización de la película pasiva y al inicio de un proceso de corrosión localizada, con la consiguiente pérdida de las propiedades durables del hormigón armado.

Las estructuras pretensadas son incluso más sensibles al proceso de corrosión debido a que se puede acabar produciendo fragilización en el acero de pretensado por problemas de corrosión bajo tensión al estar sometido a una carga mecánica durante su vida en servicio. La corrosión de los aceros pretensados es la principal causa de deterioro de las estructuras que incorporan este tipo de materiales, lo que ha llevado a convertirse en un campo de interés para conocer la vida útil de este tipo de estructuras. Entre las posibles alternativas para alargar la vida útil de estas estructuras, el empleo de los Aceros Inoxidables de Alta Resistencia (AIAR) destaca como una de las más prometedoras.

Los AIAR se producen mediante un proceso de deformación en frío (trefilado) que mejora el límite elástico y la tensión a rotura de los aceros inoxidables convencionales ya que se deben cumplir unos requisitos mecánicos mínimos si el interés es su empleo como cables o tendones en estructuras pretensadas. La experiencia práctica con este tipo de AIAR se ha centrado en aplicaciones que no requieren superar los $\sigma_{max} \cong 1400$ MPa, trabajando en servicio al 40% de su carga de rotura y expuestos a la atmósfera. Sin embargo, en estructuras de hormigón pretensado las exigencias mecánicas son mayores ($\sigma_{max} \cong 1700$MPa) y el acero debe soportar cargas en servicio del 70-80% de su carga de rotura. Este tipo de estructuras además sitúan al AIAR en contacto con medios muy alcalinos como son el hormigón o los conductos (vainas) rellenos de lechada de cemento. Estas exigencias en servicio hacen que la experiencia de los AIAR en cables a la atmósfera no sea directamente aplicable a las circunstancias de los AIAR para estructuras de hormigón pretensado.

Las primeras investigaciones para evaluar el comportamiento frente a la corrosión de los AIAR en hormigón se llevaron a cabo sobre aceros de tipo austenítico. A pesar de que los resultados obtenidos han mostrado una elevada resistencia a la corrosión, incluso en condiciones ambientales de elevada agresividad, se ha observado una transformación en la microestructura austenítica a martensita asociada al proceso de trefilado, lo que puede afectara la susceptibilidad a la corrosión de estos AIAR, aumentando el riesgo de fragilización por hidrógeno.

El elevado coste de los AIAR austeníticos debido fundamentalmente a su alto contenido en Ni y el riesgo de formación de fases martensíticas durante el proceso

trefilado está dando lugar a la introducción de AIAR tipo dúplex como alternativa para estructuras pretensadas. Sin embargo, hoy en día el empleo de estos materiales en hormigón pretensado esta limitado debido a la falta de conocimiento y respuesta a largo plazo de su comportamiento frente a la corrosión cuando se encuentran embebidos en hormigón o ambientes alcalinos de base cemento, así como a la necesidad de optimizar sus prestaciones mecánicas.

Los aceros inoxidables austeníticos se pasivan en el ambiente alcalino del hormigón. De igual forma se espera que ocurra con los AIAR tipo dúplex. La mayor parte de los estudios de corrosión publicados han empleado aceros inoxidables sin trefilar en medios alcalinos, y han permitido concluir que la formación de la capa pasiva y su respuesta electroquímica frente al acción del cloruro depende fundamentalmente de la composición de la aleación y del medio de exposición (alcalinidad, contenido en cloruro etc.).

Ante la elevada incertidumbre existente respecto a la respuesta electroquímica y capacidad protectora de los AIAR tipo dúplex en el entorno alcalino propio de un hormigón, la presente tesis se centra en evaluar este tipo de materiales con prestaciones mecánicas adecuadas para su aplicación en estructuras de hormigón pretensado. En el estudio se analiza la acción desestabilizante del ión cloruro en medio alcalino, considerando tanto los procesos de pasivación como los de despasivación.

Los objetivos específicos son:

1. Estudiar los procesos de pasivación de distintos tipos de aceros inoxidables dúplex trefilados y sin trefilar en ambientes de elevada alcalinidad, y la respuesta de la película pasiva ante la acción del ión cloruro en distintas condiciones de exposición.
2. Conocer los procesos de despasivación de este tipo de aceros inoxidables y determinar la concentración crítica de cloruro necesaria para generar una corrosión activa que permita cuantificar la contribución de los AIAR-dúplex a alargar la vida útil de las estructuras pretensadas.
3. Evaluar la propagación de la corrosión una vez iniciado el proceso de corrosión, en condiciones extremas de exposición, elevada temperatura y elevado contenido en Cl^-.

Se han estudiado dos tipos de acero inoxidable dúplex de alta resistencia ambos trefilados en frío (Ø = 4 mm) y sus alambrones de partida, (Ø = 9 mm), de las series 2205 (3,7 wt% Mo) (σ_{trf}=1710, σ_{alb}=970) y 2304 (0,1 wt% Mo) (σ_{trf}=1630, σ_{alb}=865). El contenido en Mo en los aceros inoxidables dúplex y la microestructura de los mismos han sido parámetros críticos para el desarrollo del estudio, y se ha analizado su influencia tanto en el proceso de pasivación como en el de despasivación de los aceros expuestos al medio alcalino con y sin cloruros. La influencia del nivel de alcalinidad del medio ha sido otro parámetro significativo tenido en cuenta.

Los ensayos se realizaron en distintos tipos de electrolito que simulan distintos ambientes de exposición:

1. En disoluciones saturadas de $Ca(OH)_2$ con diferentes concentraciones de KOH, con el fin de de obtener valores de pH de 12,5 a 13,5 que simulan la fase acuosa del hormigón. Se han añadido distintas concentraciones de cloruro en forma de cloruro sódico (NaCl) para estudiar el comportamiento de la capa pasiva en condiciones agresivas a distintas temperaturas (de 25 a 50 °C). Se han analizado los cambios en la pasivación inducidos por la presencia de cloruro (agente desestabilizante de la capa pasiva), la concentración critica de cloruro para iniciar una corrosión activa y la propagación de la corrosión en condiciones extremas de exposición.
2. En mortero se han considerado ensayos de penetración de cloruro hasta alcanzar una concentración crítica a nivel del AIAR-dúplex capaz de provocar el inicio de la corrosión. Se ha determinado también la concentración crítica de cloruro en morteros amasados con distintas cantidades de cloruro.

Para el estudio de la respuesta electroquímica de los AIAR-dúplex se han utilizado distintas técnicas electroquímicas:

I. *Voltametría cíclica*: Se utilizó para analizar los distintos procesos redox que tienen lugar en la película pasiva en contacto con el medio alcalino sin y con cloruros.

II. *Pulso potenciostático*: En el caso del estudio de pasivación, se ha evaluado el comportamiento de la capa pasiva a distintos potenciales en las zonas de pasividad y transpasividad.

Para el estudio de despasivación de los aceros inoxidables, los ensayos potenciostáticos se llevaron a cabo aplicando un potencial constante en la

región de transpasividad hasta detección del comienzo de corrosión por picadura, tanto en disolución alcalina como en mortero.

III. *Medidas periódicas de potencial de corrosión, de resistencia a la polarización y de espectroscopía de impedancia electroquímica* a diferentes tiempos de exposición en los medios alcalinos con el fin de evaluar la evolución de la respuesta electroquímica de los AIAR dúplex en presencia y en ausencia de cloruro y conocer el mecanismo electroquímico de los procesos de pasivación/despasivación.

Respecto a los procesos de generación de la capa pasiva los resultados más relevantes indican que:

- El comportamiento electroquímico de los aceros inoxidables tipo dúplex se ve afectado por las condiciones en las que se genera la capa pasiva. Se confirma que la composición química del acero y el medio de exposición son parámetros relevantes. En el caso particular del AIAR-dúplex el hecho de que el acero haya sido sometido a un proceso de deformación afecta al proceso de formación y a la respuesta electroquímica de la capa pasiva.
- El aumento de la alcalinidad del medio lleva a la formación de una película pasiva más conductora, indicando un menor grado de oxidación de los óxidos que la componen.
- El envejecimiento de la capa pasiva en el medio alcalino en el que se genera tiene lugar a través del enriquecimiento de la capa en compuestos estables con mayor grado de oxidación que disminuyen la reactividad de la película pasiva,

aumentando de este modo su capacidad de protección posiblemente por enriquecimiento en óxidos de Cr^{III} en su parte más externa.

- La presencia de Mo influye en la formación de la capa pasiva afectando tanto a la composición como a su respuesta electroquímica (probablemente debido a cambios en la composición de óxidos de hierro y cromo). Por otro lado, el comportamiento del Mo parece estar afectado por el pH del medio.

Respecto a la influencia de la presencia de cloruro en el comportamiento electroquímico de los aceros AIAR-dúplex, ambos aceros estudiados han demostrado aportar una elevada resistencia al ataque localizado provocado por el ion cloruro. De los resultados obtenidos por los AIAR-dúplex en presencia de cloruro cabe destacar los siguientes aspectos:

- La presencia de una concentración de cloruro inferior a la crítica para iniciar un proceso de corrosión activa afecta de forma significativa a los procesos de oxidación que ocurren en la capa pasiva. El aumento en la densidad de corriente de corrosión registrado y la disminución de la resistencia de la capa pasiva en presencia de cloruro estaría indicando un aumento de la disolución de la película externa de $Cr(OH)_3$ presente en la capa pasiva con formación de cromato que queda disuelto en el medio. Ante la presencia de bajas concentraciones de cloruro parece que este cromato disuelto tiene una actividad inhibidora que evita la ruptura de la capa pasiva. No obstante, el proceso de oxidación a cromato implica a su vez disminución del espesor de la capa pasiva, más acentuado con el incremento de la concentración de cloruro en el medio, aumentado la susceptibilidad de la película

pasiva al ataque por cloruro hasta que la película se rompe a una cierta concentración de este ión (concentración crítica de cloruro).

- La alcalinidad del medio influye de forma significativa en la concentración crítica de cloruros requerida para provocar una corrosión activa, que aumenta significativamente con el incremento del pH. A pesar de que este comportamiento en principio sería contradictorio con los resultados de pasividad, de los que se deducía la formación de películas pasivas más conductoras en los medios más alcalinos, puede estar explicado, sin embargo, por la menor agresividad de los medios de pH más elevado y por cambios en la estructura y composición de la propia capa pasiva.
- Respecto a la influencia de contenido en Mo en la respuesta electroquímica de los AIAR-dúplex frente a la acción del ión cloruro, los aceros con mayor contenido de Mo son más resistentes frente a la corrosión por picadura tanto a temperatura ambiente como a elevada temperatura. La concentración crítica de cloruro (CCC) determinada para estos aceros con mayor contenido en Mo, ha sido aproximadamente un orden de magnitud superior a la CCC determinada para los AIAR dúplex sin Mo, incluso en las condiciones más agresivas.
- Los aceros trefilados presentan una mayor resistencia frente a la despasivación por cloruro que los aceros originales (alambrones), confirmando el papel importante de la microestructura en el comportamiento de los aceros inoxidables frente a la corrosión.
- El valor de la CCC varía en función de la metodología aplicada para su determinación. La aplicación de ensayos potenciostáticos como un ensayo

acelerado conduce a mayores valores en comparación de los ensayos potenciodinámicos. Esto probablemente está relacionado con el tipo de la capa pasiva que se forma.

- Respecto a la determinación potenciostática de la CCC de los AIAR-dúplex en morteros (ensayos de penetración del cloruro) en el caso de los aceros dúplex 2304, se ha observado que la concentración crítica de estos aceros varían de 3,06 ± 0,5 %Cl^- totales (referido al peso de cemento) para el acero trefilado a 2,3 ± 0,2 % Cl^- totales para el alambrón de partida. En el caso de los aceros trefilados tipo 2205, no se ha detectado un inicio de corrosión por picadura durante el ensayo, sin embargo, en algunos casos se ha observado un ataque superficial generalizado que puede estar relacionado a la duración y condiciones del ensayo.

  La determinación de la concentración crítica de cloruro de los aceros 2304 tipo dúplex en morteros amasados con distintas cantidades de cloruro conducen a menor concentración crítica (de 1,8 ± 0,2 a 2,1 ± 0,5 % Cl^- totales) respecto al ensayo de penetración de cloruro.
- Los resultados del comportamiento de los AIAR-dúplex a la propagación de la corrosión por picadura en medios alcalinos a elevada temperatura indican que la temperatura crítica de picadura (TCP) aumenta en el caso de AIAR-dúplex con Mo en su composición. También el aumento de la alcalinidad del medio parece llevar asociado un incremento en la TCP.
- La evolución de la carga de picadura en condiciones extremas de elevada temperatura confirma que la corrosión se propaga en forma más rápida en el caso de los aceros inoxidables tipo dúplex no sometidos al proceso de trefilado, de modo

que se ha podido observar un efecto positivo del proceso de deformación en frío sobre el comportamiento electroquímico de los aceros inoxidables dúplex, lo que puede estar relacionado con la ausencia de generación de fases martensíticas en los aceros trefilados tipo dúplex siendo el estado superficial y tamaño de grano más fino son factores determinantes y una menos rugosidad superficial.

CONTENTS

I. Introduction

I. Introduction

Concrete is the most widely used construction material in the world. Right now, it is estimated that 6 billion tons concrete are produced annually. Conventional concrete is obtained by mixing aggregates, cement, being the Ordinary Portland Cement (OPC) the most employed type of cement, and water. When these materials enter in contact, water interacts with the anhydrous cement particles producing the hydrated solid phases that form a porous matrix of cement paste surrounding the aggregates. The cement paste has different types of pore that play an important role in concrete properties. The pores in hardened concrete are totally or partially filled with an aqueous solution, as has been schematized in Fig. I.1. In OPC concrete, the pore water solution contains mostly K^+, Na^+, Ca^{2+}, and OH^- ions, which define the alkalinity of concrete [1].

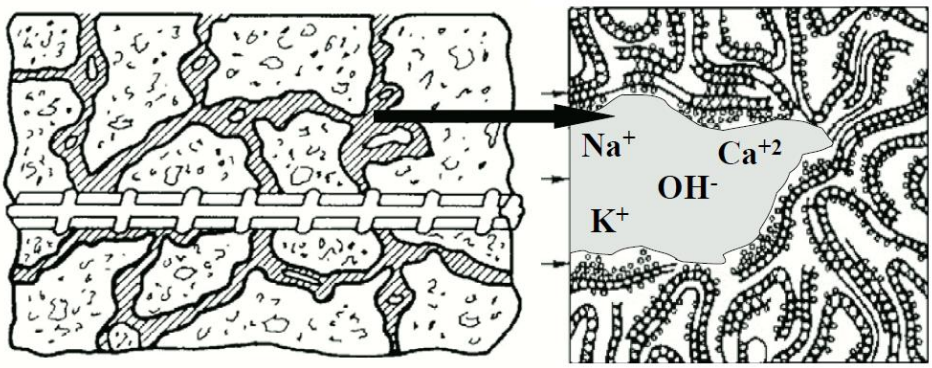

Fig. I.1 Schematic representation of the porous structure of concrete and the chemical composition of aqueous phase pore solution (Adapted from [2-3]).

It is assumed that the pore solution is always saturated in $Ca(OH)_2$, which causes the precipitation of $Ca(OH)_2$ in crystalline form within the pores, maintaining the pH of the pore solution at values higher than 12.6 [2,4-5]. The pH of the aqueous phase pore solution in OPC-based concrete varies from 12.6 to 14 as a function of the cement type (OPC or blend cements and the alkaline content K^+, Na^+) and the dosage employed for the fabrication of concrete [4-5].

It is well known that concrete has a high compressive strength and a low tensile strength. This led to the production of reinforced concrete in which the combination of concrete and steel reinforcements produces structural elements that joint the advantages of each individual material [6].

Consequently, reinforced concrete is a composite material in which reinforcing steel bars have been integrated to improve the relatively low tensile strength and ductility of concrete. Reinforced concrete has been universally accepted as a construction material because it can be molded into any shape or form, is inherently rigid and inherently fire-resistant. Furthermore, the concrete acts as a physical barrier protecting the embedded reinforcements from the environmental and climatic conditions.

Furthermore, the alkaline environment of the concrete promotes the generation of a stable passive oxide layer on the surface of the embedded steel reinforcement, which ensures a suitable protection against corrosion and high durability for reinforced concrete.

The loss of durability of the reinforcement in concrete, apart from the problems due to a poor design or construction, occurs when the passive film formed on the embedded

steel becomes unstable due to the penetration of aggressive agents through the concrete pores. The carbonation process caused by the penetration of atmospheric CO_2-gas throughout the porous matrix of the concrete reduces the alkalinity of the pore solution around the steel promoting the general corrosion of the steel surface. On the other hand, the ingression of the aggressive ions, like chloride, to the steel/concrete interface can also induce the local breakdown of the passive layer and the formation of pits even in an alkaline protective environment.

The phenomenological model proposed by Tuutti [7] gives a qualitative description of the service life of the reinforced concrete as schematized in Fig. I.2.

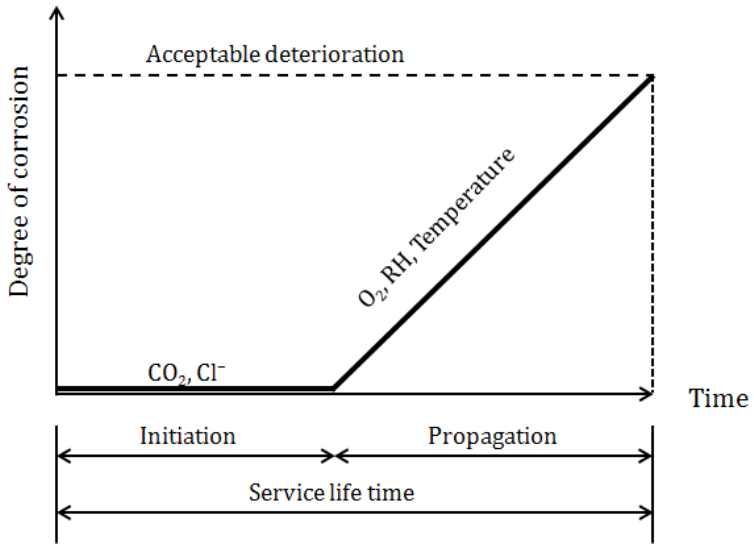

Fig.I.2. Schematic illustration of Tuutti's diagram [7].

This model distinguishes between two periods of time along the reinforced concrete service life:

Initiation period (t_{init}): This period is related to the required time for the initiation of the corrosion process on the embedded steel surface. In the case of chloride induced corrosion, the breakdown of the passive film occurs when the minimum concentration of chloride able to initiate the corrosion process, known as critical chloride concentration (CCT), is reached at the level of the rebar [8-9].

Propagation period ($t_{pro.}$) starts immediately after the corrosion process is initiated. In this period, an active corrosion process, with loss of material and loss of the section of the rebar, takes place until a certain level of damage, considered as an acceptable level due to the performance loss is reached.

The durability of reinforced concrete becomes an important investigation issue of concern for construction specialists with the aim to minimize the risk of the corrosion of reinforcing steels. To limit the corrosion of the embedded steels, certain requirements for the concrete and the reinforcing materials must be considered to improve the durability of the reinforced concrete structures.

Many methods have been developed to improve the corrosion resistance of reinforcements. These methods can be divided into four different categories, based on how they provide protection [10-11]:

1. *Alternative reinforcements:* the reinforcement corrosion resistance can be enhanced in two different ways: by applying a coating on the steel reinforcement or by replacing it with a more corrosion-resistant material such as Galvanized steel, Stainless Steel, or Polymeric fiber reinforcements.

2. *Corrosion inhibitors:* they are chemicals that can slow down or prevent reinforcement corrosion. They are typically divided into three categories: anodic inhibitors, cathodic inhibitors and mixed inhibitors [11-12]. The application of corrosion inhibitors to concrete can be carried out by the addition of the inhibitors as additives to fresh concrete during casting or by application on the hardened concrete surface [13].
3. *Surface treatment of concrete:* Surface treatment and concrete coatings have the ability of slowing down the rate of carbonation, chloride ingress, or humidity access in the concrete [11]. Invisible hydrophobic silane impregnations, polyurethane, and epoxy are the most common coatings for concrete application [11].
4. *Cathodic protection aim*s to protect the reinforcement by maintaining all areas of the reinforcement surface as cathode through connecting it to an external anode and applying a constant amount of direct current (DC) [0.0001 to 0.05 A/m^2 of reinforcement] [11].

I.1 Prestressed concrete

Prestressed concrete is a type of reinforced concrete in which the embedded steel is permanently stressed to guarantee the performance of the final structure working under mechanical loads.

Prestressed concrete combines concrete with high-strength steel in an active manner. This is achieved by tensioning the steel and anchoring it against the concrete, which produces the desirable strains and stresses to improve the tensile strength of

concrete. The most common methods for prestressing the steel are known as pretensioning and post-tensioning [14].

For the pretension of the concrete, the steel is first tensioned in a frame or between external anchorages and then the concrete is casted around it. After the concrete has developed sufficient strength, the tension is slowly released from the frame or anchorage to transfer the stress to the concrete to which the tendons have become bonded. The force is transmitted to the concrete over a certain distance from each end of the member, known as the transfer length.

Post-tensioned concrete is made by casting concrete that contains ducts through which tendons can be threaded. An alternative is to cast the concrete around tendons that are greased or encased in a plastic sleeve. When the concrete has sufficient strength the tendons are tensioned by means of portable jacks. The load is transmitted to the concrete through permanent anchorages embedded in the concrete at the ends of the tendons. Ducts are usually grouted later or filled with grease to protect the tendons against corrosion [14].

I.1.1. Production of high strength steels

For prestressed concrete structures, the maximum strength of conventional reinforcement is not high enough for application as prestressing steel. To increase the strength of the steels, a cold drawn deformation process is applied to eutectoid steel wires [15-19], where the maximum tensile strength increases with increasing the cold drawn degree [16]. High strength steels can be obtained by 50-80% cold drawing degree. This

process aims to reduce the cross section of the steels by stretching the steel wires, passing through a hole with lower diameter than the original wire diameter, as shown in Fig.I.3a.

Furthermore, the cold drawn deformation process produces microstructural changes in the prestressing high strength steels [17-19], as shown in Fig.I.3.b. In particular, cold drawn is the responsible for the decrease of the intergranular spacing and the progressive longitudinal orientation of pearlitic lamellae in the drawing direction [15].

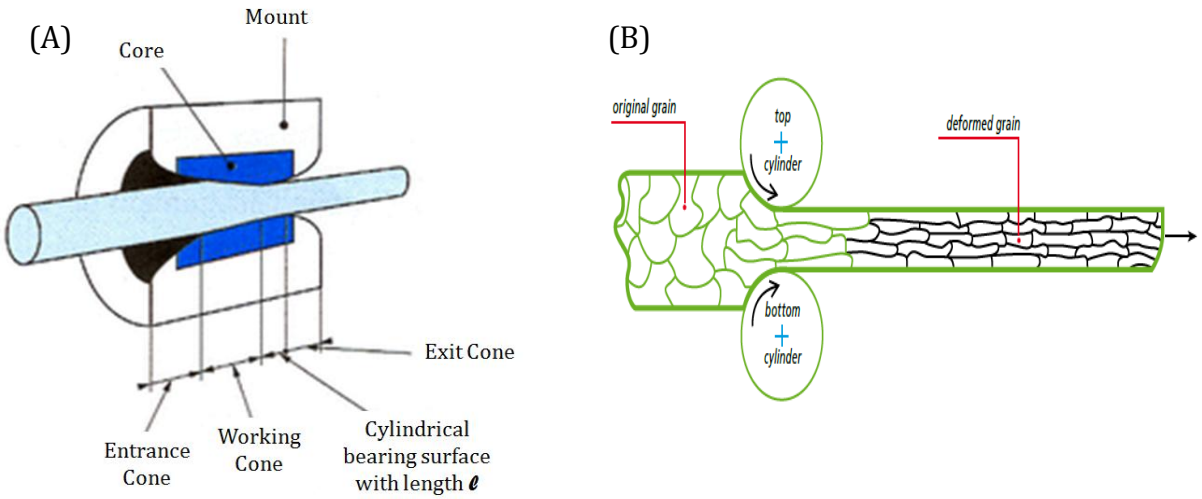

Fig. I.3 Schematic illustration of (A) cold-drawn deformation process, and (B) the induced change in the steel microstructure.

The microscopic examination of typical cold drawn prestressing steels is a highly anisotropic pearlitic microstructure with alternating lamellae of ferrite and cementite [15-17]. It is worth mentioning that, this pearlitic microstructure has been formed during the cooling process of the eutectoid steels at temperature below 723 ° C where, austenite is transformed by a process of nucleation and growth to pearlite phase [16].

I.1.2. Durability of prestressed concrete structures

Prestressed concrete structures have been worldwide used since many years. Although the corrosion protection design of prestressed concrete structures was well advanced in the past, there is still insufficient clarified corrosion problems in this filed. Such problems are not only because of the fact that the prestressed concrete is susceptible to corrosive attacks, but also traced back to unawareness of the corrosion behaviour of the prestressing materials, unsatisfied processing, unanticipated aggressive corrosion conditions as well as the occasional application of prestressing steels which are sensitive to aggressive corrosion attacks [20-22].

The corrosion risk of prestressing steels arose from the exposure to tensile stress in a corrosive environment. Fig.I.4 displays the mechanical fracture of prestressed steels as a result of the combination of induced localized attack caused by Cl^- with the external tensile stress. The high strength steel assisted cracking in aggressive environments results from hydrogen assisted embrittlement (HE), stress corrosion cracking (SCC) or a combination of both HE and SCC [21].

Fig.I.4. Photographs of corroded prestressed steels.

I.1.2.1. Protection of prestressed concrete structures

Nowadays, several corrosion protection systems, mainly based on the use of new materials [22], are available to improve the corrosion resistance of the prestressing bars in order to increase the durability of these types of concrete structures:

a) Non metallic prestressing materials:

They are characterized by their high resistance against the chemical attack and their low weight. For example, carbon fiber and glass fiber reinforced polymers. These materials show good mechanical properties in axial direction, but they are sensitive to lateral loads.

b) Prestressing metallic materials:

Different types of metallic steels can be considered as a practical solution for prestressed concrete structures to fulfill their high durability requirements. These types can be summarized as following:

Micro alloyed steels: They are high tensile strength steels at which small amounts of chromium, silicon and vanadium are added. They are characterized by their higher corrosion resistance [23].

Galvanized steels: The galvanized steels used in the prestressed structures are zinc coated wires by hot-dip galvanization. The process of forming zinc layer on steel bars is carried out by immersion in molten zinc at about 450 °C. In general terms, it takes about 20-120 sec of immersion to achieve a zinc layer thickness of 80-200 μm [24]. They are characterized by a high corrosion resistance so they can be used in aggressive atmospheric

environments, cable-stayed bridges and carbonated or chloride contaminated concrete [25-26].

High strength stainless steels (HSSS): The use of HSSS with strength up to 1700 MPa as prestressed steels is proposed as one of the most reliable alternatives for improving the durability of prestressed concrete structures in high aggressive environments [27-28]. However, they are not yet utilized because they are not fully developed to fulfill the prestressed concrete requirements. Besides, there is a lack of understanding their corrosion behaviour and mechanical performance in contact with concrete.

I.2. High Strength Stainless Steels (HSSS)

HSSSs are a type of stainless steels with certain specific mechanical properties to allow their use as prestressing reinforcements. Generally, stainless steels are corrosion resistant alloys that contain at least 12% chromium and can be divided into three groups according to their metallurgical structure [29]:

- ***Ferritic stainless steels***: contain 12 to 30% Cr which stabilize the ferrite. Some ferritic grades contain molybdenum up to 4% to increase the pitting corrosion resistance. Their crevice corrosion resistance is lower in comparison with the austenitic stainless steels. Also, they are less welded than other types of stainless steels.
- ***Austenitic stainless steels:*** they have a relatively high Ni content as an austenitic stabilizer (8-26% Ni) and the Cr-content is ranged between 17-25%. This type of stainless steels has a wide use due to their high corrosion resistance and their workability. Different alloying elements like Mo and N can be added to improve their resistance against the crevice corrosion.
- ***Duplex stainless steels:*** they present a binary microstructure of two phases (ferrite and austenite). The Cr content in duplex stainless steels is in the range between 22-28%, while the Ni content is lower than in austenitic stainless steels, 4-8%. Mo is one of the most important alloying elements added to duplex stainless steels in order to improve their corrosion resistance against pitting corrosion. The mechanical properties of duplex stainless steels are controlled by ferritic and austenitic microstructures.

Chromium content in stainless steels plays an important role in preventing the rust formation in aggressive environments. The corrosion resistance of stainless steels increases with the amount of chromium [29], as shown in Figure I.5.

The amount of chromium permissible in stainless steel is limited to the range 12 to 25% to assure the adequate passivation without the risk of precipitation at the grain boundary promoting the formation of sigma (σ) phase, which embrittles the steel [30]. In addition, sigma phase is also detrimental to the crevice and pitting corrosion resistance of the stainless steel alloys due to this precipitation of chromium at the grain boundaries [31-32].

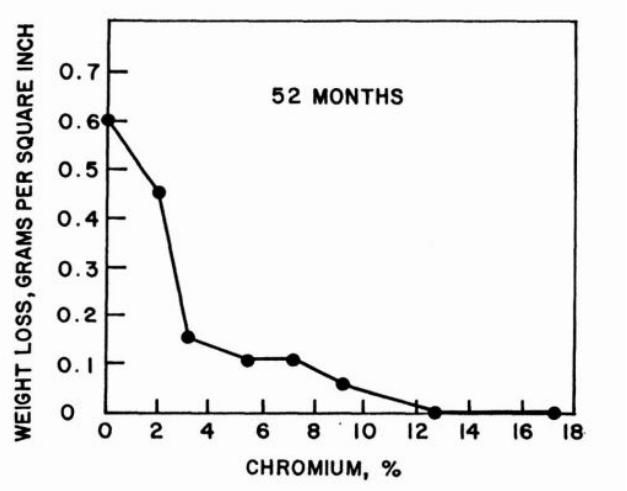

Fig. I.5 Influence of chromium content on the atmospheric corrosion of steel in an industrial atmosphere [29].

Nickel is a powerful austenizing alloying element which increases the corrosion resistance of stainless steels, especially in acidic media [29]. Furthermore, the presence of molybdenum is widely recognized for its beneficial effect on the resistance of the stainless steels [33], as the Mo has powerful effects in improving the resistance to pitting in chloride environments and to prevent crevice corrosion [34]. However, high molybdenum contents

promote the formation of the sigma phase in austenitic as well as in ferritic steels and therefore, the molybdenum content in stainless steel is normally restricted to less than 4% [30].

I.2.1. Production of HSSS

HSSS are also produced by a cold drawn deformation process [27,35-38]. Fig.I.6 indicates the variation in stainless steel tensile strength as a function of the cold drawn degree. Similarly than in case of conventional prestressing steels, the data confirm that, the maximum tensile strength of SS also increases with increasing the cold drawn degree [38]. Meanwhile, the characteristic elongation value fall down although remain in an enough high level [27].

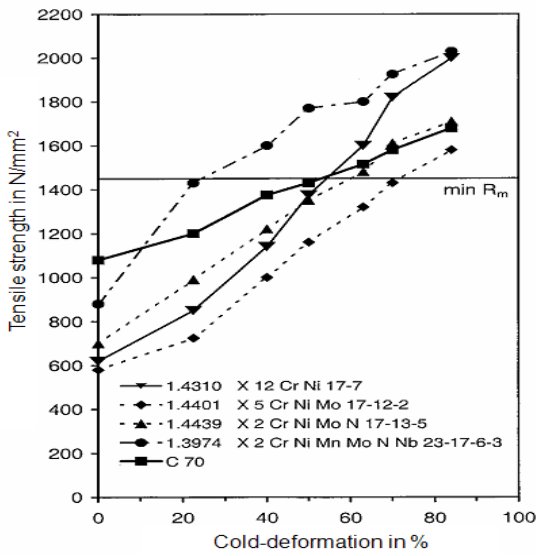

Fig. I.6 The evolution of the tensile strength of different reinforcing steels (conventional steels and stainless steels) by cold drawn degree [38].

Cold drawn deformation process in case of austenitic stainless steels may cause a transformation of the austenitic phase to martensite, especially in stainless steels with unstable austenitic microstructure (stainless steels with low content of alloying elements like Ni, N and Mn) [39-41]. The microstructure change to martensite reduces the resistance of HSSS to local corrosion and hydrogen assisted embrittlement or stress corrosion cracking [39].

Most of the published studies in high alkaline media (concrete, mortar, or simulating pore-solution) have been based on stainless steels, and few studies have been focused on cold drawn SS (HSSS). Furthermore, investigation of HSSS in literature has focused on the mechanical behaviour rather than the corrosion resistance [42-44].

Since there are few available data in literature concerning the protective and the corrosion properties of HSSS when exposed to high alkaline media, the experience on conventional normal stainless steels in contact with alkaline media has been taken into account as reference condition to understand the protective behaviour of HSSS.

I.2.2. Protective properties of stainless steels in concrete

Stainless steels have an excellent long-term corrosion resistance in natural environments and in contact with concrete [45-46] due to the formation of stable passive films on their surface [46], which can resist high aggressive environments with elevated chloride content. However, stainless steels can be subjected to localized corrosion if the chloride content in the concrete cover at the level of the reinforcement exceeds a certain critical value, known as critical chloride threshold (CCT).

I.2.2.1. Passivation of stainless steel in high alkaline media

The high corrosion resistance of the stainless steel arises from a passive, chromium-rich, oxide film spontaneously formed on the surface of the stainless steel when exposed to the alkaline conditions of concrete. Although is extremely thin, 1-5 nanometers thick, this protective film formed on stainless steels embedded in concrete is strongly adherent and chemically stable [29-30]. The passivation of stainless steels becomes a question of considerable importance for highlighting the nature of this oxide layer, the film formation mechanism and the factors affecting the passive layer growth. The passive film depends on the alloy composition, the medium characteristics and the conditions in which it is generated, causing the passivation of stainless steel to be a very complex process [33,45-48].

In literature, the electrochemical properties of the passive layer grown under spontaneous and controlled conditions (potentiostatic and potentiodynamic tests) have been analyzed by employing various electrochemical and surface analysis techniques for stainless steels exposed to alkaline media similar than the concrete aqueous phase. Concerning the passive film grown under controlled conditions, Veleva et al [47-48] performed a comparative study of passive films of austenitic AISI 316 stainless steels potentiodynamically grown in cement extract and in $Ca(OH)_2$ solutions. They found significant differences in the thickness and composition of the passive film formed in the two different solutions, cement extract and $Ca(OH)_2$. Abreu et al [33] have applied similar method for the generation of a thick passive layer by repetitive potentiodynamic cycling on austenitic AISI 304L and duplex 2205 stainless steels in 0.1 M NaOH. They observed by

sputter depth profiling analysis that, Cr/Fe ratio for duplex stainless steel was higher than for austenitic SS. In addition, the same authors investigated the long-term immersion behaviour of the potentiodynamically grown passive film in chloride containing media [33]. The results pointed out that a more oxidized iron rich layer with different Cr distribution has been found with increasing the immersion time for 41 days.

With regard to the passive film grown under potentiostatic conditions in low alkaline media that do not simulate concrete, Gojić et al [49] studied the electrochemical behaviour of duplex stainless steels in a borate buffer solution of pH 9-10 by using electrochemical impedance spectroscopy and chronoamperometric techniques. They concluded that the passive film thickness increased in the potential range from 0.1 to 0.4 V vs. SCE. Moreover, Aleksandra Kocijan et al [50] have also analyzed the potentiostatically generated passive film at similar exposure conditions. The X-ray photoelectron spectroscopy (XPS) analysis of the passive film formed on austenitic AISI 316 and AISI 304 wires at -0.36 and 0.64 V revealed a slight decrease of the chromium content close to the oxide/solution interface at more anodic potentials and this fact was explained on the basis of the selective solubility of oxides at the applied potentials.

On the other side, the spontaneous growing of the passive film on stainless steel by ageing has been studied elsewhere [51-55] by a combination of electrochemical measurements: corrosion potential, corrosion current density, capacitance and photocurrent, and electrochemical impedance spectroscopy. Bautista el al [51] and Freire et al [52] concluded that the passive film thickness and the electrochemical properties of the passive film formed in alkaline media of concrete is very pH-dependant. The exposure

to more alkaline media increases the relative amount of Fe^{II}-oxides in the grown passive film. The comparative analysis of the passive film formed on austenitic, ferritic and duplex stainless steels with ageing in NaOH solution performed by Addari et al [55] indicated that the naturally formed passive film on ferritic and duplex stainless steels became enriched in chromium oxy-hydroxide and the austenitic wires strongly enriched in nickel hydroxide. Furthermore, they reported that neither the composition of the pore solution nor the addition of 0.1 M NaCl significantly influences the passive film composition.

Although these results are available in literature to explain the passivation of the passive film grown on stainless steels under spontaneous and controlled conditions, it remains as open question if similar electrochemical response will be deduced for the passive film formed under spontaneous and induced conditions. In addition, there is still a lack in understanding the variation in the redox processes occurring in the passive film as a function of: the exposure conditions (especially pH), the stainless steels type (especially chemical composition and microstructure) and long-term immersion aging in absence and presence of chloride.

The application of surface analysis techniques to the study of the formation of the passive film on stainless steels in alkaline media has allowed to suggest that the passive film formed on alkaline media can be considered as a bilayer structure with an inner layer enriched in chromium oxide and an outer hydroxide layer [46,51-53,55-59].

According to literature [52-54], the bilayer of the passive film consisted in an outer layer enriched in Fe^{III} and Cr^{III} hydroxides and an inner layer compounded by anhydrous mixed-Fe-Cr-Ni oxides, most probably with a spinel structure. The spinel is enriched in Cr

species with the octahedral sites preferentially occupied by Cr^{III} and Fe^{II}. Abreu et al. [46] assumed that nickel may replace iron and/or chromium in the spinel and consequently it may affect the conductive behaviour of the passive film.

Ferreira et al. [54] explained that the inner layer of the passive film is composed mainly of chromium oxide due to the higher mobility of iron ions in the film as well as the higher stability of iron oxides in the passive film/electrolyte interface in comparison with chromium oxides.

Two oxidation states of iron oxides in the bilayer model of the passive film have been reported, which could correspond to a Fe_3O_4 or a mixture of FeO and Fe_2O_3 oxides. As Fe_3O_4, an inverse spinel, is structurally similar to a mixture of FeO and Fe_2O_3 [60], no difference between the two oxides was measured using XPS or AES, and thus it was not possible to determine whether the oxide film is a mixture of two oxides (Cr_2O_3 + Fe_3O_4) or whether it is an iron spinel with chromium replacing some of the iron positions [46, 59].

Liu [61] and Bastidas [62] revealed that $Cr(OH)_3$ was detected as primary constituent in the outermost layer beside iron oxides. Furthermore, molybdenum oxides are present in the film in form of a bilayer- an outer Mo^{VI}-rich layer and an inner Mo^{III} and Mo^{IV}- rich layer. The Mo species in the inner layer act as a barrier side by side with Cr_2O_3 to prevent the outward dissolution through the passive film [62]. In addition, the concentration of $Cr(OH)_3$ in the film will tend to increase with increasing the passivation time.

I. The role of some alloying elements in the passivation of stainless steels

➢ ***Effect of Ni***

The nickel content in stainless steel alloys modifies the properties of the corresponding passive film. The influence of Ni in the electrochemical behaviour of the passive film of stainless steels in high alkaline media was evaluated by several authors [58, 63-65]. Abreu et al [58] suggested that the external region of the passive film formed in high alkaline media (pH 13) is a nickel-iron spinel, probably $NiFe_2O_4$. The presence of this spinel $NiFe_2O_4$ was also confirmed elsewhere [63-64]**.** The presence of spinel $NiFe_2O_4$ enhances the formation of an homogeneous and thin passive film.

Maffi et al. [63] have confirmed the presence of NiO in the outer regions of the spontaneously formed passive film at high pH values (pH 11- 13).

In addition, a possible diffusion of Ni-metal from the substrate towards the outer oxide layer was reported in literature [58]. The Ni-enrichment at outermost part of the passive film as a result of Ni diffusion or Ni^{2+} reduction by Fe^{2+} [58] can explain why austenitic SS presents higher corrosion resistance.

➢ ***Effect of Mo***

Several attempts have been made to investigate the effects of Mo content on the passivity of stainless steels. Most of these studies have been performed in aqueous NaCl solution [66-67] or in acidic media [68]. Few works have been carried out in alkaline media [33,55].

Different hypothesis about the role of Mo in the passivation mechanism of the stainless steels in different media (NaCl solution, acidic and alkaline media) have been reported in literature [33,66-78]. In aqueous NaCl solutions and in acidic media, Mo can enhance the stability of the passive film acting from the solution on the external part of the layer [69]. The presence of Mo in the oxide film controls the dissolution rate of Fe and Cr [66,68]. Besides, Mo can enhance the effect of other passivation elements [33,49].

1) *Effect of Mo on the external part of the passive layer*

Sakashita & Sato [69] have detected that, in aqueous chloride solutions, Mo modifies the polarity of the passive film by formation of molybdates: the presence of negative MoO^{-n} ions in the outer part of the film changes its intrinsically anionic selectivity into a cationic one, inducing the formation of a bipolar layer. The latter promotes the formation of Cr_2O_3, or promotes the dissolution of chromium via the formation of soluble molybdates or Cr-Mo species that accelerate the extraction of Cr^{VI} from the most outer layer of the anodic film [62, 67, 69-71].

Bipolar model of passivity also suggests that the adsorbed molybdate in the passive film/solution interface can rectify the transport of ions through the passive film, and consequently inhibiting the ingress of chloride ions that aid in the dissolution of the film [71-72].

2) *Effect of Mo species inside the passive film*

Some authors [74-79] concluded that Mo prevents Cl^- ingress rendering the passive not only due to adsorbed molybdate in the interface, but also due to the presence of MoO_2

or MoO_3 species in the passive layer. Furthermore, Mo-oxides can improve the repassivation behaviour or the deactivation of growing pits [80-81].

Moreover, the presence of molybdenum in the passive film is widely recognized for its effect on its semiconducting properties. Stainless steels with higher Mo content show higher pitting corrosion resistance as a result of the effect of Mo in increasing the band-gap of the passive film [82-85].

The role of Mo in the stainless steel passivation process has also been reviewed by Jarglius-Pettersson et al [86], who suggested that there will be point defects in the oxide lattice of the film that are dominated by tri-valent species. The presence of the tetra and hexa molybdates tent to cancel these point defects. For an almost defect-free film it will be more difficult for anions to penetrate [87]. According to the point defect model proposed by Digby D. Macdonald [88] for the passive film formed under controlled conditions (potentiostatic control), the presence of Mo^{VI}-species in the passive film interacts with the cationic vacancies, resulting in the decrease of the vacancies flow in the passive film from film/electrolyte interface to the metal/film interface, preventing the condensation of the vacancies and the latter rupture of the passive film.

3) *Effect of Mo on the other passivation species*

In alkaline media, Abreu et al. [33] and Aleksandra Kocijan et al [50] indicated that the Mo promotes the enrichment of Cr_2O_3 and CrO_3 species in the film enhancing the effect of other passivation species more than acting directly on the passivation process of the stainless steels.

To summarize, the studies concerning the role of Mo content on the passivity of stainless steels in high alkaline media indicates that the passive film composition and electrochemical behaviour are highly affected by the presence of Mo. Thus, the evaluation of the role of this alloying element in the electrochemical response and the redox processes taking place during the passive film formation, especially in high alkaline media, has utmost importance for understanding not only the passivity of the stainless steel but also their corrosion behaviour in presence of aggressive agents like chlorides. On the other side, the effect of the exposure media, especially pH, on the role of Mo in passivation process is still a question that only few authors have taken into account.

II. The effect of the pH of the exposure media on the passivation of stainless steels

The composition of the passive film and the oxidation state of the elements in the film can be influenced by other parameters, such as the pH of the surrounding solution [89]. An important effect of pH on the passive film dissolution rate in both acidic and alkaline conditions has been reported elsewhere [90-92]. The pH increase promotes the decrease of the passive film dissolution rate and a thicker film with higher iron content, since iron oxide are more stable at higher pH. Consequently, as the pH becomes more alkaline, the solubility is lower for Fe and higher for Cr; this affects the level of chromium enrichment in the film [90]. Schmutz and Landolt [92] detected a mass increase corresponding to a net film growth and low dissolution rate in the alkaline media. In addition, Carroll and Walsh [93] found that lowering the pH from 11 to 2 at fixed chloride level (0.5M) alters the stability of the passive film formed on the stainless steels, basically related to the decrease of the passive film thickness.

In case of alkaline media simulating the aqueous phase of concrete pore, Freire et al. [52] indicated that the chemical composition of the passive film changes with pH from 9 to 13. The film becomes enriched in Cr^{III} and Fe^{III} species and depleted in Fe^{II} and Ni species as the pH decreases. So the film becomes depleted in magnetite as the pH decrease. Bautista et al. [51] have confirmed this change in the chemical composition of the passive film, as the Fe^{II}/Fe^{III} ratio in the passive layer increases when exposed to high alkaline solutions. While in carbonated solutions favors the formation of Fe^{III} implying an increase of the oxidized Fe content and the Fe^{II}/Fe^{III} tends to decrease.

For acidic and neutral environments, Elsener and Rossi [94] deduced that the pH of the surrounding environment affects both the film thickness and the passive film composition. The pH increase from 2 to 7 results in a passive film with more oxidized iron oxides in the film with higher thickness [95]. Furthermore, higher Cr^{III} hydroxide content [94].

I.2.2.2. Corrosion of stainless steel in high alkaline media

Even though the high corrosion resistance of stainless steels, they can suffer from certain types of corrosion [96] when exposed to high aggressive conditions. The different types of corrosion that can affect stainless steels can be categorized as following: General Corrosion, Galvanic Corrosion, Pitting Corrosion, Crevice Corrosion, Stress Corrosion Cracking, and Intergranular Corrosion. In the present thesis, the pitting corrosion is the main focus.

General corrosion promotes a general and uniform destroy of the passive film and mainly occurs in acids or hot alkaline solutions [97-98]. The temperature has a marked

effect on the general corrosion rate which is doubled when the temperature increases by 10 °C [99].

As a guideline, the risk of the general corrosion starts when the corrosion rate expressed as a loss of the film thickness, increases more than 0.1 mm/ year [100]. The durability of stainless steels exposed to general corrosion process is relatively easy to estimate with high reliability by the evaluation of the material loss and the film thickness reduction as a function of the exposure time to the aggressive environment [101]. Increasing the chromium content in the passive film improves the corrosion resistance of stainless steel against this type of corrosion [98].

Galvanic corrosion occurs when two different materials are in contact in the same electrolyte, and hence, a galvanic couple is formed. There will be a difference in the potential between the two materials, which will be the driving force for the severely attacked anode. The other metal will be the cathode and will be protected against corrosion. The corrosion resistance of the two coupled metals might differ significantly from their behavior when uncoupled. In many environments stainless steels are nobler than other construction metals and stay passive if coupled to a less noble material.

Actually, according to the data obtained by Bertolini el al [102-103], the galvanic corrosion that can arise when both passive carbon steel and stainless-steel rebars, embedded in aerated concrete, are in contact has no appreciable effects, since the two types of steel have almost the same free corrosion potential. Indeed, in this environment, carbon steel is even slightly nobler than stainless steel [104]. In any case, both carbon steel and stainless steel remain passive even after connection.

Under the combined effect of stress and certain corrosive environments, usually chloride containing media, stainless steels can be subjected to a very rapid and severe form of corrosion called stress corrosion cracking (SCC). The stresses must be tensile and can result from loads applied in service or stresses set up by the type of assembly e.g. from residual stresses resulting from the method of fabrication such as cold drawn [96].

Important surrounding factors for SCC are often the oxygen concentration, the pH and the electrode potential. The cracks might be both across or through the individual crystals of a metal (transcrystalline) and along the boundaries between crystals or grains of a metal (intercrystalline) and it often leads to brittle failures [101].

Concerning pitting corrosion of stainless steels, it usually occurs in high corrosion resistance materials. Under certain conditions, particularly involving high concentrations of chlorides (such as sodium chloride in sea water), moderately high temperatures and exacerbated by low pH (i.e. acidic conditions), the local dissolution of the passive film can occur. In addition, stainless steels embedded in concrete are susceptible to pitting corrosion initiation when the chloride content on the stainless steel surface reaches a minimum chloride concentration, known as critical chloride threshold (CCT). The attacked positions are a relative very small area with respect to the total exposed area. The high difference between the cathodic area (passive layer) and the anodic area (pits) induces the flow of a high anodic current density and, as a consequence, the increase of the corrosion propagation inside the pit.

The breakdown of the passive film, with the pit initiation, is probably the least understood aspect of the pitting corrosion phenomenon and several theories for the

passive film breakdown have been categorized in three main mechanisms: (a) The passive film penetration mechanism which involves the transport of the aggressive anions through the passive film [105-107]. (b) Adsorption mechanism of chloride ions on the outer barrier oxide [108-109]. (c) Film breaking mechanism, which considers that the passive film is in a continuous state of breaking and repair [110-111].

The most critical stage of the pitting corrosion mechanism is the initiation phase. After the pit is initiated, an autocatalytic process takes place with a fast growing of pits. The risk of the onset of pitting corrosion on stainless steel surface is controlled by a lot of parameters among them the aggressive ion concentration, the pH of the exposure media, and the stainless steel chemical composition and microstructure.

Concerning the effect of the stainless steel chemical composition, especially Mo content, it was reported that the presence of Mo in stainless steels in chloride acidic conditions reduces the number and size of both nucleated and metastable pits, decreasing the probability of generating stable pits [112]. Several works in acidic media defend that Mo promotes the repassivation process by forming insoluble molybdenum chloride complexes [113-114] or MoO_4^{2-} [115] in the active sites. The inhibition of the early stages of pit growth was also considered by Sugimoto and Sawada [116] due to the adsorption of MoO_4^{2-} in pits.

In the same context, Pardo et al. [117] and Schneider et al [113] confirmed that the presence of Mo in the Fe-Cr alloy permits the formation of insoluble salt at the bottom of the pit nucleated in acidic media, which induces the repassivation process of Mo bearing stainless steels. Moreover, Wegrelius et al. [118] concluded that Mo can form Mo-Chloride

complexes, which decreases the free chlorides ions in the passive layer, increasing its stability. Furthermore, they found that the passive film formed on Mo free alloys contains about 50% more chloride ion compared with the film formed in presence of Mo.

Most of the available studies in literature to understand the effect of the Mo in pitting corrosion initiation and propagation have been focused in acidic media. However, in the case of high alkaline media or in concrete, there is still a lack in understanding the impact of Mo content in the pitting corrosion of stainless steels in presence of chloride.

I.2.2.3. Critical chloride threshold (CCT) of stainless steels

For a detailed study of the stainless steel corrosion behaviour in aggressive environment, the concept of critical chloride threshold (CCT) should be considered. CCT is considered as an important parameter to evaluate the service life of reinforced concrete structures. CCT of stainless steels is defined as the minimum content of chlorides that causes the initiation of pitting corrosion on the embedded reinforcement in concrete [9, 119-120].

Although CCT is a key parameter in predicting the service life of reinforced concrete structures exposed to marine environments, its determination is hard to be measured rapidly and properly because the transport process of the chloride ions needs long time to reach the chloride threshold at the depth of the reinforcement [121-122]. In literature, there is no agreement between authors about the methodology employed to determine the CCT value. A simple classification of the testing methods used for chloride threshold determination in the laboratory is to consider a division in: 1) Natural and 2) Accelerated methods [120].

Methodologies based on natural chloride penetration are considered less useful for the study of stainless steel because of their higher corrosion resistance expected for these materials. Therefore, many researchers focus their investigations on developing accelerated depassivation methods for time saving.

In natural conditions, the chloride concentration slowly increases with time, due to the diffusion process through the concrete pores during the depassivation test. In case of natural testing methods, the critical chloride content has been determined in concrete considering both the chloride penetration (either in laboratory or in field) and the addition to the mix (in laboratory). Although the determination of CCT in concrete is closer to real application, CCT has also been determined in simulated pore solutions to avoid the uncontrollable parameters in case of mortar or concrete [123-124]. However, the obtained values cannot be directly applied in models for the service life prediction for reinforced concrete structures. Furthermore, natural determination of CCT of stainless steel in concrete or mortar is not a time saving method because of the high corrosion resistance of this material [125-126].

Accelerated methods have been considered the most applied in literature for the determination of CCT for stainless steels [123-139]. The more used accelerated methods for chloride threshold determination in case of stainless steels can be divided in three types: a) potentiostatic, b) potentiodynamic, and c) migration methods.

The reported CCT for stainless steels in literature for SS scatter over a large range due to different reasons, as the testing conditions and methods employed [125-127]. Furthermore, the stainless steel CCT is highly affected by the SS chemical composition and

microstructure [135,138], as well as, the stainless steel surface finishing and the welding scale [128,136,139].

In case of CCT values determined in alkaline solutions, most of work has been performed in saturated $Ca(OH)_2$ solution (pH ≈ 12.5 at 25 °C). Bautista et al. [131-133] found that 0.15 M NaCl was enough for nucleation of active pits on austenitic 304 and 316L by using potentiodynamic tests (CV). Similar CCT value was reported by Alvarez et al. [130] in duplex 2304 using the same electrochemical test. However, Bertolini et al. [136] employed potentiodynamic test after prepassivation for 48 hours, and obtained much higher CCT value: 0.8 M NaCl for the same SS (4.5% Ni) and 0.5 M NaCl for duplex 2101 SS with lower Ni content (1.8% Ni). In addition, the potentiostatic test performed by Bertolini et al. [127] at +200 mV_{SCE} indicates that the CCT value for 2304 DSS is ranged between 1.3-1.4 M NaCl and 0.8 M NaCl for 2101 DSS. Comparing the potentiostatic and potentiodynamic tests performed by Bertolini et al. [127, 136], it can be concluded that the critical content of Cl^- required to initiate pitting is lower in case of potentiodynamic tests than the potentiostatic one at the same conditions. From the other side, Elsener et al [140] found that the CCT of duplex 2205 stainless steels in the same alkaline media was higher than 5 M NaCl when potentiodynamic tests are used.

Regarding the CCT variation in mortar and concrete, the values for SS are betwen 1-8 % Cl^- respect the total cement weight [35,131-132,133-134].

Table I.1 summarizes the results obtained by U. Nürnberger et al. [35], which illustrates the corrosion degree based on pitting depth and weight loss. The listed data in table I.1 indicates that the strongest attack for both mild steels and ferritic stainless steels occurs in

carbonated and high chloride contaminated concrete. Furthermore, higher alloyed stainless steels (austenitic and duplex) have higher corrosion resistance even in carbonated concrete conditions.

Table I.1 Corrosion behaviour of stainless steels in concrete [35].

Steel	Concrete	Alkaline				Carbonated	
	Cl^- wt. %	0	1	2	> 2-5	0	2
Unalloyed	Unwelded						
	Welded						
Ferritic (12 Cr)	Unwelded						
	Welded						
Austenitic 17 Cr- 12 Ni-2 Mo	Unwelded						
	Welded						
Duplex 22 Cr- 5 Ni- 3 Mo	Unwelded						
	Welded						

None Moderate Severe Very severe

Sørensen et al. [128] investigated the CCT in mortar prisms mixed-in with 0-8% Cl^-. Both 304 and 316 austenitic stainless steels were tested in both welded and unwelded conditions. The potentiostatic test of 304 and 316 stainless steels at +0.2 V vs. SCE indicated that the CCT values of these steels were between 3.5-5% Cl^- with respect to the weight of cement for unwelded austenitic stainless steels. Furthermore, the CCT determined by a potentiostatic test at lower potentials (0 V vs. SCE) was relatively higher (5-8% Cl^-). In case of weld condition, the CCT values decreased down to 1-2% Cl^- when +0.2 V vs. SCE was applied, and 3.5-5% Cl^- in case of the potentiostatic test at 0 V vs. SCE.

Concerning CCT determination of the same steels by potentiodynamic scans up to +0.2 V vs. SCE, higher CCT values were obtained for both 304 and 316 stainless steels, where the CCT values were 5% and > 8% Cl^- respectively, which probably related to the effect of the less anodic limit reached during the potentiodynamic test in comparison with Bertolini et al. [127, 136].

In agreement with the up mentioned results, Garcia Alonso et al. [125-126] obtained CCT higher than 5 % Cl^- for 304 and 316 austenitic stainless steels is in case of chloride mixed-in mortar [126], while pits were potentiodynamically nucleated in case chloride mixed-in concrete [125] samples with 4% total Cl^-.

The accelerated chloride threshold testing method developed by David Trejo et al. [129] concluded that CCT value for austenitic 304 and 316LN stainless steels were 1.2 and 1.9 % Cl^- respectively, which were the lowest CCT values reported in literature for stainless steels embedded in mortar.

The CCT value of austenitic and duplex stainless steels (304, 316, 2304, 2101) were estimated by Bertolini et al. in concrete [127] indicates that for 304 and 316 austenitic steels, the CCT were 8 % Cl^- respect cement weight, while the duplex 2101 and 2304 wires, the CCT were 2.5 and 3 % Cl^- respect cement weight respectively.

I.2.3. High Strength Stainless Steels (HSSS)

I.2.3.1. Passivation of HSSS in alkaline media

In literature, few studies have been focused in the evaluation of passivation of HSSS in alkaline media [141]. Alonso et al [141] reported that austenitic HSSS presented a passive behaviour in contact with alkaline media with the formation of less electrochemically resistant passive film with increasing the alkalinity of the surrounding media. Furthermore, they [141] concluded that the passive film electrochemical properties varied with the increment in temperature of the alkaline media, where higher steady state current density values were measured for the passive film formed in high temperature alkaline solutions. On the other side, the application of an external mechanical load of 80% of the HSSS maximum strength did not show substantial changes in the stainless steel passivation process [141].

The passivation of HSSS in alkaline media is still a question of considerable importance because there is a lack in the available information in literature to highlight the electrochemical response of the passive film formed on HSSS in contact with concrete or alkaline media simulating the aqueous phase of concrete.

I.2.3.2. Corrosion of HSSS

First attempts to evaluate the corrosion behavior of the HSSS in concrete were performed on austenitic stainless steels [27,35-41,141-144]. The relevant types of corrosion expected for HSSS can be summarized as following:

A. Pitting corrosion and crevice corrosion in alkaline or carbonated concrete containing chloride. The pitting potentials of the HSSS fall with decreasing the content of alloying elements and with increasing the chloride content [27]. For the carbonated concrete with high chloride content the pitting potential is more negative indicating a higher risk of pitting corrosion than in the alkaline chloride-containing concretes [27].

Alonso et al. [40,141] have deduced that the pitting potential of HSSS is shifted to more cathodic values by decreasing the Mo and Ni contents, which means less pitting corrosion resistance. Furthermore, the carbonated concrete is more aggressive than the alkaline concrete for the same chloride content, as also obtained in [27].

Nürnberger et al. [27] observed a recognizable reduction of the pitting corrosion potential in case of prestressing austenitic 304 stainless steels compared with conventional reinforcement 304 steels, especially in chloride containing alkaline concrete and in carbonated concrete, which was related to the unstable austenitic microstructure and the formation of martensite phase.

B. Stress corrosion cracking (SCC), which is the corrosion process initiated by tiny corrosion pits growing in the steel surface in presence of load. SCC risk rises with the falling of the pH-value, increases with the chloride concentration and with the temperature of the environment.

Nürnberger et al. [27] have concluded that the life time of the stressed HSSS increases with increasing the pH-value and with decreasing the temperature of the

environment. The temperature threshold, which is the critical temperature below which no SCC is detected, depends on the pH-value as the temperature threshold increases with the pH-value so alkaline solutions have higher temperature threshold than for acidic solutions.

C. Hydrogen Embrittlement (HE), which is produced due to the penetration of the atomic hydrogen in the microstructure of martensite in stainless steels that increases the susceptibility to initiate embrittlement [27,39]. The microstructural change of austenitic to martensite induced by cold drawn deformation process affects the susceptibility of the cold drawn steels to HE. The HE susceptibility depends on the chemical composition of HSSS and on the surface [39].

In literature [39], it was outlined that HE susceptibility of austenitic SS increases with decreasing the austenitic stabilizing alloying elements, as Ni contents, which favour the martensite formation during the cold drawn process. High alloyed austenitic HSSS are expected to be less susceptible to suffer HE [27,39, 142].

I.2.3.3. Critical chloride threshold of HSSS

For austenitic (AISI 316, 317 and 304) and duplex (2101, 2304, and 2205) HSSS, many attempts to define their CCT value were carried out [27, 35, 40, 41, 137,141-143]. The most relevant CCT values of HSSSs in simulated alkaline concrete pore solutions and in mortar are listed in table I.2 and table I.3 respectively.

Studies conducted by Recio [41] using potentiodynamic accelerated techniques in simulated pore solutions (Sat. $Ca(OH)_2$+ 0.5 M KOH, pH 13.5) showed that the CCT of

austenitic 316 stainless steels is above 1.5 M. In addition, CCT value of stainless steel decreases with decreasing the pH of the alkaline solution. Alonso et al. [40] detected that pits were nucleated on the surface of austenitic 304 HSSS when the chloride content increased up to 0.75 M in Sat. $Ca(OH)_2$+ 0.2 M KOH solutions (pH 13.2), and the application of external loads induced the nucleation of pits in presence of relatively lower chloride concentrations (0.5 M).

On the other side, Moser et al. [142-143] also used the potentiodynamic tests for the study of the chloride induced corrosion of HSSS with tensile strength ≅ 1200 MPa in alkaline solutions. The estimated CCT values of austenitic 316 and 304 SS in alkaline solutions of pH 12.5 were 0.25 M and 0.5 M respectively. Concerning carbonated solutions, 316 HSSS presents higher corrosion resistance in comparison with 304 SS. According to Moser et al results [143], duplex stainless steels (2304 and 2205) were the only candidates of HSSS that exhibited high corrosion resistance at Cl^- concentrations up to 0.5 M. In all the conditions examined, 2205 HSSS exhibited higher corrosion resistance than the other HSSS studied.

Table I.2. CCT values of HSSS in simulated pore solutions.

Ref.	HSSS	Test	Temp.	Environment	pH	CCT-value/ M
[41]	316	Potentiodynamic	RT	Sat. $Ca(OH)_2$	12.5	0.5
				Sat. $Ca(OH)_2$+ 0.2 M KOH	13.2	1.5
				Sat. $Ca(OH)_2$+ 0.5 M KOH	13.5	> 1.5
[137]	316	Potentiodynamic	RT	Sat. $Ca(OH)_2$+ 0.2 M KOH	13.2	1.5
	304					0.5
[40]	304	Potentiodynamic	RT	Sat. $Ca(OH)_2$+ 0.2 M KOH	13.2	0.75
						0.5*
[143]	316	Potentiodynamic	RT	4 g/l $Ca(OH)_2$	12.5	0.25
	304					0.5
	2101					0.5
	2304					1
	2205					> 1
[143]	316	Potentiodynamic	RT	0.3 M $NaHCO_3$ + 0.1 M Na_2CO_3	9.5	0.5
	304					0.25
	2101					0.25
	2304					0.25
	2205					> 1

* In presence of external load of 70% of the steel tensile strength.

Table I.3. CCT values of HSSS in mortar.

Ref.	HSSS	Environment	CCT-value/ %Cl^-
[27,35]	304	Alkaline mortar	5
	316		5
	317		> 5
	316	Carbonated mortar	2
	317		3

Among the limited previous studies that examined HSSS, most have focused on austenitic stainless steels and no previous studies have investigated the corrosion resistance of duplex HSSS of $\sigma_{max} \cong 1700$ MPa. The lack of knowledge of long-term response and the corrosion behavior of duplex HSSS steels, especially when they are embedded in concrete or cement-based alkaline environments, are the main reasons that limit the extended application of duplex HSSSs in prestressed concrete structures. Moser et al [142-143] is the only study in literature which investigate the corrosion behaviour of duplex HSSS in alkaline media with chlorides, which concluded that these steels exhibit high corrosion resistance. Notwithstanding the mechanical properties of the tested duplex HSSS (σ_{max} of 1100-1200 MPa) were still insufficient for use in prestressed concrete structures, and the electrochemical response can be significantly different if HSSS with high maximum strength are considered.

II. Objectives

II. Objectives

The first attempts in literature to study the behaviour of HSSS have been concentrated in the austenitic type. Previous studies have shown that the heavy cold drawn deformation used for the production of austenitic HSSS results in the formation of strain-induced martensite, which affects their corrosion behaviour in aggressive environments. The higher cost of austenitic HSSS due to their high Ni content and the risk of the formation of the martensitic phase during the cold drawn deformation process give a way for the application of duplex HSSS in prestressed concrete structures as new alternatives to austenitic HSSS. The study of the long-term electrochemical response and the corrosion behaviour of the duplex HSSS in concrete or in cement-based alkaline environments are still insufficient. Consequently, the aim of the present thesis focuses on the assessment of the protective capacity of these high strength stainless steels in alkaline media through the study of the electrochemical response of duplex HSSS in different exposure conditions. The present study focuses on analyzing both passivation and depassivation processes of duplex HSSS in alkaline solutions that simulate the aqueous concrete pore phase and in mortar as well.

Concerning the analysis of the passivation of duplex HSSS in alkaline media, the following specific objectives have been considered:

I. Evaluation of the effect of the exposure media, especially the pH, on the electrochemical response of the passive film formed on duplex HSSS.

II. Study the effect of the stainless steel chemical composition, especially Mo content, in the passivation properties of the passive film. In addition, the effect of the microstructures of CD-DSS on the passivation process has been also considered.
III. Short and long-term assessment of the electrochemical behaviour of the passive film formed on duplex HSSS at different exposure conditions.
IV. Assessment of the influence of the passivation conditions on the electrochemical response of the passive layer: spontaneous and accelerated passive film formation for duplex HSSS in alkaline media.

On the other side, the corrosion behaviour of duplex HSSS in presence of chloride has been studied in alkaline media by application of spontaneous and accelerated depassivation methods to highlight the behaviour of these stainless steels in different aggressive electrolytes containing various chloride concentrations and at different temperatures. In this case, four aspects have been analyzed:

I. The progressive alteration of the passive film due to the presence of the chloride ion in the passive film/electrolyte interface before the corrosion initiation process.
II. Evaluation of depassivation processes of duplex HSSS and determination of the critical concentration of chloride (CCT) required to initiate active pits on the steel surface at different conditions.
III. Analysis of corrosion propagation period on duplex HSSS once the corrosion process is initiated in high aggressive conditions.
IV. Assessment of different accelerated electrochemical techniques for CCT determination.

III. Experimental procedure

III. Experimental procedure

The experimental procedure of the present thesis has been divided in two main parts in order to give answer to the objectives mentioned in the previous chapter:

1. Passivation process of duplex high strength stainless steels (DHSSS) in alkaline media.
2. Corrosion behaviour of HSSS in presence of chlorides in alkaline media.

The passivation and depassivation of duplex SS were analyzed by studying the electrochemical response of the passive layers formed during ageing in alkaline solutions simulating the aqueous phase of concrete pores and in mortar.

The corrosion behaviour of duplex SS was studied in alkaline media in presence of different concentrations of chloride. Moreover, to simulate more real conditions, the duplex SS susceptibility to pitting corrosion was also analyzed for stainless steels embedded in mortar, where different methods have been assessed to determine the critical chloride threshold required for the depassivation of duplex stainless steels. The working plan carried out has been schemed in Fig.III.1.

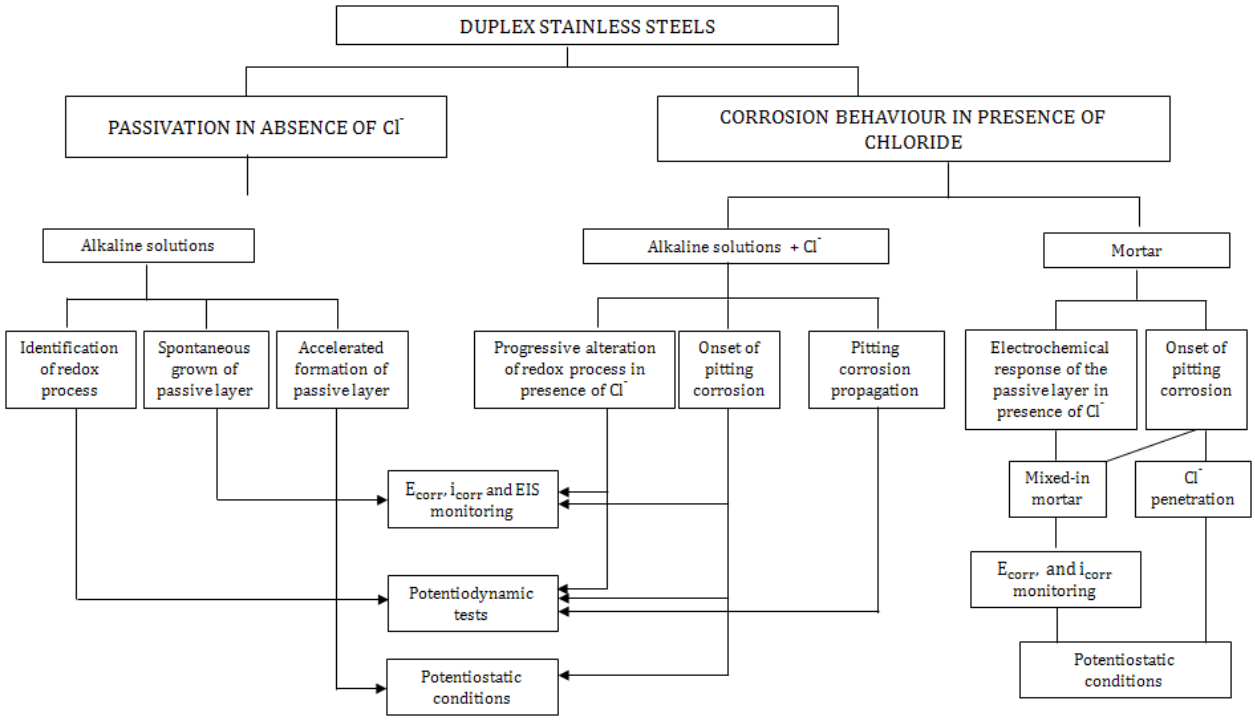

Fig.III.1 Experimental working plan.

III.1. Materials

Two duplex stainless steels (DSS) with different composition have been studied: 2304 and 2205. For each case, both parent (P) and cold-drawn (CD) wires have been considered. Fig. III.2 shows the photograph of the surface of the studied P and CD steels.

The initial surface of cold drawn and parent DSS is quite different as the cold drawn DSS have brighter and smoother surface in comparison with the parent DSS. These differences in the surface are produced during the cold drawn deformation process. Besides, some defects in the cold drawn direction appear in case of CD-DSS.

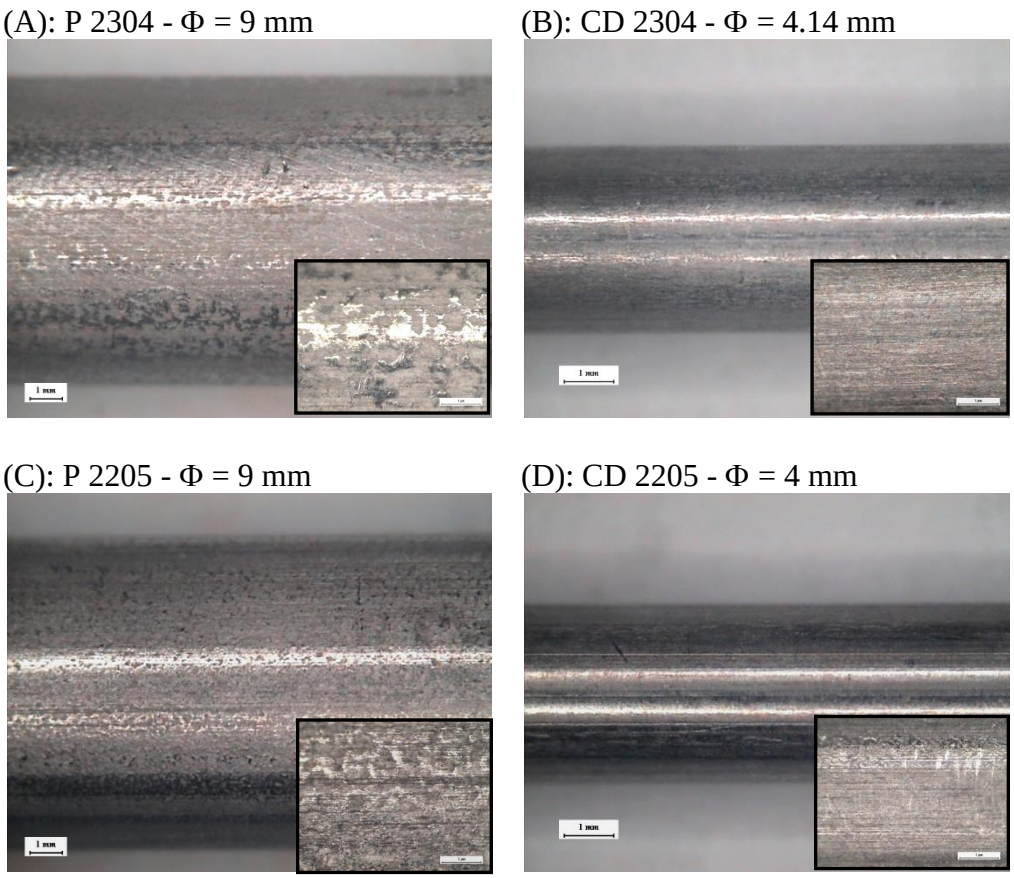

Fig.III.2. Duplex stainless steels wires: (A) parent 2304, (B) cold drawn 2304, (C) parent 2205, and (D) cold drawn 2205.

III.1.1. Alloy composition of duplex SS

The chemical composition of 2304 and 2205 duplex stainless steels is shown in table III.1, where the mass percent of each alloying element is listed depending on the steel manufacture standards followed up by the producer.

The 2304 and 2205 duplex stainless steels have a similar content in Cr and Ni. The main difference between both steels lays on the Mo content: the mass percent of Mo in 2304 SS is lower (0.1% wt) in comparison with 2205 SS which contains 3.7 % wt.

Table III.1. Chemical composition of the stainless steels in wt%.

Steel name(ASTM)	%C	%Cr	%Ni	%Mo	%Mn	%Si
2304*	0.03	22.9	4.29	0.1	1.79	0.6
2205*	0.04	23.3	4.3	3.7	2.1	0.6

∗ *The cold drawn and the parent stainless steels have the same chemical compositions.*

III.1.2. Microstructure and mechanical properties

The high strength stainless steels grades were obtained after a cold drawn treatment of the parent steels. The cold draw deformation process induces changes in the stainless steel microstructure and improves their tensile strength. In the present work, the parent grades were employed in order to analyze the impact of cold drawn process on the electrochemical behaviour of the studied stainless steels.

Equation III.1 has been employed to calculate the cold drawn degree (P) for the production of 2304 and 2205 HSSS considering the initial and the final cross section areas of the stainless steels wires before and after the cold drawn deformation:

$$P = \left(1 - \frac{s}{S}\right) \text{ x } 100 = \left(1 - \left(\frac{d}{D}\right)^2\right) \text{ x } 100 \qquad eq.III.1$$

Where, s and d are the cross section and diameter of the cold drawn wires respectively, while the S and D are the cross section and the diameter of the undrawn (Parent) bars respectively. Table III.2 shows the cold drawn degree employed for the 2304 and 2205 HSSS studied in present thesis.

Table III.2. Cold drawn degree of the HSSS.

Steel name(ASTM)	Type	D (mm)	d (mm)	P (%)
2304	Duplex	9	4.14	80
2205	Duplex	9	4	80

In order to analyse the effect of the cold drawn process on the stainless steel microstructure, stainless steel samples were cut in transverse and longitudinal axis and embedded in epoxy resin to facilitate the polishing of these samples, as shown in Fig. III.3.

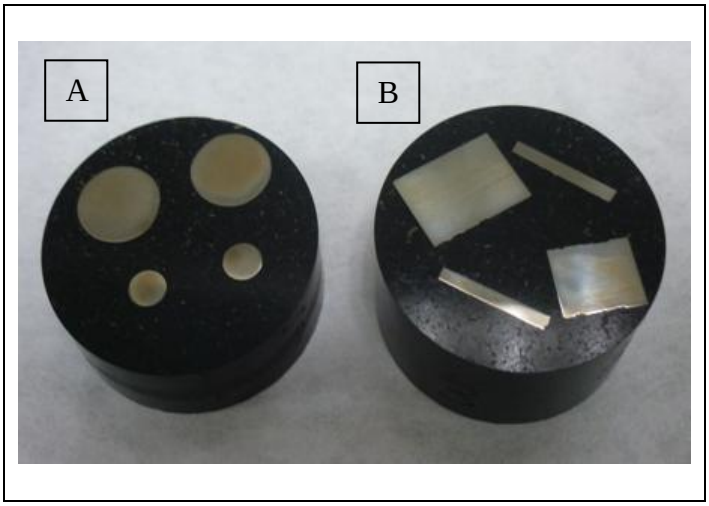

Fig.III.3. (A) Cross-sections and (B) longitudinal-sections of P and CD 2304 and 2205 stainless steels embedded in epoxy resin.

A mirror-like surface was prepared for all tested samples by a three step procedure:

1. Grinding with successive grades of SiC emery paper up to 4000 grade.
2. Polishing with 1μm diamond paste.

3. Ultrasonic degreased in acetone, then washed with distilled water and dried with hot air.

The cross and longitudinal sections were attacked by using tint etching colour metallography, which allows the identification of the different phases present in the duplex microstructure of the cold drawn (CD) and parent (P) stainless steels. The coloured revealing of the austenitic and ferritic phases was carried out by the immersion of the polished samples for 50 seconds in Bloech and Wedl coloured etching agent [145].

The solution of Bloech and Wedl coloured etching agent was prepared as following:

1. Dissolving 500 mg of potassium metabisulfite ($K_2S_2O_5$) in 100 ml of distilled water.
2. Acidifying the solution by adding 15 ml of 33% HCl.

After etching, the samples were optically examined with an Olympus GX51 optical microscope, as can be observed in Fig.III.4 for the 2304 stainless steel and in Fig.III.5 for the 2205 stainless steel.

For both 2304 and 2205 duplex stainless steels, the characteristic grains of austenite (bright) and ferrite (dark brown) are clearly observed inside the matrix. Furthermore, after the cold drawn process, the stainless steel microstructure presents a more refined grain size for both the austenitic and the ferritic phases. The formation of martensite as a consequence of the cold drawn process of duplex stainless steels is not observed at these magnifications. In table III.3 the mechanical properties of the studied duplex stainless steels are resumed.

2304	Longitudinal section	Cross section
Parent	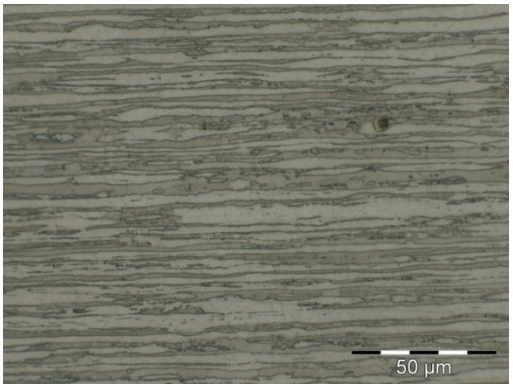	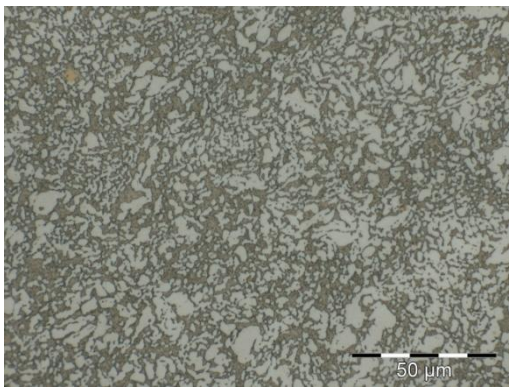
Cold drawn	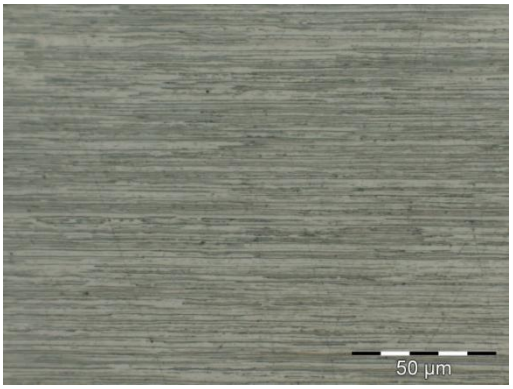	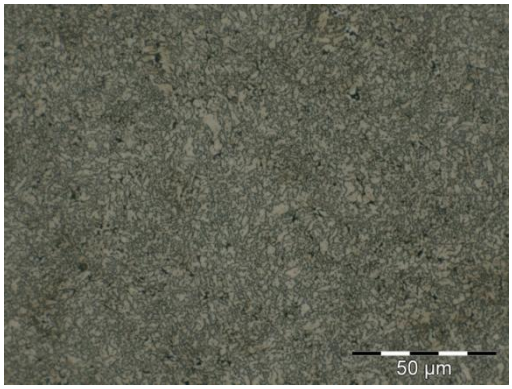

Fig. III. 4. Microstructure of the longitudinal and cross sections of 2304 SS containing austenite (bright) and ferrite (dark brown).

2205	Longitudinal	Transverse
Parent	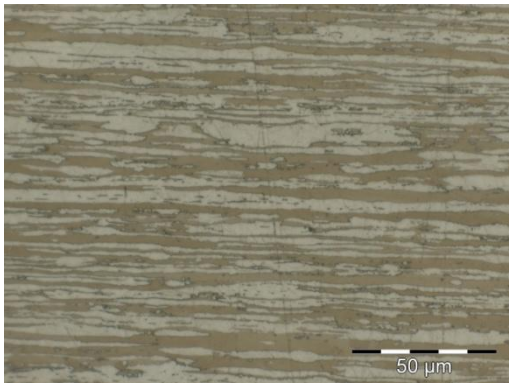	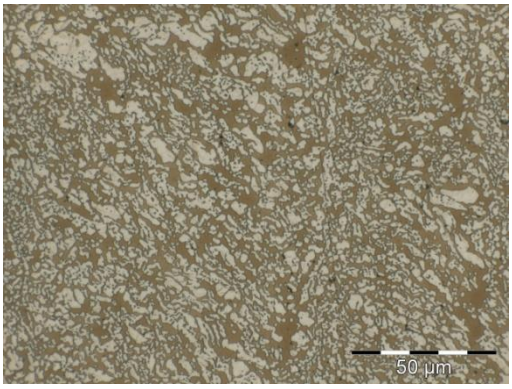
Cold drawn	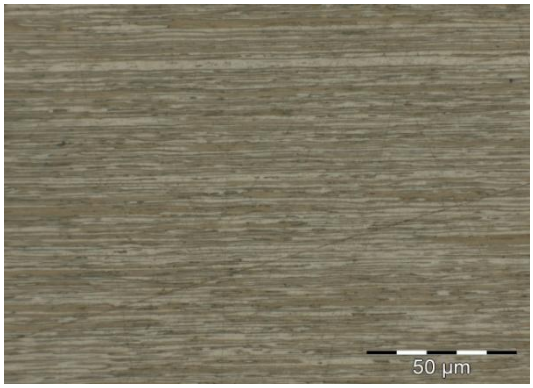	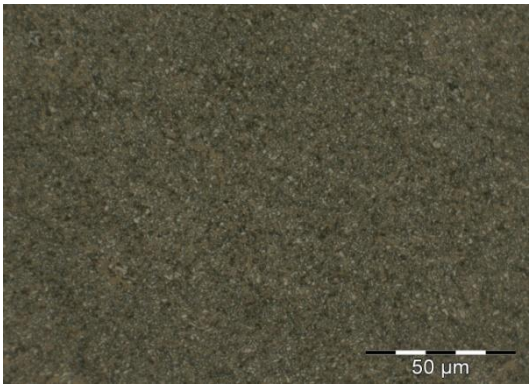

Fig. III. 5. Microstructure of the longitudinal and cross sections of 2205 SS containing austenite (bright) and ferrite (dark brown).

Table III.3. Mechanical properties of duplex stainless steels.

Stainless steel name / Mechanical properties	2304		2205	
	Parent	Cold drawn	Parent	Cold drawn
Maximum stress / MPa	865	1629	976	1712
Yield strength / MPa	569	1586	633	1527
Young Modulus (*E*) / GPa	171	178	186	208

As can be seen in table III.3, the maximum stress at which the material breaks with a sudden release of the stored elastic energy is drastically increased by the cold drawn deformation. Furthermore, the yield strength is also improved in the cold drawn duplex stainless steels which can support higher amount of stress before moving from the elastic deformation into the plastic deformation. In addition, a slight increase in Young's modulus was also induced by the cold drawn process.

Furthermore, the microhardness of both P and CD stainless steels was measured by using Struers Duramin-2 Vickers microhardness tester with a Vichers diamond pyramid as indenter. The testing procedure is very similar to that of the standard Vickers hardness test but on microscopic scale and with higher precision instruments. Fig. III.6 shows the scheme of the microhardness Vickers test.

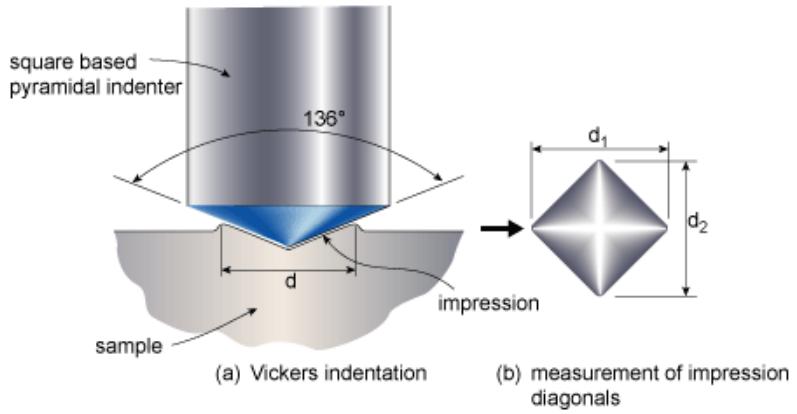

Fig. III. 6. Scheme of a microhardness Vickers hardness test.

The cross and longitudinal sections of the polished stainless steels samples embedded in epoxy resin were also used to measure the microhardness. Each sample was

tested 12 times by the application of 0.1 kilogram force (kgf) for 5 seconds to obtain the impression diagonals for each test, d1 and d2 (Fig. III.6.b).

The Vickers hardness number was calculated automatically by equation III.2:

$$HV = \left(\frac{1.8544\ F}{d^2}\right) \qquad eq.III.2$$

Where, F is the applied load in kilogram force units (kgf), d is the arithmetic mean of the two diagonals, d1 and d2 in mm, HV is the Vickers hardness.

Fig. III.7 shows the print of Vickers indentation of both cross and longitudinal sections for 2304 P and CD duplex stainless steels. Higher values of diagonals d1 and d2 were measured in the case of parent stainless steels due to its lower hardness.

2304	Cross section	Longitudinal section
Parent	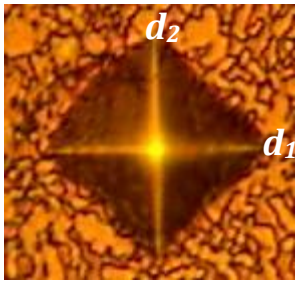 d_1 = 25.1 µm, L_2 = 25.6 µm	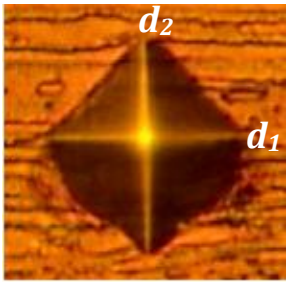 d_1 = 23.5 µm, L_2 = 24.7 µm
Cold drawn	 d_1 = 21.5 µm, d_2 = 21.0 µm	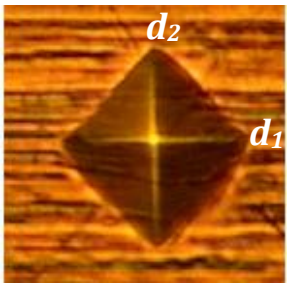 d_1 = 22.3 µm, d_2 = 22.5 µm

Fig. III.7. Vickers indentation of cross and longitudinal sections of P and CD 2304 stainless steels.

Table III.4 depicts the arithmetic mean values of Vickers hardness of 12 tests of each sample for 2304 and 2205 cold drawn and parent duplex stainless steels.

A significant effect on the Vickers hardness can be attributed to the cold drawn process, as can be deduced from table III.4: while cold drawn duplex stainless steels shows a Vickers hardness higher than 450, the parent stainless steels presents a Vickers hardness lower than 350. However, no significant differences on Vickers hardness can be distinguished due to the different composition of 2304 and 2205 stainless steels. In addition, the hardness in longitudinal section is generally slightly lower than in the cross-section especially in CD-DSS.

Table III.4. Vickers Hardness values of cross and longitudinal sections of the tested stainless steels.

DSS	Treatment	Sample type	HV (kgf/mm^2)	Stand. Dev.	Co-eff. of variation
2304	**Parent**	Cross-section	289	5.3	1.8
		Longitudinal-section	304	9.5	3.1
2205	**Parent**	Cross-section	347	9.1	2.2
		Longitudinal-section	331	11.4	3.4
2304	**Cold drawn**	Cross-section	523	5.0	1.0
		Longitudinal-section	462	4.2	0.9
2205	**Cold drawn**	Cross-section	523	4.0	0.8
		Longitudinal-section	478	6.2	1.3

III.2. Electrochemical cell

The passivation and corrosion behaviour of 2304 and 2205 duplex stainless steels were analysed by studying the electrochemical response of the passive film formed due to the alkaline nature of the electrolyte. The electrochemical response of the stainless steel wires was studied in an electrochemical cell in which the stainless steels were used as working electrodes. Different designs for the electrochemical cells were employed depending on the specific experimental conditions of each electrochemical test.

III.2.1. Electrochemical cell type I

The electrochemical cell type I was used to study both the passivation and the corrosion behaviour of the 2304 and 2205 parent and cold drawn DSS when exposed to alkaline media of different pH without and with different concentrations of chloride ions.

A three-electrode cell arrangement was employed, as can be observed in Fig. III.8:

a) *Working electrode:* the tested stainless steel.
b) *Counter electrode:* a graphite rod of 5 mm in diameter and 6 cm in length.
c) *Reference electrode*: the s*tandard calomel electrode* (SCE).

A polyethylene cell container suitable for high alkaline electrolytes was used. In addition, two working electrodes per cell were tested to guarantee the testing repeatability. The average values of the measurements were recorded to decrease the error ratio.

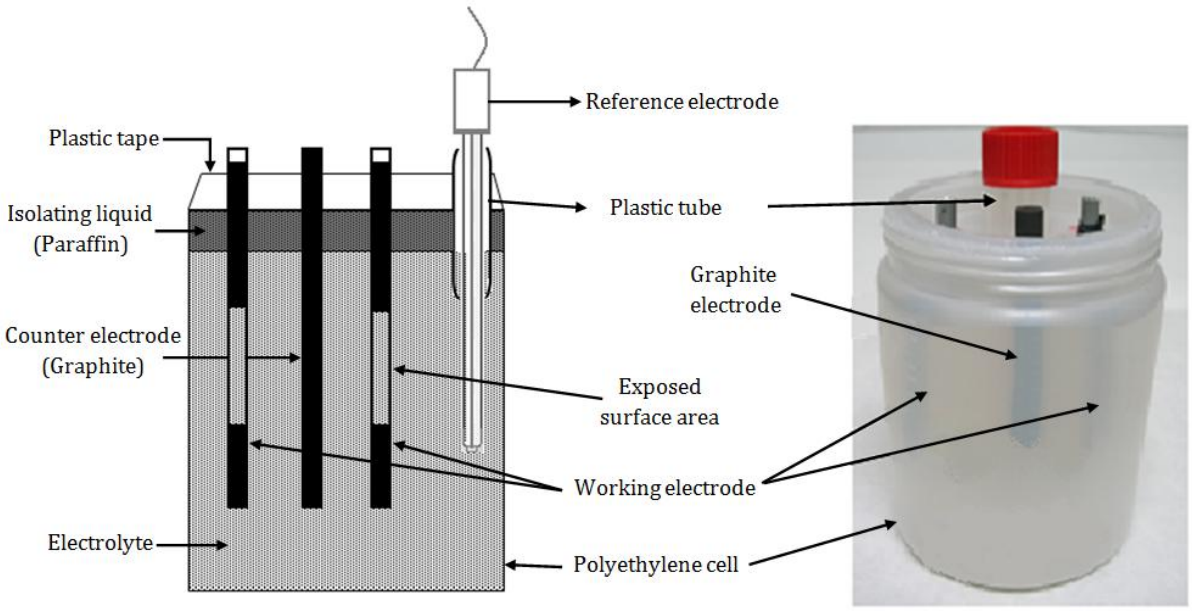

Fig.III.8. Electrochemical cell type I.

III.2.1.1. ***Working electrode preparation***

In the case of the electrochemical cell type I, rebars of 6 cm length were prepared from as received stainless steels wires to be used as working electrodes, as depicted in Fig.III.9.

The specimens were cut, then rinsed ultrasonically with acetone and washed with distilled water to remove any precipitated residue from the fabrication process that may affects the electrochemical measurements. The length of the exposed rebar was delimited to a 1 cm with electrical insulating tape. In table III.5 the exposed area of the prepared electrodes is shown.

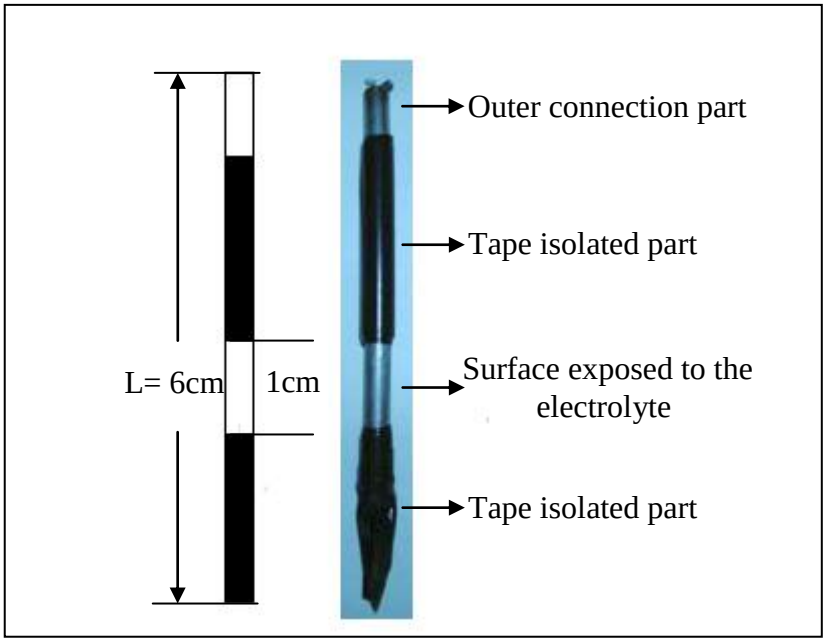

Fig.III.9. Scheme and photograph shape of the as-received DSS working electrodes preparation for the electrochemical cell type I.

Table III.5. Exposed areas of the stainless steels.

Steel name	Parent		Cold drawn	
	2304	2205	2304	2205
Exposed surface area / cm^2	2.74	2.74	1.30	1.25

III.2.1.2. ***Electrolytes***

a) Passivation in alkaline media

Alkaline electrolytes were prepared to simulate the aqueous phase of the concrete pores, considering that the pH of the concrete pore solution normally ranged from 12.5 to 13.5.

Solutions of calcium hydroxide with different concentrations of alkalis were prepared to simulate the aqueous phase of the concrete pore:

a) Sat. $Ca(OH)_2$ +0.5 M KOH with characteristic pH 13.5 at 25 °C.

b) Sat. $Ca(OH)_2$ with characteristic pH 12.5 at 25 °C.

Decarbonated distilled water was used as solvent to prepare the test solutions. The decarbonation of the distilled water was achieved by boiling the distilled water for 20 min. Then, it was kept in a reservoir for spontaneous cooling in absence of air to prevent the carbonation by the atmospheric carbon dioxide.

b) Corrosion behaviour in chloride containing electrolytes

Different concentrations of chloride in form of sodium chloride were added to the up mentioned alkaline solutions of pH 12.5 and 13.5 to study the pitting corrosion behaviour of the DSS. The added NaCl concentrations were determined depending on the test target, as resumed in table III.6.

Table III.6. Added chloride concentrations.

Electrochemical test	Electrolyte	$[Cl^-]$ / M
Spontaneous depassivation		
• 2304	Sat. $Ca(OH)_2$	0, 0.5, 0.75, 1.0, 2.0
Accelerated depassivation		
a. Potentiodynamic		
• 2304	Sat. $Ca(OH)_2$	0, 0.05, 0.1, 0.2, 0.3, 0.5, 0.75, 1, 1.5, 2.0
	Sat. $Ca(OH)_2$+ 0.5M KOH	0,1.0, 1.75, 2.0, 2.2, 2.5, 3.0
• 2205	Sat. $Ca(OH)_2$	0, 0.5, 1.0, 1.5, 2.0, 3.0, 3.5, 5.0, 5.5
	Sat. $Ca(OH)_2$+ 0.5M KOH	0, 0.5, 1.0, 1.5, 2.0, 3.0, 3.5, 5.0, 5.5
b. Potentiostatic		
• 2304	Sat. $Ca(OH)_2$	From 0 to 1 – 0.25M/24 h
• 2205	Sat. $Ca(OH)_2$	From 0 to 6 – 0.25M/24 h

During the experimental time, the temperature was kept constant by using circulating water bath, as represented in Fig.III.10.

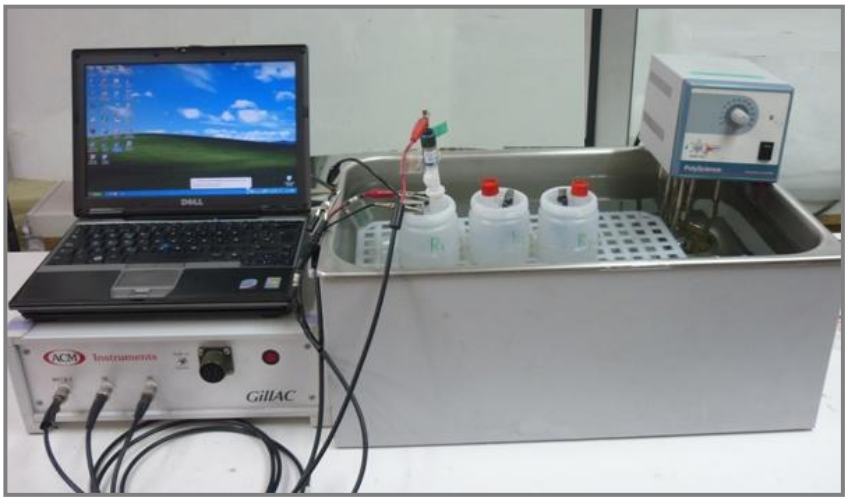

Fig.III.10. Experimental arrangement of electrochemical cell type I with control of temperature.

III.2.2. Electrochemical cell type II

The electrochemical cell type II was employed to evaluate the pitting corrosion behaviour of 2304 and 2205 DSS when exposed to higher temperature conditions (above 25 °C).

Two different studies were carried out with this electrochemical cell:

a) Determination of the critical pitting temperature (CPT) of the stainless steels in alkaline electrolytes with different chloride concentrations.
b) Analysis of the stainless steel corrosion propagation in critical aggressive conditions: high temperature and high chloride content.

The electrochemical cell type II arrangement is similar to the electrochemical cell type I, with the same preparation procedure of the working electrode. However, in the case

of cell type II, the reference electrode is isolated from the electrolyte by using a Luggin capillary at room temperature to assure no effect of the employed high temperatures on the stability of the reference electrode. In addition, a graphite sheet surrounding the working electrode was used as counter electrode. The scheme of the electrochemical cell type II with three electrode arrangement is included in Fig.III.11 where the main components of the electrochemical cell are detailed.

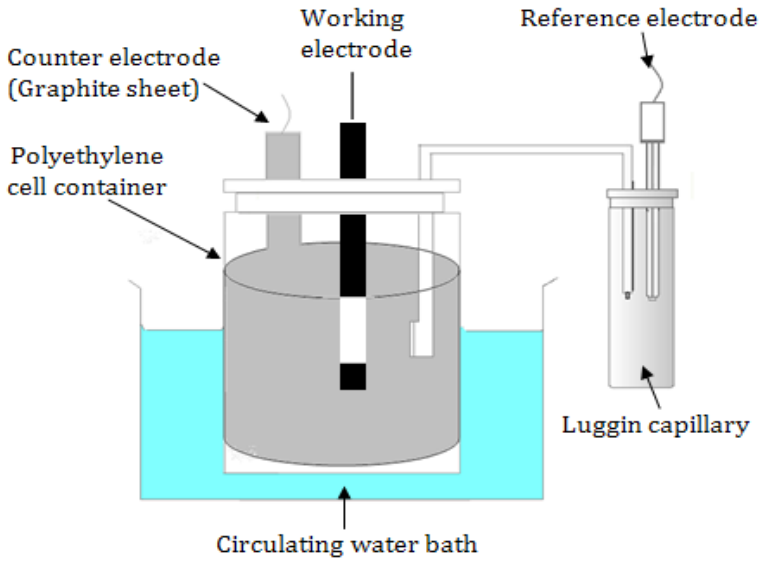

Fig.III.11. Scheme of the electrochemical cell type II.

III.2.2.1. ***Electrolytes***

Two different alkaline solutions with two different concentrations of chloride (1 M and 2 M) were employed in this study:

a) Saturated $Ca(OH)_2$ + NaCl.

b) Saturated $Ca(OH)_2$ + 0.5 M KOH + NaCl.

To determine the influence of the temperature in the pitting corrosion initiation and propagation of both 2304 and 2205 DSS, potentiodynamic measurements at different temperatures were carried out: 25, 30, 40, 50, 60, and 70 °C. The temperature of the electrolyte was increased with a constant rate of 0.5 degree/min, starting from the room temperature until reaching the required temperature, and then it was maintained constant in each case during the whole potentiodynamic measurement by the immersion of the electrochemical cell in a thermostatic circulating water bath (Fig.III.11).

The effect of the temperature increase on the pH of both saturated $Ca(OH)_2$ and saturated $Ca(OH)_2$-0.5M KOH alkaline solutions, with and without chlorides, was monitored by measuring periodically the pH at different temperatures, from room temperature until 100 °C.

III.2.3. Electrochemical cell type III

Stainless steels embedded in prestressed concrete structures are exposed to an external load that can affect the corrosion response of these stainless steels in presence of aggressive environments.

The electrochemical cell type III was used to evaluate the electrochemical response of HSSS subjected to a constant load of 70% of the stainless steel maximum tensile strength as expected in service conditions for prestressed concrete structures.

A methacrylate cell with a 15 cm in diameter and 10 cm in length was employed to perform the electrochemical tests under a constant load. Fig.III.13 shows the schematic

picture of this electrochemical cell. The cell consists in a double hollow cylinder where the internal cylinder is the electrochemical cell and the external cylinder allows controlling the temperature by water circulation, as shown in Fig.III.12.

The main components of the electrochemical cell type III are:

a) *Working electrode:* specimens of 35 cm length of 2304 and 2205 DSS. A length of 5 cm of the working electrode was exposed to the test solution, and 15 cm of each cell side were left free for coupling with tensile testing machine employed for the application of the required load.
b) *Counter electrode:* stainless steel mesh surrounding the working electrode.
c) *Reference electrode*: *standard calomel electrode* (SCE).

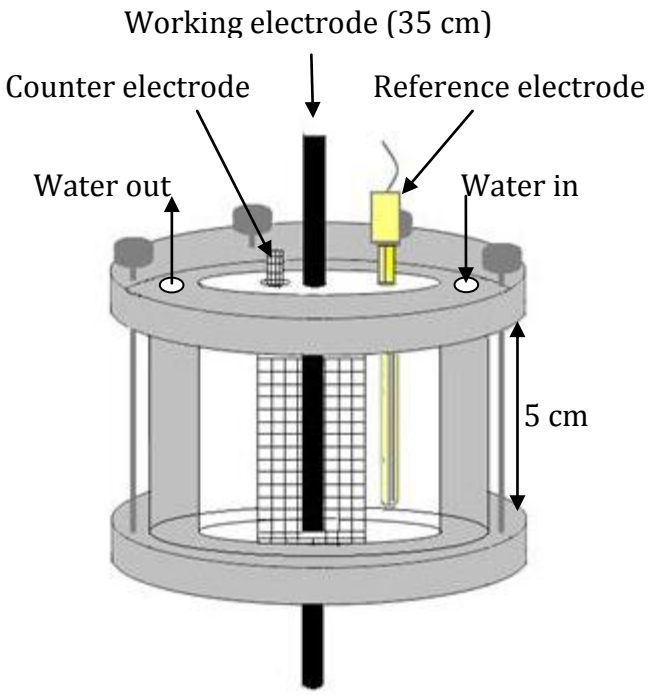

Fig.III.12. Scheme of the electrochemical cell type III.

Fig. III.13 shows the coupling of the electrochemical cell type III with the tension machine. The working electrode was stressed up to 70% of its maximum tensile strength to simulate the prestressed steels embedded in concrete.

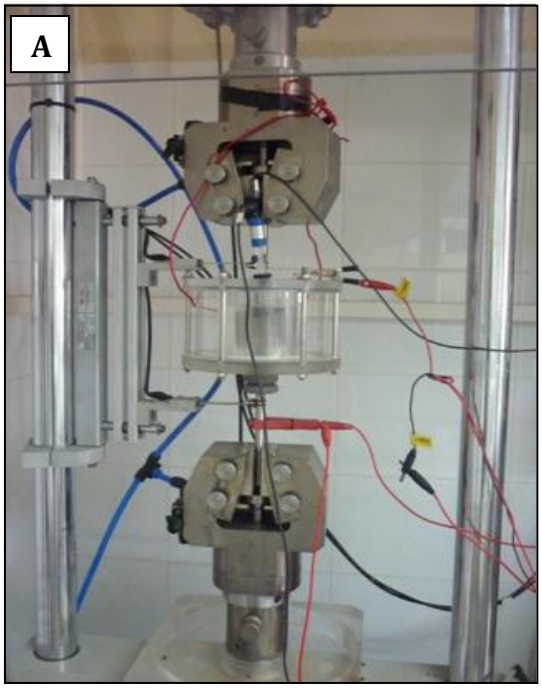

Fig. III.13 Photograph of tension machine used for the application of the external load.

The load was not suddenly applied but gradually increased at certain rate to reach the required load in 10 min. The applied rates are listed in table III.7.

Table III.7. The 70% maximum tensile strength of 2304 and 2205 SS and the applied velocity to reach the 70% maximum tensile strength of each SS in 10 min.

Stainless steel	70% Max. Stress / kN	Velocity / (N/s)
2304		
• Cold drawn	15.05	25.08
• Parent	7.69	12.81
2205		
• Cold drawn	14.48	24.12
• Parent	8.67	14.45

III.2.4. Electrochemical cell type IV

The electrochemical cell type IV was used the electrochemical behaviour of the tested DSS in mortar and to determine their critical chloride threshold.

Different mortar samples were used depending on the testing conditions as two different experimental arrangements were used for the potentiostatic tests.

III.2.4.1. Penetration of chloride from the external environment in chloride-free mortar

The scheme of the electrochemical cell has been represented in Fig.III.14. In this case the arrangement of the electrochemical cell type IV (Fig.III.14) was:

a) *Working electrodes*: cylindrical samples of mortar with embedded stainless steels. The procedure of working electrode preparation is detailed below.
b) *Counter electrode*: a stainless steel mesh lined in all internal sides of the cell container.

c) *Reference electrode*: Ag/AgCl in saturated KCl solution.

d) *Electrolyte*: aqueous solution of 1M NaCl. Chloride ion will penetrate through the mortar pores until the rebar surface promoting the pitting of the working electrode when the critical chloride concentration is reached.

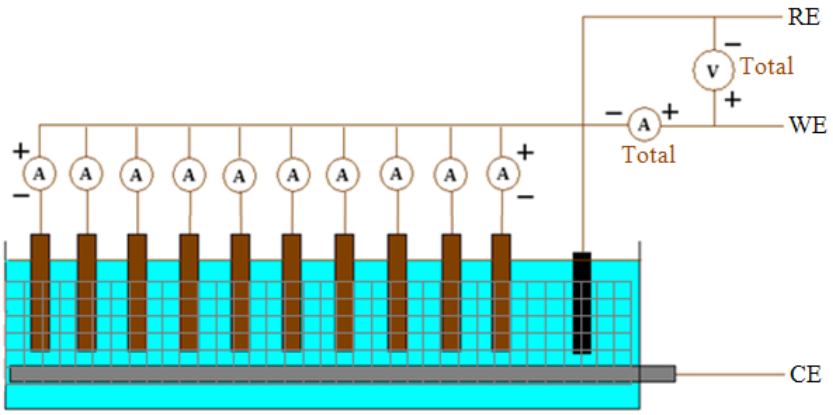

Fig.III.14 Scheme of the electrochemical cell type IV used for the potentiostatic determination of the critical chloride threshold in chloride free mortar.

III.2.4.1.1. Preparation of working electrodes

Fig.III.15 depicts the schematic shape of the mortar cylindrical samples with the embedded stainless steel wires (parent 2304 DSS and cold drawn 2304 and 2205 DSS). The embedded stainless steels length was 8 cm, with 3 cm exposed to the mortar and 1 cm left in the external part of the sample for the outer connection, and the other 4 cm were isolated with insulating tape as detailed in Fig.III.15. The mortar samples were casted using a cylindrical mould of plastic. The procedure is resumed in Fig.III.16.

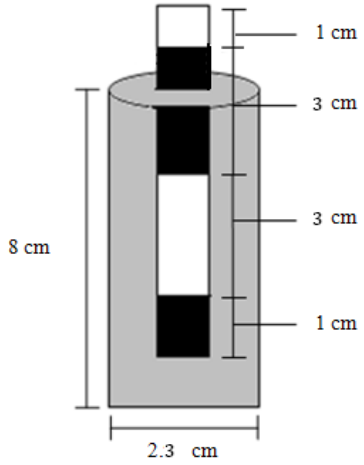

Fig.III.15 Mortar cylindrical samples of 8 cm length and 2.3 cm in diameter.

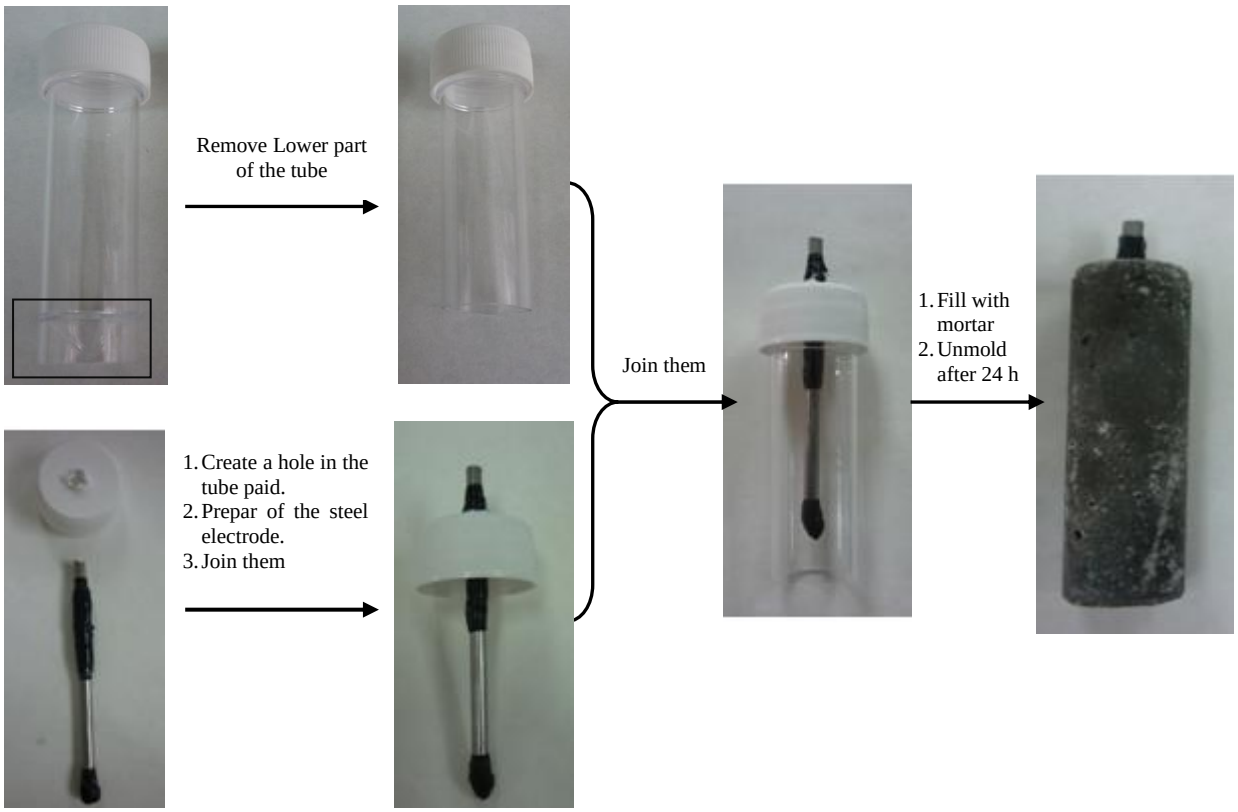

Fig.III.16 Preparation of the mortar cylindrical samples.

The mortar was prepared by using Ordinary Portland Cement, OPC, with low alkalis and aluminates content. The chemical composition of the employed OPC is presented in

table III.8. Standard sand, (CEN UNE-EN 196-1:1196), grading from 0 to 2 mm has been used for the preparation of the mortar samples. Cement:sand ratio equal to 1:3 and water/cement ratio of 0.5 were used. The mortar samples were unmolded after 24 hours, and then they were kept in a climatic chamber with 95% R.H. at 23 °C for 15 days.

Table III.8 Chemical composition (wt %) of OPC.

	SiO_2	Fe_2O_3	Al_2O_3	CaO_T	MgO	SO_3	Na_2O	K_2O	CaO_F
OPC	18.0	4.85	5.26	62.4	1.84	3.28	0.18	0.35	1.92

T = Total, F = Free.

III.2.4.2. Chloride addition to the mortar mix (mixed-in chloride mortar)

Mortar samples were made with the same OPC and standard sand. Different concentrations of chloride (0, 2, 3 and 4 % Cl- with respect to cement weight) were added to evaluate the corrosion behaviour of 2304 DSS when embedded in mortar in presence of chloride. Cylindrical mortar samples with 6 rebars (3 cold drawn+ 3 parent SS) were prepared. The counter electrode was an embedded Ti-mesh and the reference electrode was an activated Ti electrode vertically embedded in the center of the sample as can be observed from Fig. III.17.

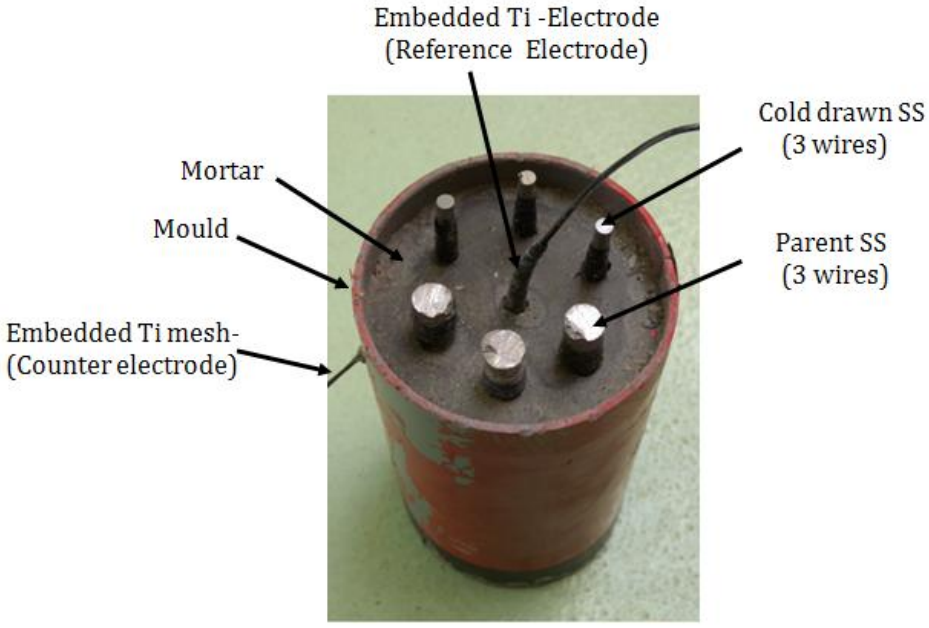

Fig. III.17 Multispecimen mixed-in chloride samples.

The potential of the embedded Ti- electrode used as a reference electrode was calibrated during the electrochemical test by using an external Ag/AgCl reference electrode.

In these samples, as-received 10 cm SS wires were embedded in the multi-specimen samples of 7 cm diameter. A mortar cover of 1 cm thickness from the sample surface to each embedded steels was maintained. The exposed areas of SS were delimited by using electric tape: 7.5 and 16.4 cm^2 for cold drawn and parent 2304 SS respectively.

After casting, the samples were exposed to 95-98 % R.H. at 23 °C for 19 days in a climatic room. Then, they were exposed to drier conditions of 80% R.H. at 23 °C for another

9 days. Finally, the samples were immersed in solutions of saturated $Ca(OH)_2$ solutions to perform the electrochemical tests.

III.2.4.3. Chloride analysis in mortar

The chloride concentrations have been analyzed in powdered mortar samples collected at the level of the rebar surface, 2 mm length from the wire bed.

The analysis of acid-soluble chloride (total chloride value) was performed by potentiometric titration [146-147], which involves (1) extraction of the chloride ions by digestion of a weighed portion of powdered mortar (2-5 g) in a boiling nitric acid solution (1:1) and separation of the resulting acid digest from the solid residue by filtration, followed by (2) titration of the extracted chloride ions dissolved in the filtrate with a standardized silver nitrate solution. As the standard silver nitrate solution is being added incrementally, the chloride ions are precipitated as silver chloride.

To summarize, the experimental conditions of the electrochemical cells used in the present study are scheme in Scheme III.1.

Scheme III.1 Experimental conditions of the electrochemical cells testing.

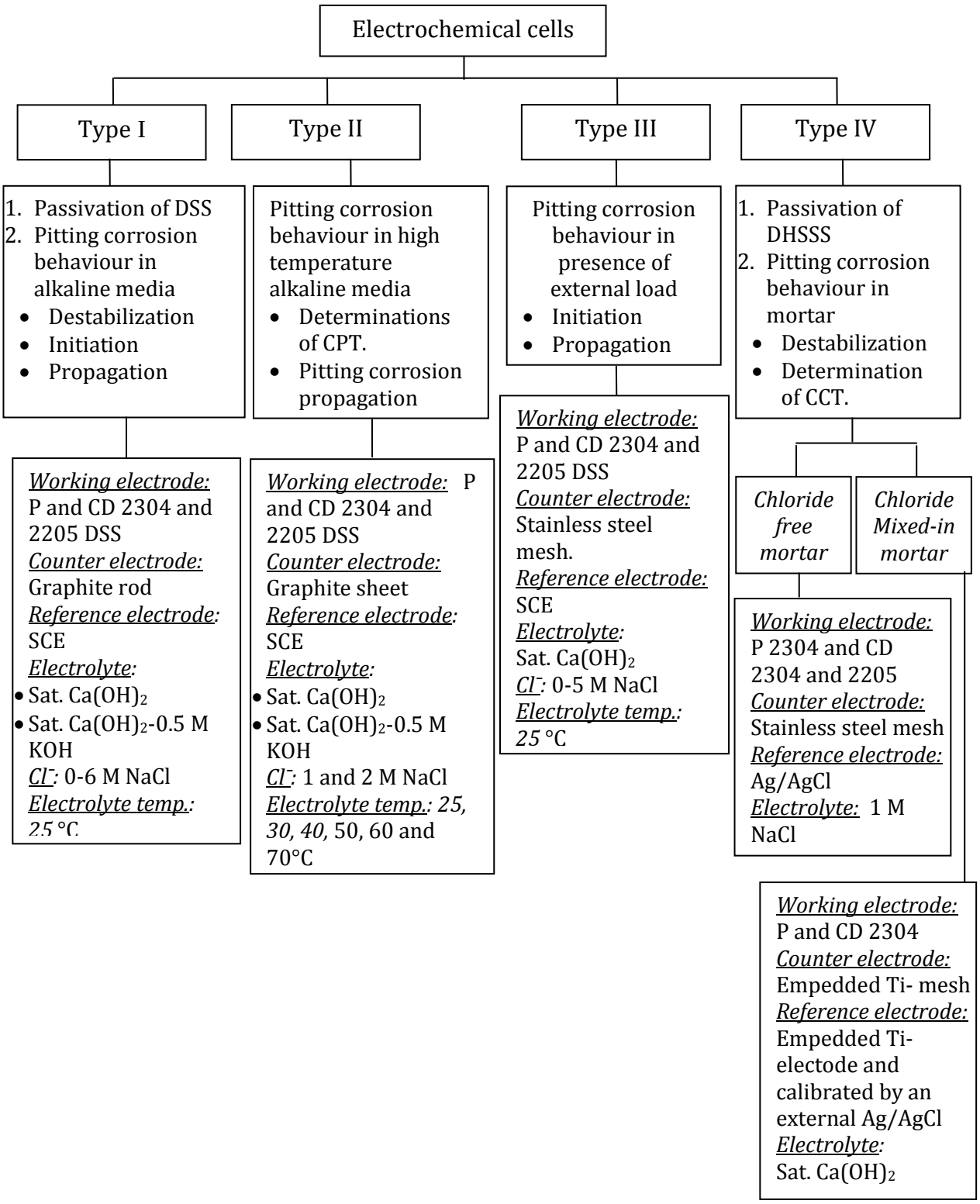

III.3. Electrochemical techniques

III.3.1. Cyclic voltammetry (CV)

Cyclic Voltammetry (CV) is the most widely used technique for acquiring qualitative information about the redox processes occurring in the stainless steel passive film [47-48, 148-151]. It is considered a destructive technique because of the high perturbation from the electrochemical equilibrium.

III.3.1.1. Experimental conditions for cyclic voltammetry (CV) application

An ACM GillAC 1199 potentiostat was used to perform the cyclic voltammetry measurements. The experimental conditions for CV measurements were established in function of the different objectives defined:

1. Passivation in alkaline media

CV measurements were carried out to identify the main redox processes involved in the passivation mechanism of 2304 and 2205 DSS. The effect of critical parameters such as the pH of the alkaline solutions and the influence of the cold drawn process on the electrochemical response of SS was analyzed by this electrochemical technique. In this case, CV measurements were carried out in the electrochemical cell type I, using a scan rate of 1 mVs^{-1} in the potential range from -1.4 to +0.7 V vs. SCE. The measurements were started in the most cathodic potential up to the most anodic one at which a reverse scan was performed to complete one cyclic potential scan.

The stability of the oxides forming the passive layer was evaluated by CV measurements in two different ways:

a) Potentiodynamic growth of the passive films by cycling 6 times in solutions of pH 12.5 and 13.5. The potential was scanned from -1.4 to +0.7 V vs. SCE. The scan rate was 1 mVs^{-1}.

b) Analysis of the effect of the ageing on passive film of 2304 DSS in an alkaline solution of pH 12.5 (Sat. $Ca(OH)_2$). The CV measurements were performed after different exposure times: 0, 7, 15, and 416 days. The scanned potential range was delimited in the range between -1.2 to +0.9 V vs. SCE, with a scanning rate of 1 mVs^{-1}.

2. Analysis of the corrosion behaviour in alkaline solutions with Cl^-

CV measurements were also carried out in aggressive media containing different concentrations of chloride. The electrochemical cell type I was used for studies at room temperature (25 °C), the electrochemical cell type II was used to study the corrosion behaviour of 2304 and 2205 DSS at high temperature and the electrochemical cell type III was employed for the potentiodynamic evaluation of the corrosion resistance of duplex SS with application of an external load (70% of the SS maximum strength). The experimental conditions for the CV measurements in the different electrochemical cells are detailed below:

a) *Electrochemical cell type I:* the progressive alteration of the redox processes in the passive film in presence of chloride, the pitting initiation and the pit propagation have been evaluated by application of potentiodynamic polarization curves at 25 °C. The potential range scanned was from -1.2 to +0.9 V vs. SCE and the scanning rate was 1 mVs^{-1}. Different concentrations of chloride were added to the alkaline solution for each SS type, as listed in table III.6.

b) *Electrochemical cell type II:* the critical pitting temperature of the 2304 and 2205 cold drawn and parent DSS was determined in solutions of sat. $Ca(OH)_2$ and solutions of sat. $Ca(OH)_2$ + 0.5M KOH with 1 and 2 M NaCl at high temperatures (30, 40, 50, 60 and 70 °C). The potential range considered was from -1.2 to +0.9 V vs. SCE, with a constant scanning rate of 1 mVs^{-1}.

c) *Electrochemical cell type III:* the corrosion resistance of the cold drawn and parent stainless steels was studied in presence of an external load of 70% of the stainless steel maximum tensile strength. In the case of 2304 cold drawn and parent DSS, the concentrations of chloride added to the alkaline solution were 0.0, 0.1, 0.2, 0.3 M, while in case of 2205 the concentrations of chloride were 0.0, 5.0 M. CV measurements were also performed in a potential range from -1.2 to +0.9 V vs. SCE, with a scanning rate of 1 mVs^{-1}.

III.3.1.2. Analysis of CV measurements

1. Identification of pitting corrosion initiation

The potentiodynamic evaluation of the pitting corrosion susceptibility in aggressive alkaline solutions was considered in order to analyze the stainless steel corrosion resistance and to determine CCT and CPT.

Three characteristic potentials are observed in the cyclic voltammograms when pitting corrosion was observed on the steel surface:

- Pitting potential (E_{pit}): it is the potential limit above which pitting corrosion is initiated. Corresponds to the potential at which there is a sharp increase in the current density. Some authors considered 100 $\mu A/cm^2$ as the current density limit at which the E_{pit} value could be depicted [152-155], while others established that the E_{pit} value corresponds to 10 $\mu A/cm^2$ [156-157]. In present work, 10 $\mu A/cm^2$ was considered as the limit current density at which the E_{pit} occurred.
- Repassivation potential (E_{rep}): it is the potential limit below which the steel is considered to recover a passive state after the pitting initiation.
- Potential range between E_{pit} and E_{rep}: refers to the potential region at which the propagation of the initiated pits is possible.

2. Electrochemical charge (Q_{pit}) of pitting propagation

The effect of different parameters (like the stainless steels microstructure, alloying elements, pH and temperature) on the pitting corrosion propagation has been studied in highly aggressive alkaline environments with chloride concentrations above the CCT.

The pitting propagation was analyzed by calculating the electrochemical charge associated to the pitting corrosion peak observed in the cyclic voltammograms (Q_{pit}) [41]. As described in [41], the Q_{pit} was calculated by integrating the peak associated to the pitting corrosion process that occurs with the increase in the current density values due to the pit initiation and propagation in both the anodic and the cathodic scans until reaching the repassivation potential (E_{rep}). The integrated area depends on the pitting corrosion potential (E_{pit}):

- When the $E_{pit} > E_{O_2}$ (oxygen evolution potential), no pitting corrosion is detected in the anodic direction but high anodic current density values, related to the pit initiation, are measured during the reverse scan in the cathodic direction until the repassivation potential (E_{rep}). In this case, Q_{pit} is the area enclosed in the loop between the oxygen evolution potential and E_{rep} in the cathodic scan of the polarization curve, as shown in Fig. III.18.a

- When the $E_{pit} < E_{O_2}$, the pit initiation is detected in the anodic scan. In this case Q_{pit} is the sum of the charges registered in the anodic scan Q_1 and in the cathodic scan Q_2, as shown in Fig. III.18.b.

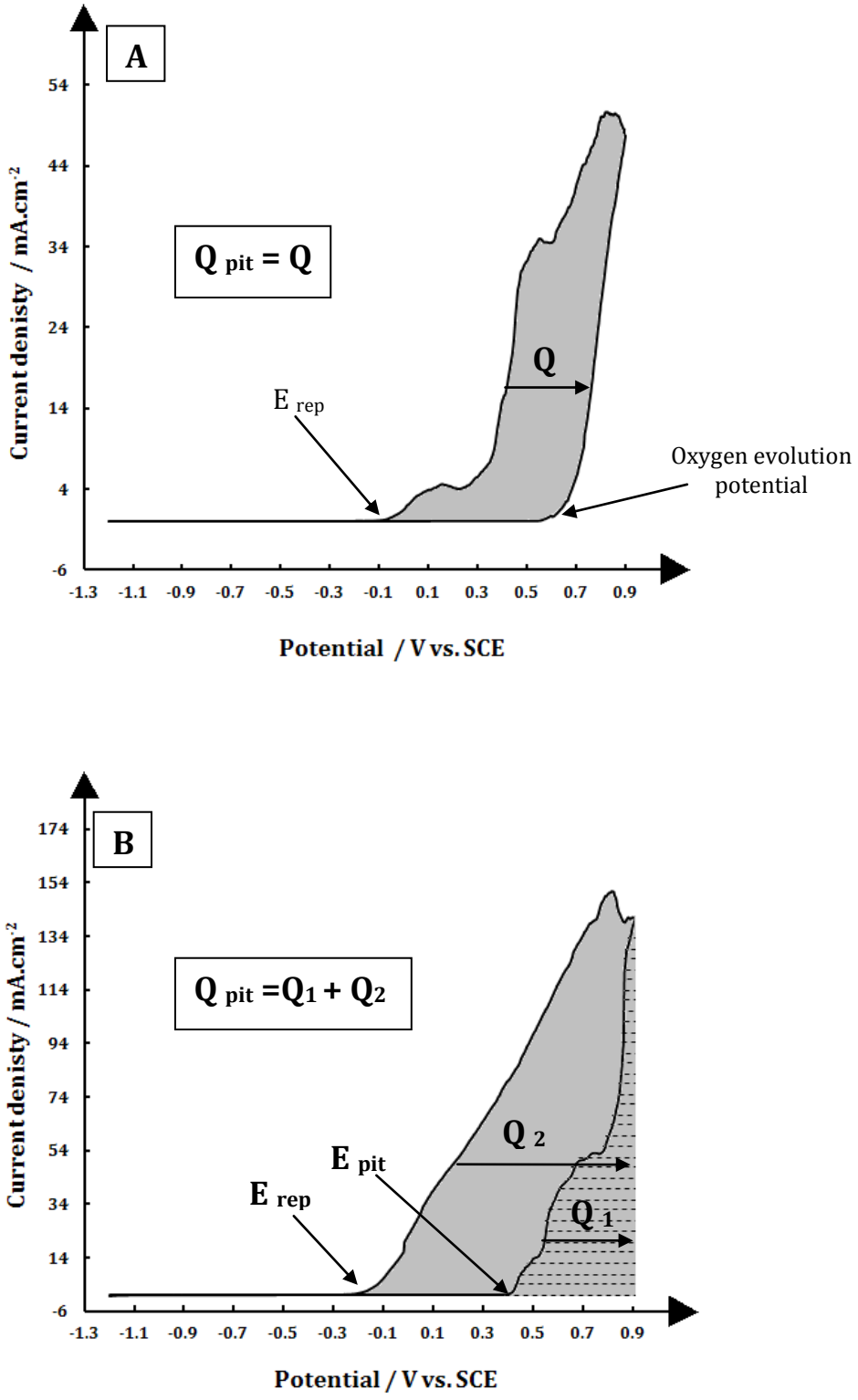

Fig.III.18 Schematic determination of the electrochemical charge (Q_{pit}) associated to pitting corrosion (A) when $E_{pit} > E_{O_2}$, and (B) when $E_{pit} < E_{O_2}$.

III.3.2. Potentiostatic tests

III.3.2.1. Electrochemical cell type I

The electrochemical cell type I was used in the chronoamperometry tests to evaluate the passive film growing at different potentials. The applied constant potentials were -0.3, +0.3, and +0.5 V vs. SCE. The current transient was reported during 60 minutes for both 2304 and 2205 cold drawn DSS immersed in solutions of saturated $Ca(OH)_2$ and saturated $Ca(OH)_2$ + 0.5 M KOH of pH 12.5 and 13.5 at 25 °C, respectively.

Furthermore, the potentiostatic determination of the CCT of 2304 and 2205 DSS was carried out in the electrochemical cell type I. In this case, the rebars were first immersed in the alkaline solutions to generate a passive film on the tested SS, and then Cl^- progressively added until detection of the concentration able to initiate corrosion. The procedure of the potentiostatic tests in electrochemical cell type I was the following:

1. Immersion of the wire in the alkaline solution and polarization at +0.25 V_{SCE} for 24 hours in order to promote the formation of the passive layer. The current of the system was recorded to identify the residual current during prepassivation period.
2. Addition of NaCl to the alkaline solution up to reach 0.5 M NaCl without switching-off the polarization of the wire. The current was recorded for further 24 hours for detection of a current increase due to the initiation of an active corrosion.
3. If no corrosion was identified, progressive 0.25 M NaCl were added to the solution every 24 hours until pitting corrosion was identified by the sudden increase in the current density.

III.3.2.2. Electrochemical cell type IV

a) Chloride-free mortar

Fig.III.19 depicts the parallel connections of the cylindrical mortar samples immersed in an aqueous solution of 1M NaCl. Two test series have been carried out to determine the CCT of DSS by chloride penetration potentiostatic test: The first tested series included six mortar samples of 2304 DSS (two parents and 4 cold drawn). The second series included 12 mortar samples of 2304 and 2205 cold drawn DSS (six for each case).

All tested stainless steels were potentiostatically kept at +0.25 V vs. SCE. The total current passing in the system was periodically measured. Moreover, the current of each stainless steel sample was also measured in order to follow up the changes with respect to the immersion time.

Before the application of the potentiostatic conditions, the initial corrosion potential (E_{corr}) and the polarization resistance (R_P) of all mortar samples were measured to guarantee the passivity of the HSSS before the potentiostatic test.

The pitting corrosion was detected by an increase in the total current. Then, the current of each mortar sample was measured in order to identify the corroding sample. The corroding sample was disconnected and the E_{corr} and R_P were measured after 5, 24, and 48 hours to confirm the depassivation of the DSS sample.

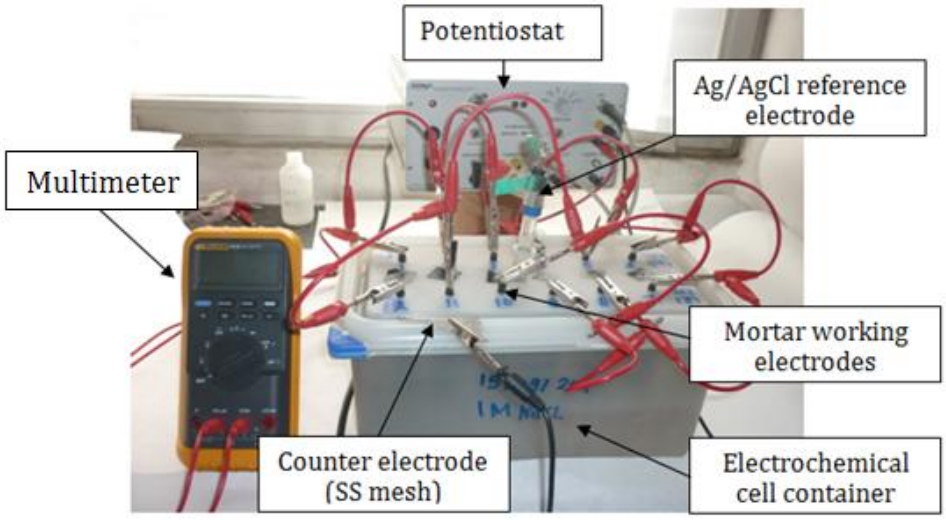

Fig.III.19 Potentiostatic test in the electrochemical cell type IV (free chloride mortar) of 2304 and 2205 cold drawn DSS with an applied potential of +0.25 V vs. SCE.

The corroding mortar samples were broken down to remove the embedded duplex stainless steel wires which were optically examined to localize the pit sites on the exposed surface.

a) Mortar mixed with chloride

After curing, the chloride mixed-in mortar samples were transferred into a container to be immersed in saturated $Ca(OH)_2$ solutions to perform the potentiostatic test, as shown in Fig.III.20, where the multi-specimen samples before (Fig.III.20.a) and after (Fig.III.20.b) immersion in test solution are observed.

Step potentiostatic tests were performed at different potentials until the detection of the corrosion initiation. The applied potentials were +0.25, +0.4 and +0.55 V_{SCE}. Each potential was maintained for 7 days and, if no corrosion was detected, the applied potential was moved to the next higher anodic potential value. As a result of the instability of the embedded Ti-reference electrode potential, the step potentiostatic tests were performed with respect to an external Ag/AgCl reference electrode immersed in the electrolyte, as shown in Fig.III.20.b.

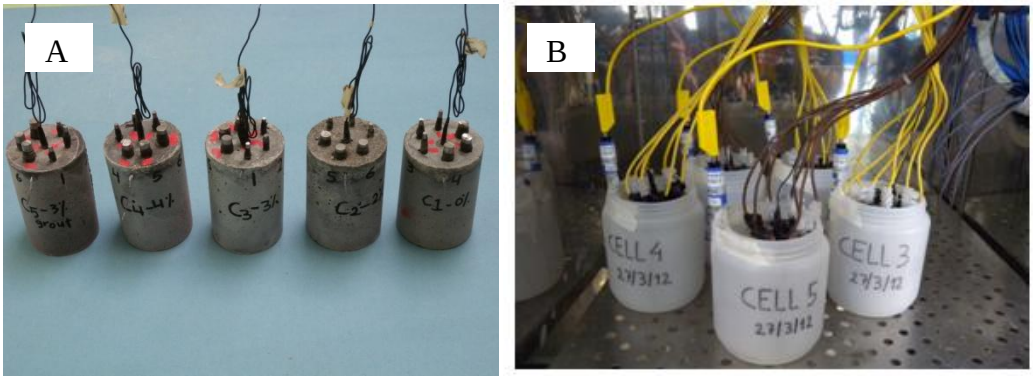

Fig.III.20 Multispecimen mixed-in chloride samples A) after casting and B) during the potentiostatic electrochemical test.

III.3.3. Corrosion potential (E_{corr}) and Polarization Resistance (R_p) monitoring

Both E_{corr} and R_p have been periodically measured to monitor the electrochemical response of the studied stainless steel wires.

The polarization resistance (R_p) was recorded by potentiodynamic measurements in a small potential range around the corrosion potential [158-160], from -20 mV to +20 mV

with respect to the corrosion potential where a linear relationship in E/i curve exists. The scan rate was 10 mV/min. The polarization resistance (R_p) is defined by the following equation III.3, where ΔE is the polarization from the corrosion potential and ΔI is the polarization current.

$$R_p = \frac{\Delta E}{\Delta I} \qquad \textit{eq. III.3}$$

This technique is non destructive because the perturbation applied around the corrosion potential does not cause a significant perturbation of the electrochemical equilibria of the system. This advantage permits the periodic measuring of the tested samples at different immersion times.

The main objective of the R_p measurements is to follow the change in the corrosion current density (i_{corr}) with time, which can be calculated by the Stern-Geary equation [161] (eq. III.4.):

$$i_{corr} = \frac{B}{R_p} \qquad \textit{eq. III.4}$$

Where, B is Stern-Geary constant which can be calculated from the Tafel slopes of the anodic and cathodic Tafel lines [162-164]. A value of B constant of 26 mV is usually used to calculate the corrosion current density (i_{corr}) of stainless steels [125-126]. Recio [41] has calculated the B-constant of austenitic 316 HSSS in alkaline media and has found a value of 31 mV of B-constant for this type of stainless steel in the studied conditions. As a result of the variation of B-constant with respect the type of stainless steel and the

exposure conditions, the experimental determination of B-constant of the tested DSS has been carried out in the present thesis and the obtained data are shown in appendix I.

In the present thesis, a mean value of 34 mV, calculated form the slopes of the Tafel lines (see appendix I), has been considered for the calculation of the corrosion current density (i_{corr}) for both DSS.

III.3.3.1. Evolution of E_{corr} and R_p in alkaline solutions using electrochemical cell type I

The electrochemical cell type I was used for the evaluation of the change in E_{corr} and R_p of duplex stainless steels by ageing in alkaline solutions in presence and in absence of chlorides:

a) Passivation of SS in alkaline solutions without chlorides

Short term evolution of E_{corr} and R_p of the tested duplex 2304 and 2205 SS during 20 days in alkaline solutions (saturated $Ca(OH)_2$ and saturated $Ca(OH)_2$ + 0.5 M KOH of pH 12.5 and 13.5 at 25 °C respectively).

b) Long-term evolution in chloride aggressive alkaline solutions:

E_{corr} and R_p of 2304 cold drawn and parent DSS were periodically measured during 416 days in saturated $Ca(OH)_2$ with 0.0, 0.5, 0.75, 1.0 and 2.0 M NaCl. Before the chloride addition, the tested SS were pre-passivated in chloride free alkaline solutions (sat. $Ca(OH)_2$) for 7 days.

III.3.3.2. Evolution of E_{corr} and R_p in chloride mixed-in mortar using electrochemical cell type IV

During the curing time of the reinforced mortar samples mixed-in with different chloride concentrations, E_{corr} and R_p of the embedded duplex stainless steels were monitored using the electrochemical cell type IV. The measurements of E_{corr} and R_p of the tested SS were performed in two different conditions:

a) Wet conditions: E_{corr} and R_p were measured during the first 19 days after casting. In this case, the prepared samples were kept in a climatic chamber with 95-98 % R.H. at 23 °C.
b) Drier conditions: the mortar samples were moved to a climatic chamber with 80 % R.H. at 23 °C for another 9 days. E_{corr} and R_p were also measured during this period.

III.3.4. Electrochemical impedance spectroscopy (EIS) monitoring

The evolution of the spontaneous passive film formed on the surface of the stainless steel in different simulating concrete pore solutions was also followed by using electrochemical impedance spectroscopy (EIS). This technique is a powerful method to study the electrochemical response of the redox processes involved in passivation/active corrosion mechanisms because it allows distinguishing between processes of different time constant within the same mechanism [165-169].

Electrochemical Impedance spectroscopy (EIS) is based on the perturbation of the electrochemical system with an alternating signal of small magnitude. EIS can only be

defined within Linear-Systems Theory (LST) which imposes four constrains to the system [165-166]:

1. The response of the system must be defined by linear equations.
2. The system must be stable, i.e., the system cannot evolve during the measurement.
3. The system must be casual.
4. Impedance values must be finite.

The compliance with these constrains can be readily tested via the Kramers-Kronig transforms [165-171].

EIS data are often interpreted in terms of electrical equivalent circuits composed only of passive elements (resistors, inductors and capacitors) [172]. Although in literature different models of equivalent electric circuits (EEC) have been proposed to interpret the impedance data of thin passive films formed on the stainless steel in alkaline media [33,151,173], in present work an equivalent electric circuit with two hierarchical parallel RC loops in series with the resistance of the electrolyte has given the best results. In Fig.III.21, the scheme of this 2RC EEC is shown and the physical meaning of the passive elements involved in the 2RC equivalent electric circuit is defined. The evolution of the parameters involved in the EEC was obtained by the fitting of experimental EIS data with a Simplex algorithm [174].

The impedance of this circuit, $Z(\omega)$, at the angular frequency ω is given by equation III.5 where RC reproduces the depressed semicircles found in the impedance complex plane plots and α_1 and α_2 model the Cole-Cole dispersion of time constants RC [52,58,150].

$$Z(\omega) = R_e + \frac{R_1}{\frac{1}{1+Z_2(\omega)/R_1} + j\omega(R_1C_1)^{\alpha_1}} \qquad \text{Being} \qquad Z_2(\omega) = \frac{R_2}{1+j\omega(R_2C_2)^{\alpha_2}} \qquad \textit{eq. III.5}$$

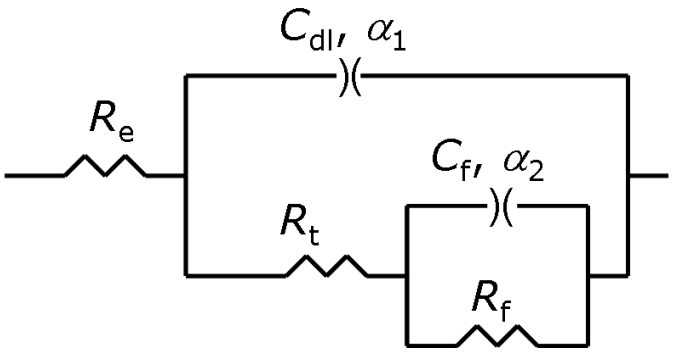

R_e: Electrolyte resistance

R_t: Charge transfer resistance

C_{dl}: Double layer capacitance

R_f: Faradic resistance of the redox processes occur in the oxide layer

C_f: Faradic pseudo-capacitance of the oxide layer

Fig.III.21 Electrochemical Equivalent Circuit (EEC) used to model the EIS data of the stainless steel passive film in alkaline media.

In present thesis an AUTOLAB PGSTAT 30 potentiostat with a frequency response analyzer (FRA) module was used for the periodic EIS measurements. The EIS data were recorded from 10 KHz down to 1 mHz (taking seven points per decade) with 10 mV rms signal amplitude. The EIS measurements were carried out to evaluate the passivation and depassivation behaviour of the analyzed stainless steels.

III.3.4.1 Passivation in alkaline solutions in electrochemical cell type I

The electrochemical cell type I has been used to perform the EIS measurements of duplex stainless steels in alkaline solutions of pH 12.5 and 13.5 without chlorides. Periodic EIS measurements were carried out during 15 days. The spectra were obtained at the open circuit potential (OCP).

III.3.4.2. Long-term evolution in chloride aggressive alkaline solutions

EIS spectra of parent and 2304 cold drawn DSS were monitored during 416 days of immersion in saturated $Ca(OH)_2$ with different NaCl concentrations (0.0, 0.5, 0.75, 1, and 2 M NaCl). The spectra were also monitored at the open circuit potential (OCP).

IV. Results

Passivation of duplex HSSS in high alkaline media

IV. Passivation of duplex stainless steels in high alkaline media

Passivation of duplex stainless steels (DSS) wires in synthetic high alkaline solutions, which simulate the aqueous phase of concrete pores, and in mortar have been investigated in the present chapter by studying the electrochemical response of the passive film formed on the DSS surface.

The effect of significant parameters controlling the passivation such as the exposure media (pH) and the type of DSS (SS alloy composition and microstructure) was analyzed in both accelerated and spontaneous passive films grown in high alkaline media.

Electrochemical techniques as cyclic voltammetry and chronoamperometry were employed to identify the redox processes occurring on the passive film and to evaluate the electrochemical response of the passive film grown under controlled conditions. Moreover, the spontaneous formation of the passive film was characterized by electrochemical impedance spectroscopy (EIS), corrosion current density (i_{corr}) and corrosion potential (E_{corr}) monitoring.

IV.1 Accelerated growth of the passive film on DSS

IV.1.1. Redox process involved in the passive film formation of DSS

Cyclic Voltammetry (CV) was used for acquisition of qualitative information about the redox processes occurring on the passive film formed on the DSS surface within the potential range considered. The tested DSS bars were submitted to 6 voltammetric cycles

to evaluate the stability of the oxides in the passive layer by analyzing the relaxation of the redox processes taking place.

IV.1.1.1. Influence of exposure media on the passive film formation on cold drawn DSS: effect of the pH

The composition of the electrolyte, and more specifically the pH, has a significant influence on the formation of the passive layer. Thus, the electrochemical response of the passive layer formed on 2304 cold drawn (CD) DSS has been evaluated in two different high alkaline solutions: 12.5 and 13.5.

Fig.IV.1 displays the cyclic voltammograms of 2304 CD-DSS exposed to saturated $Ca(OH)_2$ (pH 12.5) (Fig. IV.1.a) and to saturated $Ca(OH)_2$-0.5M KOH (pH 13.5 solution) (Fig. IV.1.b). To evaluate the stability of the oxides with the passive layer growth, 6 cycles have been performed in each case.

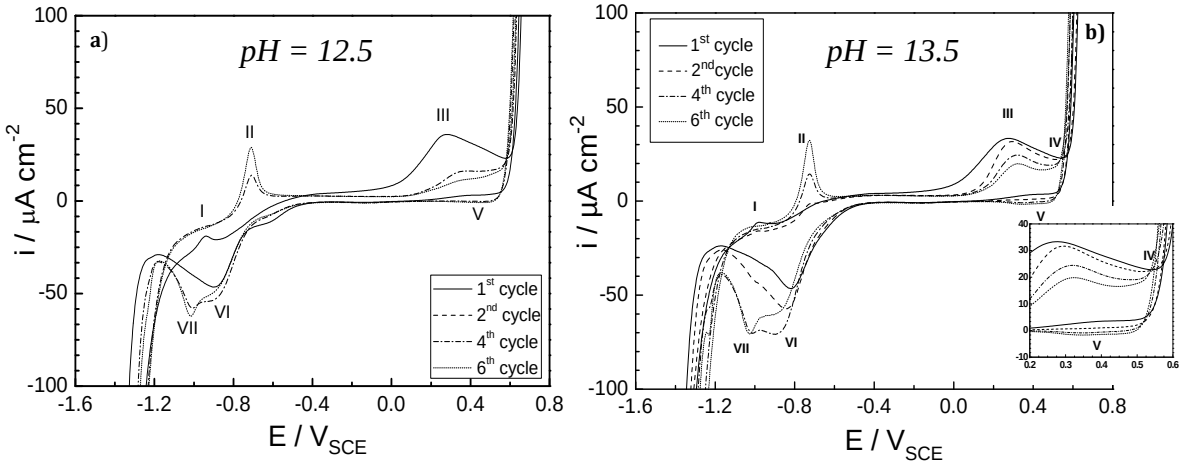

Fig. IV.1 Voltammograms for 2304 CD-DSS in a) saturated $Ca(OH)_2$ solution (pH 12.5) and b) saturated $Ca(OH)_2$ + 0.5M KOH Solution (pH 13.5).

Independently on the pH condition, three potential domains can be clearly distinguished:

a) Region of iron activity:

Two different peaks, generally assigned to iron redox processes [33,56,57,150,151,175] can be distinguished in the most cathodic region of potentials:

Peak I (E ≈ -1.1 V_{SCE}): is only observed in the first cycle and expected to be associated to the formation of Fe^{II}-oxides, as shown in equilibriums IV.1 [33,57-58]:

$$Fe + 4\ H_2O \leftrightarrow Fe(OH)_2 + 2H_3O^+ + 2\ e^- \qquad \textit{eq. IV.1}$$
$$Fe + 3\ H_2O \leftrightarrow FeO + 2H_3O^+ + 2\ e^-$$

This peak disappears after the first cycle and thus, it can be expected that Fe^0 is not anymore available on the surface to be oxidized in further cycles.

Peak II (E ≈ -0.75 V_{SCE}): corresponds to the formation of magnetite (Fe_3O_4) from the Fe^{II} oxidation, as shown in equilibriums IV.2 [151,175]:

$$3\ Fe(OH)_2 + 2OH^- \leftrightarrow Fe_3O_4 + 4\ H_2O + 2\ e^- \qquad \textit{eq. IV.2}$$
$$3\ FeO + 2OH^- \leftrightarrow Fe_3O_4 + H_2O + 2\ e^-$$

The parallel cathodic process of Fe_3O_4 [151,175] has been detailed as peak VII (E ≈ -1.2 V_{SCE}) in Fig IV.1.a and IV.1.b.

The increment of the current density of peak II observed with cycling indicates a possible enrichment in magnetite with the growing of the passive layer in agreement with the data observed by Abreu et al. [57].

Moreover, a slight shift in the *peak II* to more negative potentials is observed in more alkaline solutions, which indicates a possible increase in Fe^{II}-species in magnetite.

b) <u>Passivity region:</u>

This region is characterized by a low constant value of the current density along the whole potential interval. The formation of Fe^{III}-oxides is expected to occur in this region of potentials by the equilibriums detailed in IV.3:

$$Fe_3O_4 + OH^- + H_2O \leftrightarrow 3\ \alpha\text{-}FeO\ OH + 2e^- \qquad \textit{eq. IV.3}$$
$$2\ Fe_3O_4 + 2OH^- \leftrightarrow 3\ \gamma\text{-}Fe_2O_3 + e^-$$

The cathodic process of Fe^{III}-oxide reduction has been named as peak VI in Fig. IV.1.

The decrease observed in the current density values with the number of cycles indicates the enrichment of the passive layer in these more oxidized compounds that stabilize the passive layer due to their lesser reactivity. In table IV.1 the residual current density, i_{pass}, for the different cycles and pH conditions is resumed.

Table IV.1. Residual current density of passive region for 2304 CD-DSS in both conditions of pH (12.5 and 13.5).

	Exposure Media			
2304	**pH 12.5**		**pH 13.5**	
Cycles	**Residual current ($\mu A\ cm^{-2}$)**	**Passivity range (mV_{SCE})**	**Residual current ($\mu A\ cm^{-2}$)**	**Passivity range (mV_{SCE})**
1	7.2 ± 0.01	-610 to +11	7.5 ± 0.10	-621 to +43
2	2.8 ± 0.03	-624 to +193	3.0 ± 0.10	-625 to +109
3	2.6 ± 0.01	-602 to +209	2.9 ± 0.05	-635 to +121
4	2.6 ± 0.10	-624 to +149	3.0 ± 0.03	-621 to +127
5	2.6 ± 0.03	-560 to +219	3.0 ± 0.10	-611 to +138
6	2.7 ± 0.10	-520 to +230	3.1 ± 0.10	-611 to +145

After the first cycle, the passivity domain is extended to more anodic potentials and the residual current of passivity decreases, which reflects the formation of a more stable passive film on the stainless steel surface. Increasing the alkalinity of the exposure media promotes higher values of residual current and a decrease of the anodic limit of the passivity potential domain indicating the formation of a more conductive and less oxidized passive layer when the steel is exposed to the most alkaline solution (pH 13.5).

c) <u>Transpassivity region:</u>

An increase in the current density is observed in the transpassivity region. This region is related to the oxidation process of the alloying elements. Two main anodic peaks can be distinguished:

Peak III ($E \approx +0.3\ V_{SCE}$): assigned to the chromium oxidation process (Cr^{III}/Cr^{VI}) [46].

Peak IV (E > +0.5 V_{SCE}): the contribution of the redox process Ni^{II}/Ni^{III} can be expected at these anodic potentials. This peak seems to be strongly affected by the pH as only can be distinguished in the most alkaline condition (pH 13.5) (Fig.IV.1b).

To confirm the contribution of redox process Ni^{II}/Ni^{III} to *peak IV*, cyclic voltammograms of pure Ni electrode in the same alkaline environments were carried out. The results are shown in Fig.IV.2. The main features of the pure Ni cyclic voltammograms were the appearance of two Ni oxidation processes (Ni^0/Ni^{II} and Ni^{II}/Ni^{III}).

The Ni^{II}/Ni^{III} oxidation process (eq. IV.4) can be distinguished at +0.45 V_{SCE} in the anodic scan and the corresponding reduction peak at +0.29 V_{SCE}:

$$Ni(OH)_2 + OH^- \leftrightarrow NiOOH + H_2O + e^- \qquad \textit{eq. IV.4}$$

In high alkaline media, a clear increase in the current density corresponding to Ni^{II}/Ni^{III} oxidation process has become evident, as shown in Fig.IV.2.

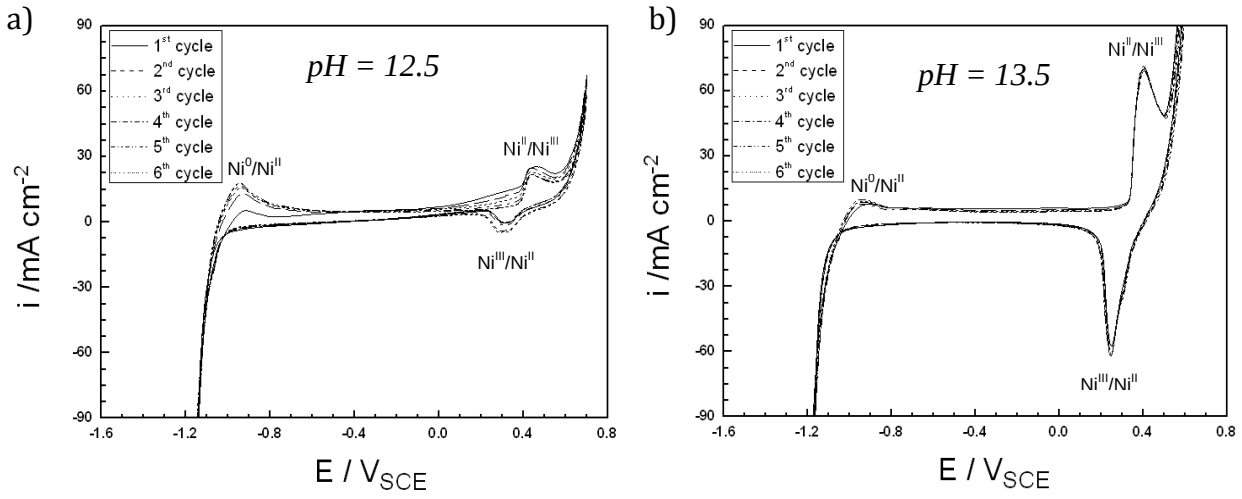

Fig. IV.2. CV of pure Ni electrode in solutions of (A) sat. $Ca(OH)_2$ of pH 12.5, and (B) sat. $Ca(OH)_2$+0.5M KOH of pH 13.5 at 25 °C.

Turning to Fig.IV.1, a sharp anodic current increase due to the oxygen evolution process is registered at +0.5 V_{SCE}. Several authors have suggested [33,46,51,52] that nickel present in the external part of the passive film exerts a catalytic effect on the oxygen evolution process promoting the shift of this process to less anodic potentials with the number of cycles.

Furthermore, the maximum current density of the transpassivity peak decreases with the number of cycles, which suggests a decrease in reactive Cr^{III}-species in the passive film as a consequence of the oxidation process of Cr^{III}-species to soluble Cr^{VI}-species. A decrease in Cr^{III}-content by XPS-analysis in a potentiodynamically generated passive film in alkaline media (pH 13) with the number of cycles has been also reported by Abreu et al [58].

Regarding the effect of the pH on the transpassivity peak (*peak III*), an intensification of the current density of this peak has been observed in more alkaline solutions of pH 13.5 (Fig.IV.1.b). Thus, an enhancement of the oxidation of Cr^{III}-species to soluble Cr^{VI}-species can be expected at this pH, and as a consequence, the passive film may become more depleted in Cr^{III}-species than the film formed in less alkaline solutions of pH 12.5 (Fig.IV.1.a).

IV.1.1.2. Influence of presence of Mo in the passive film formation on cold drawn DSS

The potentiodynamic growth of the passive film with 6 cycles of 2205 CD-DSS in alkaline solutions of pH 12.5 and 13.5 are included in Fig.IV.3a and Fig.IV.3b respectively.

The same regions of potential (iron activity, passivity and transpassivity) observed in case 2304 HSSS can be clearly distinguished in the cyclic voltammograms of 2205 CD-DSS.

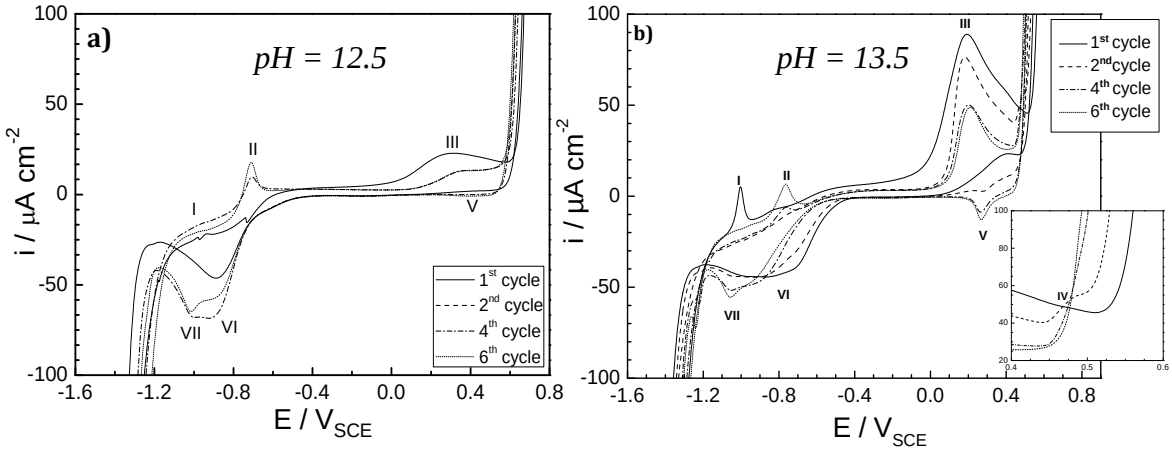

Fig. IV.3 Voltammograms with 6 cycles for 2205 CD-DSS in a) saturated $Ca(OH)_2$ solution (pH 12.5) and b) saturated $Ca(OH)_2$ + 0.5M KOH (pH 13.5).

In similar way to the data observed for 2304 CD-DSS, also the redox process taking place in the passive layer in the case of 2205 are highly affected by the pH. The current density of the *peak II* in iron activity region decreases with increasing the pH, indicating a depletion of magnetite in the passive layer formed in these conditions. The residual current density and the potential range of passive region for the different cycles and pH are listed in table IV.2. The residual current density of this region also decreases with increasing the number of cycles, and the passivity domain is extended to more anodic potentials, indicating the formation of an electrochemically more stable passive film. The pH also influences the passive region of 2205 CD-DSS (Fig.IV.3), as resumed in table IV.2: higher values of passive current density and less anodic potentials for the limit of this passive region are measured in the most alkaline pH.

In the transpassive region, a significant effect of the pH on the redox process occurring on 2205 CD-DSS surface has been distinguished by comparing Fig.IV.3a and Fig.IV.3b. Higher values of current density have been registered for the redox processes of the alloying elements taking place in this potential region when pH increases.

Table IV.2. Residual current density and range of potential in the passive region for 2205 CD-DSS in both conditions of pH (12.5 and 13.5).

	Exposure Media			
2205	**pH 12.5**		**pH 13.5**	
Cycles	**Residual current ($\mu A\ cm^{-2}$)**	**Passivity range (mV_{SCE})**	**Residual current ($\mu A\ cm^{-2}$)**	**Passivity range (mV_{SCE})**
1	4.2 ± 0.01	-540 to -57	5.5 ± 0.10	-635 to -118
2	3.3 ± 0.10	-550 to +149	3.5 ± 0.02	-630 to +19
3	2.9 ± 0.01	-630 to +152	2.1 ± 0.05	-633 to +24
4	2.9 ± 0.01	-630 to +149	2.9 ± 0.10	-631 to +4
5	2.8 ± 0.10	-650 to +157	2.6 ± 0.10	-630 to +58
6	2.7 ± 0.10	-650 to +157	3.2 ± 0.01	-639 to +69

Even though the same redox peaks can be distinguished in the cyclic voltammograms of 2304 (Fig.V.1) and 2205 (Fig.V.3) CD-DSS, significant differences occur in the current density and in the shape of these peaks when the CD-DSS are exposed to the most alkaline solutions (pH 13.5). A higher value of current density of *peak I* ($E \approx -1.1\ V_{SCE}$) and lesser current density of *peak II* ($E \approx -0.75\ V_{SCE}$) are registered in the region of iron activity domain for 2205 CD-DSS. Besides, in the transpassivity region, the current density of *peak III* ($E \approx +0.3\ V_{SCE}$) is increased in case of more alkaline solutions (pH=13.5) (Fig.IV.3.b) for 2205 CD-DSS.

The electrochemical charge associated to the oxidation peaks of magnetite formation (*peak II*) in iron activity region and chromate formation (*peak III*) in transpassive region has been estimated for both steels, 2304 and 2205, exposed to different alkaline conditions, pH 12.5 and 13.5. The results have been represented in Fig.IV.4.

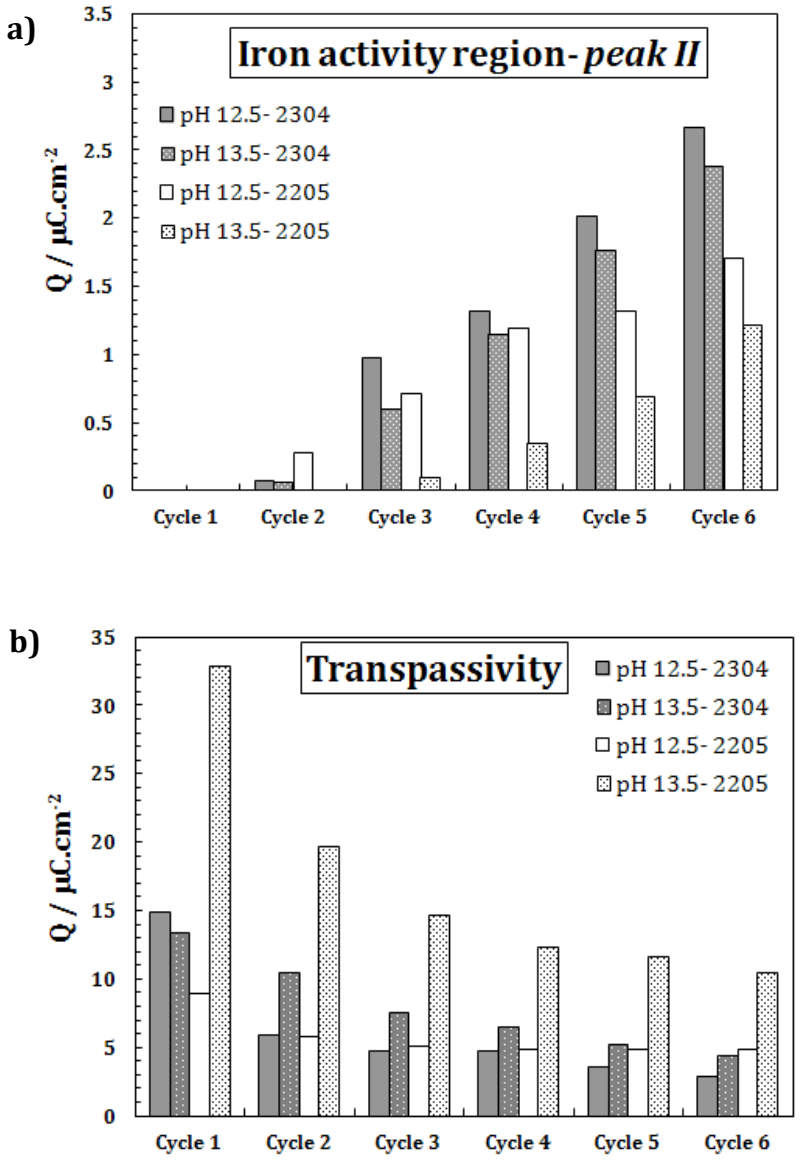

Fig. IV.4 Electrochemical charge (Q) of a) iron activity region (*Peak II*), and b) transpassivity peak of 2304 and 2205 CD-DSS obtained from voltammograms with 6 cycles in solutions of pH 12.5 and 13.5.

Concerning the effect of the number of cycles in the redox processes taking place in different potential regions, an increase of the electrochemical charge involved in the magnetite formation process (Fig. IV.4a) with the number of cycles is observed in all cases. On the other side, a clear decrease in the electrochemical charge involved in the transpassive region with cycling is detected, as shown in Fig.IV.4b. Consequently, the induced growing of the passive film on both 2304 and 2205 CD-DSS by cycling is probably accompanied by enrichment in magnetite and depletion in Cr^{III}-species in outermost of the passive film due to the progressive oxidation to soluble chromates and/or the formation of stable non-reactive Cr^{III}-oxides.

Fig.IV.4 also indicates that the variation in the electrochemical charge of both magnetite formation and transpassivity peaks depends on the pH of the surrounding media. Increasing the alkalinity induces the decrease of the electrochemical charge associated to magnetite formation (*Peak II*) and a high increment of the electrochemical charge of transpassive region. This behaviour is more evident in the case of 2205 CD-DSS than in the case of 2304 CD-DSS, as a significant enhancement of Cr^{III}/Cr^{VI} oxidation process can be observed.

As the main difference in the composition of both DSSs is the Mo-content, it can be expected that this alloying element plays an important role in the redox processes involved in the formation of the passive layer, mainly in the transpassive region, when the stainless steel is exposed to the most alkaline conditions. A synergic effect between the presence of Mo and the pH cannot be neglected.

To identify the main redox process of Mo in high alkaline media and to elucidate the influence of Mo on the electrochemical potentiodynamic response of the passive layer formed on the HSSS studied, cyclic voltammetric curves on a pure Mo electrode have been carried out in the same conditions, pH 12.5 and 13.5, as represented in Fig.IV.5 and Fig.IV.6 respectively.

The main oxidation peaks appeared in the Mo voltammograms correspond to the Mo^0/Mo^{III} (E = -1.1 V_{SCE}) and Mo^{III}/Mo^{VI} (extended from -0.4 to -0.5 V_{SCE}) process. The influence of the pH on the Mo redox process is evident. In most alkaline solutions (pH 13.5), a significant increase in the current density corresponding to Mo^{III}/Mo^{VI} peak has been measured.

Comparing the cyclic voltammograms of pure Mo electrode (Fig.IV.5 and Fig.IV.6) with the ones for 2205 CD-DSS (Fig.IV.3), the following observations can be elucidated:

- The oxidation peak appeared at more cathodic regions of (E ≈ -1.1 V_{SCE}) in the cyclic voltammograms of 2205 DSS can be also related to Mo^0/Mo^{III} oxidation process. However, this oxidative peak is clearly observed only in the most alkaline conditions (pH 13.5), as represented Fig. IV.3a. This interference of Mo oxidation process at E ≈ -1.1 V_{SCE} in the case of 2205 CD-DSS exposed to pH 13.5 is in agreement with Pourbaix diagram [174] which indicates that at this potential, the oxidation of Mo to Mo^{III}-oxides in alkaline media is more favourable than the iron Fe^0 to Fe^{II} oxidation because the iron is thermodynamically stable at this potential.

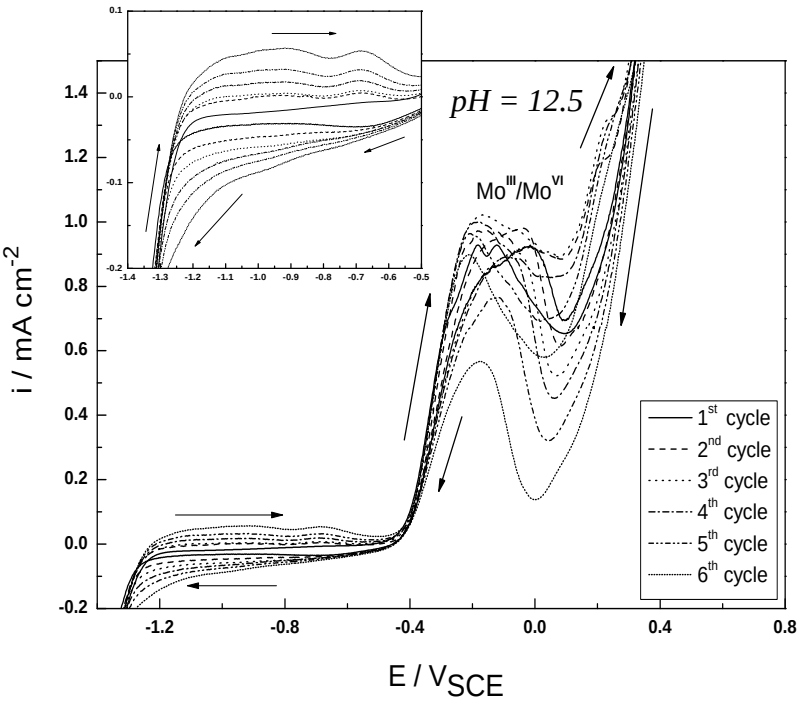

Fig. IV.5. Cyclic voltammograms of pure Mo electrode in saturated $Ca(OH)_2$ solutions (pH 12.5 at 25 °C).

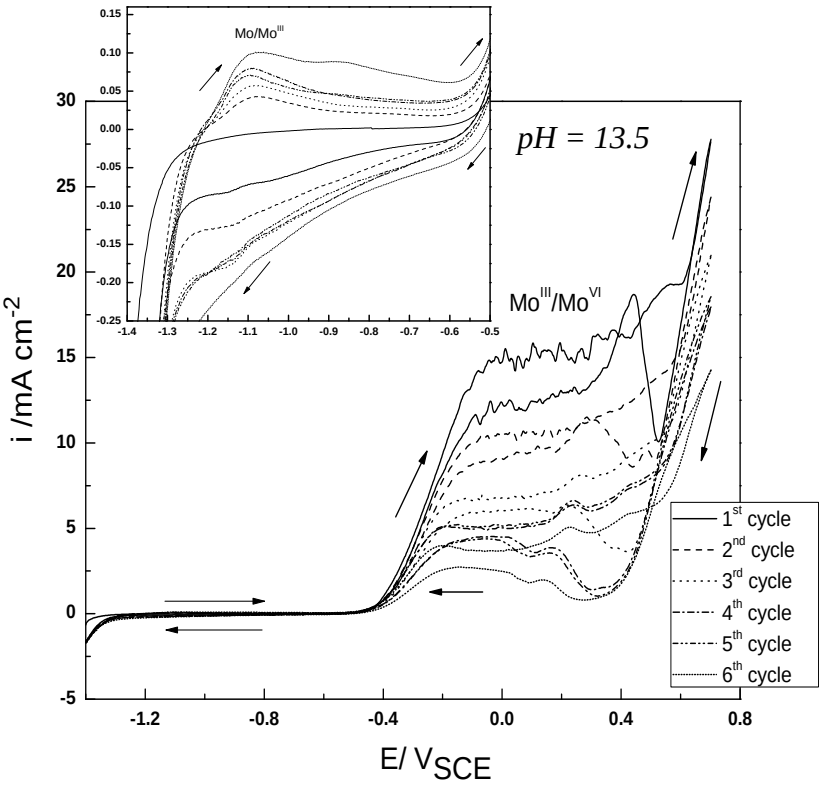

Fig. IV.6. Cyclic voltammograms of pure Mo electrode in saturated $Ca(OH)_2$+0.5M KOH solution (pH 13.5 at 25 °C).

- In the case of 2205 CD-DSS (Fig.IV.3b), the higher alkalinity of the electrolyte promotes a significant increase of the current density of associated to Cr^{III}/Cr^{VI} in similar way than Mo^{III}/Mo^{VI} process when pure Mo is exposed to the most alkaline conditions (Fig.IV.6). This increase in the transpassive current density of 2205 CD-DSS cannot be only related to the interference of molybdate formation process, where the molybdenum weight percentage is relatively small in comparison with chromium wt%. However, certain intensification of the Cr^{III}/Cr^{VI} associated to the presence of Mo in the stainless steels composition can be expected. Some authors [57, 176] suggested that the presence of Mo in the passive film promotes the dissolution of chromium in outermost layer of the passive film via the formation of soluble molybdates or Cr-Mo species that accelerates the extraction of Cr^{VI}-species from the passive layer. On the other side, it has been also reported that the Mo content can induce the enrichment of the passive layer in Cr oxides [33,55,177].

The previous results point out that the composition of the passive film and its electrochemical behaviour vary with both the alloy composition and the pH of the surrounding media. According to these results and to the literature [46,51-54, 56-59], the passive film can be described as a bilayer structure, with an outer layer enriched in iron and chromium hydroxides in the interface with the electrolyte [52-53,61], which may be involved in the electrochemical dissolution of chromates, and an inner layer consisting of an anhydrous mixed Fe-Cr-Ni oxides enriched in chromium oxides, less reactive and electrochemically more stable. In several studies [33, 46] the composition of the internal layer has been analyzed by XPS analysis, and it has been concluded that it is difficult to

indicate whether the inner oxide film is a mixture of two oxides (Cr_2O_3+Fe_3O_4) or a mixed iron-chromium spinel in which chromium and Ni can replace some of the iron positions. Abreu et al. [33, 58] reported that the Cr/Fe ratio along the passive film increases towards the oxide/metal interface and the presence of Mo species promotes a higher Cr/Fe ratio along the passive film.

IV.1.1.3. Influence of cold drawn deformation in the passive film formation on DSS

The influence of the mechanical deformation of the stainless steel due to the cold drawn treatment on the electrochemical response of the 2304 and 2205 DSS has been also evaluated. The cyclic voltammograms of parent (P) and cold drawn (CD) stainless steels when exposed to an alkaline solution of pH 12.5 have been represented in Fig.IV.7a for 2304 stainless steel and in Figure IV.7b for 2205 stainless steel.

The parent stainless steels show a wider passive domain accompanied with a smaller residual current density in comparison with the cold drawn stainless steels. Furthermore, the transpassive region is also affected by the cold drawn deformation of the stainless steels, as can be for both stainless steels (Fig.7a and Fig.7b). The main differences in the passivity and transpassivity domains of 2304 and 2205 P and CD-DSS are resumed in table IV.3.

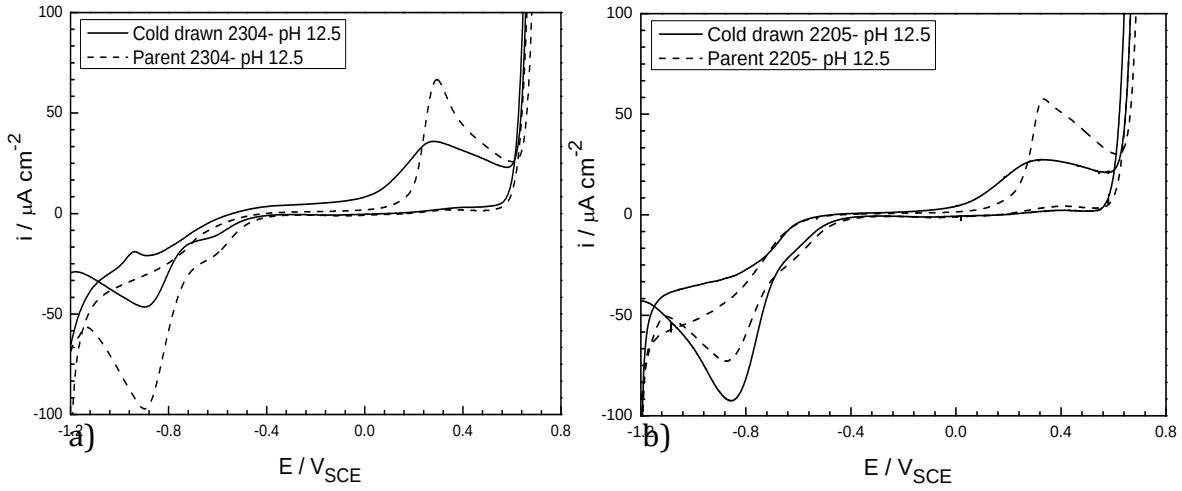

Fig. IV.7. Cyclic voltammograms of CD and P duplex stainless steels (a) 2304 and (b) 2205 exposed to saturated $Ca(OH)_2$ solution (pH 12.5 at 25 °C).

Similar response is observed for both stainless steels and no synergic effect between the steel composition and the cold drawn deformation can be distinguished. The cold drawn deformation induces a significant increase in the residual current density of passivation (i_{pass}) and decreases the potential at which the passive region ends. In the transpassivity domain, the maximum current density of the oxidation peak (i_p) and the electrochemical charge involved in this oxidative peak (Q), which mainly related to chromium dissolution process (Cr^{III}/Cr^{VI}) are smaller for the cold drawn stainless steels. Although the characteristic potential of the chromium dissolution process is nearly the same, the kinetic of this process seems to be affected by the cold drawn process, probably due to the induced changes on the stainless steel surface and microstructure as a consequence of cold drawn treatment. The higher interval of passivity, ending at a more anodic potential (Table IV.3), also allow to conclude that the P-DSS should be more

oxidized than cold drawn DSS, probably due to the major oxygen availability at the interface level of the parent SS which has a rougher surface than the cold drawn SS surface. An enrichment in Fe^{III} [46] with less residual current densities of passivation is expected in the case of parent SS. In addition, the change in the transpassivity current density of parent SS could be also associated to the different oxidability of both DSS surfaces because of the different active area for oxygen access, and the dissolution of chromate from Cr^{III} seems to be enhanced in the case of the P-DSS.

Table IV.3. Parameters of passivity and transpassivity domains of 2304 and 2205 CD and P-DSS obtained from one cyclic voltammetry.

	Passivity domain		**Transpassive domain (Cr^{III}/Cr^{VI})**		
	i_{pass} / µA cm^{-2}	E_{pass} _*range*/mV$_{SCE}$	I_p /µA cm^{-2}	E_p/ mV$_{SCE}$	Q / µC cm^{-2}
2304					
Cold drawn	7.2 ±0.01	From -450 to -74	36	278	15
Parent	0.75 ±0.03	From -460 to +171	67	295	19
2205					
Cold drawn	4.2 ±0.01	From -480 to -45	27	305	12
Parent	0.65 ±0.08	From -480 to +85	58	335	17

IV.1.2 Accelerated growth of the passive film: potentiostatic control

The aim of potentiostatic tests was to force the growth of the passive film on 2304 and 2205 CD-DSS in solutions of saturated $Ca(OH)_2$ and saturated $Ca(OH)_2$-0.5M KOH, recording the current response as a function of the applied potential. Three different potentials were considered and the test was repeated three times for each potential and (the mean values are represented): -0.3 V_{SCE} in the passive domain, +0.3 and +0.5 V_{SCE} in the transpassive domain.

The decay of the current density with time during passivation at -0.3 V_{SCE} has been included in Fig.IV.8 for both CD-DSS exposed to two different alkaline solutions.

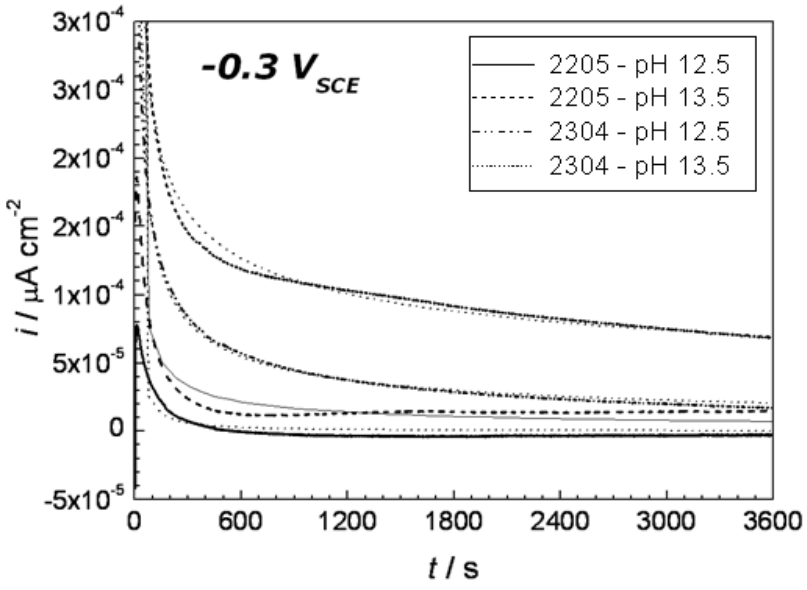

Fig. IV.8. Potentiostatic tests at -0.3 V_{SCE} on 2205 and 2304 CD-DSS in solutions of pH 12.5 and 13.5 at 25 °C.

The expression $i = A \cdot t^{-n}$ has been proposed by different authors [177-180] for studying the kinetic of passivation of Fe-Cr alloys, where *n* is associated to the repassivation rate parameter and can be considered to be an indirect measure of the growth of the oxide on the SS surface, *i* is the anodic current density, A is constant, and *t* is the time in seconds. In Fig.IV.8 the fitting of experimental data to this expression has been represented with dotted lines.

The values of *n* as well as the steady state current density for both duplex HSSS exposed to the different alkaline media have been listed in table VI.4.

Table IV.4. Significant parameters for the current density decay during the potentiostatic passivation at -0.3 V_{SCE} of both 2304 and 2205 CD-DSS.

	n		i_{ss} x 10^{-4} / μA cm^{-2}	
	pH 12.5	**pH 13.5**	**pH 12.5**	**pH 13.5**
2304	0.546 ± 0.001	0.334 ± 0.001	21.7	70.7
2205	1.090 ± 0.010	0.617 ± 0.003	4.3	7.9

Independently of the CD-DSS type, smaller values of *n* are obtained when the pH increases. In addition, the increase of the alkalinity of the solution seems to promote the formation of more conductive passive layers, as higher steady state current density values were measured in solutions of pH 13.5.

The presence of Mo in the composition of the CD-DSS is related to a significant increase of n, as listed in table IV.4. Values of n = 1 has been associated to the formation of stable oxides on the stainless steel surface. Thus, the results of potentiostatic passivation at

-0.3 V_{SCE} are coherent with the potentiodynamic formation of the passive film layer, where a more conductive passive film is expected in more alkaline conditions and for the CD-DSS without Mo (2304).

In the transpassive potential domain, the potentiostatic current density decay of 2304 and 2205 CD-DSS was recorded at +0.3 and +0.5 V_{SCE} in solutions of pH 12.5 and 13.5 at 25 °C to study the effect of the alloying elements in the redox processes occurring at the mentioned potential, as depicted in figure IV.9.

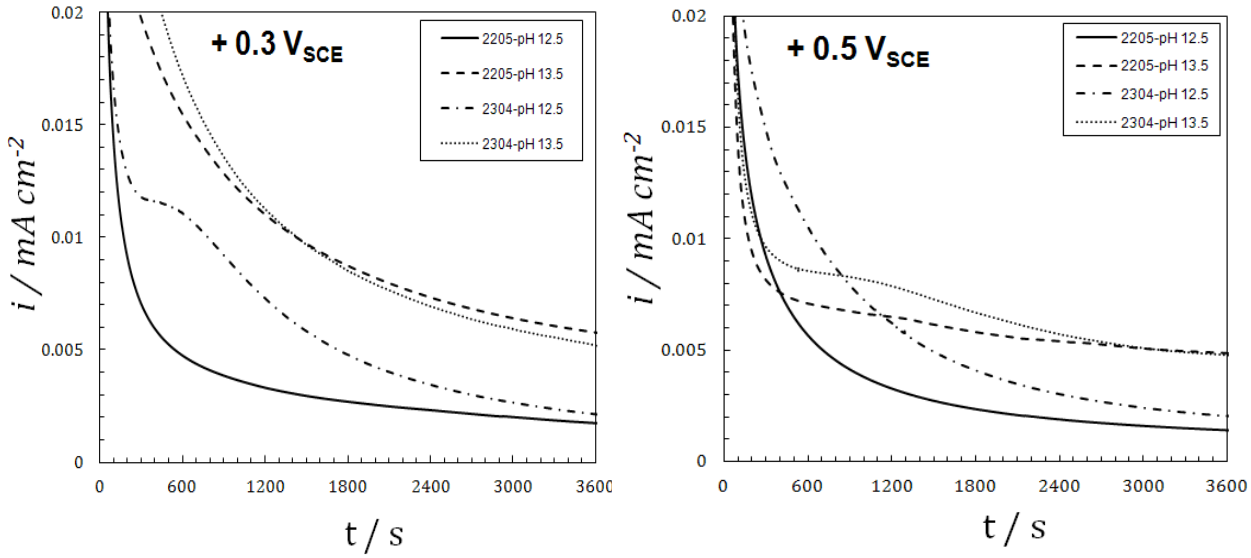

Fig. IV.9. Potentiostatic tests of 2205 and 2304 CD-DSS in solutions of pH 12.5 and 13.5 at 25 °C at +0.3 V_{SCE} and +0.5 V_{SCE}.

The results obtained at +0.3 V_{SCE} and +0.5 V_{SCE} can be summarized as following:

- Effect of pH: solutions of lower pH (12.5) for both 2205 and 2304 duplex HSSS show lower current density at both transpassive potentials, +0.3 and +0.5 V_{SCE}, confirming the enhancement of the chromates dissolution by increasing the pH of the alkaline media, that was also observed with the potentiodynamic tests.
- Influence of stainless steels compositions: in agreement to the potentiodynamic tests, the electrochemical response of the stainless steels containing Mo changes with the alkalinity of the solutions. Lesser values of steady current density are registered in less alkaline conditions for the 2205 SS than for the 2304 SS. However, when the pH increases to 13.5, the electrochemical response changes and the steady state current density is higher for 2205 stainless steels than for 2304, without Mo in its composition.

IV.2 Electrochemical response of spontaneous passive films: Ageing in alkaline media

The spontaneous passivation of DSS, 2304 and 2205, was considered in order to study the electrochemical behaviour of the passive film during its ageing in high alkaline media. The electrochemical response of the spontaneously formed passive film on DSS has been evaluated in high alkaline solutions, simulating the aqueous phase of the concrete, and in mortar in absence of aggressive agents like chloride.

The electrochemical characterization of the spontaneous passivation was carried out by non destructive electrochemical techniques as monitoring the evolution of the

corrosion potential (E_{corr}) and the corrosion current density (i_{corr}) at different immersion times in high alkaline environments. In addition, Electrochemical Impedance Spectroscopy (EIS) was also employed to follow up and to understand the changes in the passive film associated to the ageing in alkaline media.

Furthermore, destructive electrochemical techniques such as cyclic voltammetry were carried out after different ages of spontaneous passivation of the stainless steel for identifying the modifications in the redox processes occurring on the passive film at these different immersion times.

IV.2.1 Electrochemical response of spontaneous passive film formation in high alkaline solutions

The changes induced during the spontaneous passivation of DSS have been investigated during short and long term of immersion in the simulated pore solutions.

IV.2.1.1. Influence of the exposure media on the spontaneous passivation of cold drawn DSS: Effect of pH.

E_{corr} and i_{corr} monitoring

Fig.IV.10 shows the evolution of the corrosion potential, E_{corr}, for 2304 and 2205 CD-DSS with ageing in the alkaline solutions with pH 12.5 and 13.5 that simulate the aqueous phase of concrete pores. In each case, two DSS wires have been tested.

The corrosion potential (E_{corr}) is shifted to more noble potentials with ageing, indicating the spontaneous passivation attributed to the development of the oxide film on

the stainless steel surface, as suggested in literature [52,176]. This potential shift results from the predominance of the cathodic processes over the anodic one until the film acquires a stable thickness [181]. A constant potential was reached after 3 days of immersion, for both stainless steels in both alkaline conditions indicating the trend to the stabilization of the passive film composition.

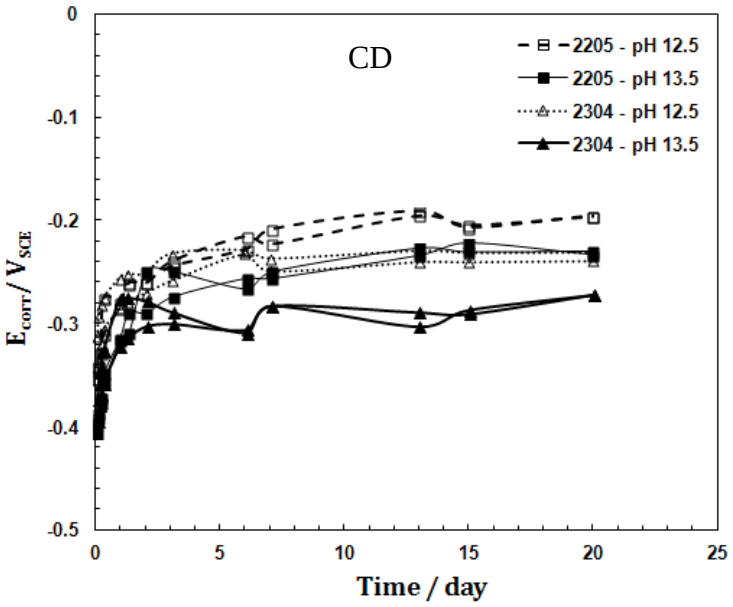

Fig. IV.10 Corrosion potential (E_{corr}) evolution for 2304 and 2205 CD-DSS in alkaline solutions at 25ºC (pH 12.5 and 13.5).

Concerning the repeatability of E_{corr} measurements, during the first 3 days, a small difference between E_{corr} values in the same experimental conditions for the same DSS have been monitored. However, similar steady state E_{corr} potentials have been measured for each stainless steel exposed to each alkaline solution after 7 days, as shown in Fig.IV.10.

The polarization resistance (R_p) was also recorded during 20 days of immersion in the same alkaline solutions for both CD-DSS to calculate the corrosion current density (i_{corr}) developed during the passivation process using a B constant value of 34 mV(see appendix I).

The evolution of i_{corr} of 2304 and 2205 CD-DSS with the immersion time in alkaline solutions of pH 12.5 and 13.5 has been represented in Fig.IV.11. Two wires have been considered in each case. A marked decay of i_{corr} with the immersion time is registered during the first stages of exposure until reaching a quasi-stationary value of i_{corr} after 4 or 6 days confirming that, this immersion period in alkaline solution is enough for the formation of an electrochemically stable oxide layer with low i_{corr} values. An acceptable repeatability of the i_{corr} measurements was confirmed in all cases.

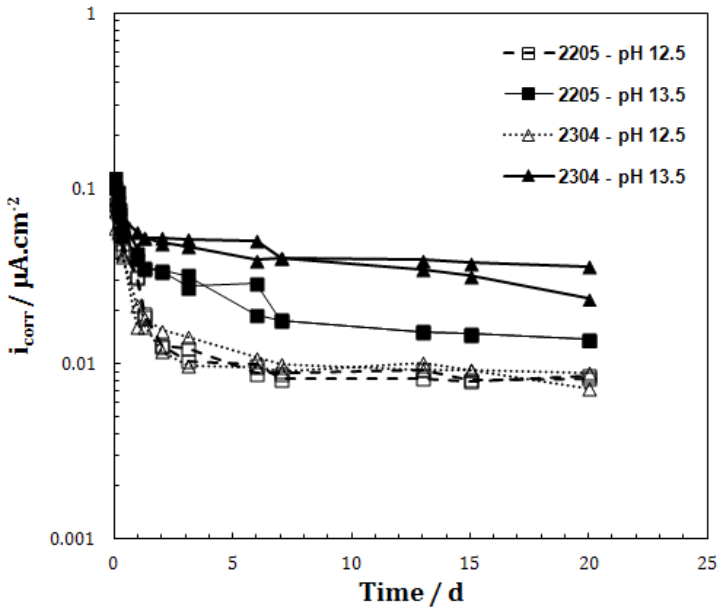

Fig. IV.11 Corrosion current density (i_{corr}) evolution of 2304 and 2205 CD-DSS during 20 days of immersion in solutions of pH 13.5 and 12.5 at 25 °C.

The results depicted in Fig. IV.10 and IV.11 show that the passive film evolution with the immersion time is pH-dependent. More anodic E_{corr} and similar i_{corr} values are registered in solution with lower alkalinity (12.5) for both tested CD-DSS.

According to the literature [51-52], the relative content of Fe^{II} in the passive film is controlled by the pH-value of the alkaline solution and higher Fe^{II}/Fe^{III} ratio in the passive film is expected in more alkaline solutions. This feature can help to explain the differences of the E_{corr} values of the passive films formed on 2304 and 2205 CD-DSS in both alkaline solutions. Although the electrochemical measurements have been carried out in aerated solutions and the oxygen reduction is expected to be the dominant cathodic reaction that defines the corrosion potential. However, Alonso et al. reported [181] that the change in Fe^{II}/Fe^{III} ratio is also an important parameter that can define the E_{corr} value. The expected increase in Fe^{II}/Fe^{III} ratio with pH induces more cathodic E_{corr} values due to the lesser content of more oxidized Fe species. The corrosion current density will also be affected by the Fe^{II}/Fe^{III} ratio as the lesser content in the most oxidized compounds promotes higher electrochemical reactivity of the passive layer. Then, the increase in the corrosion current density with the pH observed for both HSSS may be related to a higher conductivity of the passive film grown in the most alkaline solutions, as suggested by other authors for high alloyed stainless steels [51], what is also in agreement with the current density of passivity domain of potentiodynamic and potentiostatic tests carried out for both DSS at the same test conditions (see table IV.1 to table IV.4).

Regarding the influence of the DSS type on E_{corr} and i_{corr} measurements, in agreement with the previous potentiodynamic and potentiostatic results, the effect of the

stainless steel type on E_{corr} and i_{corr} values is also controlled by the pH of the alkaline solutions. In less alkaline solutions (pH 12.5), slight differences in E_{corr} and i_{corr} values of both 2304 and 2205 CD-DSS have been measured, as shown in Fig.IV.10 and Fig.IV11. On the other side, in the most alkaline solutions (pH 13.5), the passive film formed on 2304 CD-DSS shows more cathodic E_{corr} (see Fig.IV.10) and higher i_{corr} values (see Fig.IV.11) than 2205 CD-DSS, which in turn indicates that the passive film formed 2205 CD is expected to be less reactive and more electrochemical stable in comparison with 2304 CD-DSS at the same test conditions.

Electrochemical impedance spectroscopy (EIS) evolution

The evolution of the Nyquist and Bode plots measured for 2304 and 2205 CD-DSS at different immersion times in the alkaline solutions (pH 12.5 and pH 13.5) is represented in figures IV.12 and IV.13 respectively.

For both DSS, the limit of the impedance values at low frequency range increases during the first 3 days of immersion of the rebar in both alkaline media due to the growth of the passive film and the enhancement of its protective behaviour. An asymptotic tendency is observed after this period which is the time required to reach the steady state situation during the spontaneous passivation of steel in alkaline media [52, 182] as also supported the E_{corr} and i_{corr} measurements (see Fig.IV.10 and Fig.IV.11).

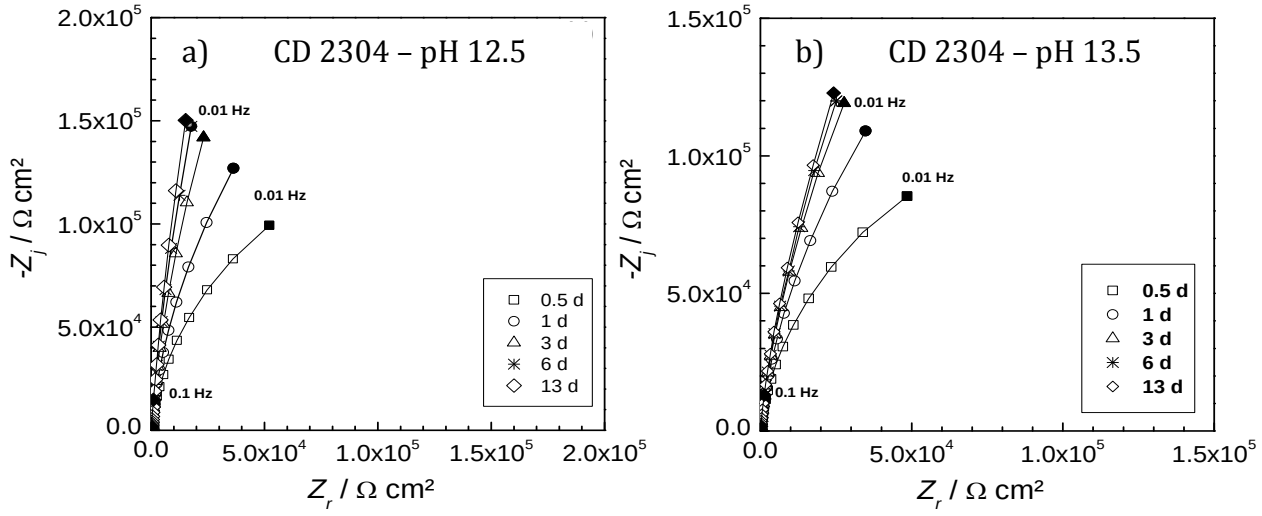

Fig. IV.12 Evolution of the impedance spectra in Nyquist plots with the immersion time (up to 13 days) of 2304 CD-DSS in: a) pH 12.5, b) pH 13.5. Experimental data (dots), fitting with 2*RC* equivalent circuit (solid lines).

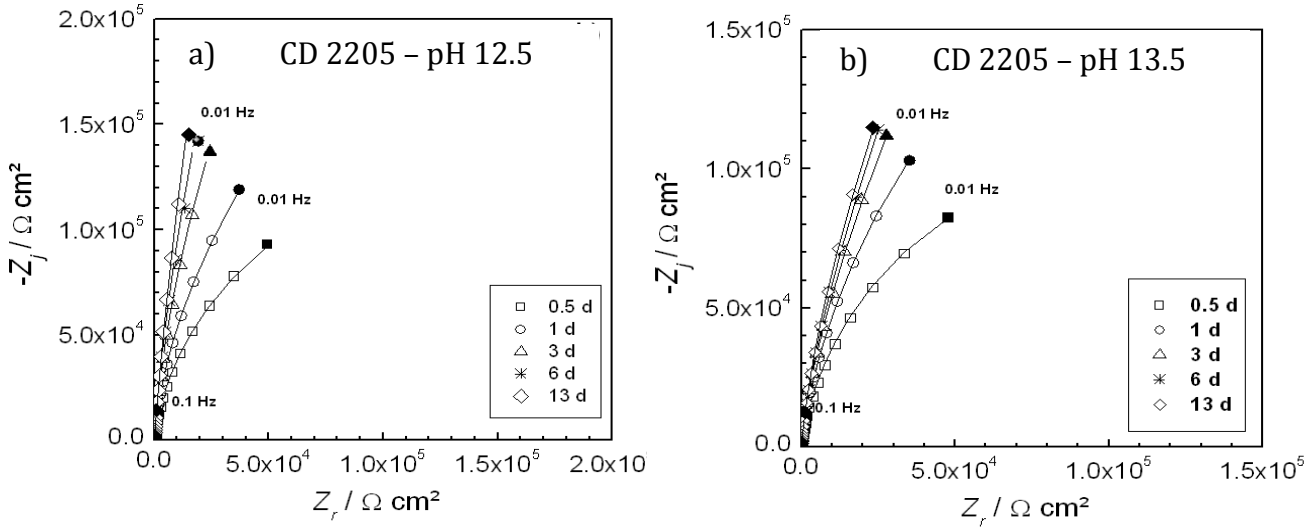

Fig. IV.13 Evolution of the impedance spectra in Nyquist plots with the immersion time (up to 13 days) of 2205 CD-DSS in: a) pH 12.5, b) pH 13.5. Experimental data (dots), fitting with 2*RC* equivalent circuit (solid lines).

The low frequency impedance values measured in alkaline solution of pH 12.5 are higher than the impedance values measured in the alkaline solution of pH 13.5, which in turn, confirms that the passive film spontaneously grown on cold drawn duplex stainless steels in solutions of pH 12.5 is less electrochemically reactive than the passive film formed in more alkaline conditions (pH 13.5). Both 2304 and 2205 CD-DSS show a similar impedance tendency with ageing.

Although different equivalent electric circuits have been suggested to interpret the impedance data of the passive films formed on the stainless steel, in present doctoral thesis an EEC consisting of two RC loops in parallel, depicted in Fig. IV.14 [51] has been used as was detailed in the experimental chapter. The quality of the fitting for 2304 and 2205 CD-DSS EIS results with the 2RC electrical equivalent circuit proposed can be observed in Fig.IV.12 and Fig.IV.13 (comparing the experimental data (dots) and the fitting data (lines)).

In figure IV.14 the evolution of R_{ct} (Fig.IV.14a) and C_{dl} (Fig. IV.14b) with the immersion time has been represented for both CD-DSS (2304 and 2205) exposed to different alkaline solutions (pH 12.5 and 13.5).

In both alkaline solutions (pH 12.5 and pH 13.5), R_{ct} increases with ageing for both CD-DSS, revealing that the charge transfer processes become more difficult due to the growth of the passive film. The capacitance (C_{dl}) values, Fig. IV.14b, ranged between 52-49 $\mu F\ cm^{-2}$, are typical of a double layer capacitance.

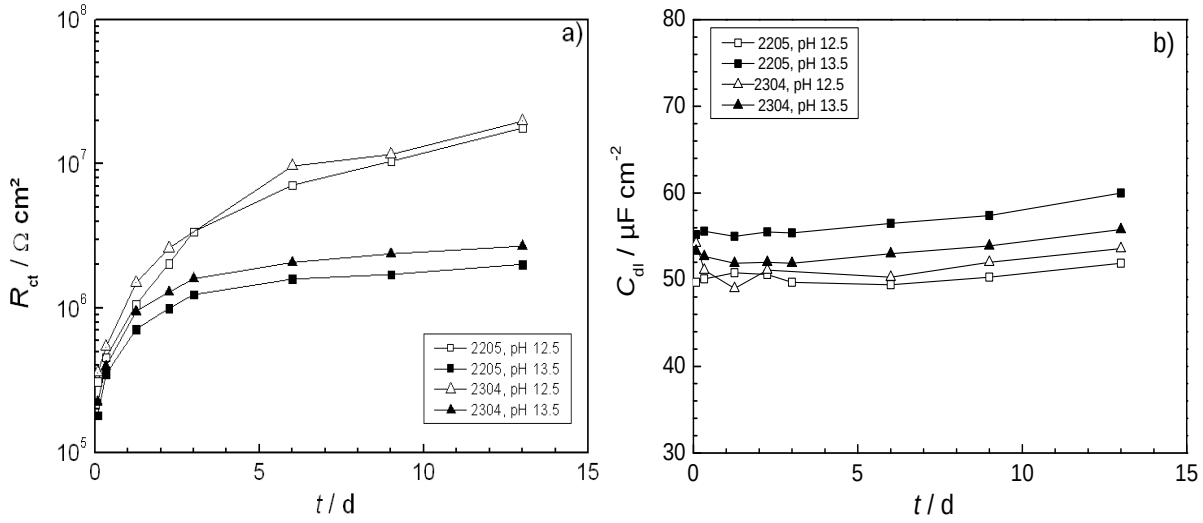

Fig. IV.14 Evolution of EEC passive elements with the immersion time for 2304 and 2205 CD-DSS in solutions of pH 12.5 and 13.5. a) Charge transfer resistance (R_{ct}), b) Double layer capacitance (C_{dl}).

The pH of the solution has a significant effect on the impedance response at high frequencies of CD-DSS. Lower charge transfer resistance values are measured for the most alkaline solution (pH 13.5) confirming the more conductive character of the passive film formed in these conditions, which is enriched in less oxidized iron oxides [51-52]. These results are in agreement with the i_{corr} evolution (Fig.IV.11) and with the potentiodynamic (Fig.IV.1 and Fig.IV.3) and potentiostatic results (Fig.IV.8). The effect of the pH on the double layer capacitance seems to be related not only with the pH value but also with the steel composition, as can be deduced from the increase of C_{dl} in the case of 2205 HSSS exposed to the most alkaline solution (pH 13.5). The possible formation of soluble chromates and molybdates in high alkaline environments induce changes in the composition of the film/electrolyte interface, affecting the double layer capacitance (C_{dl}). Furthermore, EIS response is affected by the DSS composition and lesser R_{ct} values are registered for the 2205 CD-DSS, probably due to the enhancement of the formation of

soluble chromates and molybdates on the surface of the stainless steel with higher content on Mo (2205) when exposed to the most alkaline conditions, deduced from the potentiodynamic results (Fig.IV.3).

The time constant (R_f C_f) at lower frequencies suffers an important increase with ageing in alkaline solutions, as can be observed in Fig.IV.15. The pH has also a significant influence on this parameter and higher values of R_fC_f are registered in the solutions of lower pH (pH 12.5). The higher Fe^{II}/Fe^{III} ratio expected in the passive layer formed in the most alkaline solutions increases the electrochemical reactivity of the passive layer, explaining the lower values of R_f C_f registered in these more alkaline conditions.

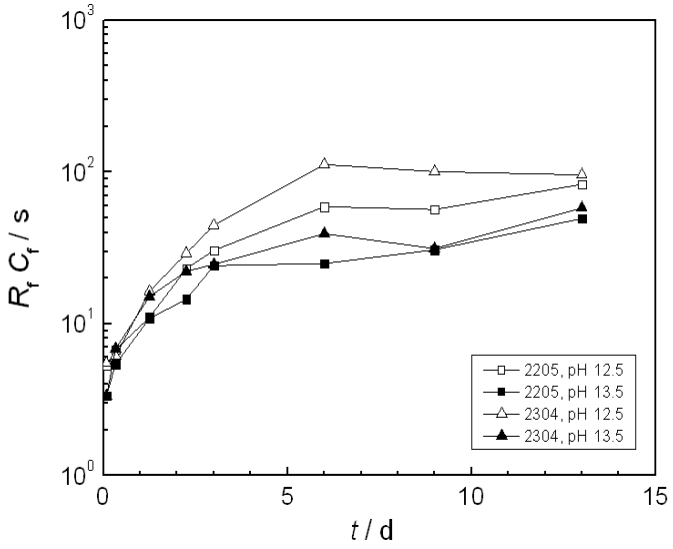

Fig. IV.15 Evolution of the time constant (R_f C_f) at the lowest frequencies for 2205 and 2304 CD-DSS with ageing in alkaline solutions (pH 12.5 and 13.5).

IV.2.1.2. Influence of presence of Mo in the passive film formation on cold drawn DSS

As has been briefly introduced in the previous section, the results depicted in Fig.IV.10 and Fig.IV.11 show that the evolution of the passive film spontaneously formed in high alkaline conditions is also controlled by the chemical composition of stainless steel. More positive steady state E_{corr} potentials are registered for 2205 duplex HSSS (Fig. IV.10). Moreover, lower i_{corr} values are measured for 2205 SS in comparison with 2304 SS, mainly in the most alkaline conditions (pH 13.5). As the main difference in composition between both stainless steels is the Mo content, the influence of this alloy element on the electrochemical response of the passive layer spontaneously formed on both stainless steels is expected.

As it was observed in potentiodynamic test (Fig.IV.3), the presence of Mo intensifies the transpassive current density especially in the case of alkaline solutions of pH 13.5, which mainly related to an enhancement of the Cr^{III}/Cr^{VI} oxidation process. However, the accumulation of chromates in the interface of the passive film with the electrolyte increases the possibility of the reduction of some adsorbed chromates by Fe^{II}-species [183-186] in the external region of passive film, as shown in equilibrium IV.5:

$$CrO_4^{--} + 3\,Fe^{II} + 5\,H_2O \rightarrow 3\,FeOOH + Cr(OH)_3 + 4H^+ \qquad eq.IV.5$$

This process induces the increment in Fe^{III} and Cr^{III} species in the outermost part of the film, enhancing the formation of a less conductive and more oxidized passive film, enriched in Fe^{III} and Cr^{III} species, in the case of 2205 SS in comparison with 2304 when exposed to alkaline solutions of pH 13.5, which would explain the smaller current density

values registered in passive conditions for stainless steels with higher Mo content (2205), even though the higher values of the transpassive region in potentiodynamic (Fig.IV.3) and potentiostatic (Fig.IV.8 and Fig.IV.9) testes were observed.

The interpretation of EIS data in terms of EEC of both types of stainless steels, 2304 and 2205, shows that certain influence of the chemical composition of the stainless steel on the electrochemical properties of the passive layer can be expected, mainly on high frequency time constant, R_tC_{dl} assigned to the oxide-electrolyte interface. The presence of Mo promotes the formation of a passive film with a slight higher C_{dl} value and lower R_{ct} values when exposed to the most alkaline conditions with pH 13.5 (Fig.IV.14). As commented above, this fact may be related with the higher production of chromate and molybdates in these exposure conditions that can be adsorbed on the passive film interface and modify the interface between the oxide film and the electrolyte. On the other hand, in alkaline solution with lower pH (12.5), no significant effect due to the presence of Mo can be identified on the parameters of the time constant at the highest frequencies, R_{ct} or C_{dl}.

Regarding the lower frequency time constant $R_f C_f$, displayed in Fig.IV.15, a slight difference between both types of HSSS can be observed after 3 days of immersion. However, it is difficult to identify if these differences in $R_f C_f$, time constant is attributed to the influence of the chemical composition of the stainless steel or it is due to an error in the fitting data due to the high capacitive behaviour of the tested DSS with aging.

IV.2.1.3. Influence of cold drawn deformation on the passive film formation of DSS

Short-term exposure to alkaline solutions

Fig.IV.16 shows the corrosion potential (E_{corr}) and the corrosion current density (i_{corr}) evolution of 2304 cold drawn and parent DSS exposed to an alkaline solution of pH 12.5 for 7 days. Five stainless steels of each type have been tested in order to evaluate the repeatability of the results.

During the earlier ages, the corrosion potential of both stainless steels increase asymptotically until reaching a steady state situation at more noble potentials after 4 days of immersion, as shown in Fig.IV.16a. This shift in E_{corr} was accompanied by a decrease in the corrosion current density (i_{corr}) values down to 6 nA cm^{-2}, indicating the formation of stable passive layer on both stainless steel surfaces.

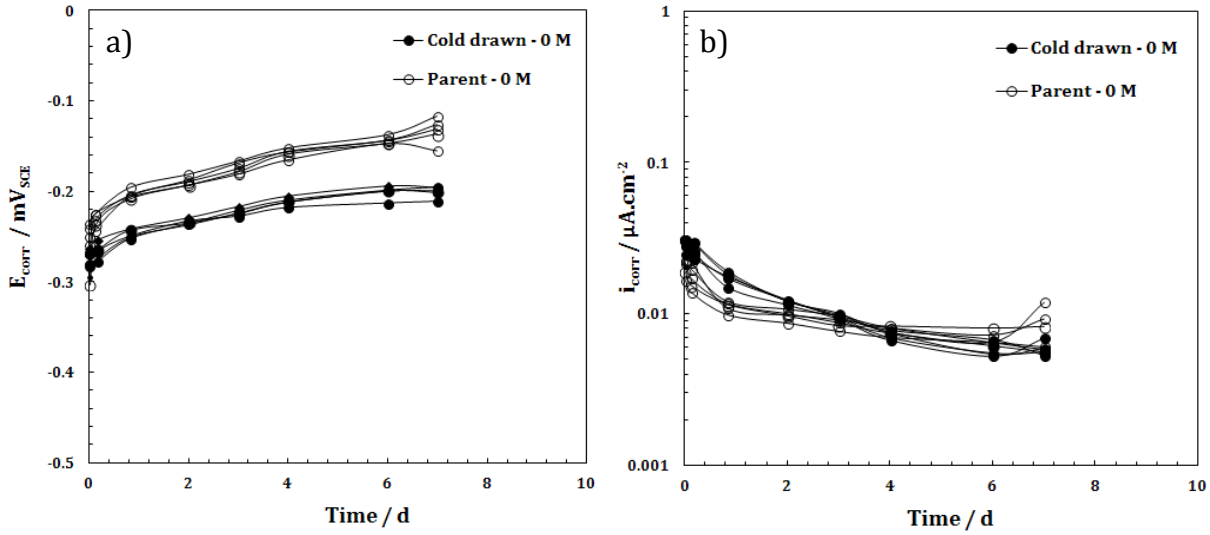

Fig. IV.16. Evolution of a) corrosion potential (E_{corr}), and b) corrosion current density (i_{corr}) of 2304 P and CD DSS in sat. $Ca(OH)_2$ (pH 12.5).

In addition to the effect of ageing in alkaline media, the cold drawn deformation process seems to affect the measured E_{corr} values, as the parent SS wires present a more anodic E_{corr} in comparison with the cold drawn SS. However, no significant differences in i_{corr} values of cold drawn and parent stainless steels were observed, see Fig.IV.16b.

The high corrosion potentials registered for the 2304 P-DSS would agree with the result of the accelerated formation of the passive film (Fig.IV.7 and table IV.3), where a more oxidized layer with a major presence of higher oxidized metal ions, probably Fe^{III} species, was expected in agreement with literature [46].

In order to clarify the electrochemical response of cold drawn and parent DSS, EIS measurements were also performed. The repeatability of these EIS measurement was confirmed by measuring 5 steels for each case. Fig.IV.17 shows the evolution of impedance spectra in Nyquist plots of one of the tested 2304 P and CD-DSS during 7 days of immersion in alkaline solutions of pH 12.5 at 25 °C. The increase of the global impedance of parent and cold drawn DSS with ageing confirms the enhancement of the protective behaviour of both SS due to the formation of an electrochemically stable passive film. The cold drawn SS presents higher impedance when compared with parent SS.

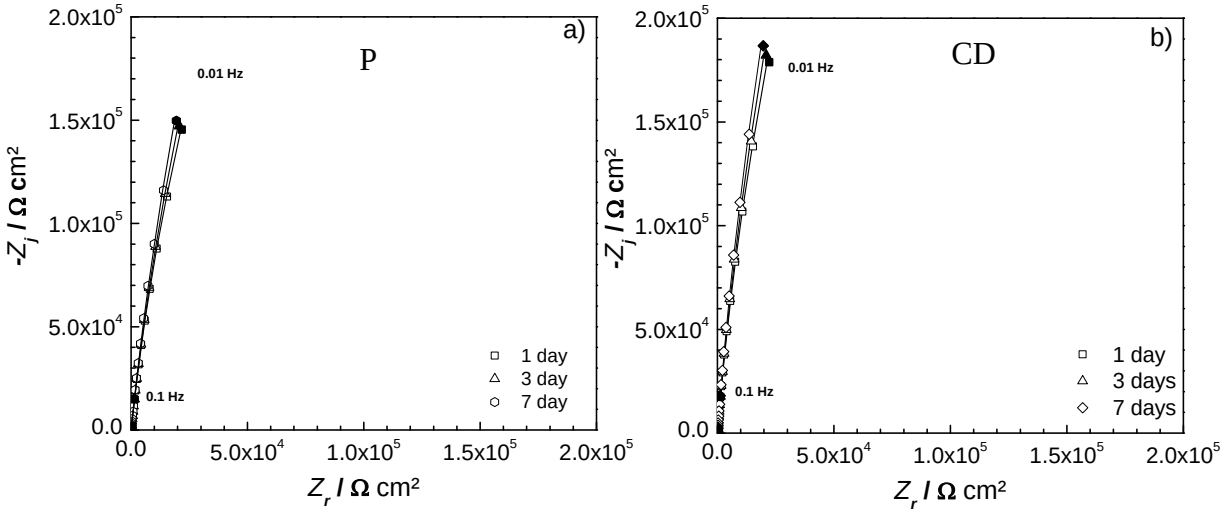

Fig. IV.17 Evolution of the Nyquist pots of 2304 a) P and b) CD DSS in alkaline solutions of pH 12.5. Experimental data (dots), fitting with 2*RC* equivalent circuit (solid lines).

The 2RC model of the electrochemical equivalent circuit (EEC) described in the experimental chapter was employed to interpret the impedance data of the passive film formed on both parent and cold drawn DSS.

The evolution of the high frequency time constant, associated with the charge transfer process throughout the double layer, and the low frequency time constant, associated with the redox processes taking place in the film of 2304 P and CD DSS are depicted in Fig.IV.18 and Fig.IV.19 respectively. For both types of SS, the obtained profile shows a similar tendency versus ageing in alkaline solutions. Furthermore, although a slight deviation value of the parameters has been observed in EIS measurements for the same type of SS exposed to the same conditions, similar evolution of all of them allows confirming the repeatability of the EIS measurements.

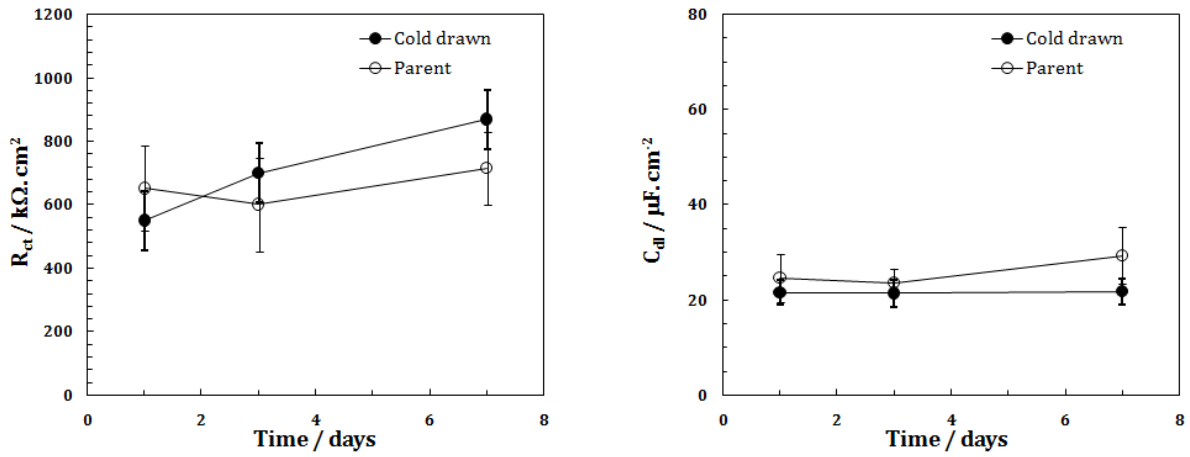

Fig. IV.18 Variation of R_t and C_{dl} parameters of 2304 (a) P and (b) CD DSS in alkaline solutions of pH 12.5.

Concerning the high frequency parameters (R_{ct} and C_{dl}), a slight increase in R_{ct}-resistance of cold drawn DSS can be observed with ageing, while almost constant values are registered in the case of parent DSS. Also an almost constant trend with ageing is observed for the C_{dl}-values for both CD-DSS (from 19 to 23 µF.cm^{-2}), as shown in Fig.IV.18b, and for P-DSS, which show a slight higher variability (from 20 to 38 µF.cm^{-2}).

On the other side, slight differences between 2304 parent and cold drawn DSS have been observed in the case of low frequency parameters (R_f C_f), as shown in Fig. IV.19. During the first 3 days, the 2304 CD-DSS presents a relatively higher R_f C_f time constant, then both DSS reaches nearly the same R_f C_f value after 7 days, as shown in Fig.IV.19.

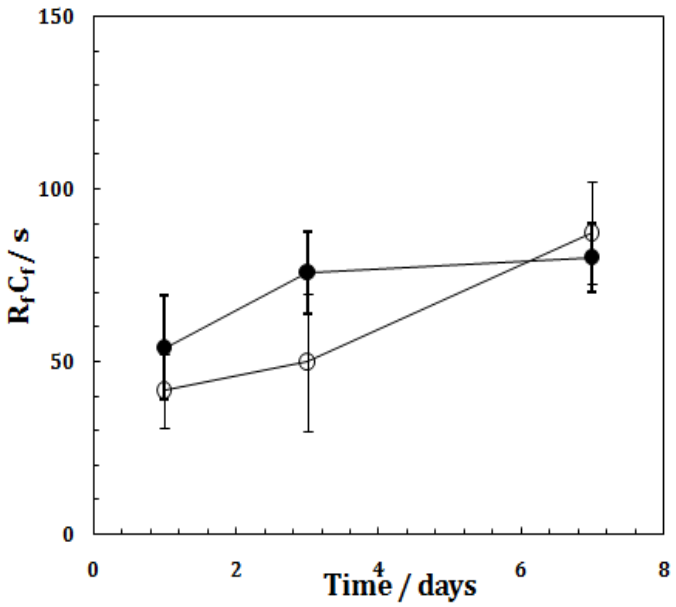

Fig. IV.19 Variation $R_f C_f$ time parameters of 2304 (a) P and (b) CD DSS in alkaline solutions of pH 12.5.

During the short-term immersion, cold drawn and parent SS generally show a similar electrochemical response, and only small differences have been observed which probably related to the different initial surface roughness in both steels. To evaluate the effect of cold draw deformation process in DSS response, longer exposure times have been considered.

Long-term exposure to alkaline solutions

Fig.IV.20 shows the long-term evolution of the corrosion potential (E_{corr}) and the corrosion current density (i_{corr}) of cold drawn and parent 2304 stainless steel in an alkaline solution of pH 12.5. The electrochemical response observed during the short-term immersion tests was maintained in the long-term immersion test, where more anodic E_{corr} was registered for parent SS than for the cold drawn wires, even after 416 days of

immersion in alkaline media. No significant differences in i_{corr} were measured for both stainless steels, as shown in Fig.IV.20b.

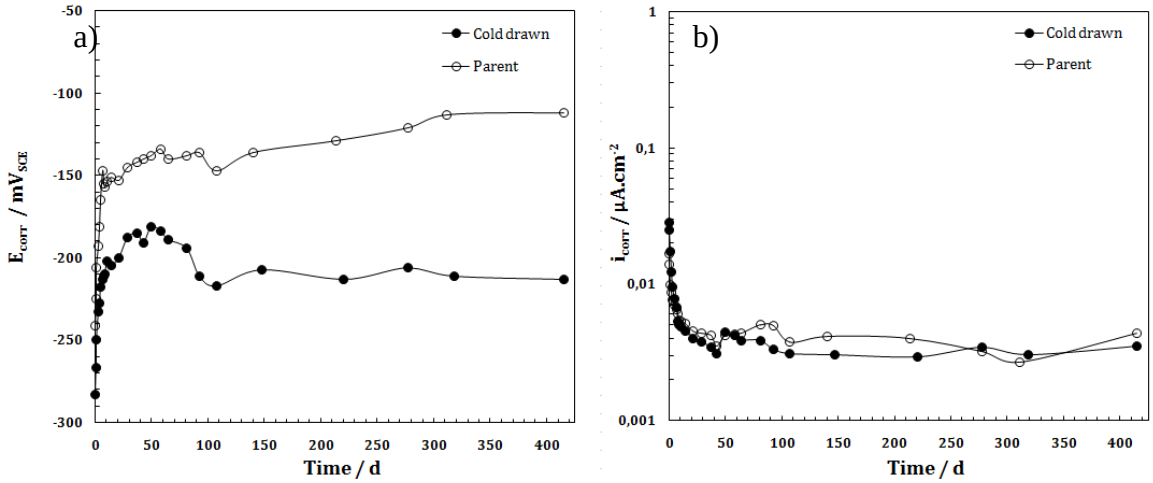

Fig. IV.20. Long-term evolution of E_{corr} and i_{corr} of 2304 P and CD DSS in sat. $Ca(OH)_2$ of pH 12.5.

The effect of the cold drawn deformation on the passive film properties at long-term immersion was also investigated throughout the evaluation of EIS spectra of 2304 P and CD DSS, as included in Fig.IV.21 (Nyquist diagrams).

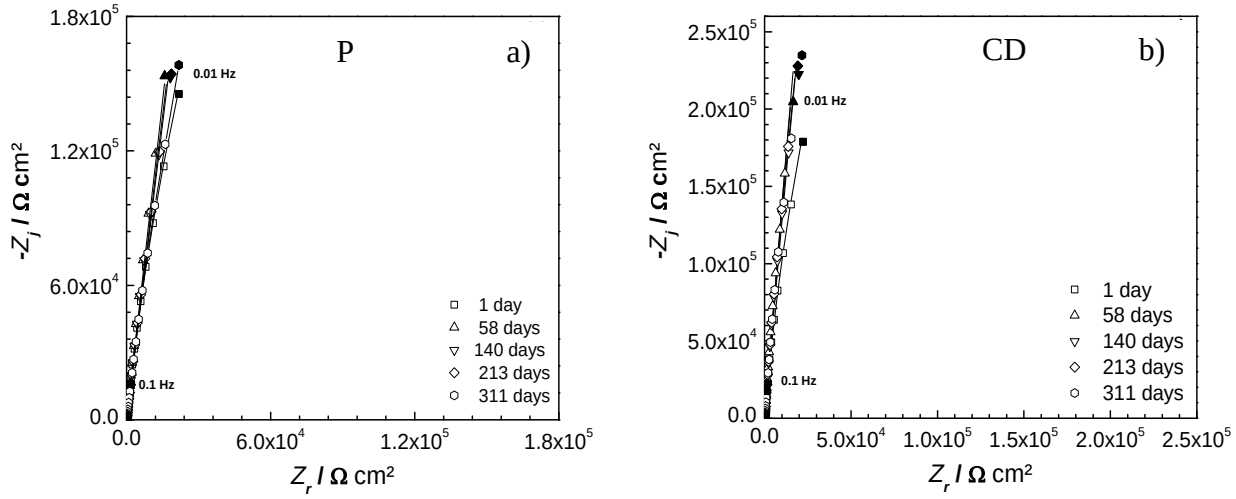

Fig. IV.21. Nyquist plots of 2304 (a) P (b) CD 2304 SS after 1, 58, 140, 213, 311 days in solution of sat. $Ca(OH)_2$ of pH 12.5. Experimental data (symbols), Fitting data with 2RC equivalent circuit (solid lines).

After a long-term immersion period, higher values of impedance at the lowest frequencies are registered for 2304 cold drawn steel than for the 2304 parent steel, indicating an enhancement of the passive properties of the oxide layer spontaneously formed on the cold drawn steel. The evolution of the passive elements of 2RC EEC considered for the fitting of EIS has been represented in Fig.IV.22 (high frequencies parameters) and in Fig.IV.23 (low frequencies time constant). A progressive increase of the charge transfer resistance of the passive film during the earlier stages of immersion in the alkaline media is observed in both the cold drawn and the parent 2304 steel, as shown in Fig. IV.22a, while at longer periods almost constant values of this parameter are registered. Cold drawn DSS shows higher charge transfer resistance than parent stainless steels.

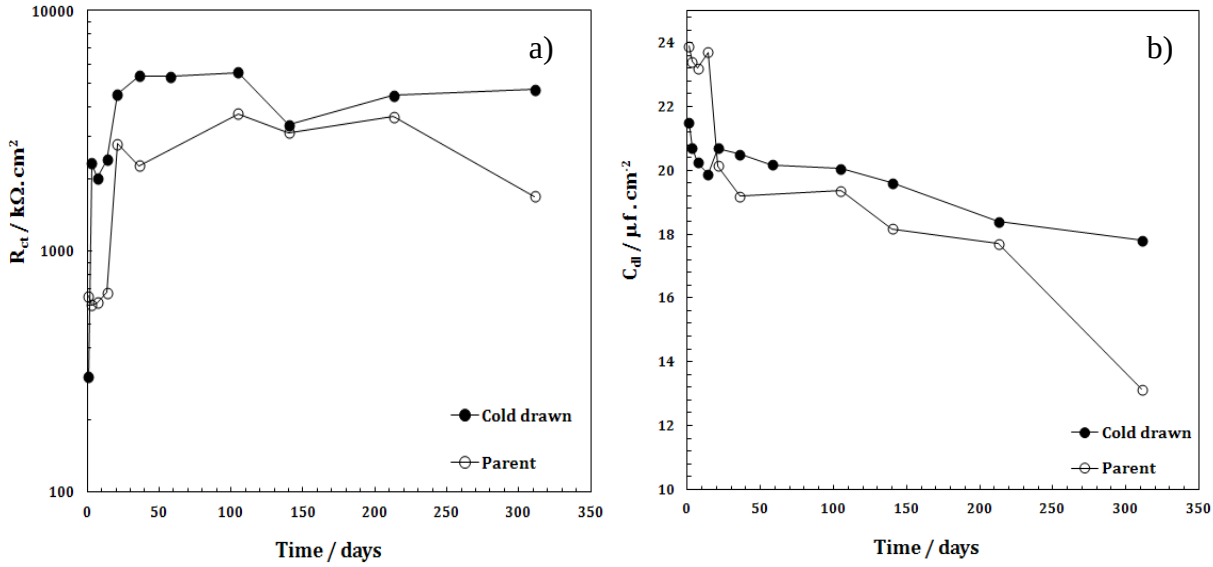

Fig. IV.22. Evolution of high frequency time constant parameters (a) charge transfer resistance (R_{ct}), and (b) double layer capacitance (C_{dl}) of 2304 P and CD DSS.

No significant difference between both DSS are monitored in C_{dl} after long-term immersion in alkaline solutions ($C_{dl} \approx$ 15-20 µF/cm^2), as shown in Fig.IV.22b.

The influence of cold drawn deformation on the stainless steel response with immersion time can be also observed in the evolution of the low frequency time constant (R_fC_f) associated to the redox processes taking place in the oxide film as shown in Fig.IV.23 for both cold drawn and parent 2304 SS exposed to an alkaline solution of pH 12.5. However, the difference between both time constants is relative small and can be affected by the high error associated to the estimation of this time constant as the fitting of the impedance values at the lowest frequencies involves an extrapolation in Nyquist diagrams of a quite opened buckle and the value of R_f can be affected by a great error.

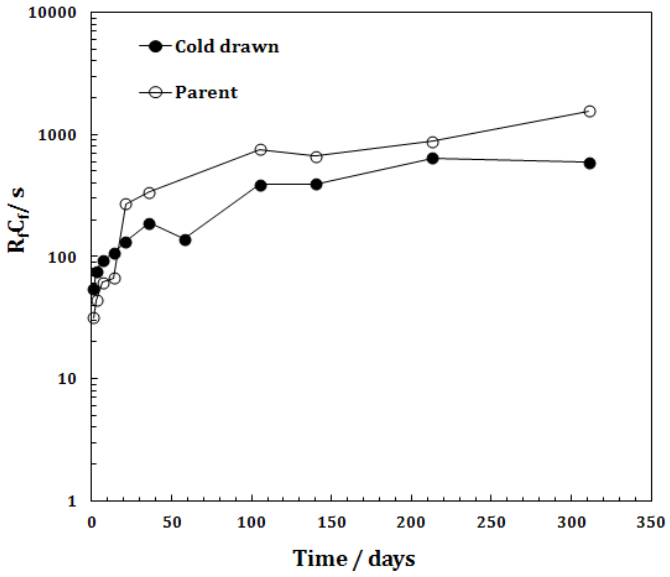

Fig. IV.23. Low frequency time constant evolution, $R_f C_f$, of 2304 P and CD DSS.

After different ages of immersion (0, 7, 15 and 416 days) in alkaline solution (pH 12.5), DSS were exposed to a cyclic voltammogram to evaluate the effects of ageing and SS microstructure in the redox processes occurring in the passive film. Cyclic voltammograms

of 2304 cold drawn DSS are shown in Fig.IV24a. Fig.IV24b displays the CV of 2304 parent DSS.

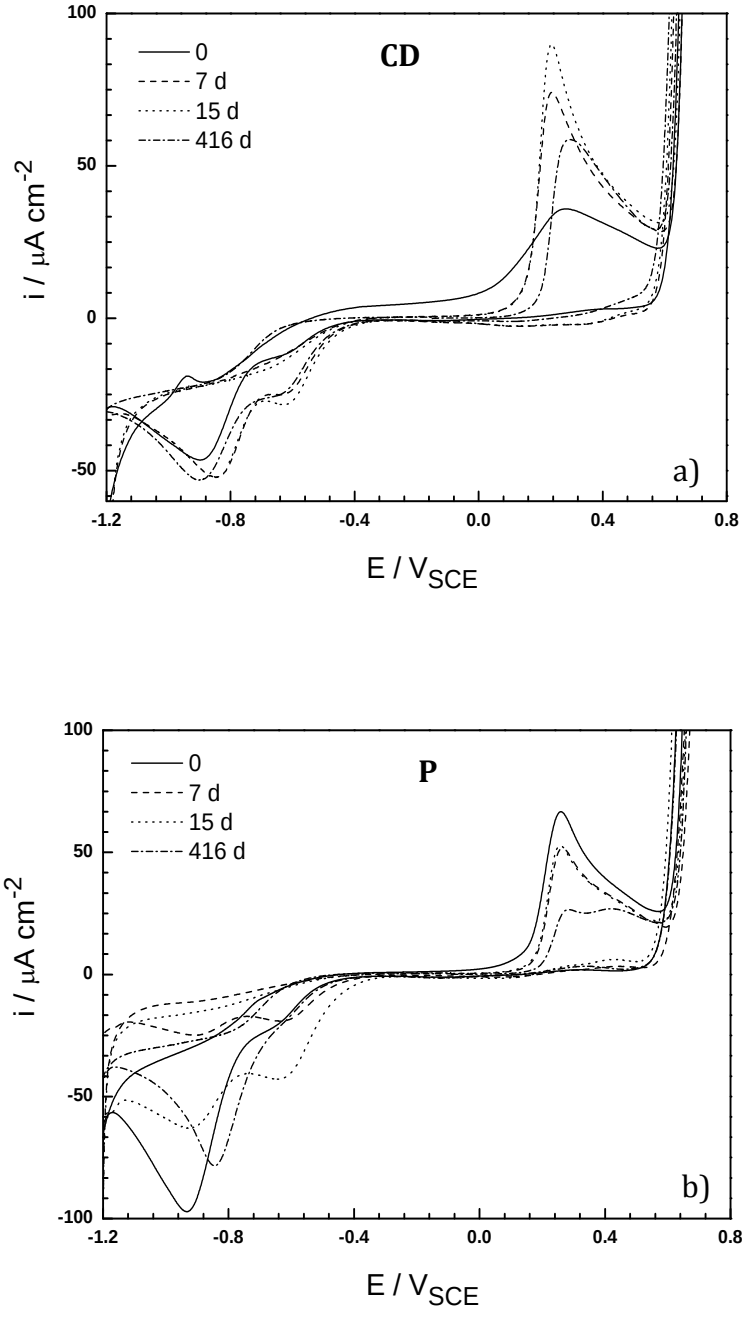

Fig. IV.24. Cyclic voltammograms of 2304 DSS after 0, 7, 15, 416 days of passivation in sat. $Ca(OH)_2$ (pH 12.5 at 25 °C). (a) CD, (b) P.

Ageing in alkaline media showed a certain effect on the transpassivity domain, suggesting a change in the Cr-content or distribution within the passive film as function of the immersion time. In addition, this evolution of the transpassivity domain depends on the SS microstructure. In the case of cold drawn 2304 (Fig.IV.24a), the maximum current density of the transpassivity peak increases with the ageing of the passive layer when short times of passivation are considered, i. e. 15 days. However, when a long-term passivation of the cold drawn steel is carried out, a decrease in the peak current density with a shifted of the peak potential to more positive values is observed. On the other side, the passive layer formed on the parent SS (Fig.IV.24b) shows a quite different electrochemical response in the transpassivity domain. Although the parent SS initially shows higher transpassive current densities values than the cold drawn SS in the same conditions, the current density of the transpassivity peak decreases with the ageing of the passive layer.

After the long-term passivation, the electrochemical response of parent 2304 in the transpassive region is quite different, as can be observed in Fig.IV.24b. Another redox process appears at E = +0.45 V_{SCE} that is expected to correspond to Ni^{II}/Ni^{III} oxidation. According to literature [187], during the growth of the passive film, chromium is oxidized to soluble Cr^{VI} species and/or is accumulated in the passive film as Cr^{III} oxy-hydroxide, with a slightly depletion in chromium at the interface with respect to the bulk composition. This depletion in the chromium content at the interface enhances the oxidation of other alloy elements, as nickel. In the voltammograms of parent stainless steel, the high current density registered in the transpassive peak of chromates dissolution could promote enhancement of this depletion of chromium at the interface and then, the appearance of

other oxidative peaks, such as Ni^{II}/Ni^{III} can be expected. Furthermore, higher current densities are measured in the transpassivity peak for parent SS if compared with CD-DSS, which indicates more dissolution of chromates in the case of the P-DSS and then, the passive film formed on cold drawn stainless steels can be expected to have higher Cr-content than parent SS, which can improve the passivity of the cold drawn steel and allows to explain the higher impedance values observed in case of cold drawn SS.

IV.2.2 Spontaneous passive film formation of DSS in mortar

The spontaneous growth of the passive film on 2304 cold drawn and parent DSS has been also investigated in chloride free mortar in order evaluate the electrochemical response of SS when exposed to more real field conditions, such as of mortar, and to analyse the reproducibility of the DSS electrochemical response in high alkaline solutions and in mortar.

Spontaneously grown passive film on 2304 DSS embedded in mortar has been assayed by monitoring E_{corr} and i_{corr} with ageing in mortar. Fig.IV.25 shows the evolution in time of E_{corr} and i_{corr} for mortar samples with embedded cold drawn and parent DSS when exposed to different climatic conditions (RH 95%, and 80% at 23 °C): firstly, the mortar samples were exposed to wet condition (RH 95%) during the first 19 days of testing and after that, they were exposed to drier conditions, RH 80%. The temperature was maintained constant at 23 °C along the whole test. Three SS wires of each DSS have been tested to confirm the repeatability of the electrochemical measurements.

During the earlier ages at the higher relative humidity, the E_{corr} is shifted to nobler potentials and i_{corr} decays with time due to the growth of the passive film on both stainless steels. Quasi-stationary values of E_{corr} and i_{corr} have been reached after 5 days of exposure to RH 95%. In similar way than occurred during the immersion of these stainless steels to the alkaline solution simulating the aqueous content of the concrete pores (pH 12.5, see Fig.IV.20), when embedded in mortar 2304 parent DSS also presents nobler values of potential than 2304 CD-DSS. The differences in the i_{corr} values of both types of SS are not much significant as also occurred when they were immersed in the alkaline solution (pH 12.5, see Fig.IV.20) and for both stainless steels small values of i_{corr} (between 0.01 to 0.02 $\mu A.cm^{-2}$ as shown in Fig.IV.25b) were measured.

However, when the mortar samples are exposed to drier conditions (RH 80%), E_{corr} of both tested DSSs suffer a slight cathodic shift but i_{corr} value seems to be not affected significantly by the RH change, although a more cathodic E_{corr} accompanied with lower i_{corr} has been measured. This change in E_{corr} when mortar samples are exposed to a climatic condition of RH 80% is probably related to a change in the oxygen availability and/or the pH of surrounding environment to the embedded DSS.

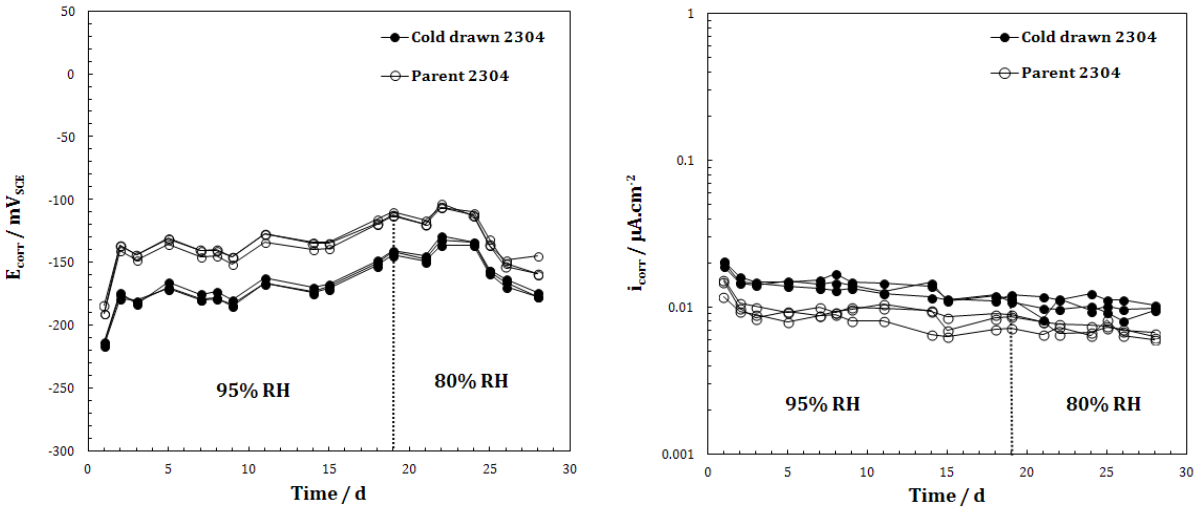

Fig. IV.25. Evolution of E_{corr} and i_{corr} of 2304 parent and cold drawn DSS in chloride free mortar.

In summary, the comparison of Fig.IV.20 and Fig.IV.25 indicates that the electrochemical response of the passive film formed on 2304 cold drawn and parent DSS in alkaline solutions (pH 12.5) and in mortar is quite similar in evolution but both parameters have different values when exposed to both exposure media.

IV.3. Main achievements in the study of CD-DSS passivation in alkaline media

The electrochemical response of the CD-DSS exposed to alkaline solutions has been analysed both under controlled and natural conditions. The results allow concluding that:

- The pH of the alkaline media in contact with duplex HSSS, the SS chemical composition and the SS microstructure are significant parameters that control the electrochemical behaviour of the passive layer.
- The higher alkalinity (pH 13.5) of the environment surrounding the CD-DSS interface promotes the enrichment of the passive film with more reactive oxides.
- The presence of Mo in the composition of the SS allows the formation of more electrochemically stable passive films attributed to changes in Fe-oxide and Cr-oxide ratio in the passive film.
- The role of the Mo in the passive film is controlled by the pH of the surrounding media, where the effect of the Mo content in the electrochemical properties of the passive film appears clearly in the highest alkaline solution (pH 13.5).
- The cold drawn deformation process induces the formation of a more refined microstructure in HSSS, which affects positively on the passive film properties at short and long-term exposure to alkaline media.
- The electrochemical response of cold drawn and parent DSS in alkaline solutions and in chloride free mortar is quite reproducible.

V. Results

Corrosion resistance of duplex high strength stainless steels in alkaline media with chloride

V. Corrosion resistance of duplex HSSS in alkaline media with chloride

In the present chapter, the corrosion resistance of 2304 and 2205 (parent and cold drawn) duplex stainless steels against to the chloride action has been evaluated through the analysis of their electrochemical response in different testing conditions, as described in the experimental part. Spontaneous and accelerated depassivation methods were used to highlight the behaviour of these stainless steel types in aggressive electrolytes containing various chloride concentrations and at various temperatures.

Three aspects have been analyzed:

a) The progressive alteration of the passive film due to the presence of chloride.

b) The critical chloride concentration to initiate an active pit.

c) The pitting growth activity.

All these aspects have been analyzed using different electrochemical techniques to understand the variations in the electrochemical response of the tested stainless steel with regard to the change in the composition and microstructure induced by various specific variables (type of duplex stainless steel, different exposure environment,…).

V.1. *Electrochemical response of the passive film formed on duplex stainless steels in presence of chloride.*

The evolution of the electrochemical response of passive films generated on the cold drawn and the parent DSS have been studied in alkaline solutions and in mortar in presence of different chloride concentrations to evaluate the variation of the passive film electrochemical properties with ageing.

Long-term immersion tests have been performed to find out the modifications induced in the passive layers by ageing in chloride-containing alkaline media. Non destructive electrochemical measurements have been employed to follow up the progressive changes in the passive film with the immersion time: corrosion potential (E_{corr}), corrosion current densities (i_{corr}), and electrochemical impedance spectroscopy (*EIS*) were monitoring.

The DSS were immersed in alkaline free-chloride solution, saturated $Ca(OH)_2$ (pH 12.5), for seven days to allow the spontaneous growth of a stable and protective passive film on the HSSS surface prior the exposure to chloride. This procedure was employed to approach the field conditions where the passive film is first formed and is present for years before the chloride ingresses through the concrete cover and reaches the rebar level. This period of 7 days was enough to ensure the formation of the passive film as shown in chapter IV (Fig.IV.10 and Fig.IV.11). After the prepassivation step, different NaCl concentrations, depending on the type of the stainless steels and on the alkalinity of the electrolyte, were added to the alkaline solution.

Regarding the evaluation of electrochemical behaviour of the passive film formed on DSS embedded in mortar, the response of the stainless steels in presence of chloride has been studied in chloride mixed-in mortar with different chloride percentage respect to the cement weight. Similar non destructive electrochemical measurements (E_{corr} and i_{corr}) have been monitored at different exposure ages to follow up the changes induced in the passive film by the presence of chloride.

V.1.1. In simulated pore-alkaline solutions

Fig. V.1 shows the long-term evolution of the corrosion potential of both 2304 parent and cold drawn DSS in saturated $Ca(OH)_2$ solution with 0.0, 0.5, 0.75, 1.0, and 2.0 M NaCl added after 7 days of prepassivation in alkaline free-chloride solutions. During the whole test, the temperature of the electrolyte was kept constant at 25 °C and the pH of the solution was periodically measured to confirm that no carbonation reaction occurred during the test.

The initial E_{corr} of parent and cold drawn stainless steel rebars, after 7 days of prepassivation, were -166 ± 8 and -220 ± 12 mV_{SCE} respectively. The mean value of the 10 steels rebars studied for each type has been considered.

After the addition of different NaCl concentrations to the alkaline media (two rebars for each case have been studied), a tendency to nobler E_{corr} values (-200 to -100 mV_{SCE}) was monitored for cold drawn and parent stainless steels due to the chloride addition. No corrosion initiation could be identified during the long-term exposure, neither for the 2304 cold drawn nor the parent DSS rebars, even at chloride concentrations up to 2 M NaCl.

However, a certain effect on the electrochemical response of the passive film can be observed in presence of chloride (Fig. V.1.). Moreover, the influence of the microstructure and the steel surface on the electrochemical behaviour of the grown passive films can also be expected as different E_{corr} values were measured for parent and cold drawn stainless steels.

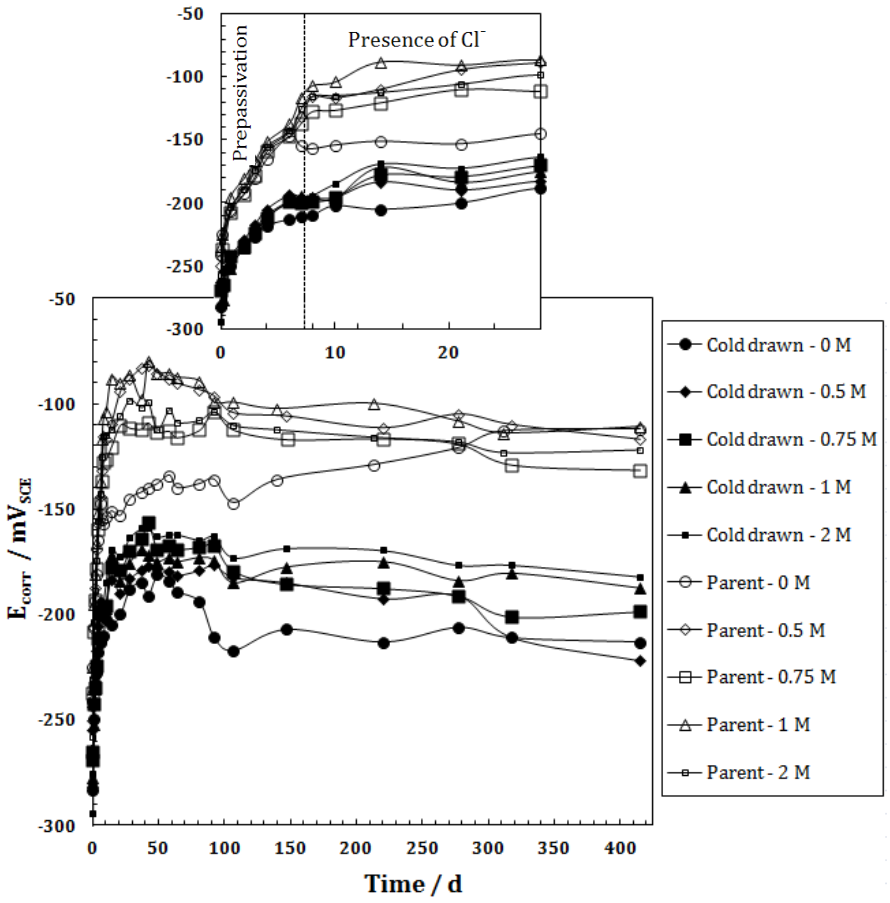

Fig. V.1 Corrosion potential (E_{corr}) evolution of 2304 P and CD DSS in saturated $Ca(OH)_2$ solution with 0.0, 0.5, 0.75, 1.0, and 2.0 M NaCl at 25 °C.

The E_{corr} shift to more positive values indicates the predominance of oxidation processes on the passive layer with the increase of the chloride content. The higher content

of chloride in the alkaline medium seems to be related with the enhancement of oxidative transformations of the elements compounding the passive layer. The enrichment of the passive layer in Fe^{III} ions have been reported as a possible cause of the E_{corr} shift to more anodic values [46], although the contribution of other oxidation processes, such as the formation of chromates, also takes place.

Furthermore, the effect of the cold drawn deformation process on the electrochemical response of the duplex stainless steel in presence of chloride can also be deduced from the E_{corr} evolution. Parent stainless steels show more anodic E_{corr} values than the cold drawn ones. This fact can be attributed to the higher surface roughness of parent DSS, see Fig.III.2, as the cold drawn deformation process usually produces a brighter smooth surface [188]. The higher surface roughness of P-DSS involves different exposed active area for oxygen access as suggested in [46,189], which enhances the formation of a more oxidized passive layer due to the major oxygen availability at the interface level, inducing higher corrosion potential values for parent stainless steels. Additionally, the cold drawn deformation process on the stainless steel rebars can modify the electrochemical properties of the steel surface. Gutman [190] has attributed this fact to the residual stress increase associated to the cold drawn deformation that promotes more cathodic values of the electrode potential.

Fig. V.2 depicts the evolution of the calculated corrosion current density (i_{corr}) For cold drawn and parent 2304 DSS. During the 7 days of prepassivation stage in alkaline solution (pH 12.5), a quasi steady state with low values of i_{corr} was reached for cold drawn and parent DSS. The addition of chloride induces the increment of i_{corr}, especially in the

case of parent DSS, which show significantly higher values of i_{corr} in presence of chloride than the cold drawn wires, as shown in Fig.V.2.

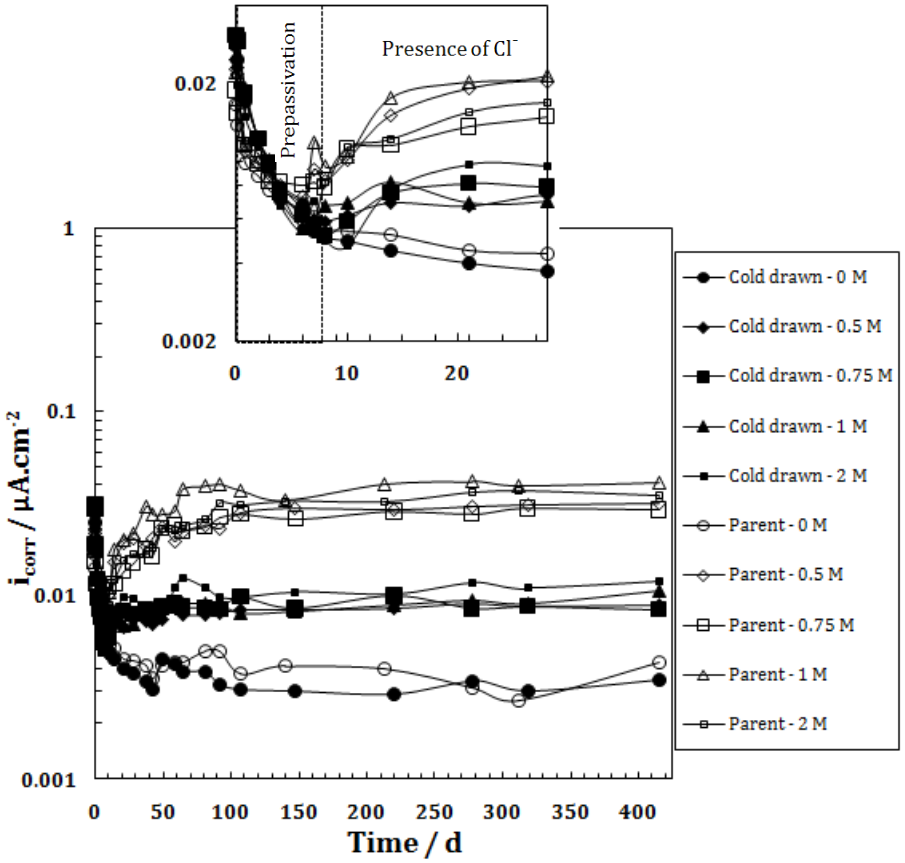

Fig. V.2 Corrosion current density (i_{corr}) of P and CD 2304 SS in saturated $Ca(OH)_2$ solution with 0.0, 0.5, 0.75, 1.0, and 2.0 M NaCl at 25 °C.

If the criteria of values of i_{corr} > 0.2 µA/cm^2, accepted for steel rebars to indicate the corrosion initiations [126], is considered as a reference in the case of SS, no indication of the initiation of an active corrosion process can be deduced from the i_{corr} results of both parent and cold drawn wires, even in presence of high concentrations of chloride (2 M).

On the other hand, the increase of i_{corr} with the chloride concentration observed for both P and CD stainless steels does not agree with the hypothesis of enrichment of the passive layer in Fe^{III} oxides expected from the nobler E_{corr} evolution (Fig. V.1), as higher presence of Fe^{III} would promote a less conductive passive film and thus, lesser values of i_{corr} should be registered. Then, the presence of chloride seems to promote the formation of other oxidized species, such as chromates, which are dissolved in the high alkaline electrolytes. In this sense, the oxidation of the external passive layer enriched in $Cr(OH)_3$ seems to be the most affected process, promoting a higher dissolution of the passive layer through the formation of soluble CrO_4^{2-} and, consequently, the diminution of the passive layer thickness. The decrease in Cr^{III} content in the passive film formed in presence of chloride was confirmed elsewhere [46] for austenitic stainless steels.

Although no significant differences between i_{corr} of parent and cold drawn SS were reported in alkaline media in absence of chloride, higher i_{corr} values have been registered for the 2304 parent DSS when chlorides are added to the alkaline solution. The activation of Cr^{III} oxidation process, giving higher i_{corr} values as observed in Fig.2, could be expected in the case of parent stainless steels as consequence of the higher roughness of its surface and/or the parent stainless steel grain size (large grains).

The comparison of E_{corr} and i_{corr} values of 2304 cold drawn and parent DSS in presence of chlorides indicates that, in addition to the changes in the chemical composition of the passive film induced by the ageing in chlorinated alkaline media, the nature of the steel surface has a significant impact on the electrochemical response of the passive film. In other words and in agreement with the observed results in previous chapter, the

roughness of the film surface can also be the origin of the different oxidability of both cold drawn and parent wires because of the different exposed active area.

Electrochemical impedance spectroscopy (*EIS*) measurements were also carried out in the same exposure conditions in order to obtain additional information about the changes in the properties of the passive film promoted by the addition of chloride to the alkaline medium, a more detailed description of the obtained results are included in Appendix II.

To point out the effect of the chloride content on the electrochemical response of the passive film, the Nyquist and the Bode plots of parent 2304 SS after 133 days of immersion in presence of 0.5, 0.75, 1, and 2 M NaCl are displayed in Fig.V.3. The impedance magnitude falls with increasing the chloride content, being more evident in 2 M NaCl (Fig.V.3a). This fact agrees with the less protective response of these passive layers as the chloride content increases (Fig.V.3b).

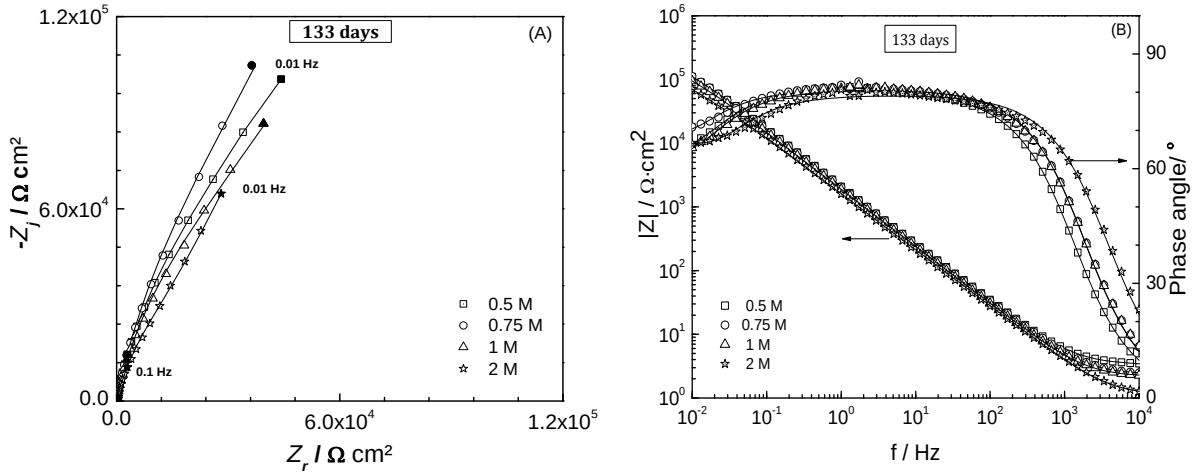

Fig. V.3 Nyquist (A) and Bode (B) plots of parent 2304 SS after 133 days of immersion in sat. $Ca(OH)_2$ solution with different chloride concentrations. Experimental data (dots), fitting with 2*RC* equivalent circuit (solid lines).

To identify the difference in the electrochemical response of both 2304 parent and cold drawn DSS by ageing, Nyquist plots of both DSS after 305 days of immersion in saturated $Ca(OH)_2$ solutions with 1 and 2 M NaCl are shown in Fig.V.4.

Comparing the parent and cold drawn EIS spectra at the same immersion time, higher capacitive behaviour is observed for the cold drawn stainless steel probably due to the formation of passive film electrochemically more stable. Furthermore, the change in the impedance value of cold drawn SS with increasing the chloride content was smaller in comparison with the values obtained for the parent SS at the same conditions, as shown in Fig.V.4, and thus, higher modifications of the passive film induced by the presence of chloride can be expected in the case of parent stainless steels, which in fact agree with the high i_{corr} of P-DSS given in Fig.V.2.

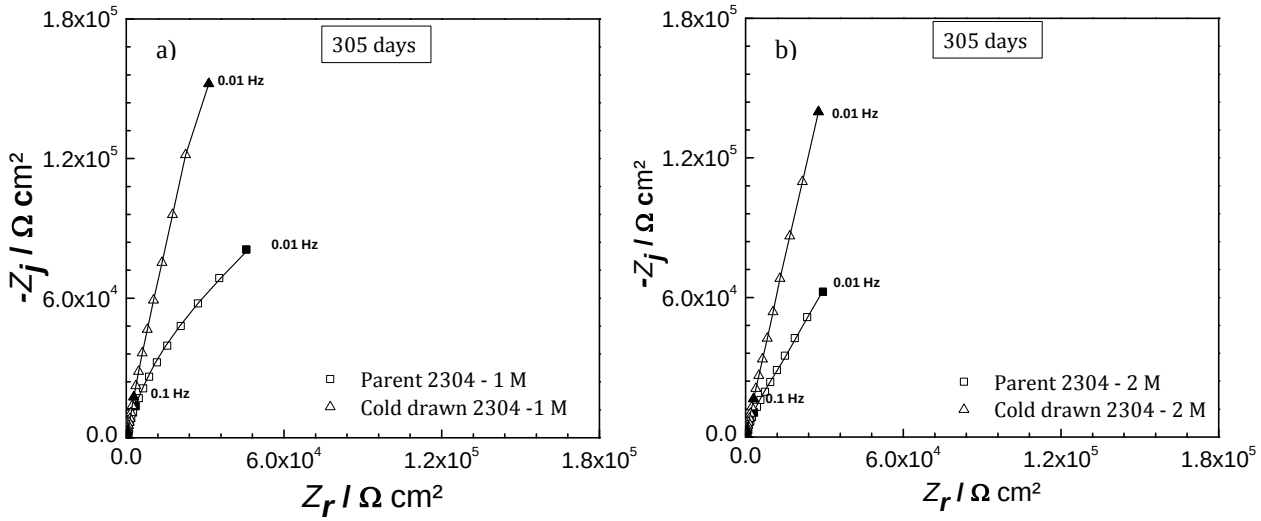

Fig. V.4 Nyquist plots of 2304 parent and cold drawn DSS after 305 days of immersion in sat. $Ca(OH)_2$ solution with (a) 1 M and (b) 2 M NaCl. Experimental data (dots), fitting with 2*RC* equivalent circuit (solid lines).

V.1.2. In chloride mixed-in mortar

The electrochemical response of the passive film formed on 2304 DSS embedded in mortar mixed-in with difference chloride percent (% Cl^- with respect to cement weight) has been analyzed by employing non destructive electrochemical measurements (E_{corr} and i_{corr}) in two different climatic conditions similar to applied conditions, in the case of passivation in mortar samples: firstly, the mortar samples were exposed to RH 95% during the first 19 days and after that, they were exposed to drier conditions, RH 80% till 30 days. The temperature was maintained constant at 23 °C along the whole test. Three wires of each DSS have been tested to confirm the repeatability of the electrochemical measurements.

Fig.V.5 shows the variation of E_{corr} of 2304 parent and cold drawn DSS embedded in chloride mixed in mortar with 2, 3 and 4% Cl^-. For all rebars, the E_{corr} is shifted to nobler potentials during the first 5 days until reaching a steady state potential: E_{corr} values were -155±5 mV_{SCE} for the parent DSS and -122±10 mV_{SCE} for the cold drawn DSS.

It is noteworthy that the parent SS presents more anodic E_{corr} than cold drawn wires in agreement with E_{corr} results in alkaline solutions that simulate the aqueous phase of concrete pores (see Fig.V.1). Besides, increasing the chloride percentage (% Cl^-) induces an anodic shift in E_{corr}, which probably related to the enhancement of oxidation processes on the passive film. These oxidative transformations seem to be affected by the RH of the surrounding environments, as the E_{corr} decreases when mortar samples were exposed to RH of 80%, as shown in Fig.V.5.

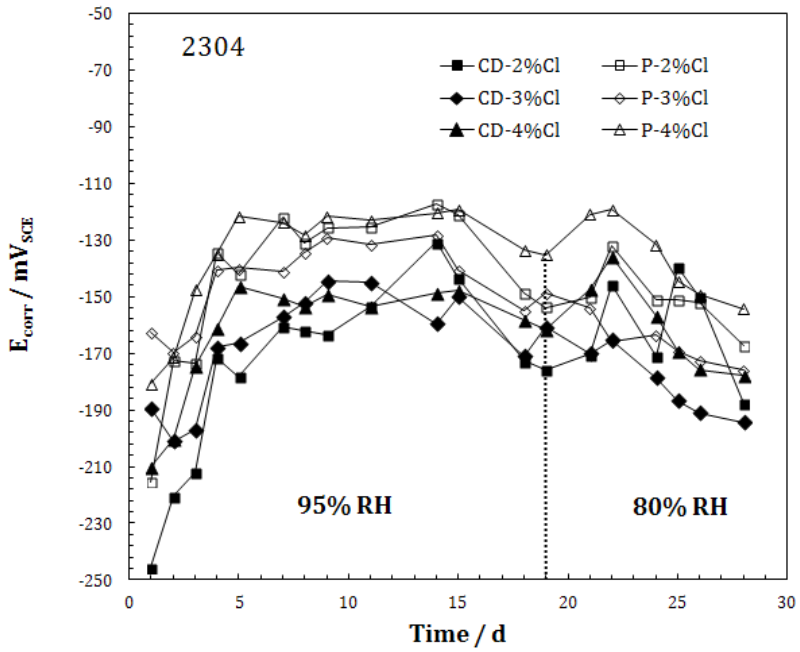

Fig.V.5 Corrosion potential (E_{corr}) evolution of parent and cold drawn 2304 SS embedded in chloride mixed-in mortar with 2,3, and 4%.

No corrosion initiation has been defined during the exposure time to chloride, even at chloride concentrations up to 4% Cl^-. However, the presence of chloride in the embedded DSS interface induces certain effects on response of the grown passive film. This variation on the electrochemical response of the passive film is highly influenced by the DSS microstructure.

Fig.V.6 displays the variation of i_{corr} of 2304 parent and cold drawn duplex DSS in the same conditions. During the first period of curing in the higher RH conditions, the i_{corr} decreases asymptotically with ageing until reaching steady state low i_{corr} values due the passive film growth on the embedded DSS surface.

Both parent and cold drawn DSS present low values of i_{corr} with ageing in chloride mixed-in mortar ($i_{corr} \approx 0.01$ μA/cm²). Although the cold drawn wires show a relatively higher i_{corr} than the parent stainless steels, i_{corr} values of cold drawn DSS corresponds to a passive state. No clear effects of the chloride concentration on i_{corr} values have been observed and no indication of active pits initiation has been identified for both DSS even in case of 4% Cl^-. Furthermore, no relevant changes in i_{corr} were measured by moving from a wet condition with 95% RH to drier conditions with 80% RH.

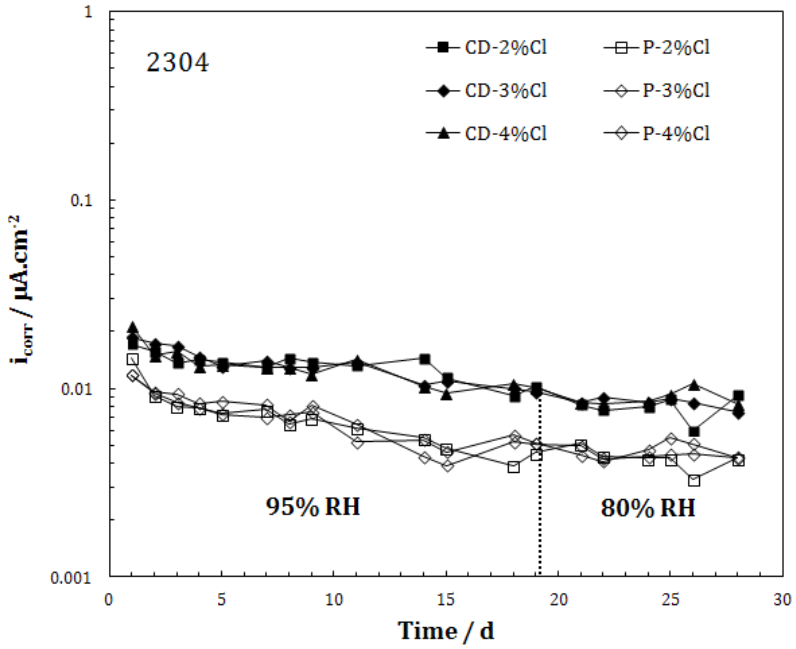

Fig.V.6 Corrosion current density (i_{corr}) of parent and cold drawn 2304 SS embedded in chloride mixed-in mortar with 2,3, and 4%.

V.2. Onset of chloride induced pitting corrosion: Critical chloride threshold determination

It is clear from the previous section that there is a noticeable impact of the chloride on the electrochemical response of the passive film before the initiation of the active pits on the DSS surface, which leads to weaken the protective properties of the passive film and finally to the nucleation of pits and the breakdown of the passive film.

The parameter named as the Critical Chloride Threshold (CCT) is usually employed to characterize the protection ability of reinforcements throughout the determination of the minimum chloride content capable to nucleate a pit and breakdown the passive film. In the case of the stainless steel, the determination of CCT is a very complex task due to its large protection ability, long testing times are expected to be consumed if using natural test. Thus, simplified and/or accelerated methods have to be employed to obtained results in reasonable testing time.

The accelerated CCT tests are less time-consuming methods. Potentiodynamic [125,127,191] and potentiostatic [123-124,127] polarization tests have been used by several authors to estimate the CCT required to initiate a pitting corrosion process.

V.2.1. In simulated alkaline pore-solutions

V.2.1.1. Potentiodynamic determination of the CCT

When potentiodynamic polarization is used to identify the breakdown of the passive film due to the presence of chloride, it is generally accepted that the pitting initiates at a

critical pitting potential (E_{pit}), which is characterized by a sharp and irreversible increase in the current density. In the case of stainless steels, due to their high corrosion resistance, the oxygen evolution peak is often reached before the E_{pit} potential [192]. Accordingly, some authors [140,151,191-194] performed the potentiodynamic polarization curves up to a potential more anodic than the limit of oxygen evolution in order to identify risk of corrosion initiation of different stainless steels wires in presence of different chloride contents.

The CCT value of 2304 and 2205 high strength and parent duplex stainless steels has been investigated by this technique and the influence of several significant parameters on the CCT value has been discussed.

a) Effect of natural ageing in presence of chloride

At the end of the long-term immersion test of 2304 parent and cold drawn DSS in alkaline solutions (pH 12.5) with different chloride concentrations, the stainless steels had not shown a clear evidence of active corrosion when non destructive electrochemical techniques was considered (E_{corr}, i_{corr} and *EIS*). Then, the application of destructive technique, such as the potentiodynamic polarization test was used to evaluate the susceptibility to pitting corrosion of the passive layer after the long-term exposure to the presence of chloride and to obtain the CCT value for both stainless steels.

Fig. V.7 shows the cyclic polarization curves of parent (Fig.V.7a) and cold drawn (Fig.V.7b) stainless steels after the long-term ageing (416 days) in Cl^- containing alkaline media. These cyclic voltammograms were performed in each wire starting at the E_{corr} value in order to not modify the existent passive film. To get the cyclic voltammograms, the

potential was firstly scanned from E_{corr} up to +0.9 V_{SCE} and secondly down to -1.2 V_{SCE}. The last step was another anodic polarization from -1.2 V_{SCE} up to the initial E_{corr} value.

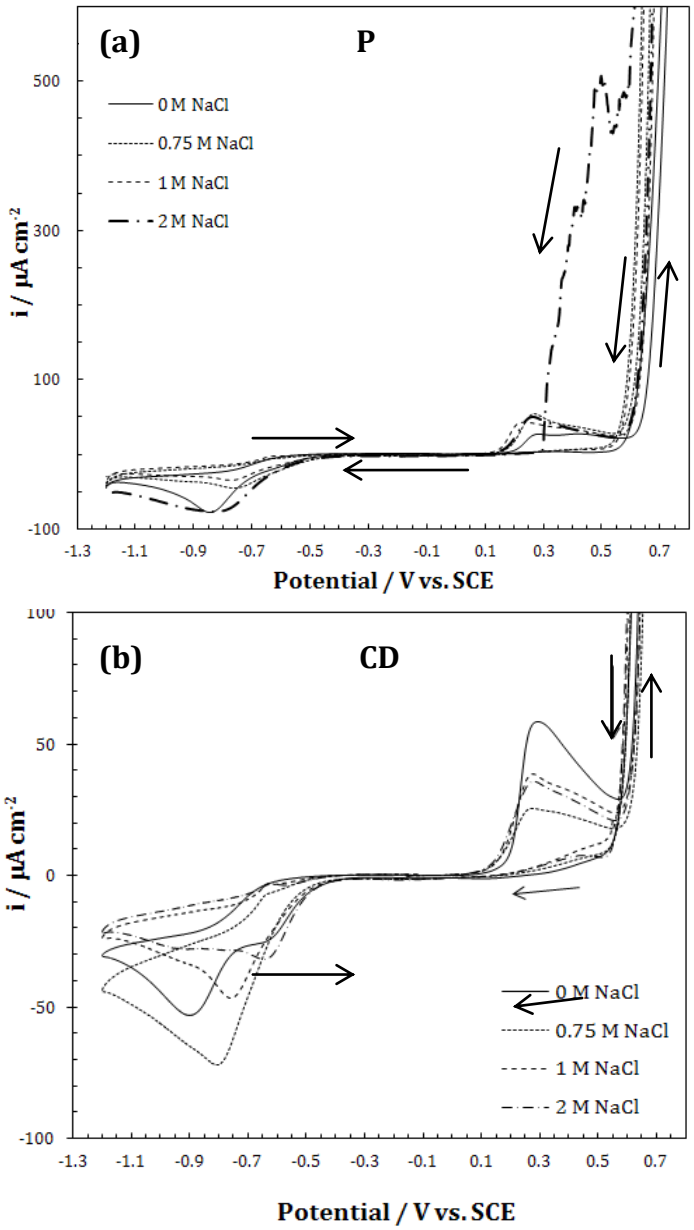

Fig. V.15. Cyclic voltammograms of 2304 (a) parent and (b) cold drawn DSS after 416 days of immersion in sat. $Ca(OH)_2$ solutions with different chloride concentration.

A wide passivity region with low residual current density due to the presence of the passive film is observed both in parent (Fig.V.7a) and in cold drawn (Fig.V.7b) stainless steels even in the highest chloride content solutions.

No clear E_{pit} can be distinguished from cyclic voltammograms in any case, even at the highest concentration of chloride (2 M) neither for parent nor for cold drawn stainless steels. At around +0.65 V_{SCE} the current sharply increases due to the oxygen evolution from water hydrolysis process.

Although no pitting potential is detected in the anodic scan, a local corrosion process is initiated in the case of 2304 parent stainless steel when the chloride content was increased up to 2 M NaCl, as can be observed from Fig.V.15a. The susceptibility to corrosion initiation in this case is detected in the cathodic scan, where high anodic current density values are registered. At these anodic potentials, the oxidation of the Cr^{III}-oxide contained in the passive layer to form CrO_4^{2-} ($Cr_2O_3 + 5\ H_2O \rightarrow 2\ CrO_4^{2-} + 10\ H^+ + 6\ e^-$) and the O_2 evolution process ($2\ H_2O \rightarrow O_2 + 4H^+ + 4\ e^-$) occur [46,43,130]. Furthermore, the formation of H^+ takes place during these oxidative reactions and thus local acidification of the steel surface can occur as suggested in [143,195]. Then a higher susceptibility to pitting corrosion is obtained for the parent duplex 2304 SS when compared with the cold drawn one, that is in agreement with the long-term electrochemical measurements carried out in alkaline media with different chloride additions (see Fig.V.4).

It has to be pointed out that the presence of chloride in the alkaline solution shows a certain effect on the transpassivity domain of the cyclic voltammograms of 2304 parent and cold draw DSS. For studying in details of this region, enlarged areas of the

transpassivity domain in the cyclic voltammograms (Fig.V.7) are shown in Fig. V.8, where the main peaks of this potential domain can be clearly distinguished. Oxidation peaks related to redox process of Cr^{III}/Cr^{VI} and Ni^{II}/Ni^{III} (eq. V.2 and eq. V.3 respectively) are occurring.

The current increase observed at about +0.3 V_{SCE} with the increase of the chloride content reveals that chromium oxide dissolution is taking place through the equation V.2 as suggested in [59, 130,151]:

$$Cr_2O_3 + 10\ OH^- \rightarrow 5\ H_2O + CrO_4^{2-} + 6e^- \qquad \textit{eq. V.2}$$

According to literature [196-197], the peak at around +0.5 V_{SCE} is related to the redox process of Ni^{II}/Ni^{III} and could be written as in equation V.3:

$$Ni(OH)_2 + OH^- \rightarrow NiOOH + H_2O + e^- \qquad \textit{eq. V.3}$$

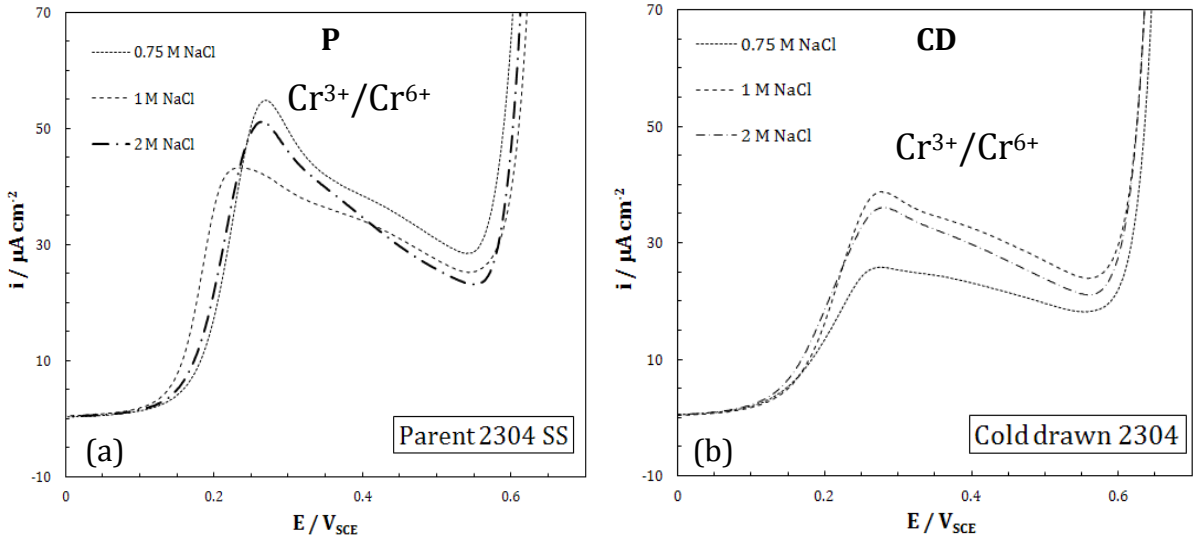

Fig. V.8. Enlarged area from Fig. V.15 (0 to +0.7 V_{SCE}) of cyclic voltammograms of (a) parent and (b) cold drawn 2304 SS after 416 days of immersion in alkaline solutions with chloride.

The results obtained from Fig.V.8a. and Fig.V.8b reveal an important increase in the current density values of the transpassivity region in both cases, parent and cold drawn stainless steels, with the increase of the chloride content probably due to a higher activation of the Cr^{III} oxidation process, as it was proposed from i_{corr} long-term measurements (Fig.V.2). The increase of the reaction rate of Cr oxidation (eq. V.2) may promote the partial loss of the protective ability of the passive film as a result of the Cr^{III}-oxy/hydroxide consume. The lesser values of current density registered in the transpassive domain for the cold drawn stainless steel (Fig. 8b) when compared with the parent SS (Fig. 8a) reflect a smaller effect of the chloride on the transpassive processes of CD, probably due to the higher stability of the passive layer growth on the cold drawn surface, in agreement with EIS measurements during the long-term test (Fig.V.4).

On the other hand, the clearer appearance of the peak assigned to Ni^{II}/Ni^{III} oxidation process (around +0.5 V_{SCE}) as a shoulder overlapped with Cr^{III} oxidation process indicates a possible enrichment in Ni-oxide in the passive film by long-term immersion in alkaline solution containing chloride. The enrichment of Ni-oxide as Ni^{II} in the passive film was also confirmed elsewhere [33,46,58,198-200] and it has been related with the depletion on Cr^{III} content in the passive layer interface due to the chromates dissolutions process [55]. This fact has been observed for both parent and cold drawn stainless steels, as shown in Fig.V.8a and Fig.V.8b.

At the end of the long-term immersion test (after 416 days), the rebar showing higher i_{corr} values of each test was removed from the solution and optically examined to study the parent and cold drawn stainless steel initial surface before the CV

electrochemical test. Furthermore, the rebars submitted to the polarization curves were also optically examined after the test.

In Fig.V.9 some photographs of the optical examination of the cold drawn and parent stainless steel wires have been displayed. After the long-term immersion test, no formation of deep pits, neither on cold drawn nor on parent SS, was observed.

Test type	Cold drawn	Parent
After natural long-term immersion	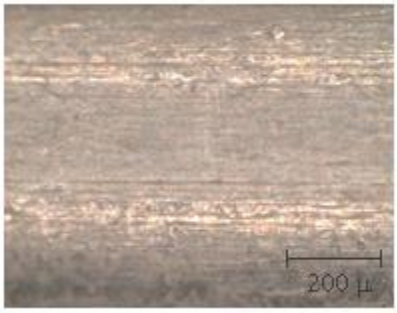	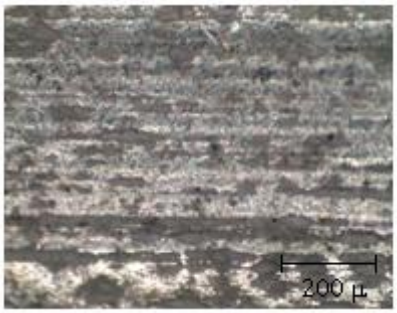
Cyclic voltammetry (CV) after natural long-term immersion test	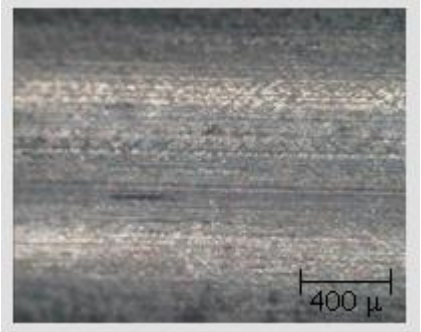	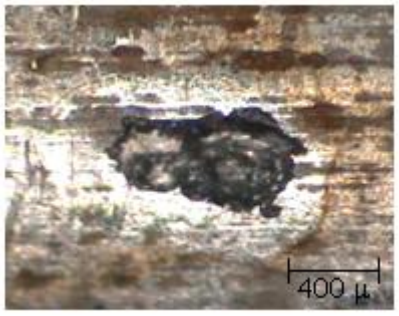

Fig. V.9 Optical examination of 2304 SS after long- term immersion and CV tests in saturated $Ca(OH)_2$ solution with 2.0 M NaCl.

After the CV test was carried out at the end of the 416 days of immersion, deep pits were nucleated on the surface of the parent stainless steels in presence of 2 M NaCl, as shown in Fig. V.9. No pitting initiation was detected in case of cold drawn stainless steel surface at the end of the immersion, neither after the polarization curve.

b) Effect of the alkalinity and cold drawn deformation

Fig.V.10 shows the case of 2304 parent and cold drawn DSS immersed in saturated $Ca(OH)_2$ solutions with different chloride concentrations from the beginning of the test, without previous pre-passivation stage. In this case, potentiodynamic polarization curves have been performed immediately after the immersion of the tested wires in the alkaline solutions containing chloride.

Specimens of the parent SS (Fig.V.10a) did not show any pitting corrosion evidence in alkaline solutions until 0.1 M NaCl, but the pitting corrosion was initiated when the chloride content increased at 0.2 M NaCl and high current densities were registered in the cathodic reverse curve, as depicted in Fig.V.10a. This concentration of chloride could be established as the CCT for parent 2304 SS when immersed in alkaline solutions of pH 12.5.

Regarding the CCT for the cold drawn SS, the potentiodynamic tests at the same conditions indicate that these SS wires are more resistant against pitting corrosion than the parent type as the corrosion in the cold drawn SS is only initiated in saturated $Ca(OH)_2$ solutions with 0.3 M NaCl added (Fig.V.10b).

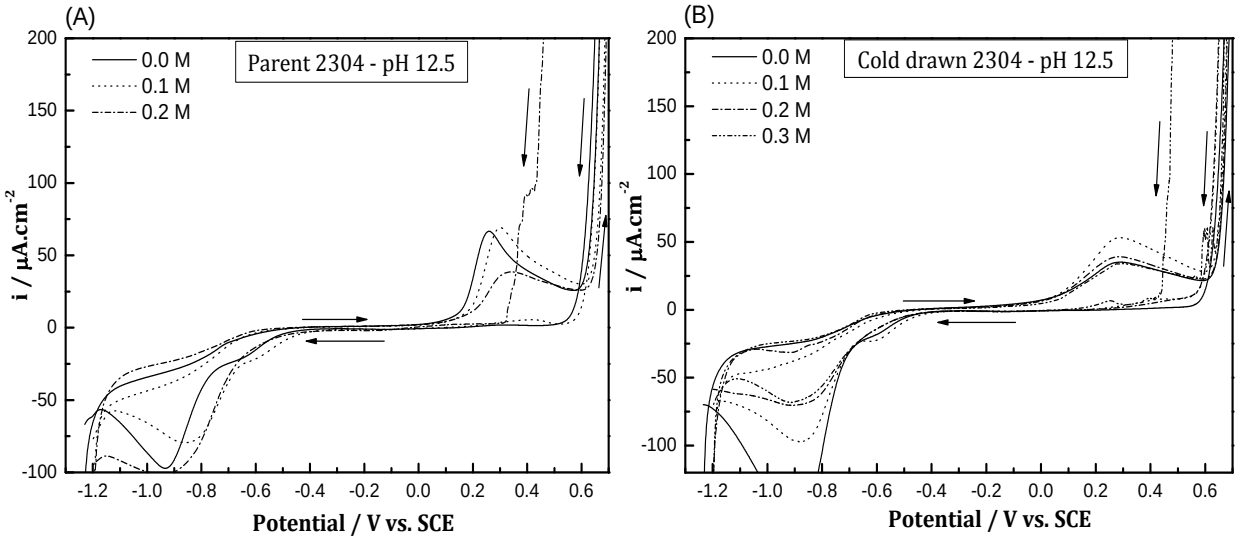

Fig. V.10. Cyclic voltammograms of 2304 (A) parent, and (B) cold drawn duplex DSS in saturated $Ca(OH)_2$ solutions with different chloride concentrations

Fig.V.11 displays the cyclic voltammograms of 2304 parent and cold drawn duplex DSS in more alkaline solutions of pH 13.5 (saturated $Ca(OH)_2$ – 0.5 M KOH solutions).

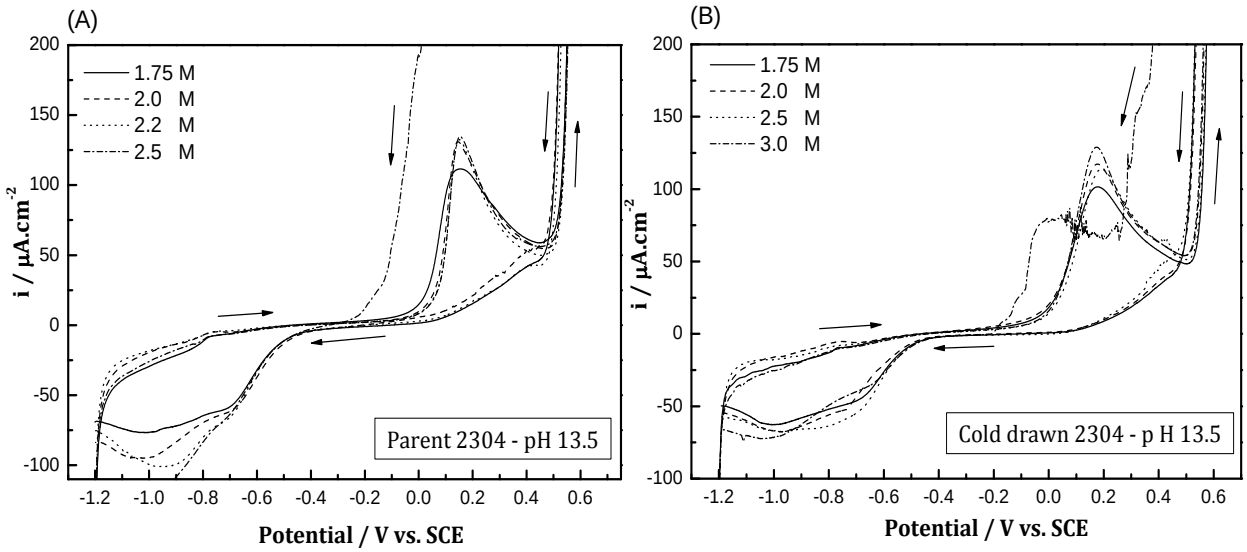

Fig. V.11. Cyclic voltammograms of 2304 (A) parent, and (B) cold drawn DSS in saturated $Ca(OH)_2$ – 0.5 M KOH solutions with different chloride concentrations.

Similar behaviour of both types of stainless steel is observed in these more alkaline conditions: parent stainless steel shows higher susceptibility to pitting corrosion than cold drawn stainless steel. With the increase of the pH from 12.5 to 13.5 the CCT increases in one order of magnitude up to 2.5 M for the parent SS and to 3 M for the cold drawn SS.

In table V.1, the CCT determined in the different experimental conditions studied has been resumed.

Table V.1 CCT of 2304 parent and cold drawn DSS after CV.

	Sat. $Ca(OH)_2$ pH ≈ 12.5 – 25 °C		**Sat. $Ca(OH)_2$ - 0.5 M KOH pH ≈ 13.5 – 25 °C**	
	Parent	**Cold-drawn**	**Parent**	**Cold-drawn**
CCT / mol.l^{-1}	0.2	0.3	2.5	3.0

Both the chloride content and the pH of the alkaline solution induce certain influence on the cyclic voltammograms of 2304 parent and cold drawn DSS, especially in the transpassivity domain. Fig.V.12 shows a detailed study of the transpassivity region for the cyclic voltammograms of both parent and cold drawn cyclic voltammograms in alkaline solutions of pH 12.5 and 13.5 in presence of different chloride concentrations.

Independently on the stainless steel type (parent or cold drawn) and on the immersion media (pH 12.5 or 13.5), the chloride addition seems to induce the increase of the transpassive current density, similarly than occurred in the case of the potentiodynamic curves obtained after the long-term immersion of the stainless steels in a saturated $Ca(OH)_2$ solution with different chloride concentrations after a 7 days of prepassivation (see Fig. V.8). In present case, where no formation of a previous passive

layer has been allowed, only one oxidation peak corresponding to the chromates formation from the oxidation of chromium (III)-hydroxide around +0.2 - +0.3 V_{SCE} can be clearly distinguished. The chromium dissolution should promote the formation of a less protective and thinner passive layer with the increase of the chloride concentration in the alkaline solutions.

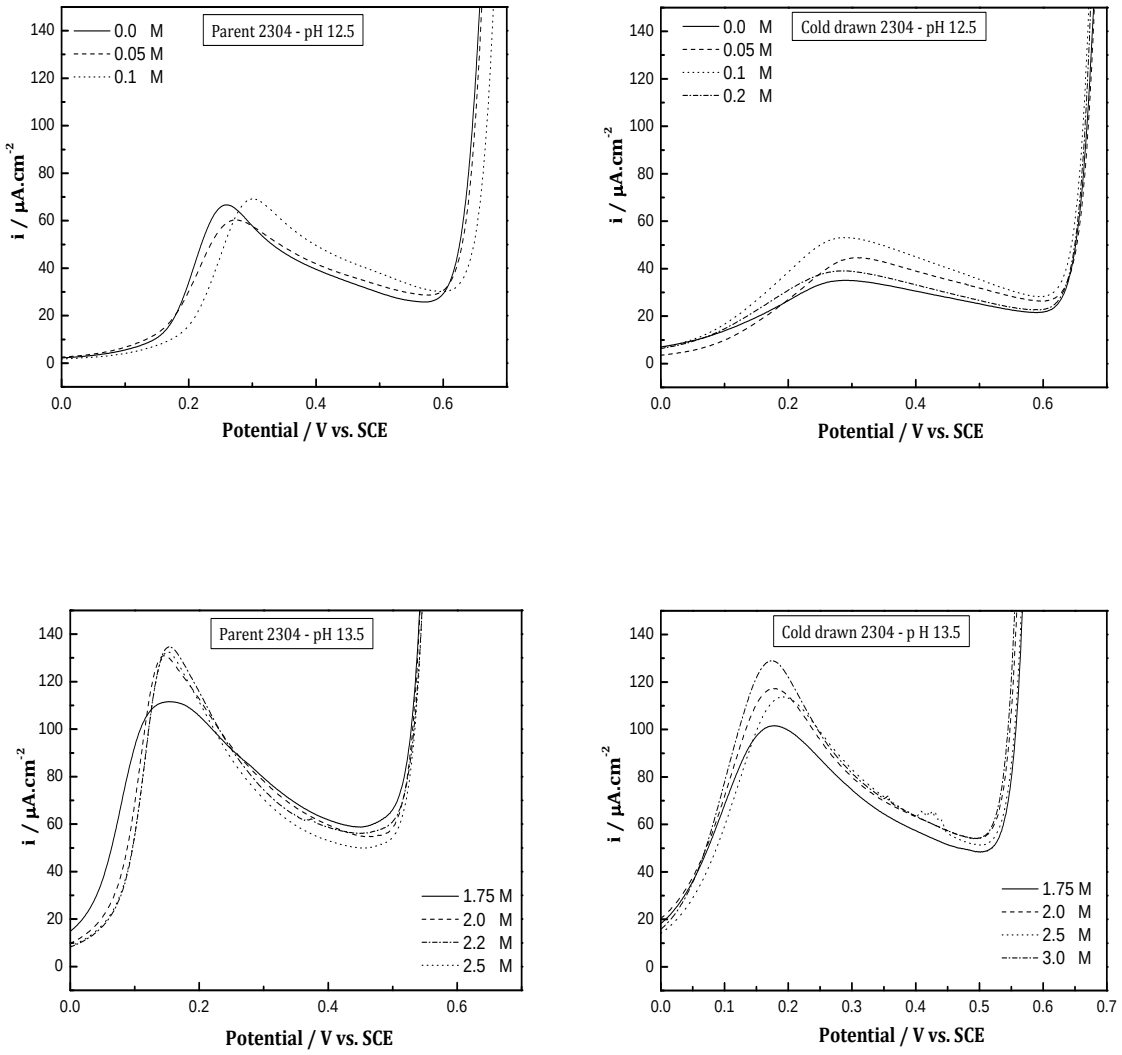

Fig. V.12. Zoom on the transpassive region of Fig.V.20 and Fig.V.21 (cyclic voltammograms of 2304 parent and cold drawn DSS in alkaline solutions of pH 12.5 and 13.5 with different chloride content).

Furthermore, a significant increase in the current density of the transpassive region is observed for the most alkaline solution (pH 13.5) when compared with alkaline solutions of pH 12.5 (Fig. V.12). As discussed in chapter IV, the higher current densities registered in this peak for the most alkaline solutions are associated with the enhancement of chromates production because of the higher pH. In the most alkaline medium the pit initiation occurs at higher CCT values (Fig.V.10 and Fig.V.11), even if the loss of the passive layer thickness is enhanced by a more active chromium dissolution process. The higher pH seems to have a positive effect on the electrochemical response of the passive layer, not only because of the smaller $[Cl^-]/[OH^-]$ ratio existent at the passive layer/electrolyte interface but probably also due to the presence of chromates at this interface that should be produced in enough concentration to have an inhibitive action [112,201-202] on the steel surface.

As also observed in Fig.V.8 for the voltammograms obtained after the stainless steel immersion in saturated $Ca(OH)_2$ solution with different chloride concentrations with a previous pre-passivation stage, the cyclic voltammograms obtained just after the immersion of the stainless steel in the aggressive solution (see Fig. V.12), without pre-pre-passivation step, agree with the smaller transpassive current density registered for the cold drawn stainless steel. Thus, the smaller chromium dissolution registered for this type of stainless steel will match with the higher pitting corrosion resistance observed for the cold drawn stainless steel.

c) Effect of Mo content

The effect of the SS alloy composition on the pitting corrosion resistance of duplex stainless may be as important as the impact of the pH and the microstructure previously discussed.

Fig.V.13 depicts the cyclic voltammograms of the parent and cold drawn 2205 duplex stainless steels exposed to a saturated $Ca(OH)_2$ solution containing different chloride contents up to 5.5 M NaCl. The hysteresis loop indicating the initiation of a pitting corrosion process was not observed at any chloride concentration neither for the parent nor for the cold drawn stainless steels.

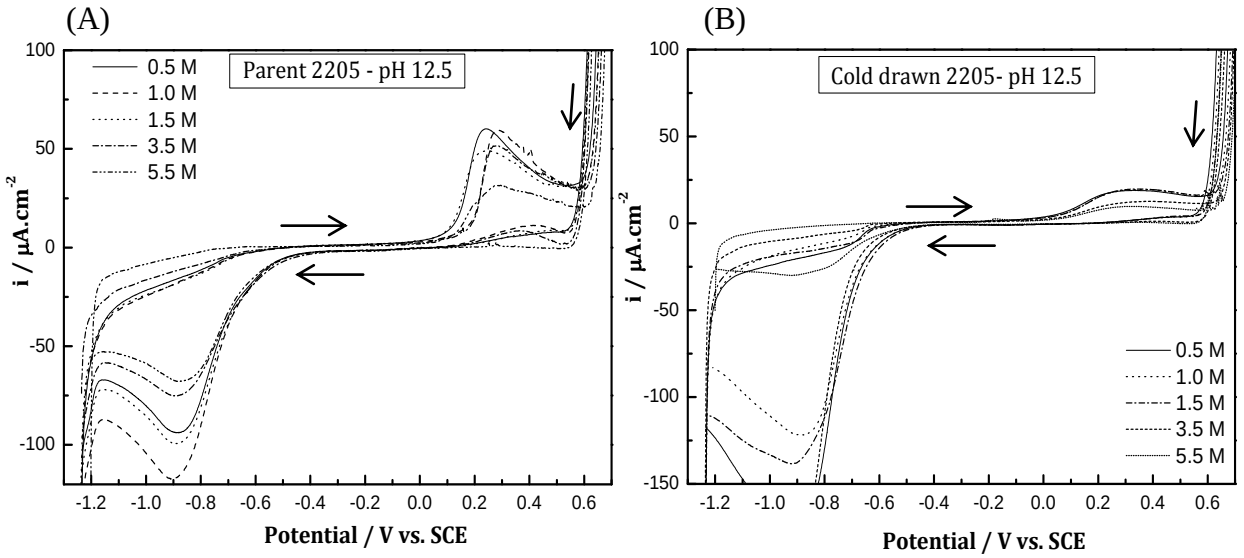

Fig. V.13. The Cyclic voltammograms of 2205 (A) parent, and (B) cold drawn DSS in saturated $Ca(OH)_2$ solutions with 0.5, 1, 1.5, 3.5 and 5.5 M NaCl at 25 ° C.

The effect of the chemical composition can be deduced comparing Fig.V.10 and Fig.V.13. In the case of the duplex 2205 SS (Fig.V.13) no pitting could be observed at any

concentration of chloride, up to 5.5 M NaCl, while in the case of the duplex 2304 SS, the CCT was 0.2 M for the parent SS and 0.3 M for the cold drawn when immersed in pH = 12.5 (Fig.V.10).

To analyze the influence of the chloride content on the transpassivity domain of duplex 2205 SS (Fig.V.13), the enlarged area of this region is shown in Fig.V.14a for the parent SS and in Fig.V.14b for the cold drawn SS.

The data displayed in Fig.V.14 indicate that both 2205 cold drawn and parent DSS behave differently from the 2304 SS in the transpassive region when the same testing conditions are considered (Fig.V.12). In the case of 2205 duplex DSS, mainly for the cold drawn SS, the broadening of the transpassive peak can be observed and lesser values of the transpassive current density with the increase of the chloride content are registered. This diminution of the transpassive current density with increasing the chloride content will probably be related to different reasons: (a) the diminution of pH of the alkaline solutions as a result of the elevated chloride concentration (this fact will be discussed in details later). (b) the variation of pH also affects the redox processes of chromium and probably lesser concentration Cr^{III} susceptible to be oxidized to chromate is expected in the less alkaline conditions.

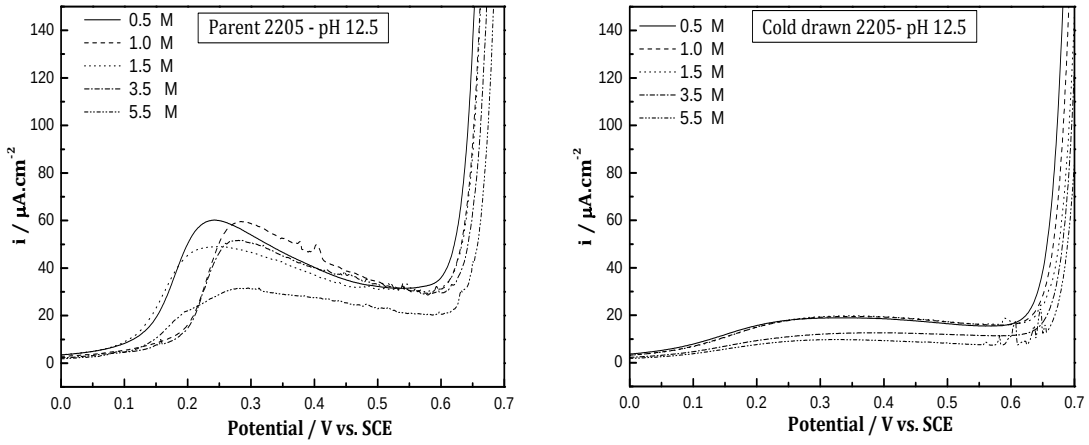

Fig. V.14. Transpassivity domain of 2205 parent and cold drawn DSS in alkaline solutions of pH 12.5 with different chloride content.

Concerning the pitting corrosion risk of 2205 parent and cold drawn DSS in more alkaline solutions of pH 13.5, Fig.V.15 shows the cyclic voltammograms of both parent (Fig.V.15a) and cold drawn 2205 (Fig.V.15b) DSSs exposed to saturated $Ca(OH)_2$ – 0.5 M KOH solutions (pH 13.5) containing 2 and 5.5 M NaCl.

The results shown in Fig.V.15 conclude that no pitting corrosion initiation has been detected in case of 2205 parent and cold drawn DSS even in presence of 5.5 M NaCl. Furthermore, similar electrochemical response of both DSS has been observed in the transpassivity domain (Fig.V.16), where the cold drawn wires showed lower transpassivity current density respect the parent SS. In addition, the transpassivity current in case of parent SS falls with increasing the chloride content (Fig.V.16a).

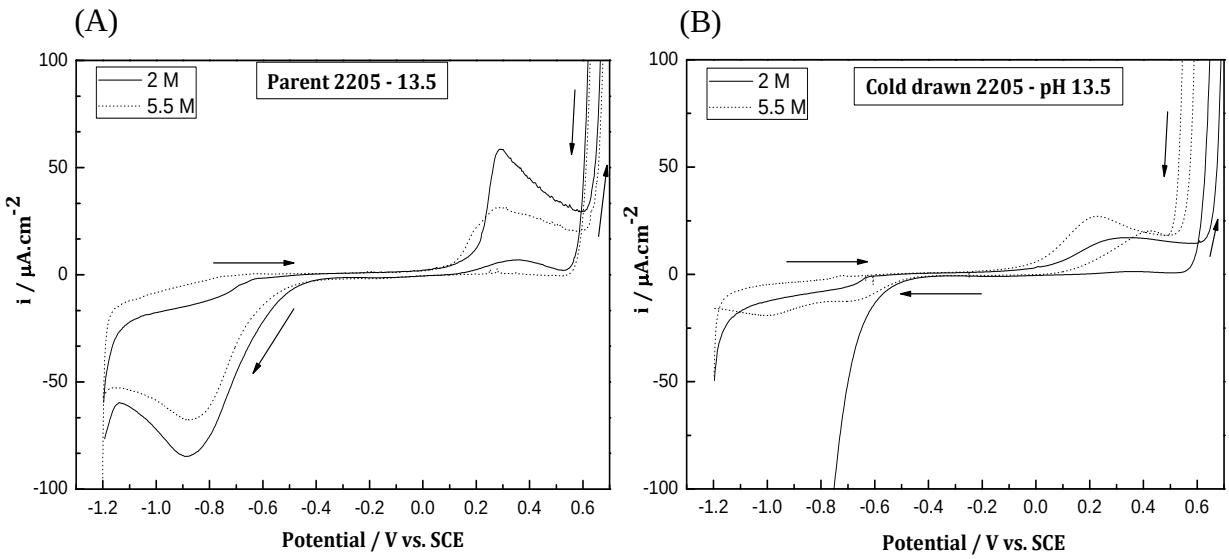

Fig. V.15. Cyclic voltammograms of 2205 (A) parent, and (B) cold drawn DSS in saturated $Ca(OH)_2$ – 0.5 M KOH solutions (pH 13.5) with 2 and 5.5 M NaCl at 25 ° C.

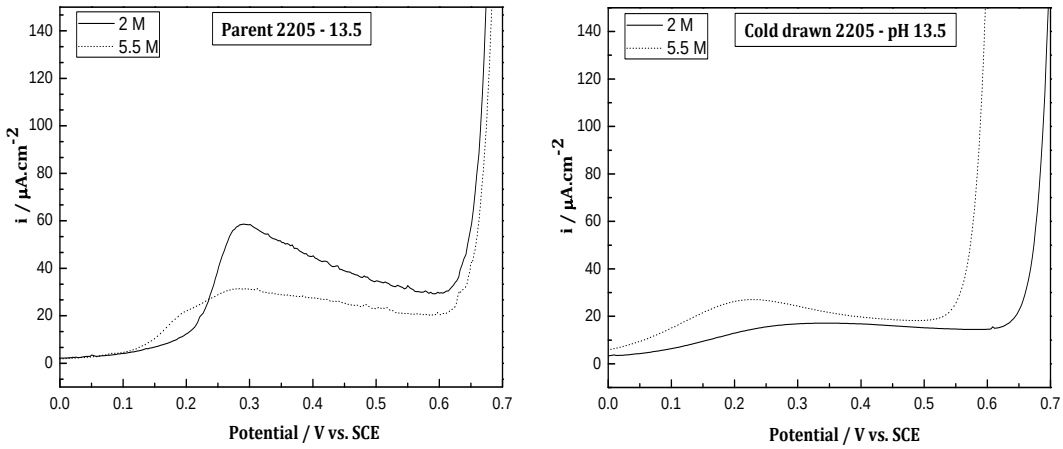

Fig. V.16. Transpassivity domain of 2205 parent and cold drawn DSS in alkaline solutions of pH 13.5 with 2 and 5.5 M NaCl.

d) Effect of external load

In the field conditions, high strength stainless steels will be exposed to an external load of 70% of its maximum strength. This load would affect the risk of pitting corrosion initiation of duplex SS. Fig.V.17 and Fig.V.18 show the cyclic voltammograms of 2304 and 2205 parent and cold drawn DSS, respectively, in saturated $Ca(OH)_2$ solutions containing different concentrations of chloride.

The results show that the application of 70% load has a negative impact on the corrosion resistance of 2304 cold drawn and parent wires (Fig. V.17) and the CCT value decreases from 0.2 M and 0.3 M for parent and cold drawn steels respectively (at 0% load) to 0.1 M for both types of SS when 70% load was maintained during the test.

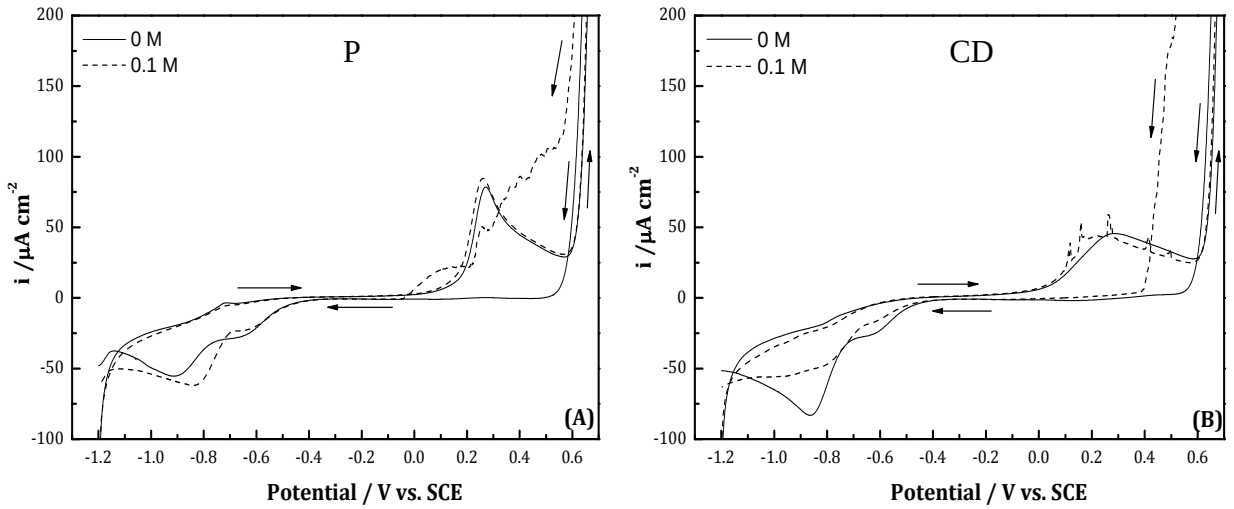

Fig.V.17. Cyclic voltammograms at 70% load of (A) parent and (B) cold drawn 2304 SS in sat. $Ca(OH)_2$ solutions with 0 and 0.1 M NaCl.

The application of 70% of the maximum strength induces certain deformation on the stainless steel surfaces which probably is the responsible of the reduction of the pitting corrosion resistance and as a consequence the reduction of CCT values [40].

Fig.V.18 shows the cyclic voltammograms of 2205 cold drawn and parent DSS at 70% load. In this case, the corrosion initiation was not detected even in 5 M NaCl neither for the parent nor the cold drawn stainless steels.

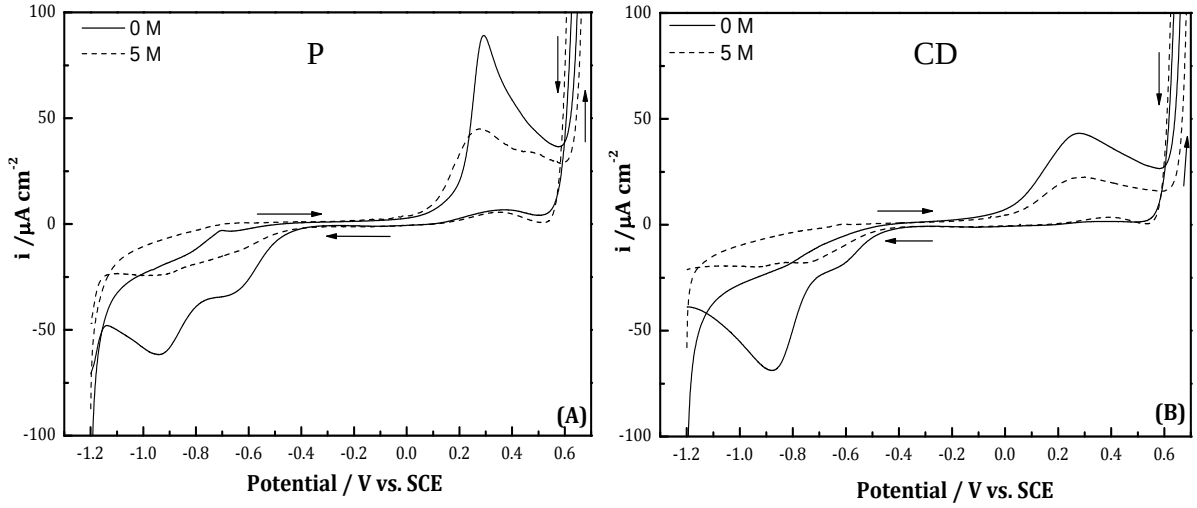

Fig.V.18. Cyclic voltammograms at 70% load of 2205 (A) parent and (B) cold drawn DSS in sat. $Ca(OH)_2$ solutions with 0 and 5 M NaCl.

In the case of 2304 stainless steel (see Fig.V.17), the comparison of parent and cold drawn 2304 wires indicates that, the parent SS presents more cathodic repassivation potential (E_{rep}), which in turn demonstrates that the pitting corrosion risk is higher in case of parent steels. This behaviour is probably related to the formation of deeper pits which

makes the repassivation process difficult that would justify the more negative E_{rep} value obtained in this case.

The stainless steels chemical composition also affects the corrosion resistance of the tested SS when exposed to an external load. Parent and cold drawn 2205 stainless steels show the highest corrosion resistance against the chloride action even when the steel wires tensioned up to 70% of their maximum strength.

e) Effect of temperature

The impact of the temperature on the CCT of the duplex stainless steels was analyzed by fixing the chloride content at lower concentration than the CCT found at 25 °C. In this test, the temperature of the solution was gradually increased until reaching the lowest temperature at which the growth of stable pits was detected. This temperature that induces the corrosion initiation has been defined as Critical Pitting Temperature (CPT) [203-204]. The effect of temperature was evaluated by performing a series of cyclic polarization tests at different temperatures in presence of constant chloride content as suggested in [204].

The testing conditions (chloride content and pH of the electrolyte) were selected taking into account the electrochemical results of tests at 25°C previously discussed. In the case of 2304 DSS, the most alkaline solution (pH 13.5) with the addition of 2 M NaCl has been considered (CCT at 25°C was 2.5 M for parent SS and 3 M for the cold drawn). In the case of 2205 SS both alkaline solutions (pH 12.5 and 13.5) with two different chloride

concentrations (1 and 2M) have been also considered (no CCT could be identified even with 5.5 M NaCl).

Fig.V.19 shows the cyclic voltammograms of 2304 parent (Fig. V.19a) and cold drawn (Fig. V.19b) DSS in sat. $Ca(OH)_2$ + 0.5M KOH with 2M NaCl at increasing temperatures until pitting initiation. For both 2304 parent and cold drawn DSS the onset of the pitting corrosion process was observed when the temperature increased up to 30 °C , which was considered the critical pitting temperature in the tested conditions for the 2304 DSS.

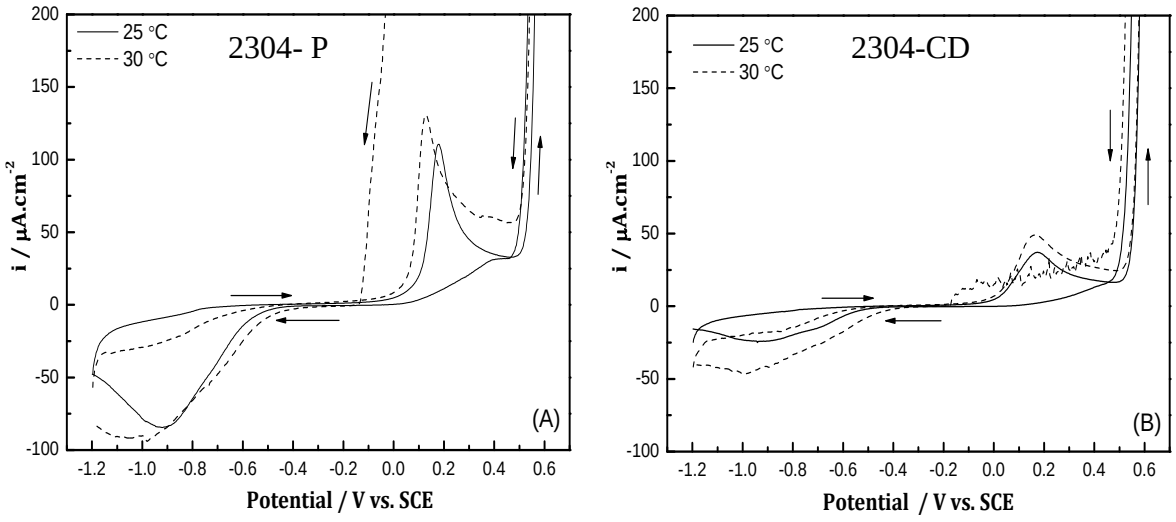

Fig. V.19. Cyclic voltammograms of 2304 (A) parent and (B) cold drawn DSS in sat. $Ca(OH)_2$ + 0.5 M KOH with 2M NaCl at different temperatures.

Fig. V.20 displays the cyclic voltammograms of the 2205 parent (Fig. V.20a) and cold drawn (Fig. V.20b) DSS in saturated $Ca(OH)_2$ + 0.5 M KOH with 2M NaCl at increasing temperatures until the detection of pitting initiation. Parent and cold drawn 2205 SS do not

showed pitting initiation even at 50 °C indicating a higher corrosion resistance for 2205 DSS than for 2304 DSS. For higher temperatures, different pitting corrosion susceptibility was registered for 2205 parent and the cold drawn DSS: the formation and propagation of stable pits was observed in the cathodic scan at 60 °C in the case of 2205 parent SS (Fig. V. 20a) while no pitting was detected, even at higher temperatures (70 °C), in the 2205 cold drawn DSS (Fig. V. 20b). Then, the influence of the microstructure induced by the cold drawn deformation can be expected to have a positive effect on the behaviour of this steel at high temperatures.

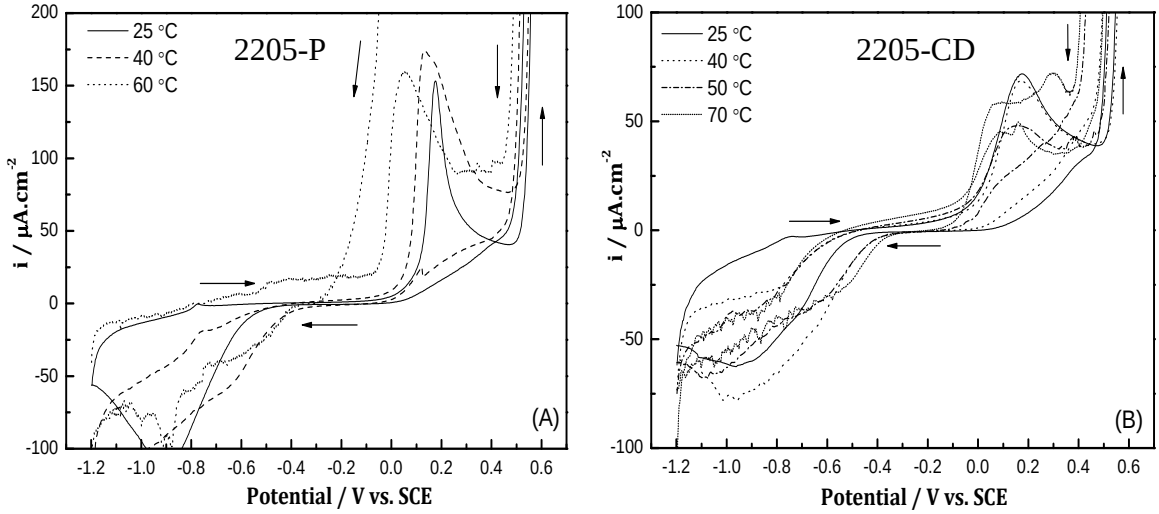

Fig. V.20. Cyclic voltammograms of 2205 (A) parent and (B) cold drawn DSS in sat. $Ca(OH)_2$ + 0.5 M KOH with 2M NaCl solutions at different temperatures.

The influence of the stainless steel composition, mainly the Mo content, seems also to have a significant influence on the corrosion resistance response at high temperature, as deduced from the clear differences observed when the potentiodynamic polarization

curves of both types of stainless steels are compared (Fig.V.19, 2304 DSS (no Mo) and Fig.V.20, 2205 DSS (3.7% Mo)).

The pH of the alkaline media also affects the pitting corrosion initiation process in high temperature conditions. Fig.V.21 shows the potentiodynamic polarization curves of parent (Fig. V. 21a) and cold drawn (Fig. V.21b) 2205 SS in an alkaline solution with lower pH (sat. $Ca(OH)_2$, pH 12.5 at 25 °C) with the addition of the same chloride content (2M NaCl) and at different temperatures.

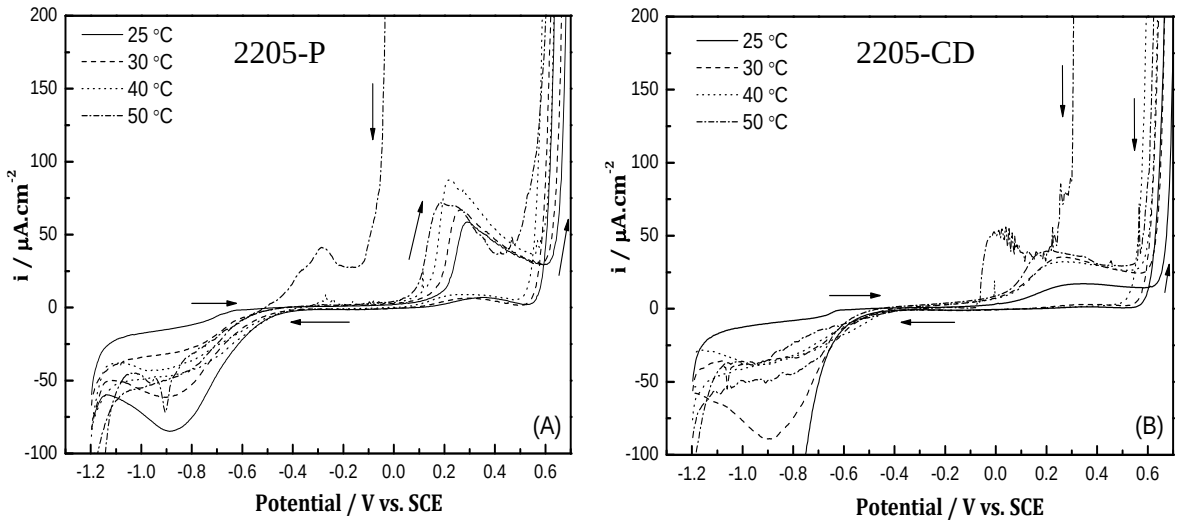

Fig. V.21. Cyclic voltammograms of 2205 (A) parent (B)cold drawn DSS in saturated $Ca(OH)_2$ + 2 M NaCl solutions at different temperatures.

The results indicate that the pitting corrosion risk at high temperature alkaline media increases with the alkalinity decrease, lower CCT values are measured for the lowest pH. In saturated $Ca(OH)_2$ + 2 M NaCl the nucleation of stables pits occurred at 50 °C for both 2205 parent and the cold drawn DSS while, as was previously discussed, no corrosion

initiation was observed at 25°C, even in presence of 5 M NaCl, neither for 2205 parent nor the cold drawn DSS.

Another important parameter to be considered to understand the influence of the temperature on the corrosion behaviour of duplex stainless steels is the chloride concentration present in the alkaline solution. Fig.V.22 depicts the cyclic polarization curves of 2205 parent (Fig. V.22a) and cold drawn (Fig. V.22b) DSS in saturated $Ca(OH)_2$ mixed in with 1 M NaCl. In the case of the parent 2205 stainless steel, no influence of the chloride concentration in the tested conditions can be observed, as the CPT (defined as the first temperature at which pitting is initiated) was 50 °C independently on the chloride concentration. However, the influence of the chloride concentration on the corrosion susceptibility of the cold drawn stainless steel can be deduced from the decrease of the CPT with the increase of the chloride concentration (CPT = 50 °C in 2M NaCl and CPT > 70 °C in 1 M NaCl).

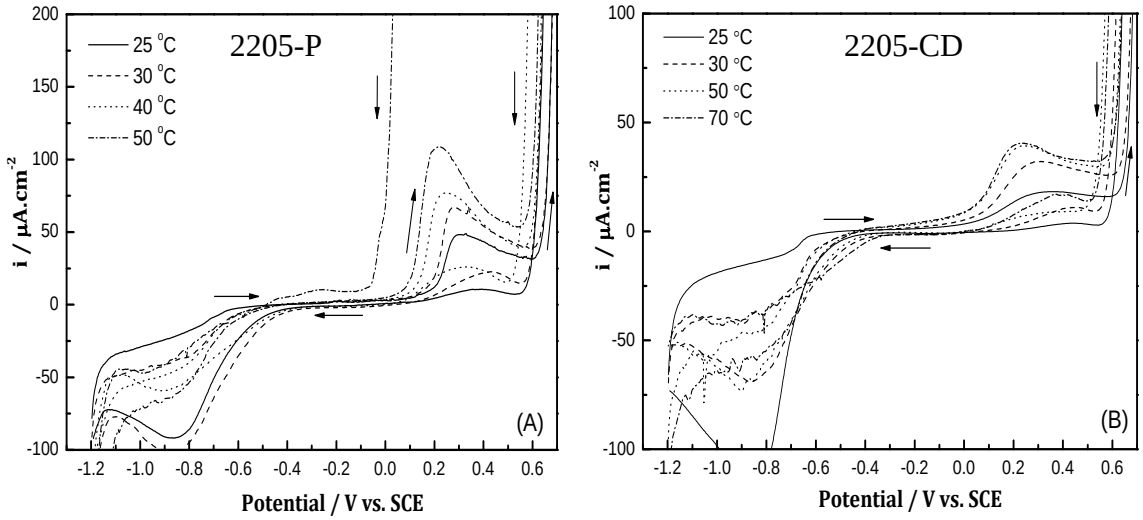

Fig. V.22. Cyclic voltammograms of 2205 (A) parent, and (B) cold draw DSS in saturated $Ca(OH)_2$ + 1 M NaCl solutions at different temperatures.

In table V.2 the summary of the CPT in the different experimental conditions studied is included.

Table V.2 Critical pitting temperature of 2304 and 2205 parent and cold drawn DSS in the different experimental conditions considered.

	CPT (ºC) 2304 SS		CPT (ºC) 2205 SS	
	Parent	**Cold-drawn**	**Parent**	**Cold-drawn**
2 M NaCl				
Sat. $Ca(OH)_2$ + 0.5 M KOH	30	30	60	>70
Sat. $Ca(OH)_2$	< 25	< 25	50	50
1 M NaCl				
Sat. $Ca(OH)_2$	< 25	< 25	50	>70

The increase of the pH of the alkaline media and the Mo content improve the corrosion resistance of the duplex stainless steel, even in high temperature conditions. Furthermore the superficial state of the stainless steel also affects its corrosion behaviour at high temperature and the higher CPT obtained for the cold drawn 2205 SS indicates a lesser susceptibility to pitting initiation at high temperature.

Focusing in the transpassivity domain of the cyclic voltammograms (Fig.V.22) of the stainless steels studied in alkaline solutions with chloride at high temperature, it can be clearly observed that both the chloride content and the temperature of the alkaline media influence the electrochemical response of the stainless steel in this region, as shown in Fig.V.23 and Fig.V.24, where the transpassive region of the cyclic voltammograms of 2205 parent and cold drawn DSS in sat. $Ca(OH)_2$ solutions with 1 and 2 M NaCl respectively.

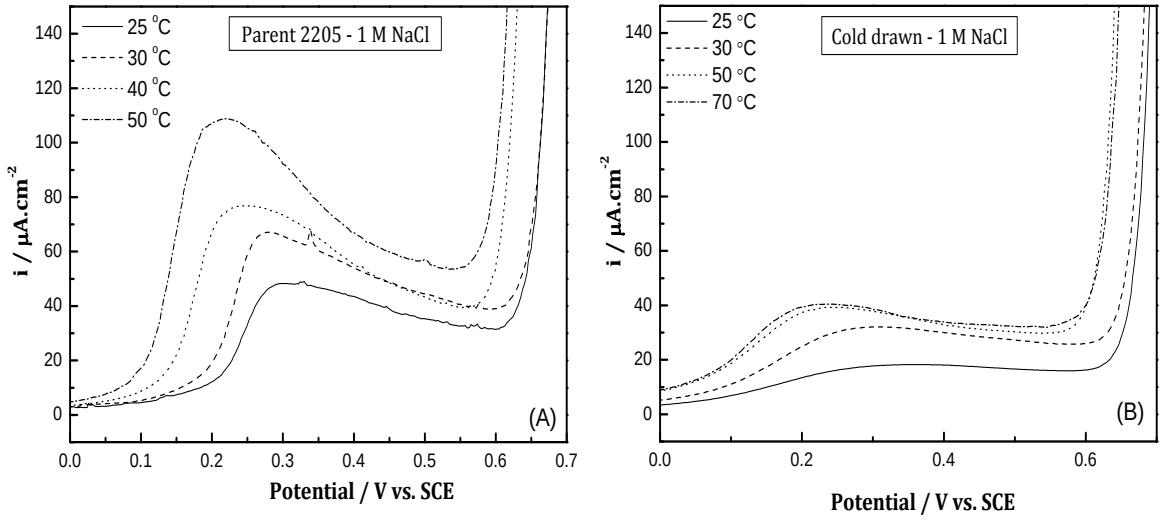

Fig. V.23. Transpassive region in voltammograms of 2205 (A) parent, and (B)cold drawn DSS in saturated $Ca(OH)_2$ + 1 M NaCl at different temperatures.

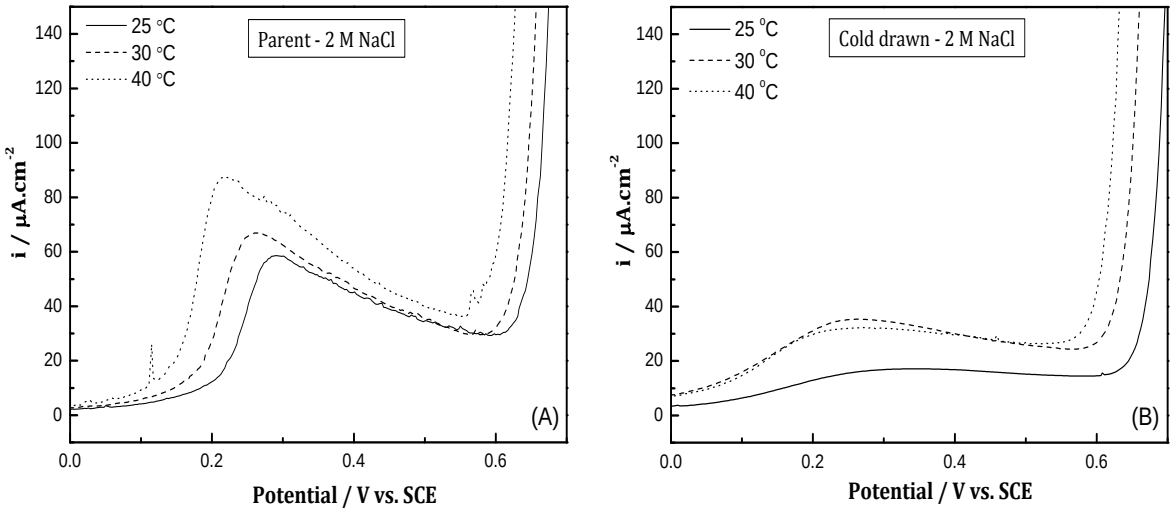

Fig. V.24. Transpassive region in voltammograms of 2205 (A) parent, and (B)cold drawn DSS in saturated $Ca(OH)_2$ + 2 M NaCl solutions at different temperatures.

Similar influence of the temperature is observed independently of the chloride concentration. From Fig.V.23 and Fig.V.24 an increase of the transpassive current density is measured with the temperature increment which could be explained by the activation of the chromium dissolution process at the highest temperature. In addition, smaller transpassive current densities are registered for the cold drawn stainless steel (Fig.V.23b and Fig.V.24b) in comparison to the parent stainless steel (Fig.V.23a and Fig.V.24a). Thus, as previously observed for T^a = 25°C, cold drawn stainless steel shows a higher resistance against pitting initiation than parent DSS, even when high temperatures are considered.

V.2.1.2. Potentiostatic determination of CCT

From the previous results carried out by potentiodynamic polarization tests it has been confirmed that CCT of duplex stainless steels shows an important dependence on the testing conditions in agreement with literature [40, 123-124,127]. Consequently, the CCT of the stainless steels has been also determined using potentiostatic conditions by applying a constant E = +0.25 V_{SCE} corresponding to the transpassive region in voltammograms of both duplex stainless steels. After 24 hours prepassivating the stainless steel in the free-chloride alkaline media, the chloride concentration was gradually increased in the test solution until reaching the CCT, detected by a sharp increase of the current density measured.

The current density measured for the stainless steels polarized at +0.25 V_{SCE} (transpassive region) with the addition of chloride with time has been represented in Fig.V.25.

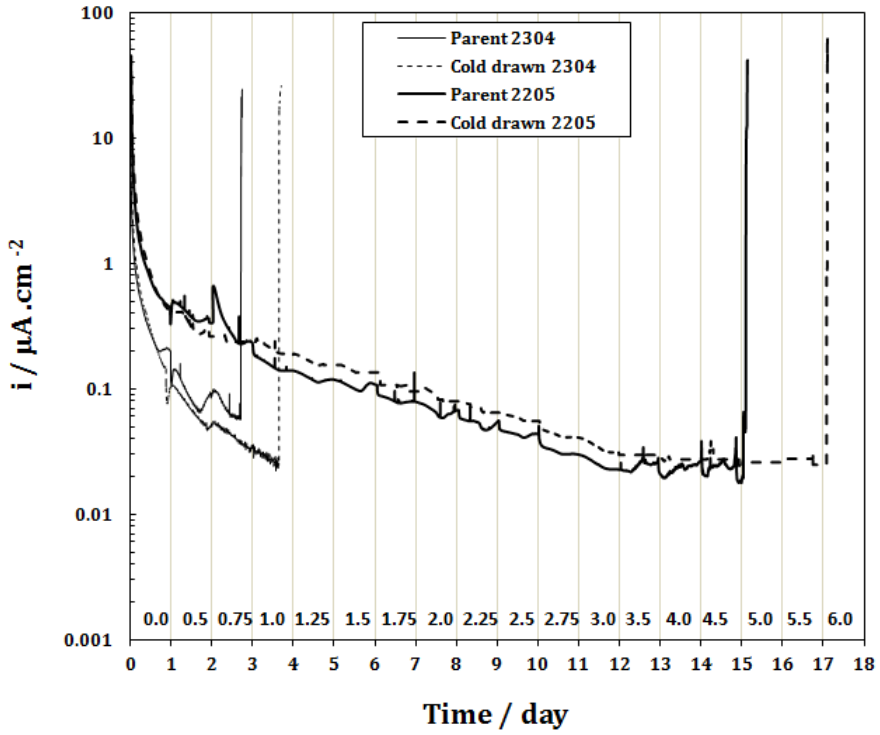

Fig. V.25 Potentiostatic test at constant E = +0.25 V_{SCE} with stepped chloride addition to saturated Ca(OH) at 25 °C solution.

After the 24 h of prepassivation period in free-chloride alkaline solution, 0.5 M NaCl was added. During this earlier stage, the measured current densities decrease gradually with the immersion time and no indication of the nucleation of stable pits on the tested stainless steels surfaces could be deduced. Then, the chloride content in the test solution was increased by the addition of 0.25 M NaCl every 24 hours. An exponential decay of the current density is registered when chloride concentrations were below the CCT for every stainless steel studied. Residual current densities lesser than 0.1 µA.cm^{-2} were reached for all cases when the passive film breakdown did not occur in the experimental conditions. A significant increase of the current density up to 10 µA cm^{-2} was established as the depassivation criterium.

From Fig.V.25, earlier depassivation, at lower chloride concentrations, has been detected for the 2304 SS in comparison with the 2205 SS. In both cases, the depassivation of the cold drawn wire occurred after the parent stainless steel, at higher concentration of chloride. In table V.3 the CCT and the depassivation time for each stainless steel are summarized. Concerning 2304 DSS, the pitting corrosion onset in case of the 2304 parent DSS was observed when the chloride content increased up to 0.75 M. However, in the case of 2304 cold drawn DSS, the presence of 1 M in the passive film/electrolyte interface was able to initiate active pits on the cold drawn SS surface. Regarding 2205 DSS, the passive film formed on 2205 cold drawn and parent DSS showed higher corrosion resistance in comparison with 2304 DSS, as shown in Fig.V.25 and table V.3. The pitting corrosion onset was observed in case of 2205 parent when the chloride content increased up to 5 M NaCl and for the cold drawn 2205 SS when the chloride content increased up to 6 M NaCl.

Table V.3 CCT and depassivation time obtained in potentiostatic conditions (+0.25 V_{SCE}).

	2304		**2205**	
	Parent	**Cold-drawn**	**Parent**	**Cold-drawn**
CCT / mol.l^{-1}	0.75	1	5	6
Depassivation time / d	2.5	3.5	15	17

Fig.V.26 shows the optical examinations and pit initiation on 2304 and 2205 DSS after potentiostatic test at +0.25 V_{SCE}.

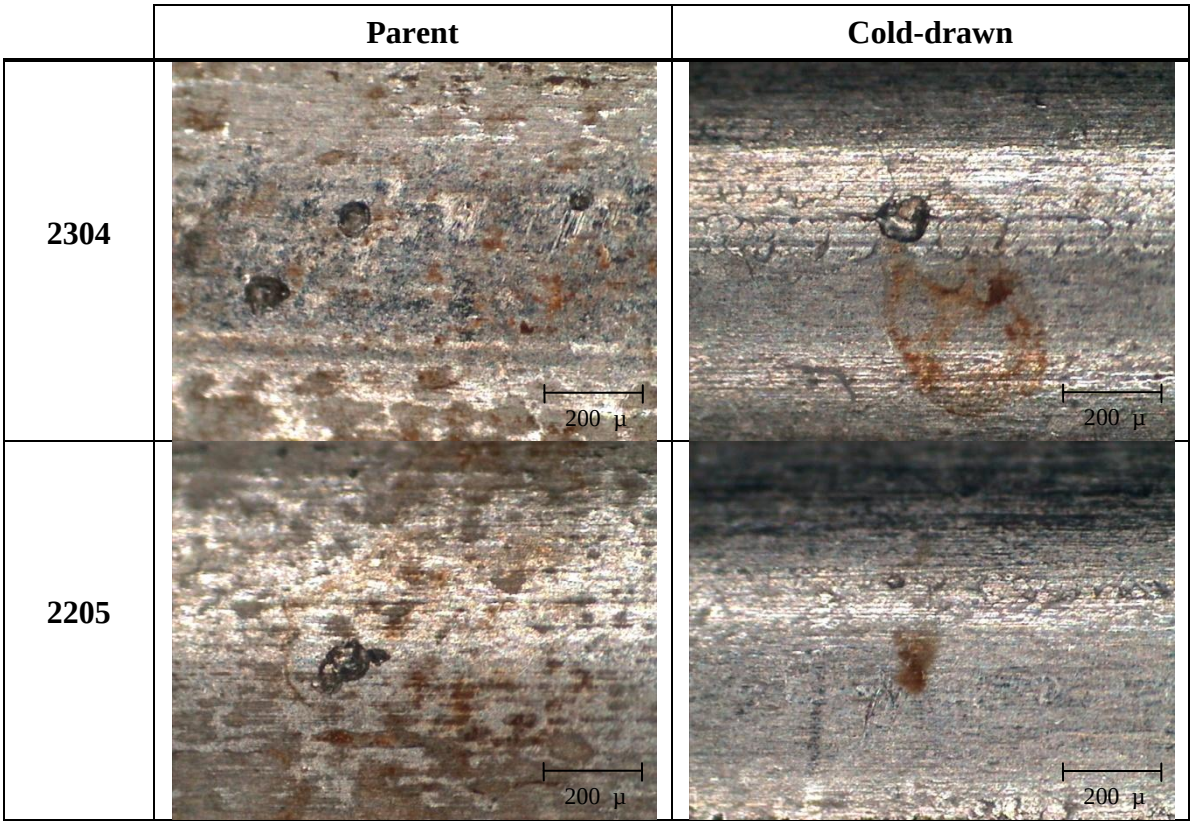

Fig. V.26 Optical examination of parent and cold drawn 2304 and 2205 DSSs after pitting corrosion initiation in potentiostatic conditions (+0.25 V_{SCE}).

V.2.1.3. Influence of the testing method in the determination of CCT for DSS in simulated alkaline pore-solutions

The influence of the testing method applied and of the experimental conditions in CCT can be deduced from Fig.V.27 where the comparison of experimental data at different testing conditions been represented. It can be observed that, for the same DSS, the CCT determined in potentiodynamic conditions is lower than the values determined in potentiostatic tests at the same experimental conditions.

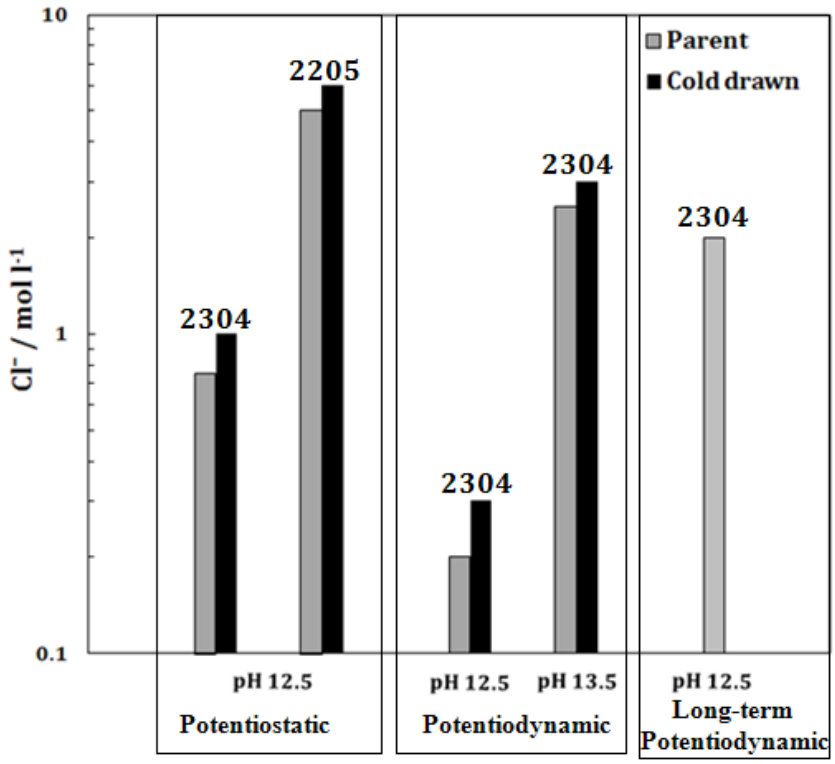

Fig.V.27 Variation of the CCT of 2304 and 2205 DSSs in high alkaline solutions (pH 12.5 and 13.5) at 25 °C using accelerated (potentiostatic and potentiodynamic) and natural tests.

This observation matches with the results obtained by Bertolini et al [127], who also reported certain differences in CCT values using potentiodynamic and potentiostatic tests. It can be considered that the differences may be related to the different electrochemical properties of passive films grown using different electrochemical techniques. Potentiodynamic polarization is a fast technique and a non stable passive film is formed during the measurement, which can explain the lower CCT values obtained under these conditions. However, the long duration of the potentiostatic test can allow the formation of a more stable and protective passive layer and then higher CCT can be expected.

It is noteworthy that, the long-term immersion in saturated $Ca(OH)_2$ solution in presence of chloride, after the spontaneous pre-passivation of the rebar for 7 days in the alkaline free-chloride solution, improves the protective capacity of the duplex stainless steels, as shown in Fig.V.27. 2304 parent stainless steel previously pre-passivated, both in the potentiostatic test and in the long-term test presents higher CCT when compared with the potentiodynamically measured CCT just after the immersion of the rebar in the same experimental conditions (pH =12.5).

Besides, the data in Fig.V.27 indicate that, in all cases, the cold drawn stainless steels always exhibit higher CCT than the parent ones, even if different methodologies are used. In addition, 2205 DSS present higher CCT in comparison with 2304 DSS at the same exposure conditions.

The up mentioned results confirm that, the CCT is controlled by many parameters including the testing condition, the method applied for the CCT determination, and stainless steel type, microstructure and surface.

V.2.1.4. Proposal of CCT determination in alkaline pore-solutions for DSS

From the up mentioned results of CCT determination using different accelerated electrochemical techniques, the following proposal for CCT determination of DSSs in high alkaline media can be suggested:

I. Potentiodynamic polarization test is a fast electrochemical technique which can affect the CCT measured. Consequently, a prepassivation in chloride free-alkaline

solutions, to confirm the formation of stable passive layer before the chloride addition, is more recommended.

II. In case of DSS, the determination of CCT can be carried out after long-term immersion up to 50 days in presence of chloride, when the long-term E_{corr}, i_{corr} and EIS monitoring indicates that the immersed DSS in alkaline solutions (pH 12.5), with chloride content up to 2 M NaCl, show a stationary state behaviour. If during this period an active corrosion has not be initiated, the pitting corrosion risk can be determined by applying a potentiodynamic test.

III. The potentiostatic determination of the CCT in alkaline solutions leads to reasonable CCT values. Nevertheless, these results cannot be transfer to the real response of DSS in mortar or concrete, and the optimization of the CCT values determined under these conditions becomes necessary.

This electrochemical test can be performed by prepassivation in chloride free alkaline media for 24 hours at the applied constant potential (+0.25 V_{SCE}). Then a progressive chloride addition (0.25 M NaCl every 24 hours) until the detection of the minimum concentration able to initiate active pits.

V.2.2. In mortar

CCT-values of duplex stainless steels have been also determined in mortar to define the corrosion behaviour of DSS in contact with concrete.

Earlier attempts to determine CCT in the case of stainless steels in mortar have been carried out by employing accelerated methods as chloride mixed-in mortar [125-126,138] and/or chloride penetration potentiostatic tests for chloride-free mortar immersed in aqueous chloride solutions [127-128].

V.2.2.1. Chloride penetration potentiostatic test

Two series of potentiostatic tests have been carried out to determine the CCT of DSS by the chloride penetration test: The first tested series (S-1) included six mortar samples of 2304 DSS (2 parent and 4 cold drawn). The second series (S-2) included 12 mortar samples of 2304 and 2205 cold drawn DSS (6 for each case).

a) 2304 DSS

The depassivation process of 2304 DSS was investigated by the evaluation of CCT of the 2304 cold drawn and parent wires in chloride-free mortar using potentiostatic polarization tests (at +0.25 V_{SCE}), similarly than the potentiostatic tests carried out in the alkaline solution simulating the aqueous phase of the concrete pores. Fig.V.28a shows an example of the change in the current density with the immersion time in mortar specimen with parent and cold drawn stainless steel for the first series (S-1). The variation in the current density for the second series (S-2) has been represented in Fig.V.28b.

Ageing in the alkaline mortar induces the passive film formation on the embedded stainless steels rebars. During this period the chloride ions penetrate through the mortar barrier until reaching a critical concentration (CCT) at the embedded SS surface, able to break the passive film.

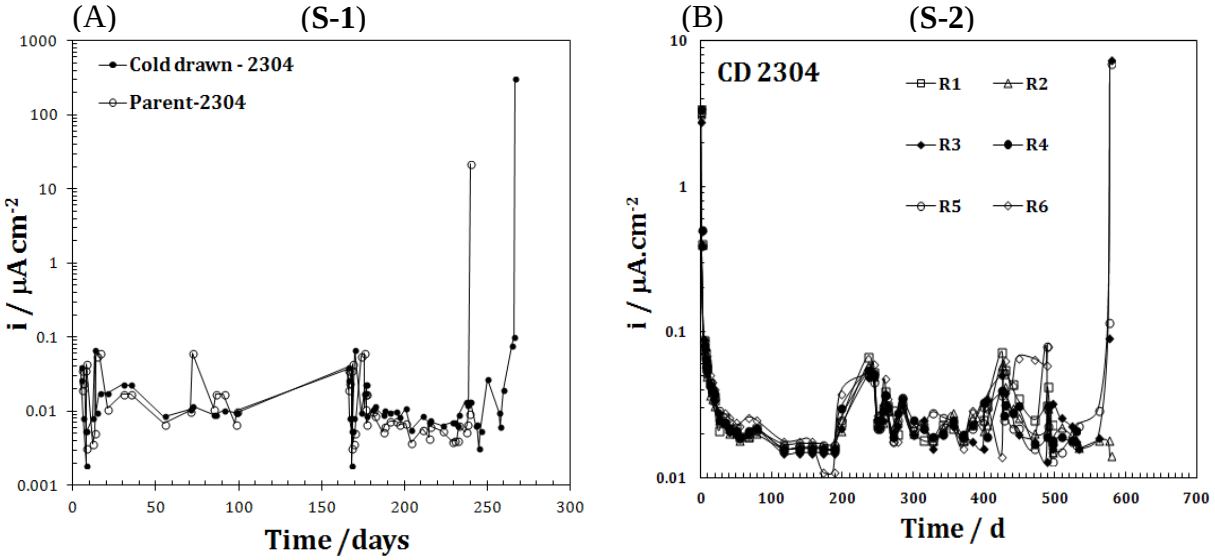

Fig.V.28. Current density variation during potentiostatic test of 2304 DSS subjected to chloride penetration test. (a) first series (S-1), and (b) second series (S-2).

In case of S-1, a sharp increase in the current has been observed after certain period of time, which indicates the initiation of active pits on DSS surfaces (see Fig.V.28a). However, in the case of S-2 (Fig.V.28b), certain fluctuations in the measure current densities were observed probably due to the formation of metastable pits able to be repassivated, some of these metastable pits can be propagated and induce an increase in the measure current density, as shown in Fig.V28b. In the last case, the evolutions of the accumulated charge (Q_{Acc}) during the potentiostatic test for each cold drawn 2304 stainless steel (S-2) are shown in Fig.V.29. The observed data in Fig.V.29 indicate that the Q_{Acc} increases asymptotically with the rebar ageing in mortar. Depending on the show data in

Fig.V.29, a critical value of $Q_{Acc} \geq 0.05 - 0.06$ C has been considered to indicate the onset of chloride induced pitting corrosion of the embedded cold drawn DSSs.

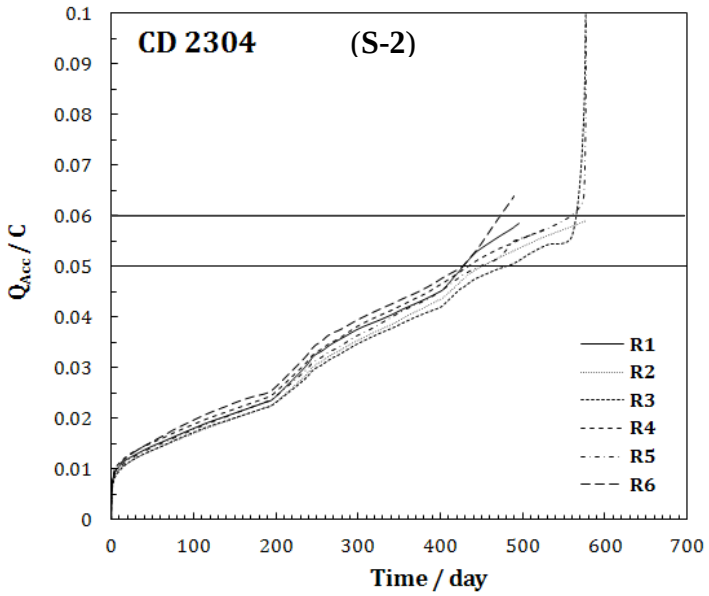

Fig.V.29. The accumulated charge during the potentiostatic CCT determination of 2304 cold drawn DSS (second series S-2) in chloride penetration test.

At the end of the test, the mortar specimens were disconnected and the E_{corr} and i_{corr} were measured for the two series after 48 hours. The E_{corr} and i_{corr} data before and after the onset of the pitting corrosion induced by chloride are listed in table V.4. Before the potentiostatic test, all the wires showed a passive state characterized by E_{corr} > -250 mV_{SCE} and i_{corr} lower than 0.07 $\mu A/cm^2$. However, when the chloride concentration on the stainless steels surface reached the CCT value, the i_{corr} were always > 0.2 $\mu A/cm^2$ indicative of a pitting corrosion onset.

Table V.4 E_{corr} and i_{corr} data of 2304 DSS in mortar before and after corrosion initiation.

	S-1				S-2			
	Before		after		Before		After	
	E_{corr}/mV_{SCE}	$i_{corr}/\mu A.cm^{-2}$	E_{corr}/mV_{SCE}	$i_{corr}/\mu A.cm^{-2}$	E_{corr}/mV_{SCE}	$i_{corr}/\mu A.cm^{-2}$	E_{corr}/mV_{SCE}	$i_{corr}/\mu A.cm^{-2}$
R1	-172*	0.016*	-381*	14.96*	-209	0.037	2.9	0.57
R2	-144*	0.073*	-401*	4.31*	-	-	-	-
R3	-189	0.012	-395	2.95	-200	0.09	-327	2.9
R4	-192	0.010	-394	3.01	-186	0.012	-65	0.21
R5	-189	0.011	-290	4.52	178	0.02	-349	6.7
R6	-137	0.056	-364	4.56	-192	0.01	66	0.75

* Parent DSS

- Still in test

Fig.V.30 displays an example of the optical examinations of the 2304 cold drawn at the end of chloride penetration potentiostatic tests. In case of the first series (S-1), deep pits were detected, which explained the reason of the observed sudden increase in the current density after pitting corrosion onset and also high values of i_{corr}, maintained after the disconnection of the potentiostatic test (see Table V.4). On the other hand, less propagated pits were monitored in case of the second series (S-2), as shown in Fig.V.30.

The chloride content analysis to determine the CCT at the rebar level has been performed after the detection of the pitting corrosion onset. The CCT values obtained for the tested stainless steels in mortar specimens are listed in table V.5. The CCT was expressed as total chloride content by the weight of cement.

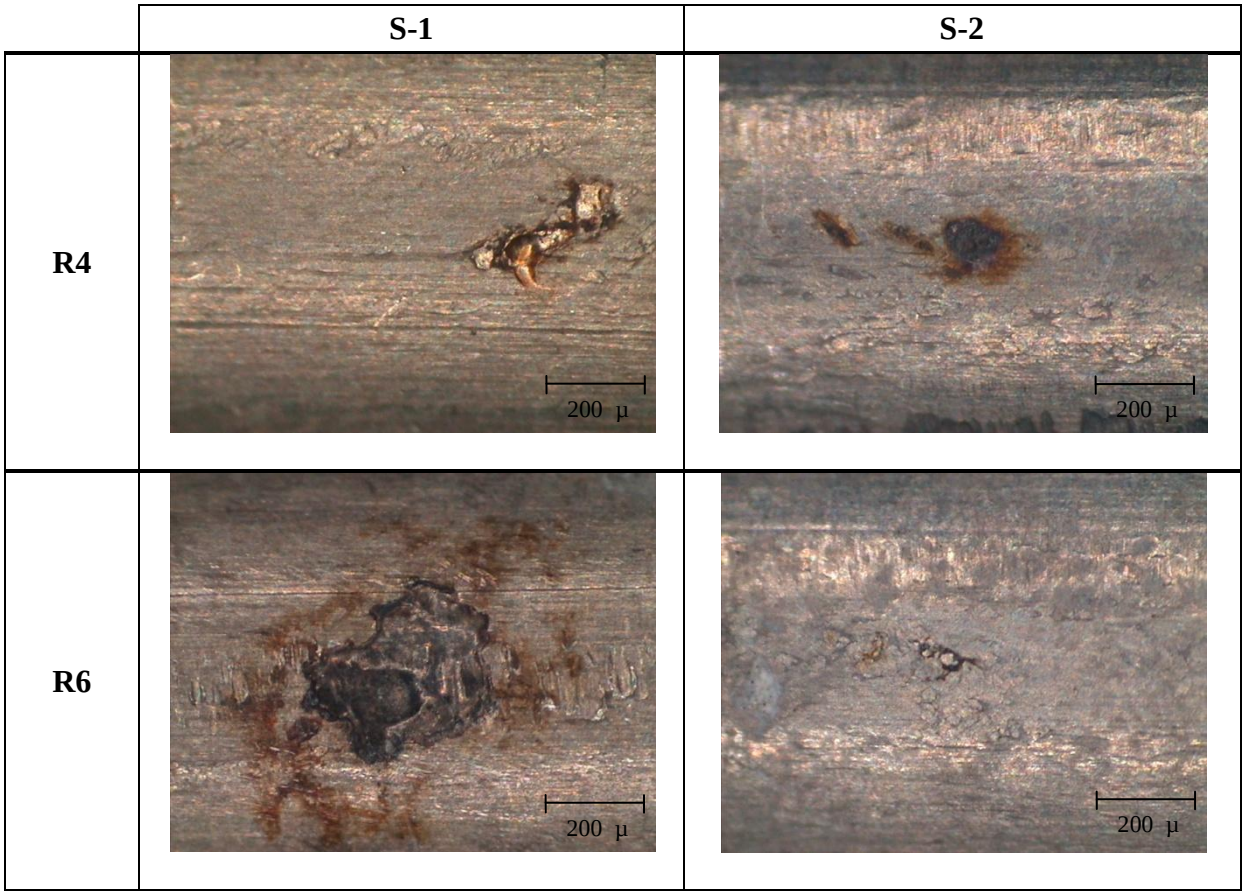

Fig.V.30 Optical examination of some examples of cold drawn 2304 DSSs after chloride penetration potentiostatic tests.

Table V.5. CCT values in % Cl^- total respect the cement weight of 2304 DSS. (A) First series S-1, and (B) Second series S-2.

(A)	S-1					
	Parent		Cold drawn			
	R1	R2	R3	R4	R5	R6
CCT - % Cl^-	2.14	2.41	2.43	2.45	3.08	2.78

(B)	S-2					
	Cold drawn					
	R1	R2	R3	R4	R5	R6
CCT - % Cl^-	3.64	-	-	3.52	-	3.52

- Still in test

The results show that the corrosion initiation was observed on the parent SS embedded in mortar when the chloride content in the steel surface increased above 2.3±0.2% total chloride, while cold drawn SS always shows higher corrosion resistance, 3.06 ± 0.6 % total chloride considering the two series.

b) 2205 DSS

To evaluate the effect of the Mo content in the depassivation of duplex HSSS when embedded in mortar, similar potentiostatic electrochemical tests have been carried out at +0.25 V_{SCE} to determine the CCT of 2205 cold drawn 2205 DSS.

Fig.V.31 shows the variation of the current densities of the 2205 cold drawn DSS during the potentiostatic test. In the earlier ages, the current density of the HSSS decreases with the immersion time indicating the formation of the passive layer on the embedded HSSS surfaces. After 200 days of potentiostic testing an increase in the current density is detected for all the rebars. Although a progressive decrease of the current density takes place after this time, certain instability in the measured current densities is registered. This could be explained by the formation of metastable pits that stabilized with time, as shown in Fig, V.31.

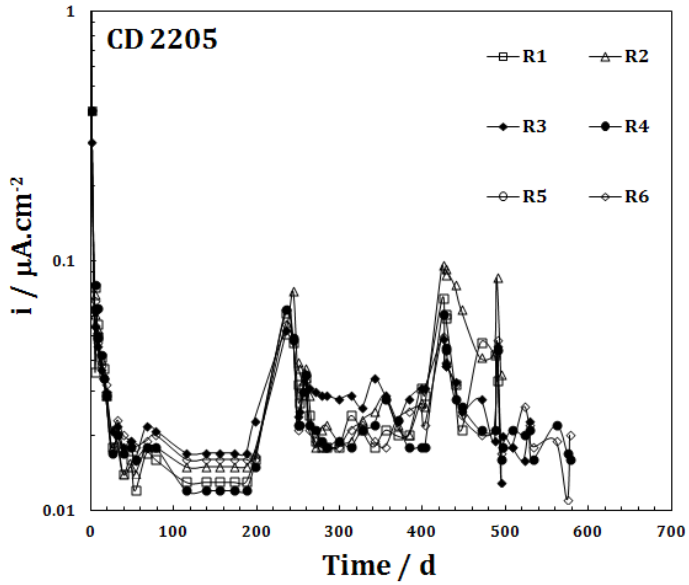

Fig.V.31. Variation of the current density during the potentiostatic test of 2205 cold drawn DSS embedded in mortar and subjected to chloride penetration.

Fig.V.32 displays the variation of Q_{Acc} of 2205 cold drawn DSS embedded in mortar during the chloride penetration potentiostatic test. Both 2205 cold drawn, (Fig.V.32), and 2304 cold drawn, (Fig.V.29), DSS show similar behaviour with ageing.

Considering the same criteria used for 2304 DSS (S-2), the cold drawn 2205 DSS were disconnected when $Q_{ACC} \geq 0.05 - 0.06$ C has been reached. Besides, the E_{corr} and i_{corr} were measured after the potentiostatic test and they were compared with values measured before the test connection. E_{corr} and i_{corr} data before and after the chloride penetration test of 2205 CD-DSS are listed table V.6

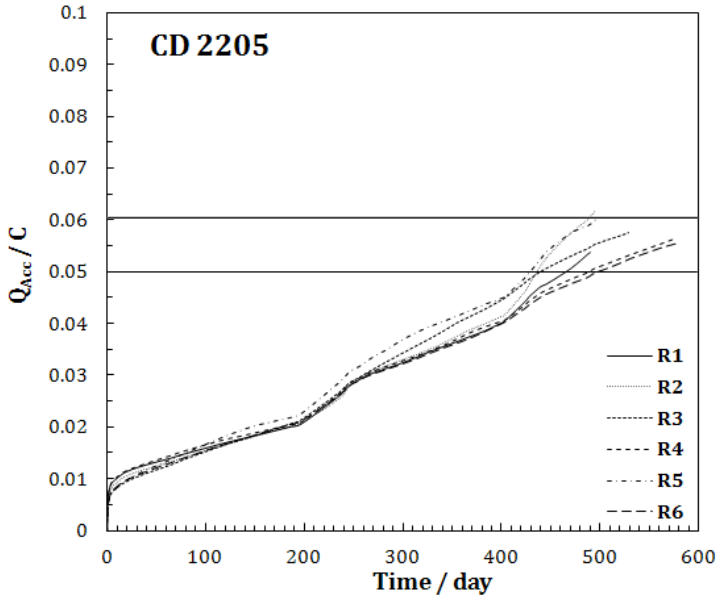

Fig.V.32. The accumulated charge (Q_{Acc}) during potentiostatic test of 2205 CD-DSS embedded in mortar and subjected to chloride penetration test.

Table V.6 E_{corr} and i_{corr} data of 2205 DSS in mortar before and after chloride penetration test.

	S-2			
	Before		After	
	E_{corr}/mV$_{SCE}$	i_{corr}/µA.cm^{-2}	E_{corr}/mV$_{SCE}$	i_{corr}/µA.cm^{-2}
R1	-188	0.016	76	0.35
R2	-177	0.011	27	0.43
R3			2.4	0.20
R4	-	-	-	-
R5			4.4	0.45
R6	-	-	-	-

- Still in test

At the end of the test, 2205 CD-DSS also exhibit i_{corr} values higher than 0.2 µA/cm², which suggested a possible corrosion onset of 2205 DSS, as shown in table V.6.

The optical examination of the 2205 CD-DSS at the end of the potentiostatic test are shown in Fig.V.33. No detection of the characteristic pits has been observed in case of 2205

CD-DSS. However, in some cases, a color change of the steel surface has been noticed, which intensified after the exposure of the embedded rebar to the atmosphere, as shown in Fig.V.33a, c. The reason of this superficial attack appeared in some cases of the 2205 DSS rebars are not clear and more studies are needed to clarify this phenomenon. Nevertheless, one possible explanation may be attributed to the effect of the polarization test duration in the case of the HSSS containing Mo, as the testing potential is located in the transpassive region, where the activation of Cr^{III} oxidation to chromates has been observed to be enhanced due to the presence of molybdenum at high alkaline pH.

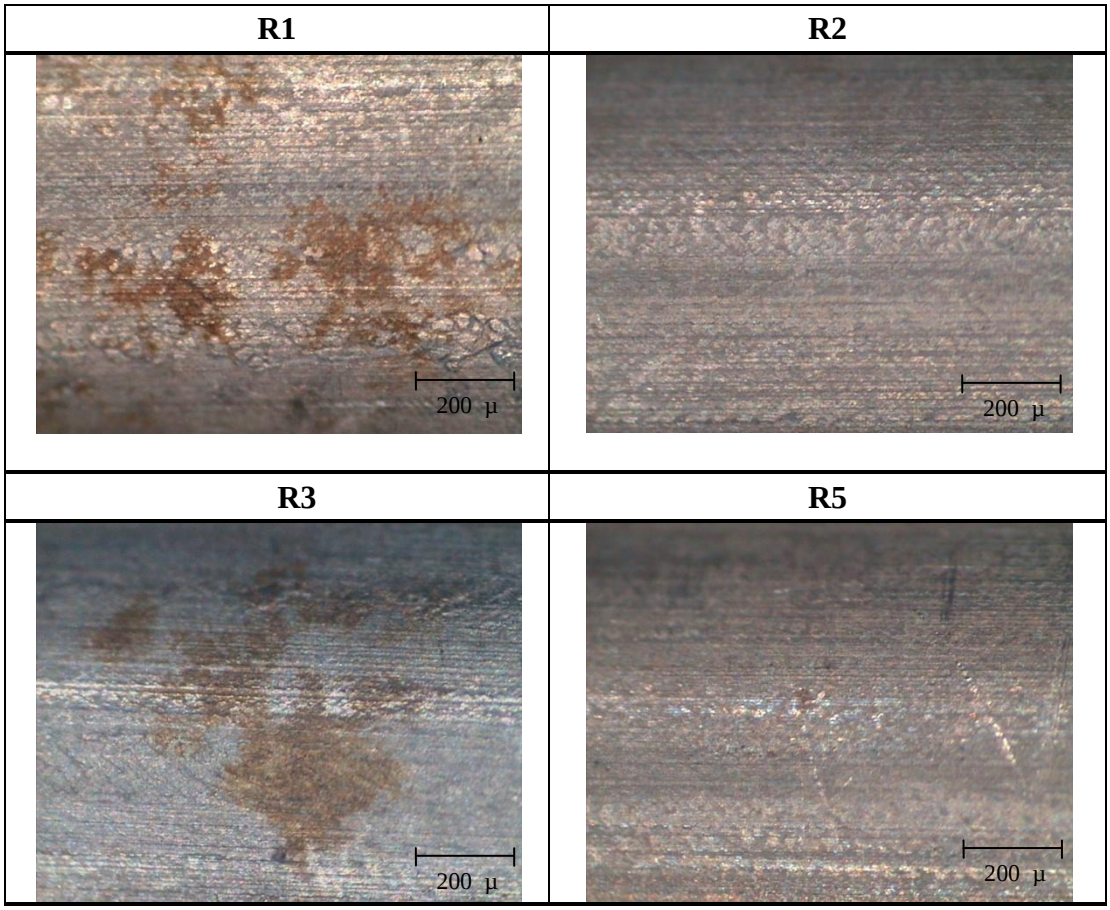

Fig.V.33 Optical examination of some examples of 2205 CD-DSS after chloride penetration test.

The chloride analysis at the end of the chloride penetration test in case of 2205 cold drawn DSS are shown in table V.7. The % Cl^- total respect the cement on the surface of the embedded 2205 DSS are in the same order like the measured % Cl^- for 2304 DSS after the same immersion period.

Table V.7. % Cl^- total respect the cement weight of 2205 CD-DSS after the chloride penetration potentiostatic test.

	Cold drawn					
	R1	**R2**	**R3**	**R4**	**R5**	**R6**
% Cl^-	3.64	3.8	3.74	-	3.81	-

- Still in test

V.2.2.2. Chloride mixed mortar

Mixed-in chlorides mortar have been used by several authors as a time saving method for the evolution of pitting corrosion initiation of embedded SS by adding a constant chloride concentration in the mortar [125-128].

The pitting corrosion risk of parent and 2304 CD-DSS embedded in chloride mixed-in mortar with different chloride concentrations up to 4% Cl^- has been evaluated by further application of step potentiostatic test, which is considered by some authors [127] as a more reliable electrochemical technique than potentiodynamic test in case of mortar.

Fig.V.34 shows the variation of the residual current density of parent and cold drawn DSS embedded in mortar samples mixed-in with 2, 3 and 4% Cl^-, and

potentiostatically tested at +0.25, +0.4 and +0.55 V_{SCE}. In each case, three stainless steel wires have been tested and the current densities shown are the mean of the three measurements. The chloride mixed-in mortars were immersed in saturated $Ca(OH)_2$ solutions during the potentiostatic test, and the potential applied was changed to nobler values every 6-8 days.

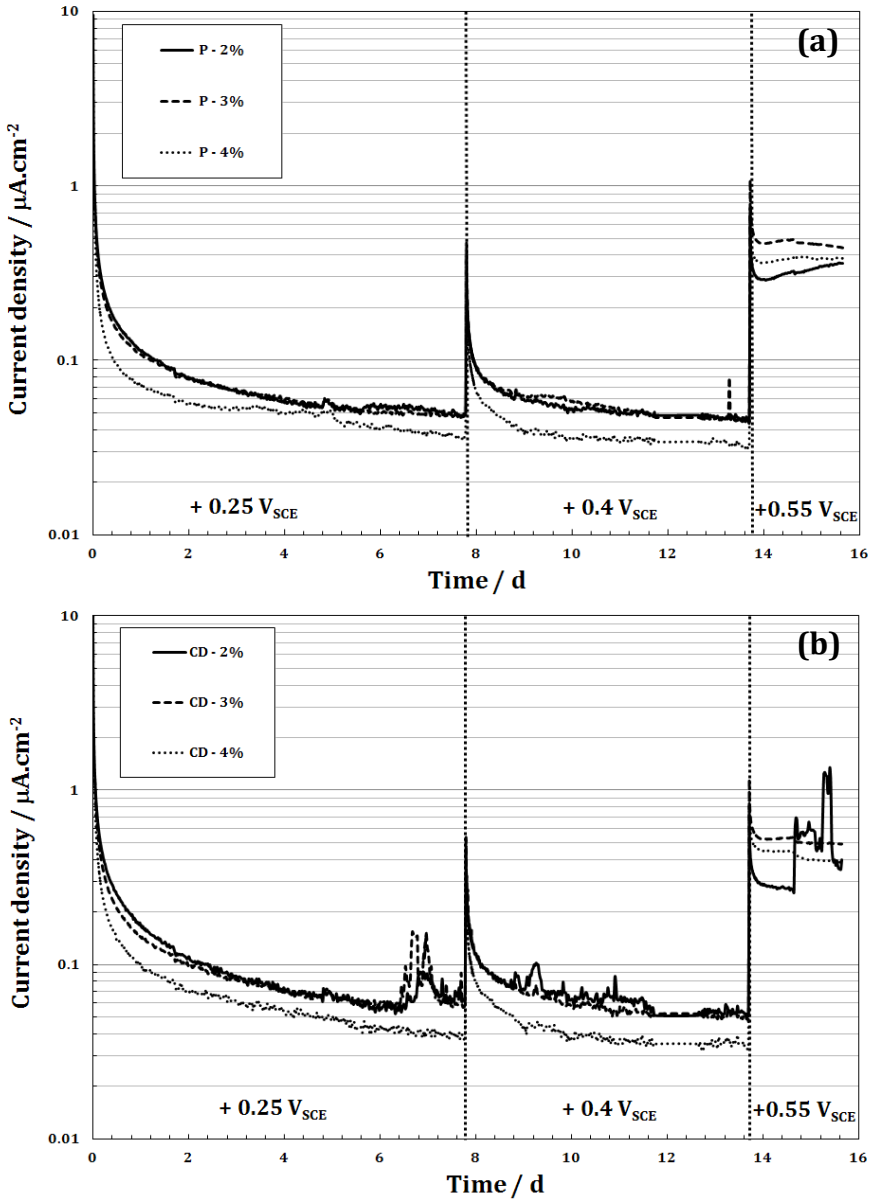

Fig.V.34 Step potentiostatic test of 2304 (a) parent and (b) cold drawn DSS embedded in embedded in chloride mixed-in mortar with 2, 3, and 4% Cl^-.

According to the potentiostatic results depicted in Fig.V.34, the residual current density decreases by ageing until reaching a steady state current density. No sudden increase has been observed in the measured residual current.

The chloride analysis at the end of the test in chloride mixed-in mortar samples (initial 2, 3 and 4 % Cl^-) at the rebar level were also performed to confirm the real chloride content in each sample. The data obtained are listed in table V.8. The results of the chloride analysis of mortar samples show that the chloride contents measured at the end of test are smaller than the initially mixed-in %Cl^-, which in turn indicates a possible leaching of chloride ions from the mortar to the external $Ca(OH)_2$ solution leading to a decrease of the content of Cl^- on the surface of the embedded stainless steels, as shown in table V.8.

Table V.8 Chloride analysis of chloride mixed-in mortar samples expressed by % total Cl^- by cement weight.

Cl^- *Mix-in samples*	**% Cl^- total**
2%	**1.8 ± 0.2**
3%	**2.1 ± 0.5**
4%	**2.9 ± 0.1**

As no clear response of the current density was detected, the pitting corrosion risk of the tested DSS was evaluated by optical examinations of the SS surface at the end of the test. Table V.9 summarizes the data of the optical examination of parent and cold drawn 2304 SS. 2304 parent DSS have been depassivated in presence of 1.8 ± 0.2 % Cl^- (by cement weight) at the interface. However, the cold drawn wires show higher corrosion resistance and pitting corrosion initiation was not observed obverted up to 2.1 ± 0.5 % Cl^-.

Table V.9. Evaluation of pitting corrosion risk by optical examination of parent and 2304 CD-DSS embedded in chloride mixed-in mortar with 2,3,4 % Cl^- after the step potentiostatic test.

	Pitting corrosion risk	
	Parent	**Cold drawn**
2 % Cl^- (1.8 ± 0.2 %)		
R1	**Yes**	No
R2	**Yes**	No
R3	**Yes**	**Yes**
3 % Cl^- (2.1 ± 0.5 %)		
R1	No	No
R2	**Yes**	**Yes**
R3	**Yes**	**Yes**
4 % Cl^- (2.9 ± 0.1 %)		
R1	**Yes**	**Yes**
R2	**Yes**	**Yes**
R3	**Yes**	No

Comparing the chloride mixed-in CCT data with the chloride penetration potentiostatic test, as shown in Fig.V.35, lower CCT values are obtained in chloride mixed-in mortar. This fact probably is attributed to the difference between the passive film grown in both cases and the duration of the electrochemical test, as the chloride mixed-in test is considered as a short term test.

Concerning chloride penetration in chloride free mortar, the passive film growth is favoured in earlier ages as a consequence of the absence of chloride and a more stable passive film is expected. However, in case of chloride mixed-in mortar, the chloride ions are

present in the interface from the beginning. The presence of chloride induces certain changes in the passive layer which affects the electrochemical properties of the layer and its lower protective capacity is expected to resist lower CCT.

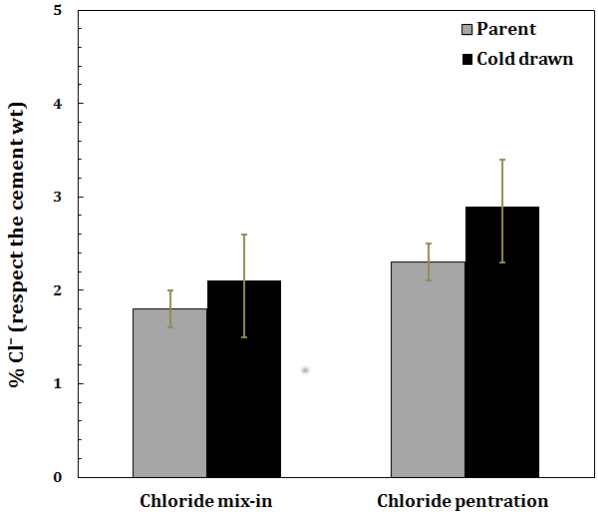

Fig.V.35. Variation in CCT values of 2304 DSSs in mortar

By the comparison of the measured CCT values by penetration potentiostatic test with CCT value in literature, it is found that, the data obtained using this accelerated electrochemical tests (chloride penetration and chloride mixed-in test) seems quite reasonable and are in agreement with those CCT data given by Bertolini et al [127] for similar SS.

V.2.2.3. Proposal of CCT determinations in mortar:

The CCT determination for DSS in mortar using accelerated tests, such as the potentiostatic chloride penetration and the chloride mixed-in potentiostatic test proposed in present doctoral thesis can be resumes as follows:

I. The potentiostatic determination of the CCT of DSS in chloride free or chloride mixed-in mortar should be carried out at constant potential in the passivity domain to avoid the interference of the redox process that occurs in the transpassivity domain, mainly related with the chromium dissolution.

II. CCT determination by using chloride penetration potentiostatic test is long-term test in comparison with chloride mixed-in method. However, some optimizations of the chloride mixed-in tests are required for application for CCT determination, even though reasonable CCT values have been measured in the studies carried in present work.

III. CCT determination using chloride mixed-in mortar should be performed in chloride containing electrolytes to prevent the chloride leaching from mortar.

V.3. Pitting corrosion propagation of duplex SS in alkaline solution

The pitting corrosion propagation in presence of chloride was analyzed by quantifying the electrochemical charge (Q) associated to the pitting corrosion process which has been calculated from the cyclic voltammograms carried out in presence of concentration of chloride higher than CCT. The values of Q from both anodic and cathodic curves were considered, from the pitting potential to the repassivation potential as was described more in detail in the experimental part (chapter III).

V.3.1. Effect of the chloride content in the pitting corrosion propagation

Fig. V.36 depicts the cyclic voltammograms of 2304 parent and cold drawn DSS in saturated $Ca(OH)_2$ with chloride concentrations above the CCT. The propagation of the pits, once the corrosion is initiated, becomes more widespread and the repassivation process becomes more difficult, as can be deduced from the more negative E_{rep} obtained, as shown in Fig.V.36.

It has to be considered that, the addition of chloride affects the pH of the alkaline media. Fig. V.37 shows the variation of the pH of sat. $Ca(OH)_2$ and sat. $Ca(OH)_2$ - 0.5 M KOH solutions with the increase of the chloride content. The measured data shows a decrease in the pH of the alkaline media with the increase of the chloride content.

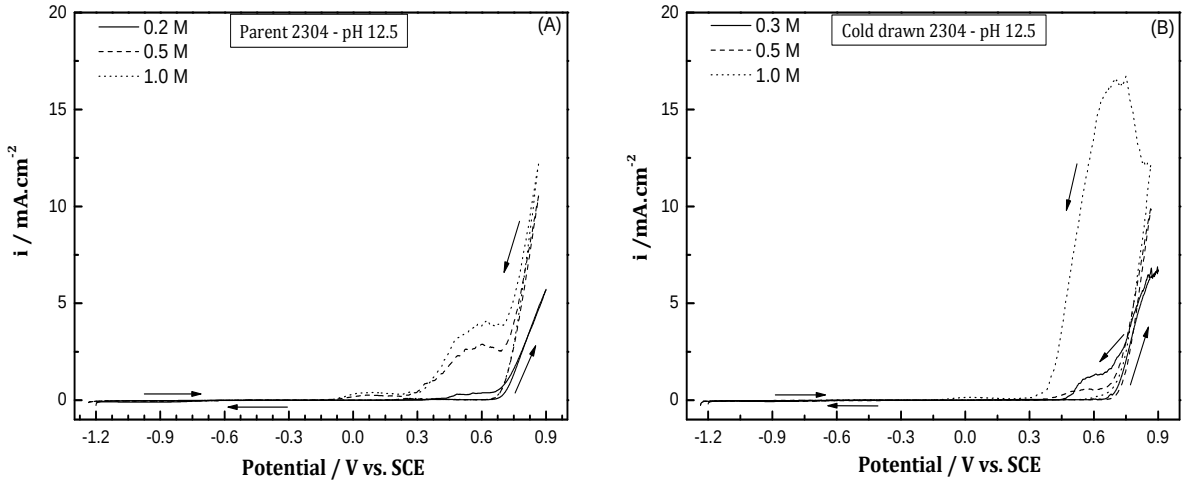

Fig.V.36 Cyclic voltammograms of 2304 (A) parent and (B) cold drawn DSS in Sat. $Ca(OH)_2$ with chloride concentration more than CCT (CCT, 0.5, 1 M NaCl) at 25 °C.

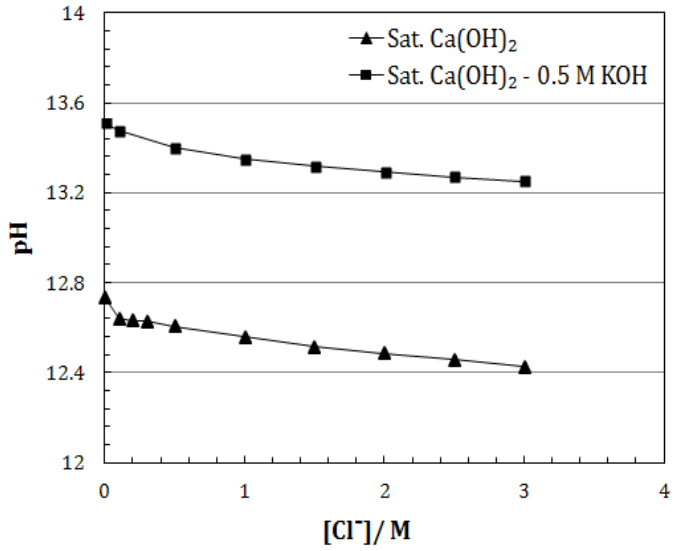

Fig.V.37 Variation of the alkaline pH as a function of the concentration of NaCl.

In Fig.V.38, the electrochemical charge associated to the pitting corrosion propagation as function of the chloride concentration is represented. Once the chloride had

induced the pitting due to the local dissolution of the passive film formed on duplex SS, the corrosion intensity of the redox processes occurring inside the pit causes its propagation, which is more intense in presence of higher chloride content and, as a consequence, the electrochemical charge of pitting increases and E_{rep} is shifted to more negative potentials.

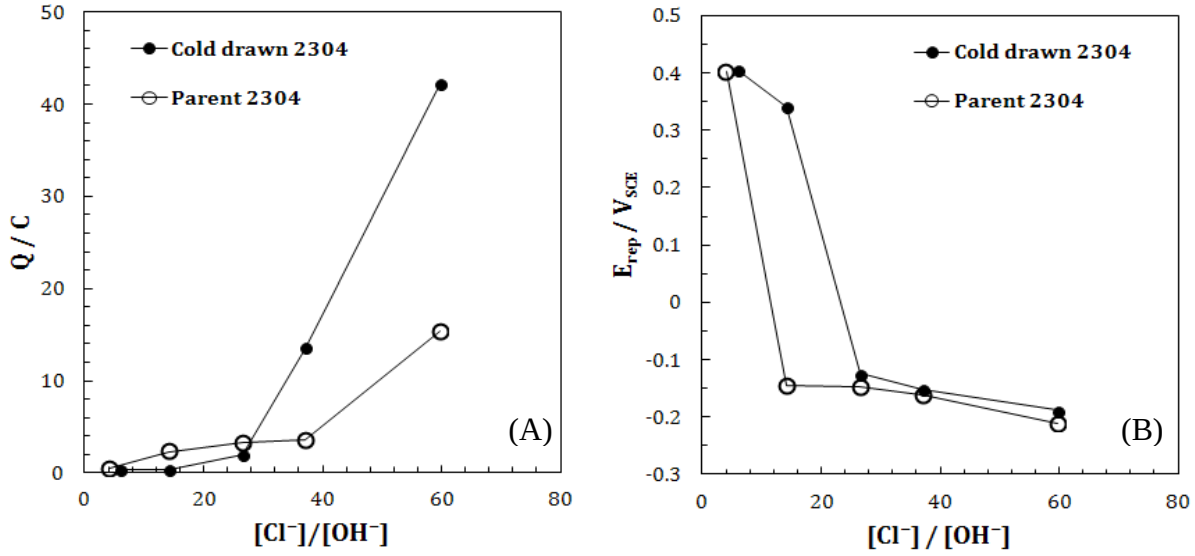

Fig.V.38 Variation in (A) electrochemical charge (Q) of pitting corrosion and (B) repassivation potential (E_{rep}) with the chloride content of 2304 SS in pH 12.5 at 25 °C.

Concerning the cold drawn DSS, the pits propagation, in presence of a chloride concentration less than 0.75 M Cl^- was slower in comparison with parent SS at the same condition. However, for higher concentrations than 0.75 M Cl^- of chloride, the propagation of the pit is more accelerated in the case of the 2304 cold drawn DSS, as shown in Fig.V.38a. In this sense, it is interesting to note that, although cold drawn stainless steel is more resistant against the action of chlorides, once the pitting is initiated, the rate of propagation is faster in presence of high chloride content.

V.3.2. Effect of the temperature on the pitting corrosion propagation

The temperature has also a relevant effect on the pH of the alkaline solution: as the temperature goes up, the pH of the saturated $Ca(OH)_2$ solution decreases as consequence of the diminishing the solubility of calcium hydroxide with the temperature increase, as shown in Fig.V.39.

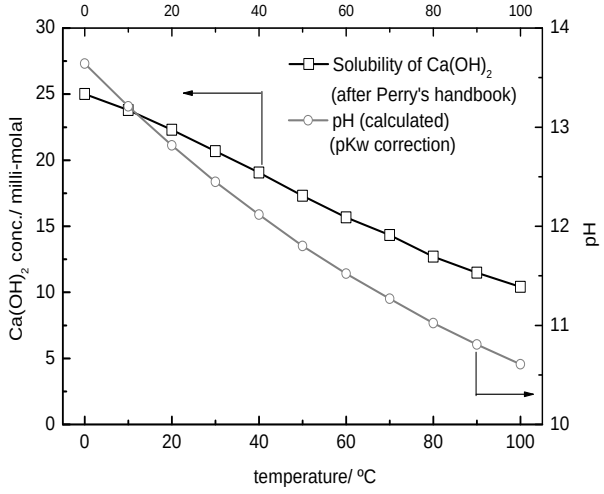

Fig. V.39 Solubility of calcium hydroxide and pH value at different temperatures.

Furthermore, both the increase of the temperature and the addition of the chloride to the alkaline solution affect the pH value, as can be deduced from Fig.V.48.

This modification of the chemistry of the alkaline solution controls the electrochemical response of the duplex stainless steels, both in the initiation and in the propagation periods, as will be shown later.

Moreover, the chloride concentration, the temperature and the pH of the alkaline solution are not independent parameters, as can be deduced from Fig. V.39 and Fig V.40,

and they have a synergic effect on the pitting corrosion propagation of the duplex SS. The synergic effect of these three parameters can be taken into account through the $[Cl^-]/[OH^-]$ ratio.

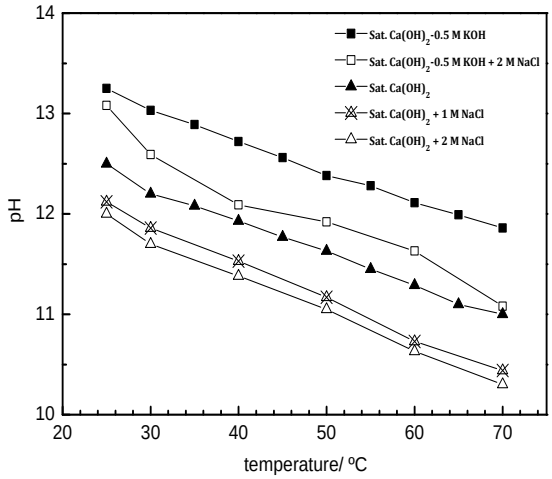

Fig. V.40 Variation of the alkaline pH as a function of the temperature and the concentration of NaCl.

Fig.V.41 depicts the evolution of the charge Q for the 2304 DSS in the saturated $Ca(OH)_2$ solution with 1 M and 2 M NaCl as a function of the temperature and the $[Cl^-]/[OH^-]$ ratio. This parameter, Q, seems to be able to quantify the pitting damage of the SS and the increase of both chloride concentration and the temperature promotes higher values of the pitting charge, Q.

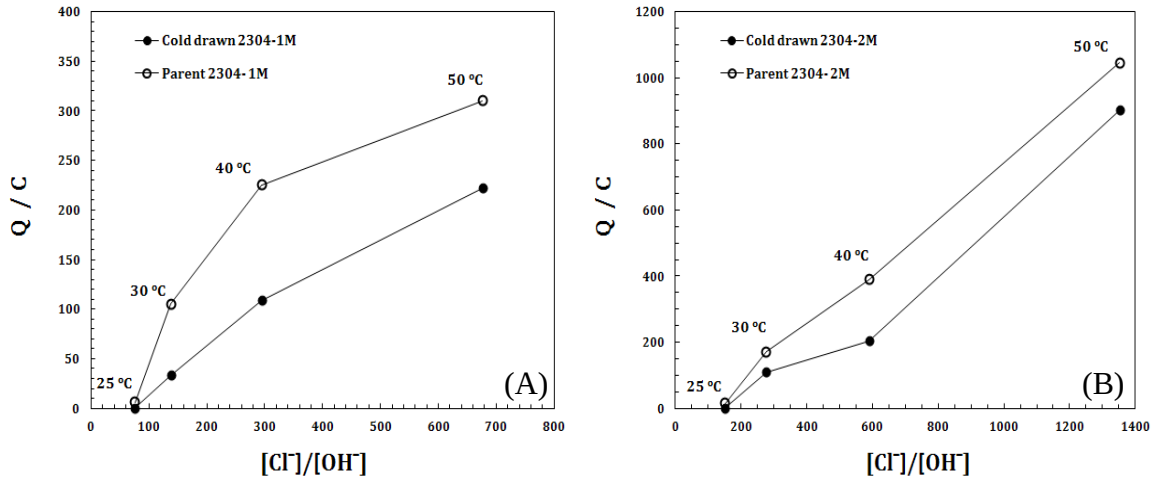

Fig. V.41. Electrochemical charge of 2304 cold drawn and parent DSS in saturated $Ca(OH)_2$ solution containing (A) 1 M and (B) 2M NaCl solutions at 25, 30, 40, and 50 °C.

Fig.V.42 and Fig.V.43 depict respectively the variation of the pitting potential (E_{pit}) and the repassivation potential (E_{rep}) of 2304 parent and the cold drawn DSS with respect to the temperature and the chloride concentration (expressed as $[Cl^-]/[OH^-]$).

The pitting potential shifts to more negative values with the temperature and chloride concentration increase. Consequently, the difference between the corrosion potential and the pitting potential is smaller in these conditions enhancing the susceptibility to pitting corrosion of duplex stainless steels. Furthermore, the cold drawn steels show a more positive pitting potential, that reflects the higher corrosion resistance of these steels in comparison with the parent stainless steels bars.

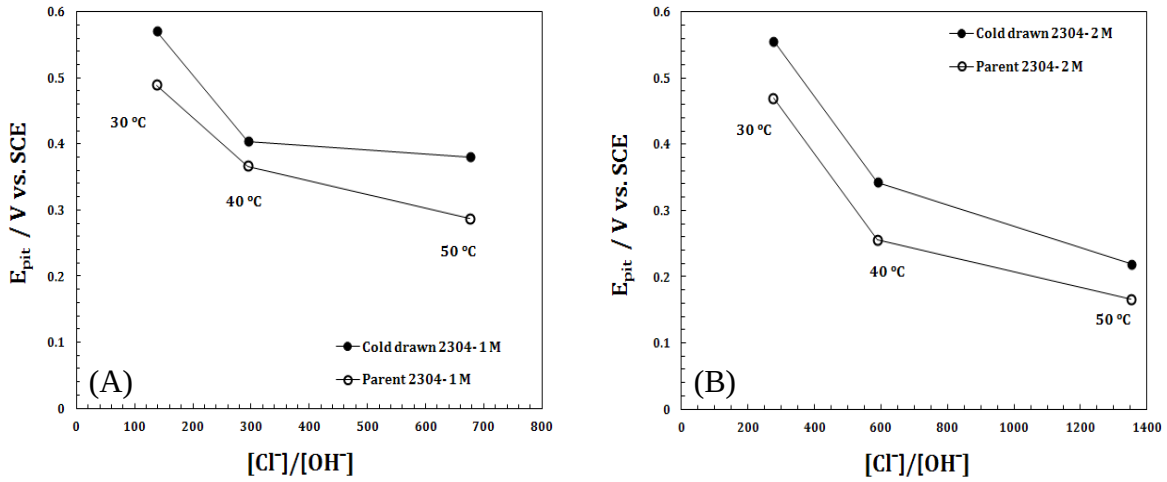

Fig. V.42. Pitting corrosion potential of 2304 cold drawn and parent DSS in sat. $Ca(OH)_2$ with (A) 1 M and (B) 2M NaCl solutions at different temperatures.

Fig. V.43 shows the repassivation potential as a function of the chloride concentration. As can be observed, the repassivation process of 2304 stainless steels becomes more difficult for the higher chloride concentrations and temperatures, and more negative E_{rep} values are registered.

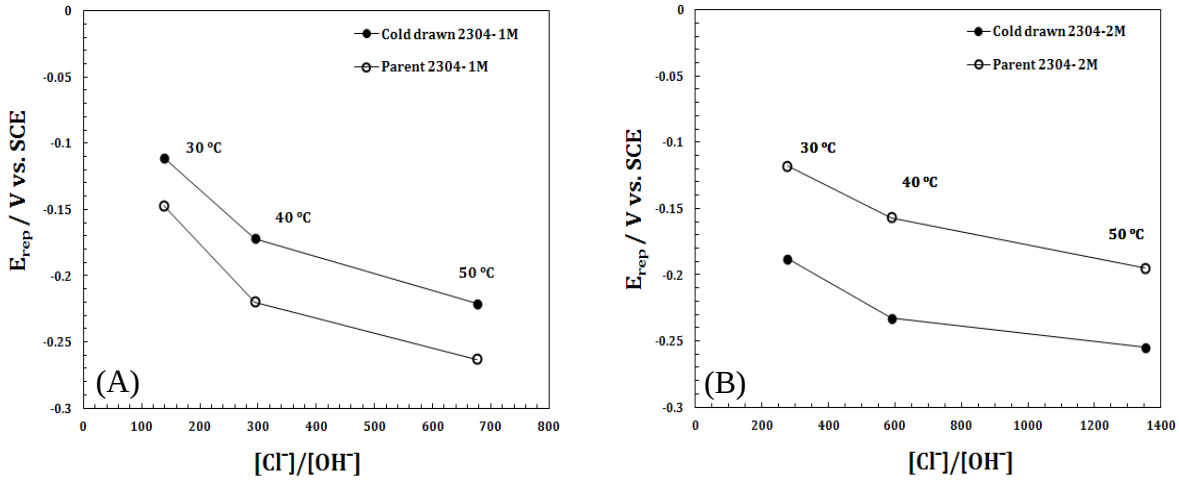

Fig. V.43. Repassivation potential of 2304 cold drawn and parent DSS in sat. $Ca(OH)_2$ with (A) 1 M and (B) 2M NaCl at different temperatures.

In the case of alkaline solutions containing 1 M NaCl, the cold drawn steels have more anodic repassivation potentials. However, when the chloride content increases up to 2 M NaCl, in case of cold drawn steel more negative E_{rep} values are obtained indicating higher difficulty for the repassivation process.

Comparing up mentioned results associated to the pit propagation parameters of 2304 parent and cold drawn DSS at 25 °C (see Fig.V.38) and at high temperature alkaline media (see Fig.V.41 and Fig.V.43), it can be concluded that the corrosion risk is accelerated with the increase of the temperature of the alkaline media for both parent and cold drawn SS. The corrosion damage of both parent and cold drawn SS at at 25 °C and 50 °C are shown in Fig.V.44. Parent SS presents higher Q than cold drawn wires (see Fig.V.41). This is probably associated to the fact that, at high temperature and aggressive environments, an extensive destroy of the passive film is occurring, as shown in Fig.V.44b, which induced the high weight loss of the material, and a as a consequence, high Q-value. However, in case of cold drawn SS, local pits were more localized on the steel surface, as shown in Fig.V.44d and lesser weight losses can be expected. Therefore, it can be concluded that, the change in the SS microstructure, not only affects the pit initiation phase but also shows a certain impact on the pit propagation process.

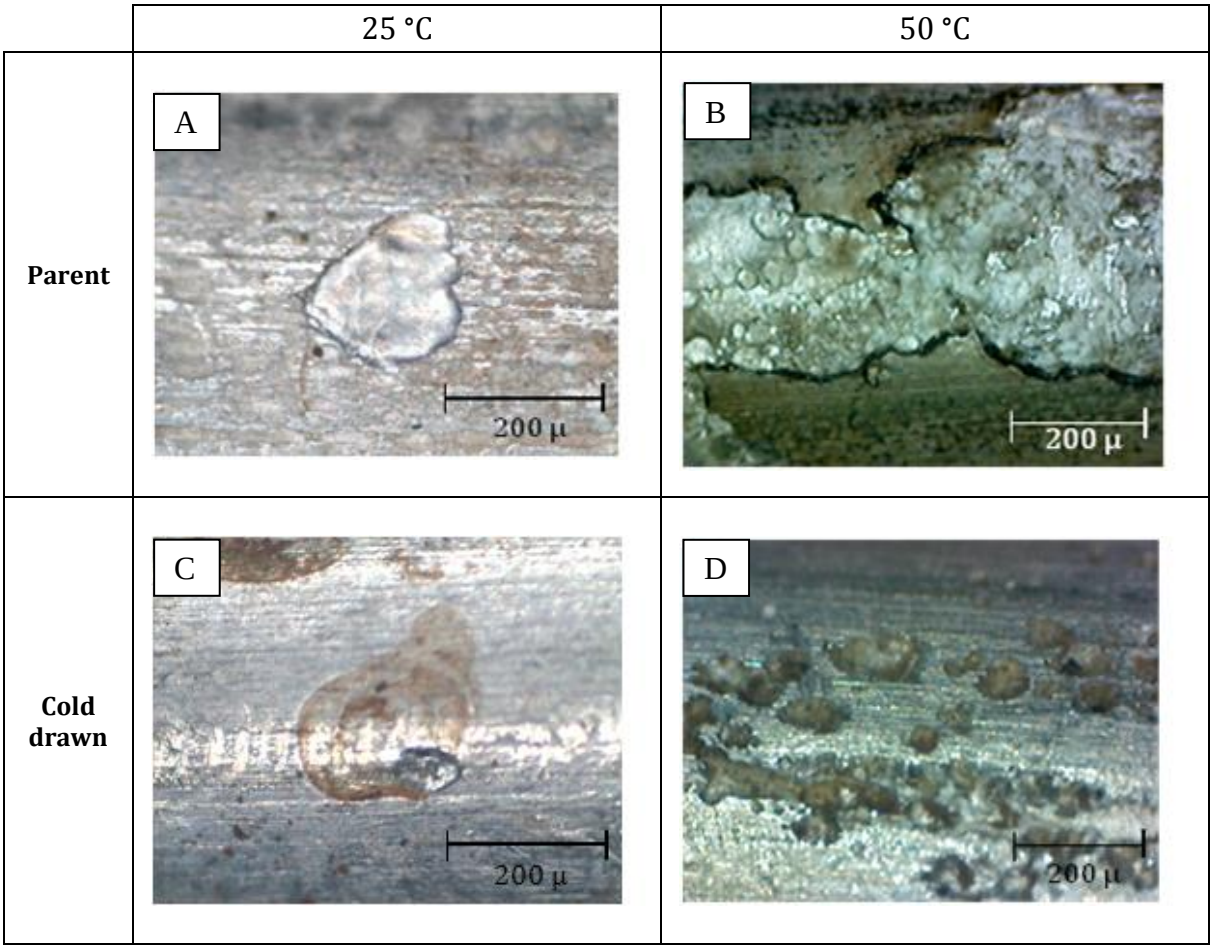

Fig. V.44 Optical examination of corrosion damage of parent and cold drawn 2304 SS after CV tests in saturated $Ca(OH)_2$ solution with 1.0 M NaCl at 25 and 50 °C.

V.3.3. Effect of SS alloy composition on the pitting corrosion propagation

In table V.10, the electrochemical charge of pitting corrosion, Q, and the repassivation potential, E_{rep}, of 2304 and 2205 parent and cold drawn DSS after CV test in saturated $Ca(OH)_2$ with 2 M NaCl at 50 °C are listed.

Table V.10 Q and E_{rep} values of parent and 2304 and 2205 CD-DSS after CV tests in saturated $Ca(OH)_2$ solution with 2.0 M NaCl at 50 °C.

	2304		**2205**	
	Parent	**Cold drawn**	**Parent**	**Cold drawn**
Q / C.cm^{-2}	1045	901	8.7	157
E_{rep} / mV$_{SCE}$	-195	-255	-54	-133

The listed data in table V.10 indicate that the stainless steel chemical composition presents a considerable impact on the pitting corrosion propagation process. At the same testing conditions, 2205 stainless steels present lower Q-value and higher E_{rep} in comparison with 2304 SS. Therefore, the pit propagation seems to be strongly hindered in 2205 SS probably due to the presence of Mo.

For highlighting the nature of the nucleated pits in case of 2205 SS, scanning electron microscope (SEM) examinations inside the pits and in the passive surface (outside the pits) have been carried out. Fig.V.45 depicts SEM images inside the pits for 2205 parent and cold drawn DSS after CV test in saturated $Ca(OH)_2$ solution with 2.0 M NaCl at 50 °C .

The morphology of the corrosion damage of 2205 parent and cold drawn DSS is different. Concerning parent SS, the pit propagation process is accompanied by a selective dissolution of the phase with less corrosion resistance, as shown in Fig.V.45a. Large corrosion pits are observed as a result of the selective dissolution process of the ferrite phase, leaving islands of austenite [130,142]. However, this selective dissolution is not clearly observed in case of cold drawn wires, as shown in Fig.V.45b.

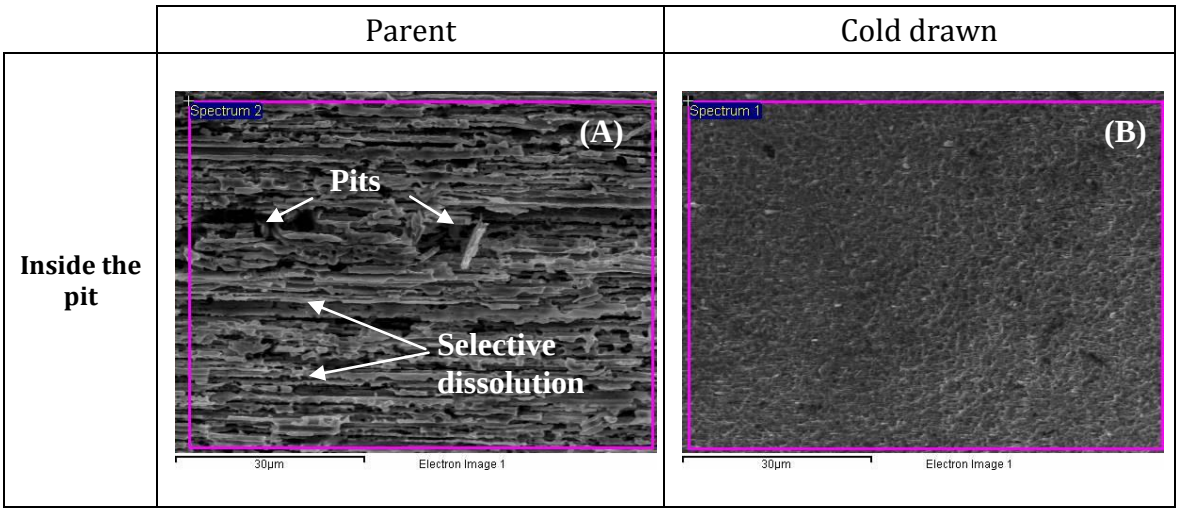

Fig. V.45 SEM images of inside and outside the nucleated pits on the surface of 2205 parent and cold drawn DSS after CV tests in saturated $Ca(OH)_2$ solution with 2.0 M NaCl at 50 °C.

The optical microscopy and SEM/EDX studies may provide useful insights into the fundamental mechanisms of corrosion initiation and propagation in duplex HSSS. Based on EDX data, the corrosion damage examined inside the propagated pit and on the passive surface outside the pit, for the 2205 SS, are composed mainly of Fe, Cr, Mo and Ni. These elements are present in slightly different concentrations inside and outside the pits, as listed in table V.11.

The weight percentages of Fe and Cr inside and outside the pit in case cold drawn SS seems to be unchanged. However, in the case of parent SS, these percentages have suffered a slight variation. Besides, for both SS, a smaller Ni weight percentage has been measured inside the pit than the Ni wt% percentage outside. This change in Ni wt% probably is related to the effect of the acidic media formed inside the pit during the corrosion propagation.

Table V.11 Weight percentages of Fe, Cr, Ni, and Mo inside and outside the pits formed on 2205 parent and cold drawn DSS after CV tests in saturated $Ca(OH)_2$ solution with 2.0 M NaCl at 50 °C.

	Parent				**Cold drawn**			
	Fe	**Cr**	**Ni**	**Mo**	**Fe**	**Cr**	**Ni**	**Mo**
Inside the pit	65.4	26.5	2.54	3.05	65.6	23.7	3.99	3.6
Outside the pit	70.6	18.4	3.33	2.52	63.6	23.2	4.42	3.2

On the other side, higher Mo wt% has been found inside the pits in the case of parent and cold drawn SS. This increase in Mo wt% may be related to the possible formation of stable Mo species in the acidic media generated inside the pits. The formation of these insoluble Mo oxides would limit the pit propagation and help the repassivation process of 2205 SS, which can explain the reason of the hindrance of the pit propagation in the case of 2205 SS in comparison with 2304 SS (see table V.10).

V.3.4. Effect of the load on the pitting corrosion propagation

The effect of the application of external load (70% of the maximum strength of the steel) on the pitting propagation process has been also evaluated by the comparison of the repassivation potential (E_{rep}) and Q-values after CV test in alkaline solutions with higher chloride concentration than CCT. E_{rep} and Q-values after CV test of tensioned 2304 parent and cold drawn DSS up to 70% of their maximum strength at 25 °C are listed in table V.12.

Table.V.12. Effect of the external load on the electrochemical charge (Q) and repassivation potential (E_{rep}) of 2304 cold drawn and parent DSS.

	Q / mC.cm^{-2}		E_{rep} / mV	
	Parent	**Cold-drawn**	**Parent**	**Cold-drawn**
Sat. $Ca(OH)_2$ + 0.3 NaCl - 0%	0.66	0.41	+325	+408
Sat. $Ca(OH)_2$ + 0.1 NaCl - 70%	907	870	-38	91
Sat. $Ca(OH)_2$ + 0.2 NaCl - 70%	1600	1296	-200	61

The shown data in table V.12 indicate the following:

I. The pitting corrosion risk and the pits propagation increase when the tested steels are exposed to an external load. In addition, higher Q-values and more negative E_{rep} are measured when an external load of 70% of the steel maximum strength is applied.

II. In all cases, parent SS presents more elevated Q-value and more negative E_{rep} than cold drawn SS. This behaviour is probably related to the high corrosion damage spread on the parent SS surface which makes the repassivation process more difficult.

III. The pitting corrosion damage is propagated with the increase of the chloride concentration for both 2304 parent and cold drawn DSS.

V.3.5. Validation of electrochemical estimations

Considering that the electrochemical charge of the pitting process is completely involved in the metal dissolution process, the estimation of the associated weight loss can

be made applying the Faraday's Law [205-210]. A conversion factor of 3.79 x 10^3 coulomb/gram was introduced as the stoichiometric dissolution of all the alloys as (Fe^{2+}, Cr^{3+}, Ni^{2+}, Mn^{2+}, and Mo^{3+}) [41,143]. A good agreement between the electrochemical weight loss and the gravimetric weight loss obtained by the gravimetric method (different of weight before and after the test) was found, as shown in Fig.V.46.

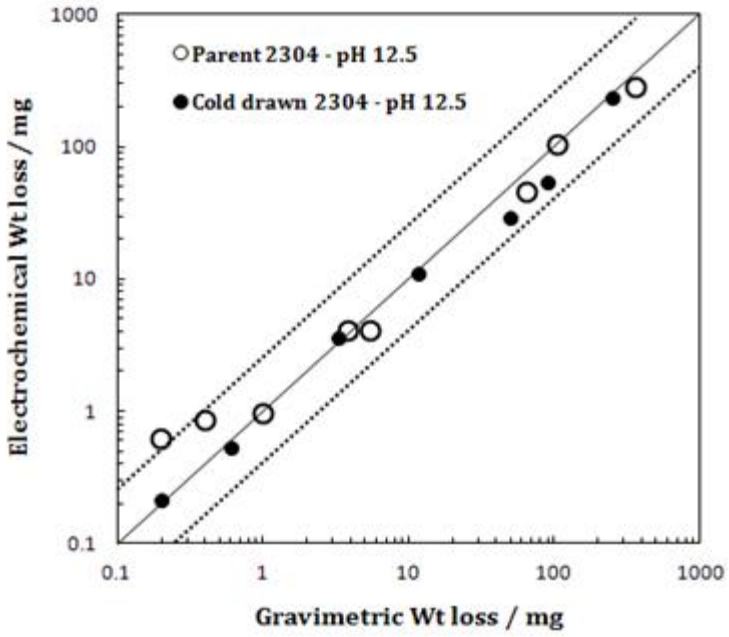

Fig. V.46. Electrochemical and gravimetric weight loss of 2304 cold drawn and parent DSS.

V.4. Main achievements in the corrosion behaviour of HSSS in alkaline media in presence of chloride

The evaluation of the corrosion resistance of duplex high strength stainless steels throughout the study of their electrochemical response in presence of chloride and the determination of CCT in aggressive alkaline solutions indicate the following main aspects:

1. Before the pitting corrosion initiation, the presence of the chloride at the film/electrolyte interface influences the passive film electrochemical response.

2. The long-term immersion in alkaline solutions with chlorides, after a previous 7 days pre-passivation stage, induces a lost in the protective properties of the passive film formed on duplex SS, which was confirmed by an increase in i_{corr} long-term measurements and by the fall in the impedance magnitude at the lowest frequencies. This modification in the passive film induced by the chloride content is more pronounced in parent steels than in cold drawn wires. This behaviour can be attributed to the decrease of the Cr^{III} content in the film as a consequence of the activation of the Cr^{III} dissolution as chromates with the increase of the chloride content in the interface.

3. The testing method influences the CCT values: CCT values determined using potentiodynamic tests are lower than CCT obtained by application of potentiostatic tests. The differences in CCT could be related to the different electrochemical properties of passive films grown using different electrochemical techniques and/or to the nature of the electrochemical test.

4. Potentiodynamic and potentiostatic estimation of CCT values of both 2304 and 2205 parent and cold drawn DSS confirm that both steels presents high corrosion resistance against pitting corrosion initiation, which allows the wide application of these steels in different environments including prestressed concrete structures.

5. Cold drawn stainless steels shown a relatively higher corrosion resistance, and consequently, higher CCT values than parent wires probably due to the more refined microstructure induced by the cold drawn deformation process.

6. The pitting corrosion susceptibility of the duplex SS decreases with the increase of the alkalinity of the surrounding media. This behaviour might be related to both the minor aggressivity of the surrounding environment and to the changes on the passive film structure with the pH increase.

7. 2205 cold drawn DSS showed the best corrosion resistance against the pitting corrosion process even in case of the application of an external load, 70% of the steel maximum strength, and in high temperature aggressive environments, which reflect the positive effect of the Mo-content in improving the inhibition action of the passive film against the chloride ion local attack.

8. Rising the temperature of the alkaline media reduces the CCT values of the cold drawn and parent duplex stainless steels. Furthermore, according the evolution of the electrochemical charge (Q) of the pitting corrosion hysteresis loop, the pit propagation in case of parent SS was more intense than cold drawn SS in alkaline solutions contaminated chloride concentrations.

9. Concerning the electrochemical tests in mortar, the results obtained highlight the following:

   - Both 2304 parent and cold drawn DSS shows high corrosion resistance against the chloride induced pitting corrosion and high CCT was measured.
   - The CCT values in mortar vary from 3.06 ± 0.5 % Cl^- (by cement weight) for cold drawn 2304 SS to 2.3 ± 0.2 %Cl^- for parent 2304 SS.
   - The stainless steel microstructure influences the CCT: the cold drawn stainless steel shows higher corrosion resistance than parent wires.
   - In agreement with the result obtained in solutions, 2205 parent and cold drawn DSS also shows higher corrosion resistance in comparison with 2304 DSS, as no detection of propagated pits has been observed in case of 2205 DSS.

VI. Conclusions

VI. Conclusions

VI.1. Passivation of duplex HSSS in alkaline media

Concerning the analysis of the passivation process of DSS in alkaline media, the results obtained allow concluding the following:

1. The electrochemical response of the passive film formed on duplex HSSS is affected by the conditions in which the passive layer is generated. The exposure conditions and the stainless steel chemical composition have been the most relevant parameters that control the passivation of duplex HSSS in alkaline media.
2. The electrochemical response of the passive film formed on cold drawn DSS was different than parent stainless steels, which indicated that, the induced changes in the stainless steel microstructure by cold drawn deformation process also controls the electrochemical response of the tested duplex stainless steels.
3. Increasing the alkalinity of the surrounding media induces the formation of more conductive passive film with lower oxidation degree of iron oxides components in the passive layer.
4. Ageing of the passive film in alkaline media induces the enrichment of stable oxides with high oxidation degree, and as a consequence, the passive film reactivity decreases. In addition, a possible enrichment in Cr^{III}-oxides in the passive layer by ageing has been also expected, which can improve the protection capacity of the passive layer.

5. The presence of Mo during the passive film formation affects the passive film composition and its electrochemical response (probably associated to the changes in the composition of the iron and chromium oxides). Furthermore, Mo behaviour in the film appears to be controlled by the pH of the surrounding media.

VI.2. Corrosion behaviour of duplex HSSS in presence of chloride

Regarding the influence of the presence of aggressive agent like chloride ion on the electrochemical behaviour of the tested duplex HSSS, both 2304 and 2205 duplex HSSS show high corrosion resistance against the localized attack caused by chloride ion. Based on the observed results in presence of chloride ion, the following conclusions have been reported:

1. The presence of chloride ion in electrolyte less than the critical chloride concentration significantly affects the oxidation processes occurring in the passive layer. The oxidation of $Cr(OH)_3$ species present in the outermost of the passive film and the formation of dissolved chromate seems to be induced by the presence of chloride in the interface. In this case, the dissolved chromate inhibits the breakdown of the passive film and the formation of active pits on duplex stainless surface. However, the oxidation process to chromate decreases the thickness of the passive layer, and as a consequence, the passive film becomes more susceptible to pitting corrosion in presence of elevated chloride ion concentrations (critical chloride concentration) as deduced from EIS results.

2. The alkalinity of the medium has a significant influence on the critical chloride concentration of duplex HSSS, where, the critical chloride concentration able to breakdown the passive film formed on duplex stainless steels increases with increasing pH of the surrounding media. Although this behaviour would be inconsistent with the results of passivation in chloride free alkaline media, which indicates the formation of more conductive passive films in more alkaline media, this behaviour can however be explained by the fact that, in higher pH alkaline solutions, the media becomes less aggressive due to the diminution of $[Cl^-]/[OH^-]$ ratio in the passive film/electrolyte interface.
3. Concerning the influence of Mo content in the electrochemical response of duplex HSSS in presence of chloride ion, duplex HSSS with high Mo content exhibits high resistance against pitting corrosion in aggressive environments at room and elevated temperatures.
4. Cold drawn duplex HSSS are more resistant to chloride depassivation process in comparison with parent duplex stainless steels, which in turn confirms the role of the stainless steel microstructure in the electrochemical behavior of stainless steels.
5. The critical concentration of chloride for duplex stainless steel with high Mo content is about an order of magnitude higher than those without Mo.
6. The critical chloride concentration varies depending on the applied methodology for its determination. The potentiostatic determinations leads to higher values compared to the potentiodynamic tests. This is probably related to the nature of the formed passive layer during potentiodynamic and potentiostatic test.

7. Regarding the potentiostatic determination of the critical chloride concentration of duplex stainless steels in mortars by chloride penetration test, the critical chloride concentrations for duplex 2304 stainless steels varies from 3.06 ± 0.5 % total Cl^- (by cement weight) for cold drawn HSSS to 2.3 ± 0.2 % total Cl^- for parent duplex stainless steel. Concerning 2205 HSSS, no detection of active pits has been observed during potentiostatic chloride penetration test. However, in some case, a certain superficial oxidation has been noticed in case of cold drawn 2205, which was intensified after the exposure to atmosphere. This fact is probably related the duration of the polarization and Mo influence in Cr oxidation process.

   On the other side, a relatively lower CCT for 2304 DSS has been potentiostatically determined in chloride mixed-in mortar (1.8 to 2.1 % total Cl^- by cement weight).

8. Pitting propagation results of the duplex HSSS in alkaline media at high temperatures indicate that, DSS with high Mo content shows elevated critical pitting temperature (CPT). Furthermore, increasing the alkalinity of the medium increases the CPT of the tested steels. Beside, cold drawn DSS also presents higher corrosion resistance in high temperature aggressive environments than parent stainless steels.

9. The evolution of the pitting corrosion electrochemical charge confirms that pitting corrosion risk and propagation in case of parent duplex stainless steels is higher than cold drawn duplex SS, which in turn confirms the positive effect of cold drawn deformation process on the electrochemical behaviour of duplex stainless steels.

Conclusiones

VI. Conclusiones

Ante la elevada incertidumbre existente respecto a la respuesta electroquímica y a la capacidad protectora de los Aceros Inoxidables de Alta Resistencia (AIAR) tipo dúplex en entorno alcalino propio de un hormigón, el objetivo principal de la presente tesis se ha focalizado en evaluar este tipo de materiales con prestaciones mecánicas adecuadas para su aplicación en estructuras de hormigón pretensado. Con base de los resultados obtenidos en presente estudio, las siguientes secciones presentan las conclusiones principales de cada parte del estudio experimental.

VI.1 Pasivación de AIAR en medios alcalinos

En cuanto al análisis del proceso de pasivación de HSSS dúplex en medios alcalinos, los resultados obtenidos permiten concluir lo siguiente:

1. El comportamiento electroquímico de los AIAR tipo dúplex se ve afectado por las condiciones en las que se genera la capa pasiva. Se confirma que la composición química del acero y el medio de exposición son parámetros relevantes. En el caso particular del AIAR-dúplex el hecho de que el acero haya sido sometido a un proceso de deformación afecta al proceso de formación y respuesta de la capa pasiva.
2. El aumento de la alcalinidad del medio lleva a la formación de una película pasiva más conductora, indicando un menor grado de oxidación de los óxidos de hierro que la componen.
3. El envejecimiento de la capa pasiva en el medio alcalino en el que se genera tiene lugar a través del enriquecimiento de la capa en compuestos estables con mayor grado de

oxidación que disminuyen la reactividad de la película pasiva, aumentando de este modo su capacidad de protección posiblemente por el enriquecimiento en óxidos de Cr^{III} en su parte más exterior.

4. La presencia de Mo influye en la formación de la capa pasiva afectando tanto a la composición como en su respuesta electroquímica (probablemente asociada a cambios en la composición de óxidos de hierro y cromo). Por otro lado, el comportamiento del Mo parece estar afectado por el pH del medio ya que la elevada alcalinidad favorece la formación de molibdatos que son disueltos de la película pasiva.

VI.2 Corrosion del AIAR en presencia de cloruro

Respecto a la influencia de la presencia de cloruro en el comportamiento electroquímico de los aceros AIAR-dúplex, ambos aceros estudiados han demostrado aportar una elevada resistencia al ataque localizado provocado por el ion cloruro. De los resultados obtenidos por los AIAR-dúplex en presencia de cloruro cabe destacar los siguientes aspectos:

1. La presencia de una concentración de cloruro inferior a la crítica para iniciar un proceso de corrosión activa afecta de forma significativa a los procesos de oxidación que ocurren en la capa pasiva. La disolución de la película externa de $Cr(OH)_3$ presente en la película pasiva parece estar favorecida por la presencia de cloruro en el medio. Se trata de un proceso de oxidación con formación de cromato que se disuelve en el medio. Ante la presencia de bajas concentraciones de cloruro parece que este cromato disuelto tiene una actividad inhibidora que evita la ruptura de la capa pasiva. No obstante, el proceso de oxidación a cromato implica a su vez disminución del espesor de la capa pasiva, más

acentuado con el incremento de la concentración de cloruro en el medio. De este modo, la susceptibilidad de la película pasiva al ataque por cloruro aumenta hasta que la película se rompe a una cierta concentración de este ión (concentración crítica de cloruro).

2. La alcalinidad del medio influye de forma significativa en la concentración crítica de cloruros para una corrosión activa, que aumenta significativamente con el incremento del pH. A pesar de que este comportamiento en principio sería contradictorio con los resultados de pasividad, de los que se deducía la formación de películas pasivas más conductoras en los medios más alcalinos, puede sin embargo estar explicado por la menor agresividad de los medios de pH más elevado y por cambios en la estructura y composición de la propia capa pasiva y solubilización de la propia capa pasiva.

3. Respecto a la influencia de contenido de Mo en la respuesta de los AIAR-dúplex frente a la acción del ión cloruro, los aceros con elevado contenido de Mo presentan una resistencia mayor frente a la corrosión por picadura tanto a temperatura ambiente como a elevada temperatura.

4. Los aceros trefilados presentan una mayor resistencia frente a la despasivación por cloruro que los aceros originales (alambrones), confirmando el papel importante de la microestructura en el comportamiento de los aceros inoxidables frente a la corrosión.
5. La concentración crítica de cloruro (CCC) para mantener una corrosión activa determinada para estos aceros, incluso en las condiciones más agresivas, ha sido aproximadamente un orden de magnitud superior a la CCC determinada para los AIAR dúplex sin Mo.

6. El valor de la CCC varía en función de la metodología aplicada para su determinación. La aplicación de ensayos potenciostáticos como un ensayo acelerado conduce a mayores valores en comparación de los ensayos potenciodinámicos. Esto probablemente está relacionado al tipo de la capa pasiva que se forma.

7. Respecto a la determinación potenciostática de la CCC de los AIAR-dúplex en morteros, en el caso de penetración del cloruro (con proceso de generación y envejecimiento inicial de la capa pasiva) las concentraciones críticas encontradas varían de 3,06 ± 0,5 % Cl^- totales (respeto el peso de cemento) para los aceros AIAR-dúplex (trefilados) a 2,3 ± 0,2 % Cl^- totales para los alambrones en el caso del AIAR-dúplex tipo 2304. En caso de los aceros trefilados tipo 2205, no se ha detectado un inicio de corrosión por picadura durante el ensayos, sin embargo, en unos casos, se ha observado un ataque generalizado lo que puede estar relacionado a la duración del ensayo.

   Por otro lado, la determinación de la concentración critica de cloruro de los aceros 2304 tipo dúplex en morteros amasados con distintas cantidades de cloruro conducen a menores valores relativamente (de 1,8 a 2,1 % Cl^- totales).

8. Los resultados del comportamiento de los AIAR-dúplex a la propagación de la corrosión por picadura en medios alcalinos a elevada temperatura indican que, la temperatura crítica de picadura (TCP) aumenta en el caso de AIAR-dúplex con Mo en su composición. También el aumento de la alcalinidad del medio parece estar asociado a un incremento en la TCP. En el caso de los aceros trefilados se ha registrado una mejora del comportamiento a alta temperatura en comparación con los aceros de partida sin trefilar (alambrones).

9. La evolución de la carga de picadura confirma que la corrosión se propaga en forma mas rápida en el caso de los aceros AIAR-dúplex no sometidos al proceso de trefilado, de modo que no se ha podido observar un efecto positivo del proceso de deformación en frío sobre el comportamiento electroquímico de los aceros inoxidables dúplex, lo que puede estar relacionado con la ausencia de generación de fases martensiticas en los AIAR tipo dúplex trefilados siendo el estado superficial un factor más determinante y un tamaño de grano más fino.

Appendix I

Determination of B-constant by using Tafel lines slopes

The B-constant value for the tested duplex HSSS was estimated by the determination of the Tafel slopes of the linear anodic and cathodic branches of the polarization curve. The potentiodynamic measurements used to estimate the Tafel lines slopes were performed at a potential scanning rate of $1mVs^{-1}$ in the potential range from -200 mV to +200 mV vs. corrosion potential after two hours immersion in the test solutions. Butler-Volmer equation (Eq.I) was used to fit the experimental curves:

$$i = i_o \left[10^{\frac{(E-Eo,a)}{ba}} - 10^{\frac{-(E-Eo,c)}{bc}} \right] \qquad eq.\ I$$

Where b_a and b_c are the anodic and cathodic Tafel slopes, respectively. B-constant of Stern and Geary equation can be defined from these Tafel slopes (equation II):

$$B = \frac{ba \cdot bc}{2.3\ (ba+bc)} \qquad eq.\ II$$

The linear extrapolation of the cathodic and anodic branches starting at least at 50 – 100 mV away from E_{corr} [166-168], gives the values of Tafel slopes.

In literatures [41,167,182] there were two strategies to determine the B-constant value. The first one was carried out by one direct measurement of the cathodic and anodic Tafel lines starting from the cathodic potentials and using the same steel samples [167]. Fig.I show the potentiodynamic polarization curves of both 2205 and 2304 duplex HSSS in solutions of pH 12.5 and 13.5 at 25 °C.

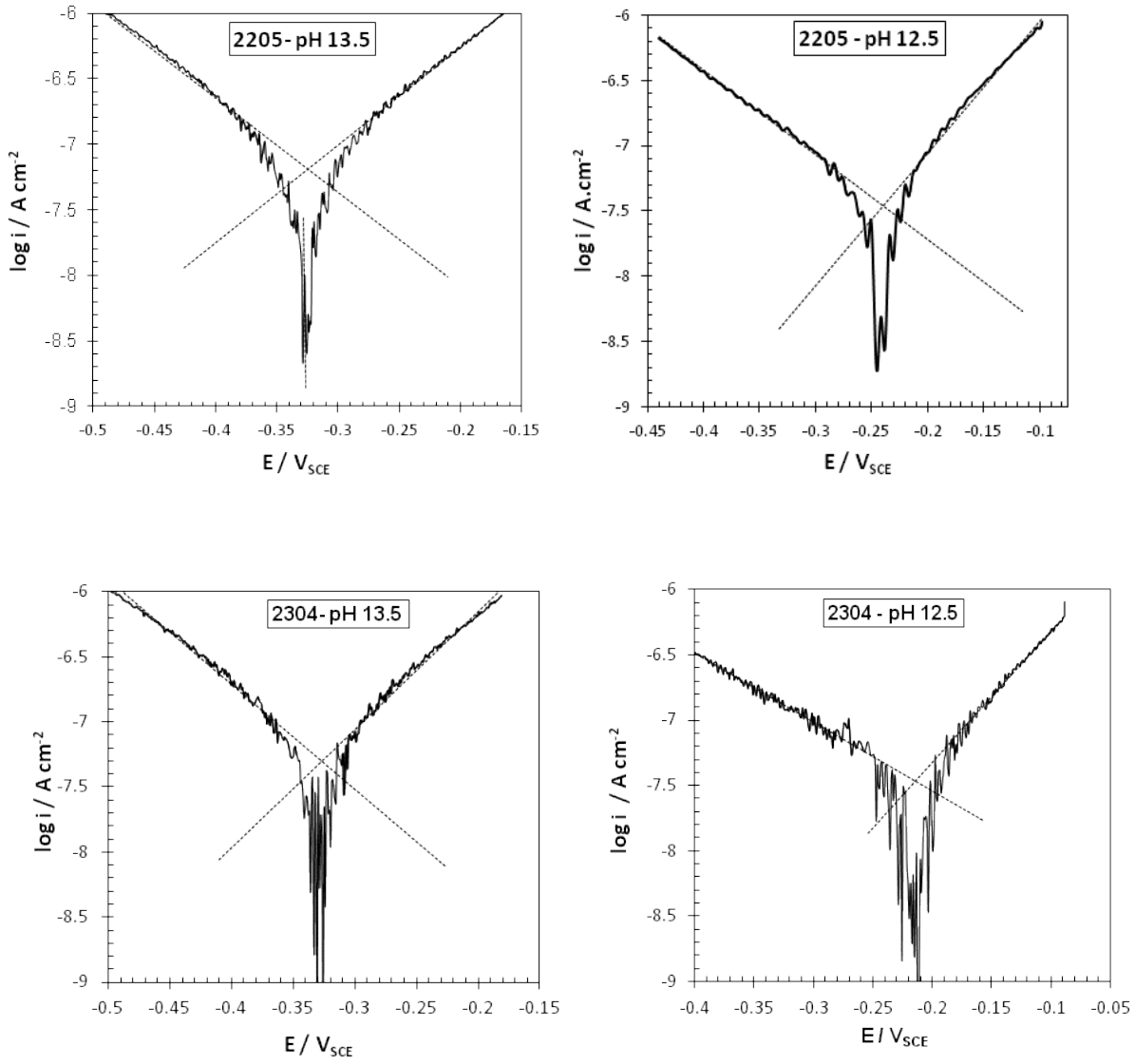

Fig. I Anodic and cathodic polarization curves of 2205 and 2304 duplex HSSS after immersion for 2 hours in alkaline media of pH 12.5 and 13.5, at 25 °C using only one steel sample. Potential range: ± 0.2 V from E_{corr}.

The fitting to Tafel behaviour by linear extrapolation of the cathodic and anodic branches starting at least at 0.05-0.1 V away from E_{corr} [167] gives the value of Tafel slopes b_a and b_c. The electrochemical parameters estimated situations (b_a, b_c, and *B-constant*) are

listed in table I. A mean value of 34 mV can be detected for the B-constant by using this method.

The limitation of this method was the possibility of the polarization of the tested stainless steel bar which may affects the Tafel lines slopes because of the use of only one rebar.

Table I The anodic and the cathodic Tafel lines slopes and B constant values of 2205 and 2304 duplex HSSS immersed in solutions of pH 13.5 and 12.5, using one steel sample.

HSSS	pH	b_a, mV dec^{-1}	b_c, mV dec^{-1}	B, mV
2205	13.5	368	120	39
	12.5	270	102	32
2304	13.5	270	107	33
	12.5	287	96	31

In order to study the reproducibility of the determined B-constant, another strategy was used for B-constant determinations. This strategy was mentioned in literature [41], where two stainless steel working electrodes were used to set the anodic and the cathodic polarization curve to avoid the possibility of the steel polarization during the test.

Fig.II depicts the anodic and the cathodic potentiodynamic polarization curves of both 2205 and 2304 duplex HSSS in solutions of pH 12.5 and 13.5 at 25 °C, in which two different stainless steel samples were used for measuring the cathodic and anodic branch.

The B-constant estimated values by the determinations of the Tafel slopes of the anodic and cathodic polarization curves are listed in table II. The mean value of the determined B-

constant using two stainless steels samples to measure the anodic and the cathodic polarization curves was 42 mV. The use of different surfaces seems to affect the measured Tafel slopes.

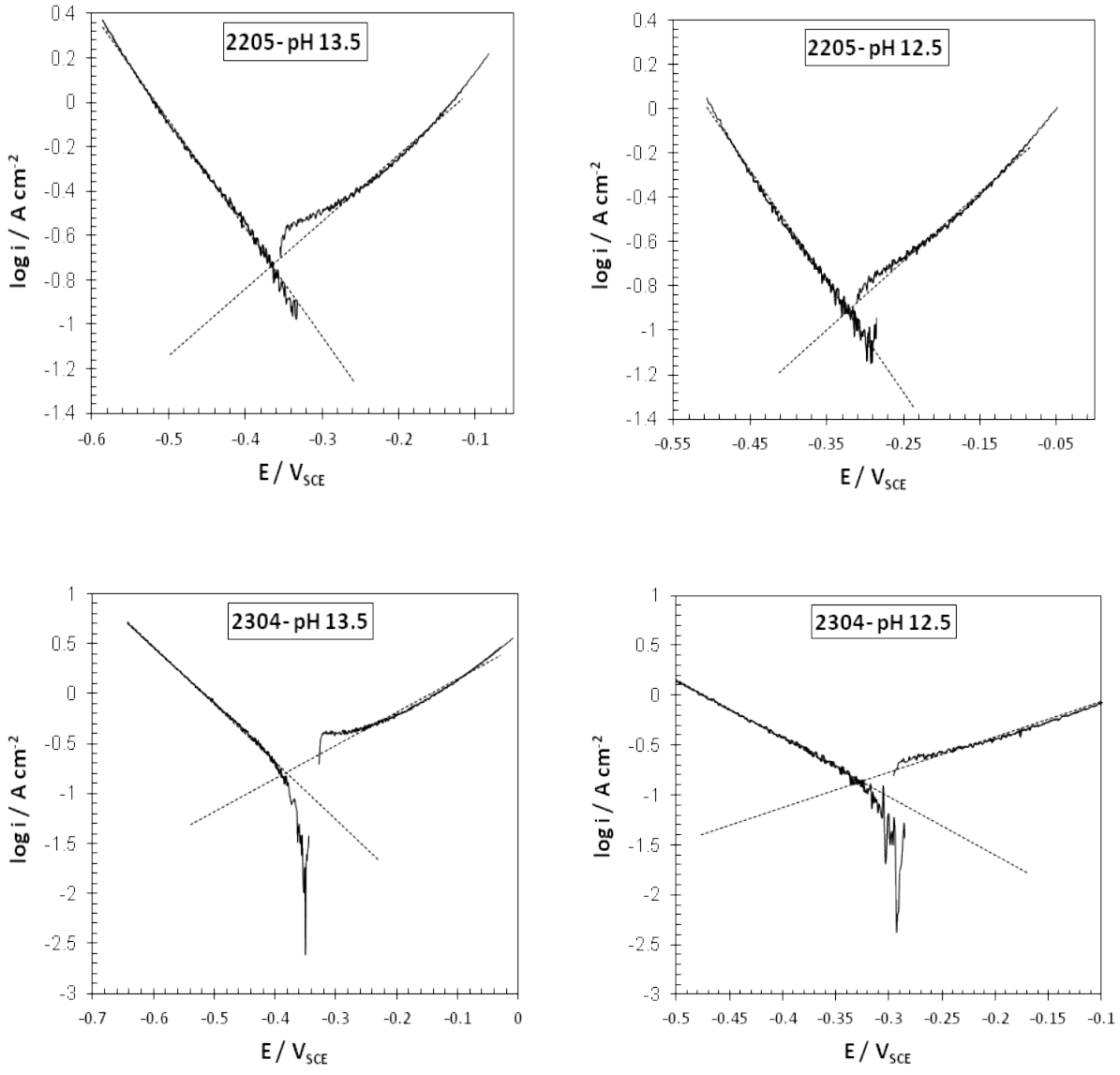

Fig. II Anodic and cathodic polarization curves of 2205 and 2304 duplex HSSS after immersion for 2 hours in alkaline media of pH 12.5 and 13.5, at 25 °C using two steel samples.

Table II The anodic and the cathodic Tafel lines slopes and B constant values of 2205 and 2304 duplex HSSS immersed in solutions of pH 13.5 and 12.5, using two steel samples.

HSSS	pH	b_a, mV dec^{-1}	b_c, mV dec^{-1}	B, mV
2205	13.5	208	202	45
	12.5	237	149	40
2304	13.5	219	179	43
	12.5	245	166	43

The difference in the B-constant value estimated using the two strategies was not relevant and the mean value of 34 mV obtained by the method of using one stainless steel was considered in present doctoral thesis to estimate i_{corr} values from the R_P measurements as higher variability of B-constant value has been obtained with the two stainless steels method.

Appendix II

Electrochemical Impedance Spectroscopy (EIS) monitoring of 2304 parent and cold drawn DSS in alkaline media of pH 12.5

Parent 2304 SS

The EIS spectra were recorded at different immersion times of the stainless steel bars in the different experimental conditions studied. The evolution of the Nyquist and Bode diagrams are represented in Fig.I and Fig.II for the specific case of parent 2304 DSS.

A continuous decrease of the impedance in the low frequency limit with the immersion time in the chloride containing solutions can be observed in Fig.I. Higher chloride concentrations give smaller impedance values at the lowest frequency limit, which is in agreement with the higher i_{corr} values measured (Fig.V.2). The decrease in the low frequency limit can be considered as a measure of the dissolution rate of the passive oxide film [134].

The Bode diagrams depicted in Fig.II show the tendency to less capacitive behaviour at low frequency limit by ageing in presence of chloride ion. This electrochemical response can be attributed to the formation of a more conductive passive layer, as suggested in [59].

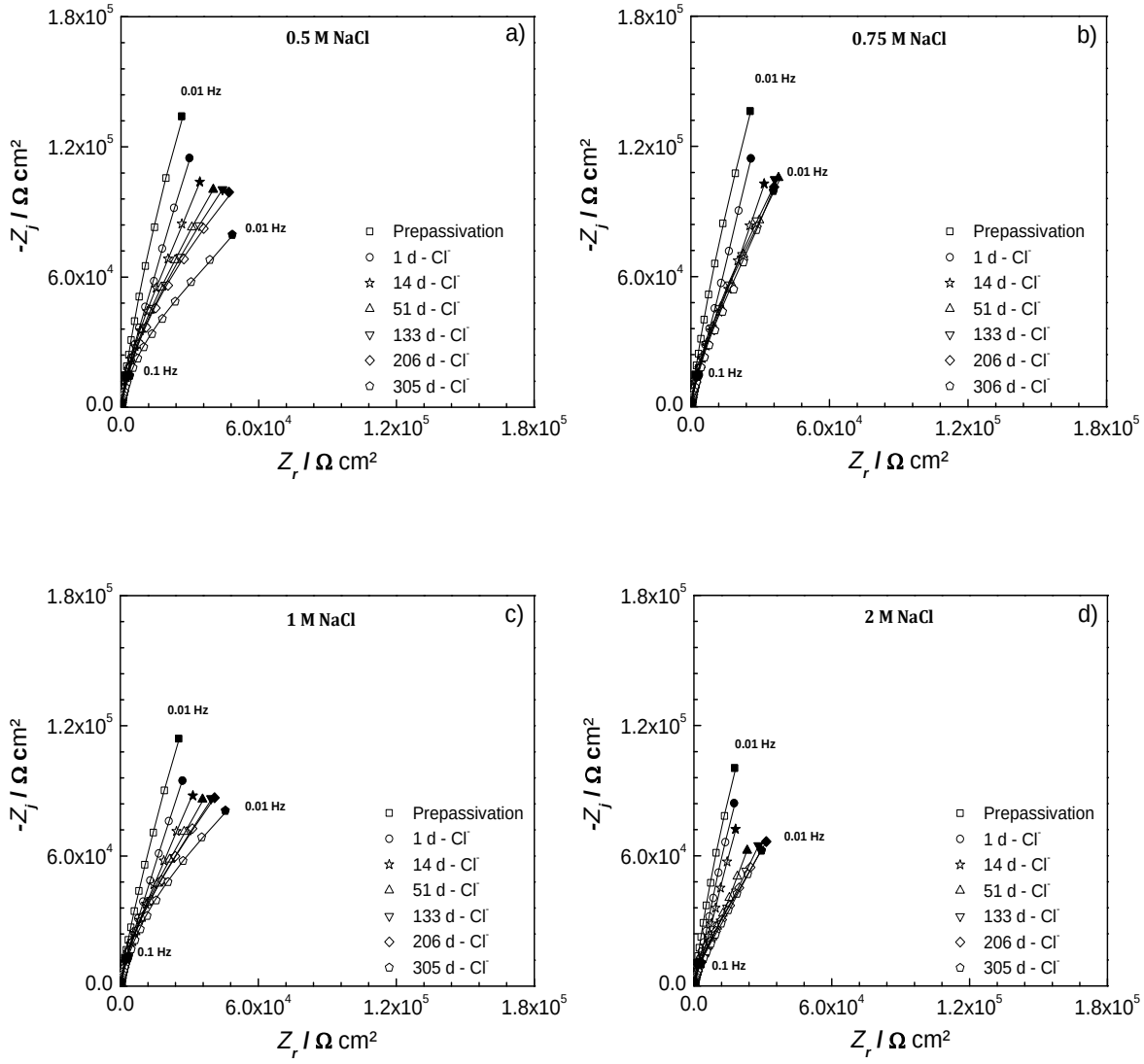

Fig. I Evolution of Nyquist impedance spectrum of 2304 parent SS in sat. $Ca(OH)_2$ solution with (a) 0.5, (b) 0.75, (c) 1.0, and (d) 2.0 M NaCl. Experimental data (dots), fitting with 2*RC* equivalent circuit (solid lines).

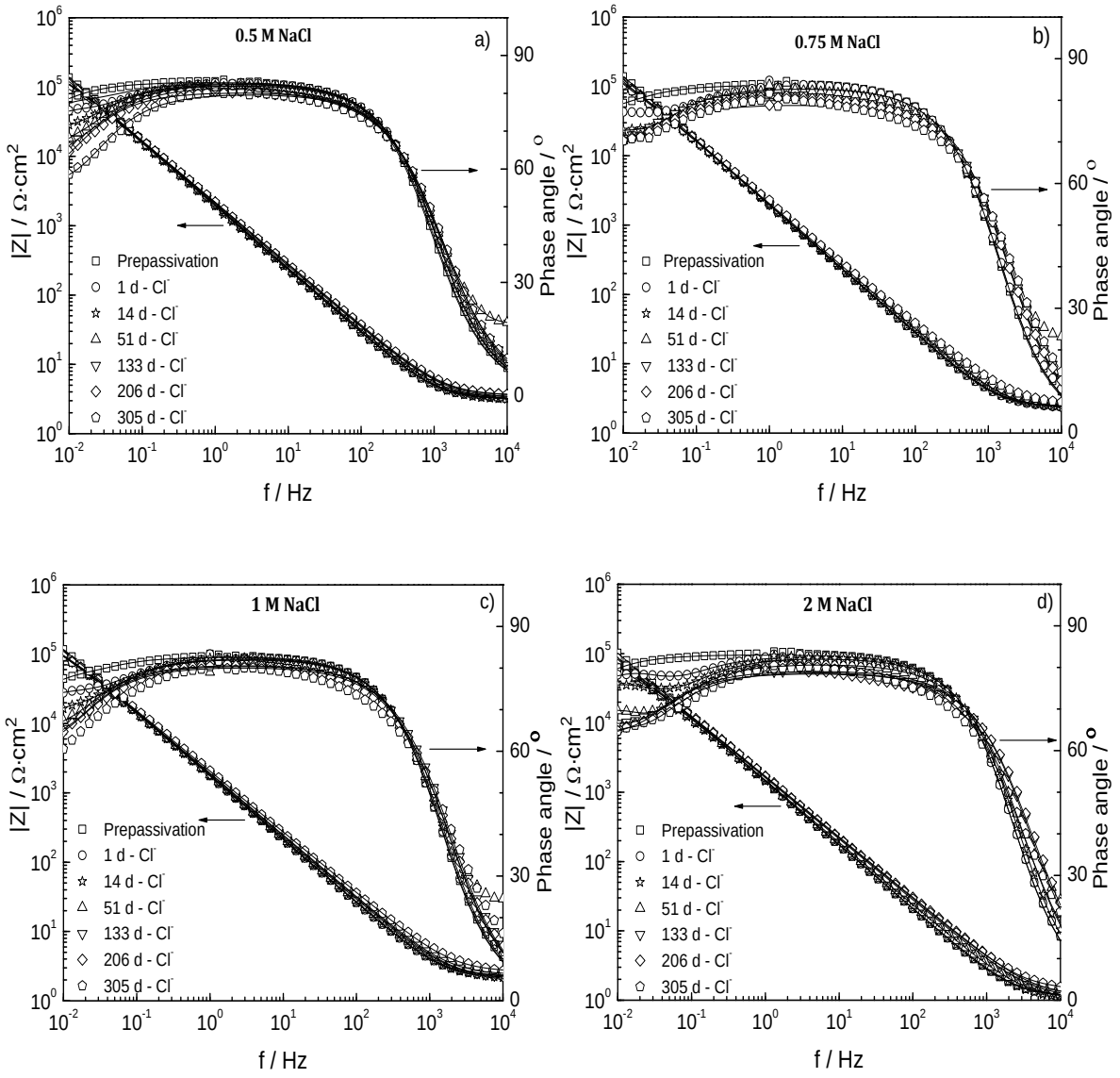

Fig. V.II Evolution of Bode plots of 2304 parent SS in sat. $Ca(OH)_2$ solution with (a) 0.5, (b) 0.75, (c) 1.0, and (d) 2.0 M NaCl. Experimental data (dots), fitting with 2*RC* equivalent circuit (solid lines).

To point out the effect of the chloride content on the electrochemical response of the passive film, the Nyquist and the Bode plots of parent 2304 SS after 133 days of immersion in presence of 0.5, 0.75, 1, and 2 M NaCl are displayed in Fig.III. The impedance magnitude falls with increasing the chloride content, being more evident in 2 M NaCl (Fig.IIIa). This fact agrees with the less protective response of these passive layers as the chloride content increases (Fig.IIIb).

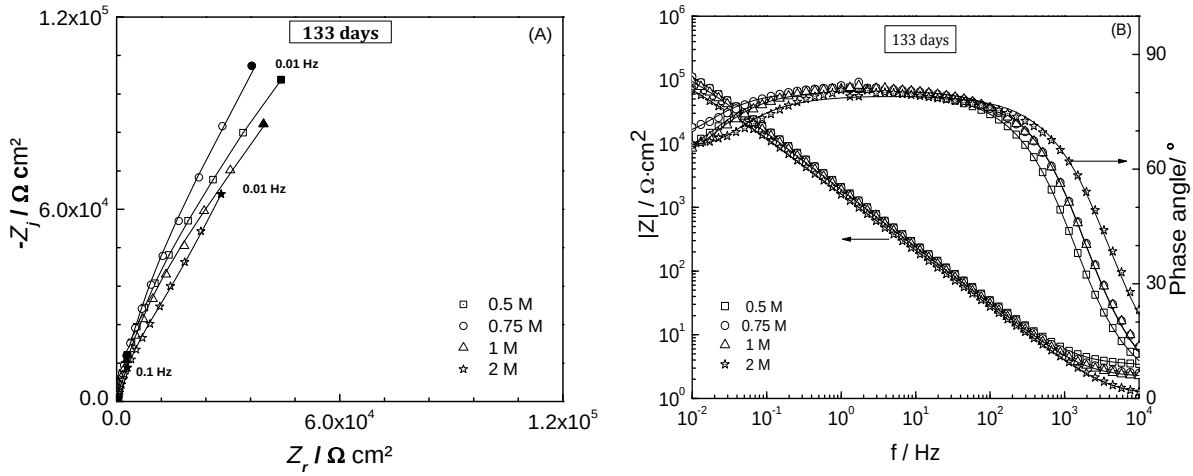

Fig. III Nyquist (A) and Bode (B) plots of 2304 parent SS after 133 days of immersion in sat. $Ca(OH)_2$ solution with different chloride concentrations. Experimental data (dots), fitting with 2*RC* equivalent circuit (solid lines).

Two time constants can be distinguished from impedance spectra. EIS data included in Fig.I and Fig.II have been interpreted by using the same EEC described in experimental parte (chapters III) with two RC connected in parallel. A good agreement between the experimental data (dots) and the fitted data (solid lines) can be confirmed in Fig.I, Fig.II and Fig.III.

The evolution of the passive elements involved in the EEC has been represented in Fig.IV and Fig.V for the parent 2304 duplex stainless steel exposed to different chloride concentrations in the saturated $Ca(OH)_2$ alkaline solutions.

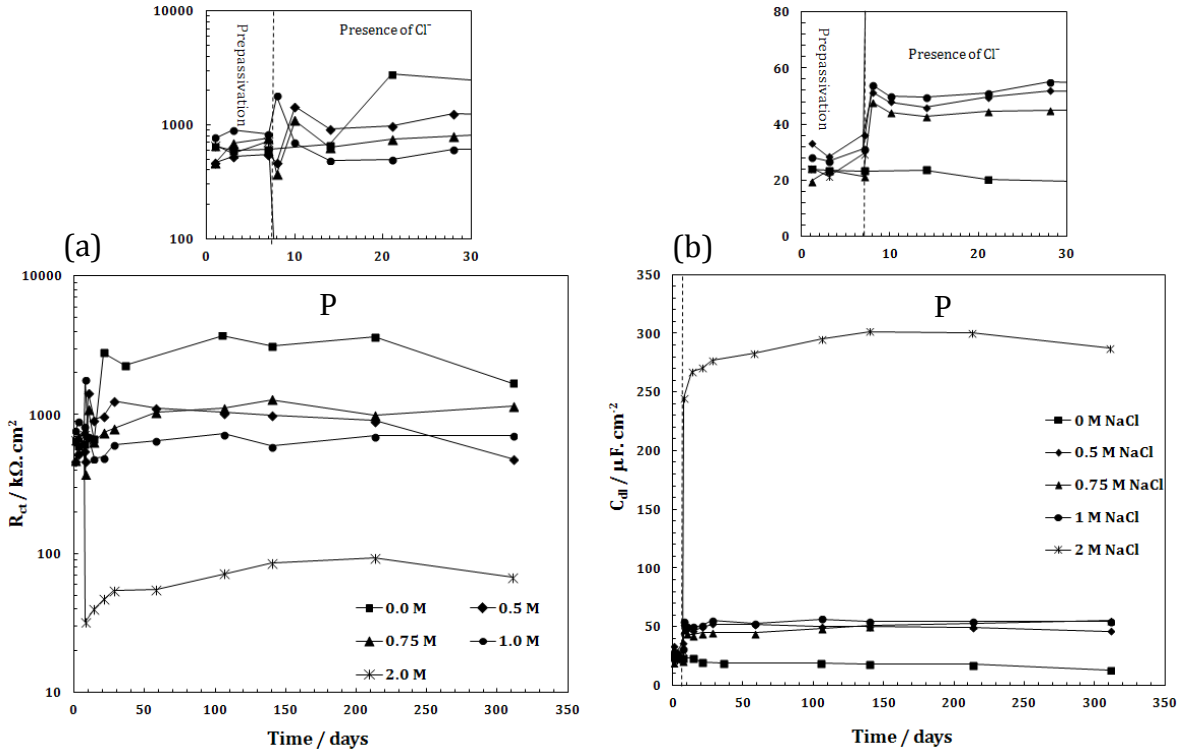

Fig. IV Evolution of EEC parameters for 2304 parent SS in alkaline sat. $Ca(OH)_2$ with different chloride concentrations. a) Charge transfer resistance (R_{ct}), b) Double layer capacitance (C_{dl})

Concerning the R_{ct} evolution, Fig.IVa, an increase of this parameter is observed with the ageing in alkaline solutions in absence of chloride, indicating that the transfer of charge through the film becomes difficult due to the formation of stable passive film, as described in passive state (chapter IV). The addition of chloride promotes a progressive decrease of R_{ct} with the chloride content (up to 1 M). The stabilization of this parameter with ageing is reached in each case indicating that the amount of chloride is not enough to destroy the

generated passive layer on the SS surface. When higher concentrations of Cl^- are added to the alkaline solution (2M), a significant decrease in R_{ct} values is observed, which evidences the faster charge transfer across the double layer, and agrees with higher i_{corr} results observed in this more aggressive condition (Fig.V.2).

As observed from Fig.IVb, C_{dl}, considered as the double layer capacitance in the proposed ECC, has an almost constant value with the immersion time in all cases, both in absence and in presence of chloride.

In chloride free solutions, values of C_{dl} oscillating between 20 and 30 μF cm^{-2}, in agreement with [46], where similar values corresponding to the double layer capacitance have been reported. The addition of chloride to the alkaline solution promotes the increase of C_{dl} with the chloride content that may be related to a certain decrease of the film thickness when chloride is present in the solution. For chloride concentration up to 1 M, slight increase of C_{dl} (45 – 55 μF cm^{-2}) is registered, but a sharp increase of C_{dl} is observed up to 260 - 285 μF cm^{-2} in the case of the highest chloride concentration (2 M), indicating a strong decrease of the passive film thickness that could be related with a more active dissolution of Cr^{III} present in the passive layer through the oxidation to chromates.

Fig. V displays the evolution of R_f and C_f values with the exposure time of 2304 parent SS in alkaline media with different concentrations of chloride. The influence of the chloride on the electrochemical properties of the passive layer is also confirmed from the R_f response, as observed in Fig.Va. While an increase of R_f value is registered in absence of chloride, a clear decrease of this parameter occurs with the chloride addition. The higher the chloride concentration, the higher diminution of R_f reaching values even two order of

magnitude lesser in the case of the highest concentration of chloride (2 M). Thus, the formation of a less oxidized passive layer with major presence of Fe^{II}-oxides in the spinel structure of iron-oxides can be expected with the increase of the chloride content in the electrolyte.

The capacitance C_f can be associated to the total amount of transformable charge (q) stored in the oxide layer according to Eq. (I), as suggested in [52,195,211-212]:

$$C_f = q\frac{d\theta}{dE} \qquad eq.I$$

Where, θ represents the transformation degree achieved at a given electrode potential, E.

The transformation degree indicates a passive film more o less oxidized depending on the applied potential to the electrode, the open circuit potential in this case. The lower C_f pseudocapacitance values of the passive film formed in absence of chloride ions indicate a diminution of the amount of charge susceptible to be transformed in comparison with the higher capacitance values registered when chloride is added. In presence of chloride, C_f increases asymptotically until reaching an almost constant value, more significantly for the highest chloride content (2 M).

This fact indicates that the presence of the chloride ions in the passive film/electrolyte interface affects the passive film structure and induces changes in the oxidation degree of the oxides layer as suggested in [46], even if no corrosion initiation can be detected from the corrosion current density values (Fig.V.2).

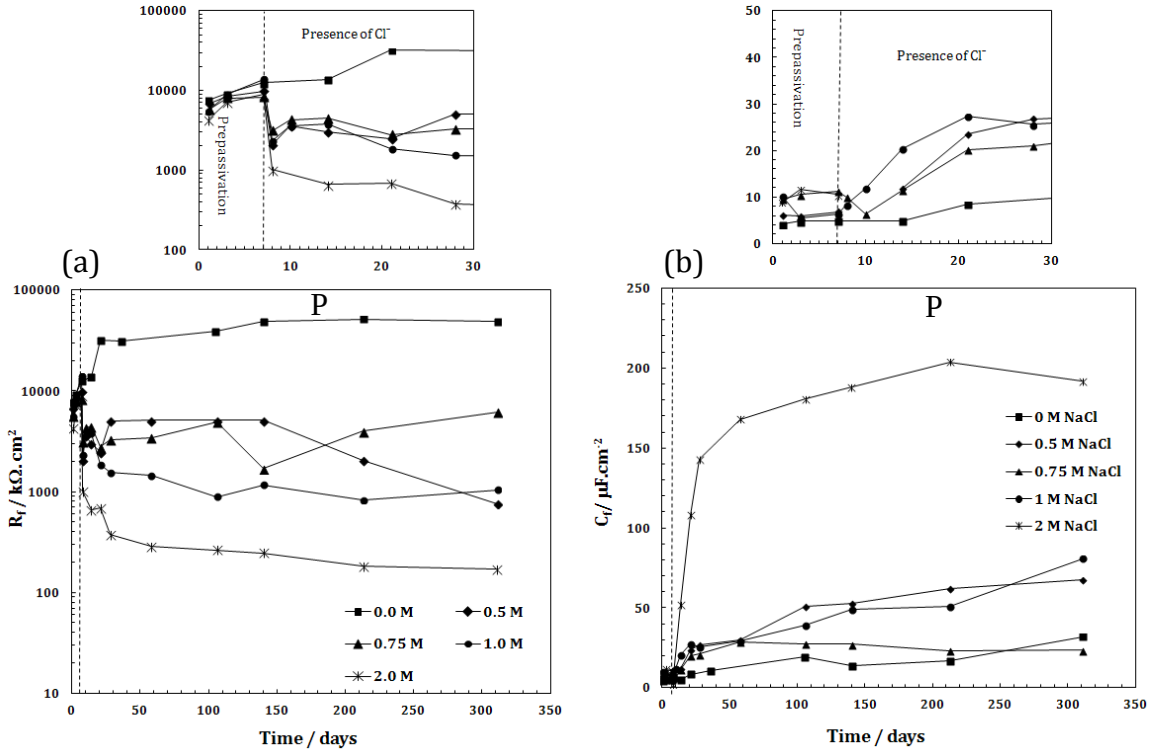

Fig. V Evolution of (a) R_f , and (b) C_f obtained by fitting the impedance data of 2304 parent SS in Sat. $Ca(OH)_2$ solution with 0, 0.5, 0.75, 1, and 2 M NaCl.

Cold drawn 2304 SS

In order to report the effect of the stainless steel deformation after the cold drawn process, EIS measurements of cold drawn 2304 wires were performed. Nyquist and Bode diagrams at different times of immersion in alkaline solutions with 0.5, 0.75, 1 and 2 M NaCl are shown in Fig.VI and Fig.VII respectively.

The displayed data in Fig.VI and Fig.VII show that the low frequency limit of the impedance was slightly diminished by increasing the chloride content. Furthermore, ageing in the alkaline solution with the highest concentration of chloride (2 M) promotes a clear decrease in the impedance at the lowest frequencies.

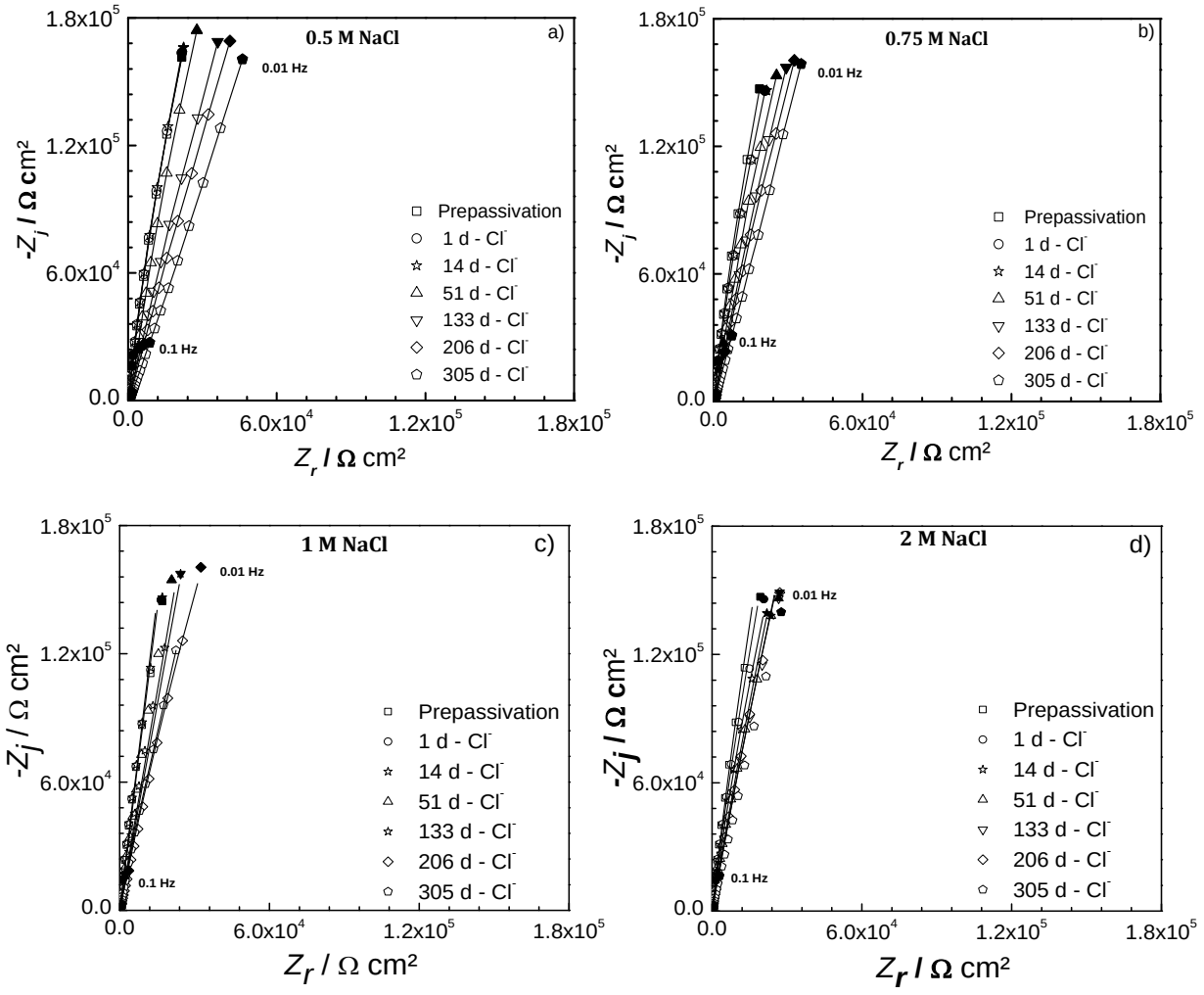

Fig. VI Evolution of Nyquist plots of 2304 cold drawn SS in sat. $Ca(OH)_2$ solution with (a) 0.5, (b)0.75, (c)1.0, and (d) 2 M NaCl. Experimental data (dots), fitting with $2RC$ equivalent circuit (solid lines).

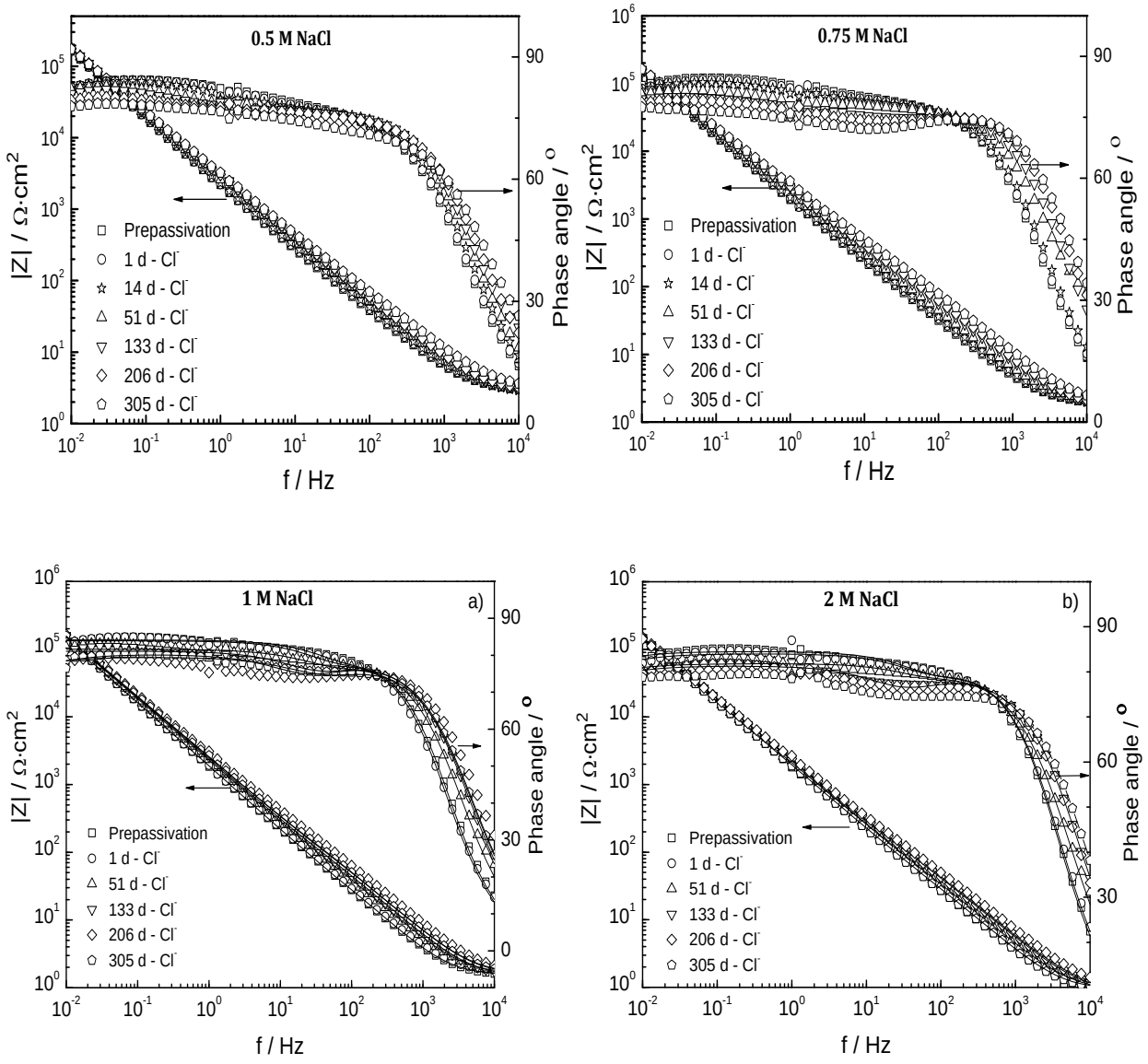

Fig. VII Evolution of Bode diagrams of 2304 cold drawn SS in sat. $Ca(OH)_2$ solution with (a)0.5, (b)0.75, (c)1.0, and (d) 2 M NaCl. Experimental data (dots), fitting with 2*RC* equivalent circuit (solid lines).

The fitting data obtained for EIS spectra of 2304 cold drawn DSS using the 2RC equivalent electric circuit are displayed in Fig.VIII and Fig.IX.

The charge transfer through the passive film/electrolyte interface becomes more difficult as the R_{ct} resistance increases as a result of the passive film grown, Fig.VIIIa. However, in presence of chloride, lower values of R_{ct} are measured, indicating a faster charge transfer across the double layer in the oxide layer formed on CD-DSS.

The higher R_{ct} values reported for cold drawn compared with parent stainless steel probably is an indication of the formation of a more compact and stable passive layer.

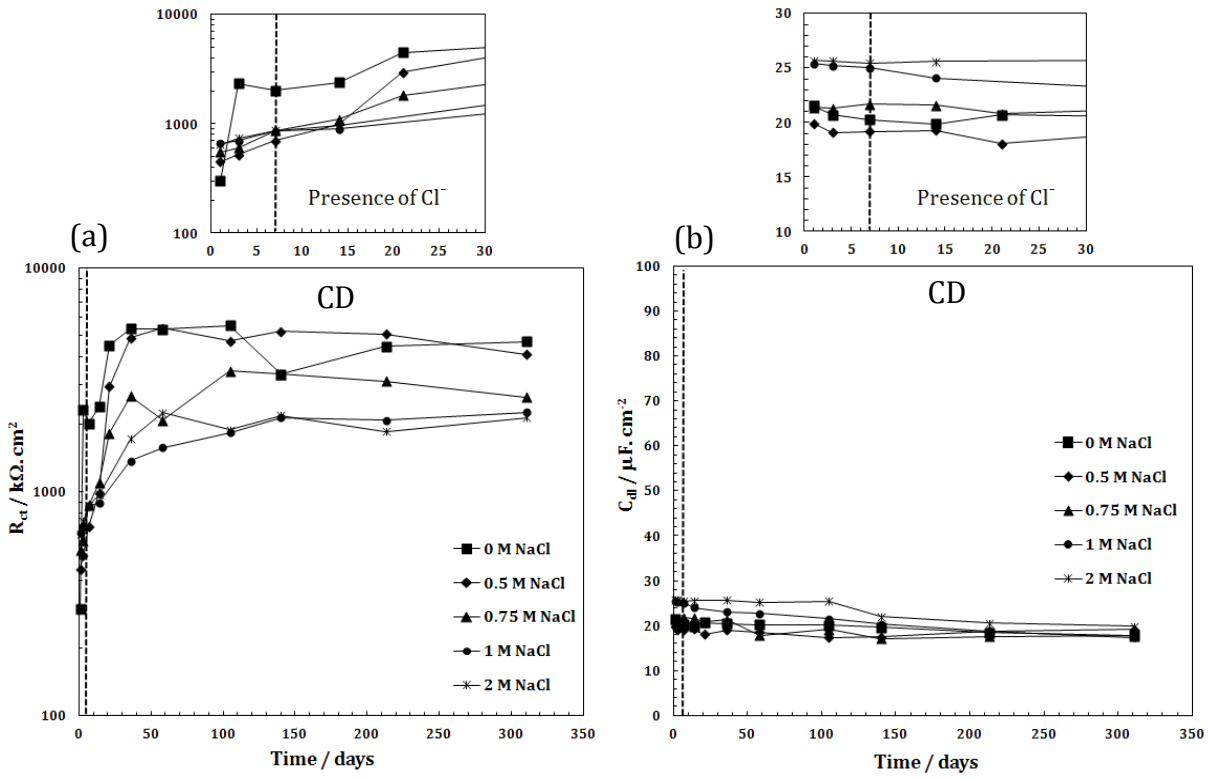

Fig. VIII Evolution of EEC passive parameters for cold drawn 2304 SS in alkaline sat. $Ca(OH)_2$ with different chloride concentrations. a) Charge transfer resistance (R_{ct}) , b) Double layer capacitance (C_{dl})

The capacitance values at the highest frequencies of the passive film grown on the cold drawn steel surface are limited between 18-25 $\mu F.cm^{-2}$ (Fig.VIIIb), even in presence of high concentration of chloride (2 M). These capacitance values, similar to the C_{dl} values

measured in the case of parent stainless steel in absence of chloride (Fig. IVb), are expected to correspond to the double layer capacitance and seem not to be affected by the presence of chloride, even in high concentrations (2 M). Thus, no relevant changes in the thickness of the passive layer are expected to occur in the studied exposure conditions when cold drawn stainless steel is considered, suggesting the formation of more stable passive layer on this type of stainless steel.

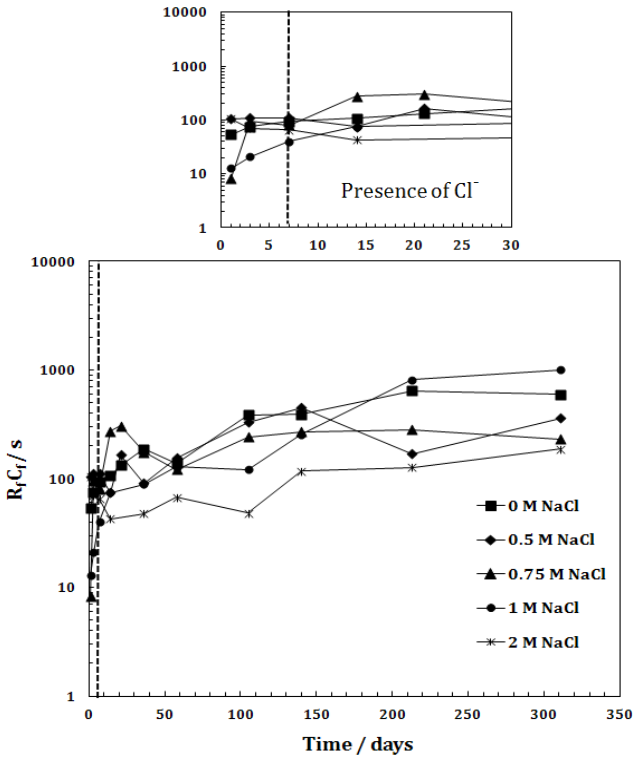

Fig. IX Variation of R_f C_f time constant of cold drawn 2304 SS in solutions of Sat. $Ca(OH)_2$ with 0, 1, and 2 M NaCl at different immersion time.

Concerning the low frequency time constant, shown in Fig.IX, $R_f \cdot C_f$ decreases with the increase of the chloride content. For concentrations up to 1 M, $R_f . C_f$ increases with the immersion time and the formation of an electrochemically more stable passive layer with ageing can be expected. However, for the highest chloride content (2 M) a significant

decrease of R_fC_f values is observed, which in turn suggests a perturbation of the passive film redox process.

The comparison of R_f C_f time constant for both cold drawn and parent stainless steels indicates that the reported changes induced by ageing in presence of chloride observed for the parent stainless steel cannot be clearly identified in the cold drawn SS.

References

1. H. F. W. Taylor. A method for predicting alkali ion concentrations in cement pore solutions. Advances in Cement Research 1 (1987) 5–16.

2. R. F. Feldman, P. J. Sereda. A new model for hydrated Portland cement and its practical implications. Engineering Journal (Canada) 53, 8/9 (1970) 53-59.

3. S. Feliu, C. Andrade, et al. Manual de inspección de obras dañadas por corrosión de armaduras. Edt ACOR 23 (1989).

4. José Luis García Calvo. Desarrollo de materiales de construcción con cemento de bajo pH, compatible con la barrera de ingeniería de un almacenamiento geológico profundo de residuos radiactivos de alta actividad. Tesis Doctoral Universidad Autónoma de Madrid, Spain – 2012.

5. A. Moragües, A. Macías, C. Andrade. Equilibria of the chemical composition of the concrete pore solution. Part 1. Comparative study of synthetic and extracted solutions. Cement and Concrete Research 17 (1987) 173-182.

6. B. Bhattacharjee. Sustainability of concrete construction in Indian context. The Indian Concrete Journal (2010) 45-51.

7. K. Tutti. Corrosion of steel in concrete. Report No. Fo 4. Swedish. Cement and Concrete Research Institute. Stockholm (1982).

8. R. Alizadeh, P. Ghods, M. Chini. M. Hoseini, M. Shekarchi. Durability based design of RC structure in Persian Gulf region using DuraPCulf moldel. Concrete Repair, Rehabilitation and Retrofitting- Alexandre (eds.) Taylor and Francis Group, London, ISBN 0 415 39654 9. (2006).

9. Ueli Angst, Bernhard Elsener, Claus K. Larsen, Øystein Vennesland. Critical chloride content in reinforced concrete- A review. Cement and Concrete Research 39 (2009) 1122-1138.

10. A. Volkwein. Corrosion protection by concrete, part 1 – preventative measures, Cost Action 521 final report, Corrosion of steel in reinforced concrete structure, Edt. R. Cigna, C. Andrade, U. Nürnberger, R. Polder, R. Weydert, E. Seitz, European Commission. (2003) pp. 8-18.

11. Jennifer L. Kepler, David Darwin, Carl E. Locke. Evaluation of corrosion protection methods for reinforced concrete highway structures. A report on research sponsored by the Kansas department of transportation, University of Kansas center for research, INC. (2000) 1-53.

12. Vedul S. Sastri. Corrosion Inhibitors-Principles and Applications. John Wiley and Sons, Chichester, (1998).

13. Mercedes Sánchez Moreno. Películas pasivas modificadas por el empleo de inhibidores de corrosión para la protección de armaduras. Sistemas de prevención de la corrosión. Doctoral Thesis (2007).

14. T. Y. Lin, NED H. Burns. Design of prestressed concrete structures. Third Edition. John Wilky & Sons Inc. (1981) 1-38.

15. J. Toribio, E. Ovejero. Effect of cold drawing on microstructure and corrosion performance of high-strength steel. Mech. Time-Depend. Mater. 1 (1998) 307-319.

16. B. González, J. C. Matos, J. Toribio. Relación microestructura-propiedades mecánicas en acero perlitico progresivamente trefilado. Anales de Mecánica de la Fractura 26 (2009) 142147.

17. M. Dollar, I.M. Bernstein, A.W. Thompson. Influence of deformation substructure in flow and fracture of fully pearlitic steel. Acta Metall. 36 (1988) 311-320.

18. C.C. Kumria, W.H. Hartt, R.J. Kessler. Influencing of chlorides, pH and precharging upon embrittlement of cathodically polarized prestressing steel. Procedure corrosion 90, Las Vegas, Nevada, April (1990) paper number 322.

19. R.N. Parkins, M. Elices, V. Sánchez-Gálvez, L. Caballero. Environment sensitive cracking of pres-stressing steels. Corrosion Science 22 (1982) 379-405.

20. Ulf Nürnberger. Corrosion induced failure mechanisms of prestressing steel. Materials and corrosion 53 (2002) 591-601.

21. Ulf Nürnberger. Influence of material and processing on stress cracking of prestressing steel. Materials and Corrosion 48 (1997) 602-612.

22. Maria Cruz Alonso, Miguel Ángel Villegas, Enrique de las Heras. Developments in steel tendons. Design and materials, COST 534 final report of "New materials and systems for prestressed concrete structures", Edt. R.B. Polder, M.C. Alonso, D.J. Cleland, B. Elsener, E. Proverbio, Ø. Vennesland, A. Raharinnaivo. European commission (2007) 6-34.

23. Young Sang Ko, Jin Woo Park, Hyounsoo Park, Jong Dae Lim, and David K. Matlock. Application of high strength microalloyed steel in a new automotive crankshaft. Proceedings of International Conference on New Developments in Long and Forged Products: Metallurgy and Applications, edited by J.G. Speer, E.B. Damm and C.V. Darragh, AIST, Warrendale, PA, USA (2006) 3-10.

24. R. Narayan Swamy. Design for durability with galvanized reinforcement. Galvanized Steel Reinforcement in Concrete. S. R. Yeomans (Editor). International lead zinc research organization. Inc. Research Triangle Park, Raleigh Durham. North Carolina, USA. (2004) 31-69.

25. E. Riecke. Investigations on the influence of zinc on the corrosion behaviour of high strength steels. Material and Corrosion 30 (1979) 619-631.

26. F.J. Recio, M.C. Alonso, L. Gaillet, M. Sánchez. Hydrogen embrittlement risk of high strength galvanized steel in contact with alkaline media. Corrosion Science (2011) 2853-2560.

27. Y. Wu, U. Nürnberger. Corrosion-technical properties of high-strength stainless steel for the application in prestressed concrete structures. Materials and Corrosion 60 (2009) 771-780.

28. Y Katada, M Sagara, Y Kobayashi, T. Kodama. Fabrication of High strength nitrogen stainless steels with excellent corrosion resistance and its mechanical properties. Materials and Manufacturing Process 19 (2004) 19-30.

29. A.John Sedriks. Corrosion of stainless steel, second edition, corrosion monograph series, sponsored by the electrochemical society. John Wiley & Sons. Inc., (1996) 1-13.

30. David Talbot, James Talbot. Corrosion science and technology (CRC series in materials science and technology), by CRC Press LLC, chapter 8 (1998).

31. N. Lopez, M. Cid and M. Puiggali. Influence of σ-phase on mechanical and corrosion resistance of duplex stainless steels. Corrosion Science 41 (1999) 1615-1631.

32. M. Wilms, V. Gagil, J. Krougman, F. Ijsseling. Effect of σ-phase precipitation at 800 °C on the corrosion resistance in sea-water of high alloyed duplex stainless steel. Corrosion Science 36 (1994) 871-881.

33. C.M. Abreu, M.J. Cristóbal, R. Losada, X.R. Nóvoa, G. Pena, M.C. Pérez. Comparative study of the passive films of different stainless steels developed on alkaline medium. Electrochimica Acta (49) (2004) 3049-3056.

34. K. Hashimoto, K. Asami, K. Teramoto. An X-ray photo-electron spectroscopy study of the passivity of Ferritic 19Cr stainless steels in 1N HCL. Corrosion Science 19 (1979) 251-260.

35. U. Nürnberger, Y. Wu. Stainless steel in concrete structure and in fastening technique. Materials and Corrosion 59 (2008) 144-158.

36. W. Schmidt, H. H. Dolmalski, W. Schaffrath. Zur verfestigung chemisch bestandiger austenitischer drahte durch Kaltumformung. Thyssen Edelstahl Technische Berichte 12 (1985) 101-111.

37. P. Gümpel, F. Helmut. Über die Eigenschaften von kaltverformten Drähten aus stickstoffhaltigen nichtrostenden Stählen für die Seilherstellung. Thyssen Edelstahl Technische Berichte 14 (1988) 25-38.

38. Ulf Nürnberger. Prestressing steel- corrosion damages and application of stainless steels tendons. Cost 534 – Final work shop, Toulouse, France (2007).

39. F.J. Recio, Y. Wu, M.C. Alonso, U. Nürnberger. Hydrogen embrittlement risk in cold-drawn stainless steels. Materials Science & Engineering A 564 (2013) 57-64.

40. M.C. Alonso, M. Sánchez, E. Mazarío, F.J. Recio, H. Mahmoud, R. Hingorani. High strength stainless steels 14301 for prestressed concrete structure protection. 6th international conference on Concrete under severe conditions (CONSEC 10) - Mexico (2010) 1047-1054.

41. F. Javier Recio, Corrosión de aceros inoxidable y galvanizados de alta resistencia, como alternativa a los aceros convencionales de pretensado, PhD Thesis, Universidad Autónoma de Madrid, Spain, (2010).

42. Andrés Valiente, Mihaela Iordachescu. Damage tolerance of cold drawn ferritic-austenitic stainless steels wires for prestressed concrete. Construction and Building Materials 36 (2012) 874-880.

43. A. Hedayati, A. Najafizadeh, A. Kermanpur, F. Forouzan. The effect of cold rolling regime on microstructure and mechanical properties of AISI 304L stainless steels. J. Mater Process Technol 210 (2010) 1017-1022.

44. M. Milada, N. Zreibaa, F. Elhalouanib, C. Baradaib. The effect of cold work on structure and properties of AISI 304 stainless steel. J. Mater Process Technol 203 (2008) 80-85.

45. Marijana Serdar, Lidija Valek Žuli, Dubravka Bjehovic. Long-term corrosion behaviour of stainless reinforcing steel in mortar exposed to chloride environment. Corrosion Science 69 (2013) 149-157.

46. C.M. Abreu, M.J. Cristóbal, R. Losada, X.R. Nóvoa, G. Pena, M.C. Pérez. Long-term behaviour of AISI 304L passive layer in chloride containing medium. Electrochimica Acta 51 (2006) 1881-1890.

47. Lucien Veleva, Mario A. Alpuche-Aviles, Melissa K. Graves-Brook, David O. Wipf. Voltammetry and surface analysis of AISI 316 stainless steel in chloride-containing simulated concrete pore environment. Journal of Electroanalytical Chemistry 578 (2005) 45–53.

48. Lucien Veleva, Mario A. Alpuche-Aviles, Melissa K. Graves-Brook, David O. Wipf. Comparative cyclic voltammetry and surface analysis of passive films grown on stainless steel 316 in concrete pore model solutions. Journal of Electroanalytical Chemistry 537 (2002) 85-93.

49. M. Gojic, D. Marijan, L. Kosec, Electrochemical Behavior of Duplex Stainless Steel in Borate Buffer Solution. Corrosion 56 (2000) 839-848.

50. Aleksandra Kocijan, Crtomir Donik, Monika Jenko. Electrochemical and XPS studies of the passive film formed on stainless steels in borate buffer and chloride solutions. Corrosion Science 49 (2007) 2083-2098.

51. A. Bautista, G. Blanco, F. Velasco, A. Gutiérrez, L. Soriano, F. J. Palomares, H. Takenouti. Changes in the passive layer of corrugated austenitic stainless steel of low nickel content due to exposure to simulated pore solutions. Corrosion Science 51 (2009) 785-792.

52. L. Freire, M. J. Carmezim, M. G. S. Ferreira, M. F. Montemor. The passive film behavior of AISI 316 in alkaline media and the effect of pH: A combined electrochemical and analytical study. Electrochimica Acta 55 (2010) 6174-6181.

53. M.J. Carmezim, A.M. Simões, M.F. Montemor, M. Da Cunha Belo. Capacitance behaviour of passive films on ferritic and austenitic stainless steel. Corrosion Science 47 (2005) 581.

54. M.G.S. Ferreira, M. Da Cunha Belo, N. E. Hakiki, G. Goodlet, M.F. Montemor, A.M. Simões. Semiconducting properties of the oxide and passive film formed on AISI 304 Stainless steels and Alloy 600. J. Braz. Chem. Soc. 13 (2002) 433-440.

55. D. Addari, B. Elsener, A. Rossi. Electrochemistry and surface chemistry of stainless steels in alkaline media simulating concrete pore solutions. Electrochimica Acta 53 (2008) 8078-8086.

56. C.M. Abreu, M.J. Cristóbal, R. Losada, X.R. Nóvoa, G. Pena, M.C. Pérez. Electrochemical behaviour of an AISI 304L stainless steel implanted with nitrogen. Electrochimica Acta 53 (2008) 6000-6007.

57. C.M. Abreu, M.J. Cristóbal, R. Losada, X.R. Nóvoa, G. Pena, M.C. Pérez. High frequency impedance spectroscopy study of passive films formed on AISI 316 stainless steel in alkaline medium. Electroanalytical Chemistry 572 (2004) 335-345.

58. C.M. Abreu, M.J. Cristóbal, R. Losada, X.R. Nóvoa, G. Pena, M.C. Pérez. The effect of Ni in the electrochemical properties of the oxide layers grown on stainless steels. Electrochimica Acta 51 (2006) 2991-3000.

59. C.M. Abreu, M.J. Cristóbal, X.R. Nóvoa, G. Pena, M.C. Pérez, R. J. Rodriguez Modification of the stainless steel passive film induced by cerium implantation. Surface and Coating Technology 158-159 (2002) 582-587.

60. C. Giacovezzo. Fundamentals of Crystallography, third ed., Oxford University Press, New York (1995) 442-493.

61. C. T. Liu. J. K. Wu. Influence of pH on the passivation behaviour of 254SMO stainless steel in 3.5% NaCl solutions. Corrosion Science 49 (2007) 2198-2209.

62. J. M. Bastidas. C. L. Torres, E Cano, J. L. Polo. Influence of molybdenum on passivation of polarized stainless steels in chloride environment. Corrosion Science 44 (2002) 625-633.

63. S. Maffi. B. Bozzini, A. Fanigliulo, L. Peralado Bicelli. A photoelectrochemical and spectroscopic investigation of oxide layers on AISI 301 in sulfate solution at different pH. J. of Applied Electrochemistry 34 (2004) 71-77.

64. B. Beverskog, I. Puigdomenech**.** Pourbaix Diagrams for the Ternary System of Iron-Chromium-Nickel. Corrosion 55 (1999) 1077-1082.

65. M. da Cunha Belo, M. Walls. N.E. Hakiki. J. Corset, E. Pickenard, G. Sagon, D. Noël. Composition, structure and properties of the oxide films formed on the stainless steel 316L in a primary type PWR environment. Corrosion Science 40 (1998) 447-463.

66. C. O. A. Olsson. The influence of nitrogen and molybdenum on passive films formed on the austeno-ferritic stainless steels 2205 study by XPS. Corrosion Science. 37 (1995) 467-479.

67. M.A. Ameer, A.M. Fekry, F. El-Taib Heakal. Electrochemical behaviour of passive films on molybdenum-containing austenitic stainless steels in aqueous solutions. Electrochimca Acta 50 (2004) 43–49.

68. C.R. Clayton, Y.C. Lu. A bipolar model of the passivity of stainless steels-III. The mechanism of MoO_4^{2-} formation and incorporation. Corrosion Science 29 (1989) 881–898.

69. M. Sakashita, N. Sato, in: Frenkental, Kruger (Eds.), Passivity of Metals, Electrochemical Society, Pennington, (1978) 479-491.

70. N. Boucherit, A. Hugot-le Goff, S. Joiret. Influence of Ni, Mo, and Cr on pitting corrosion of steels studied by Raman spectroscopy. Corrosion 48 (1992) 569–579.

71. W.J. Tobler, S. Virtanen. Effect of Mo species on metastable pitting of Fe18Cr alloys – a current transient analysis. Corrosion Science 48 (2006) 1585–1607.

72. C. R. Clayton. Y. C. Lu. A bipolar model of the passivity of stainless steels. The role of Mo addition. J. Electrochemical Society 133 (1986) 2465-2464.

73. Philippe Marcus. Corrosion Mechanisms in Theory and Practice. Second Edition, Revised and Expanded, MARCEL DEKKER, INC. NEW YORK. BASEL (2002) 225-266.

74. K. Sugimoto, Y. Sawada. The role of molybdenum additions to austenitic stainless steels in the inhibition of pitting in acid chloride solution. Corrosion Science 17 (1977) 425–445.

75. W.D. Robertson. Molybdate and tungstate as corrosion inhibitors and the mechanism of inhibition. J. Electrochemical Society 98 (1951) 94–100.

76. Y.C. Lu, C.R. Clayton, R. Brooks. A bipolar model of the passivity of stainless steels-II. The influence of aqueous molybdate. Corrosion Science 29 (1989) 863–880.

77. K. Ogura, T. Ohama. Pit formation in the cathodic polarization of passive iron IV. Repair mechanism by molybdate, chromate and tungstate. Corrosion 40 (1984) 47–51.

78. J.N. Waklyn. The role of molybdenum in the crevice corrosion of stainless steels. Corrosion Science 21 (1981) 211–225.

79. A. Ihrzo, Y. Segui, N. Bui, F. Dabosi. On the conduction mechanisms of passive films on molybdenum-containing stainless steel. Corrosion 42 (1986) 141–146.

80. F. Falkenberg, I. Olefjord. Passivation of stainless steels in hydrochloric acid. J. Electrochemical Society 146 (1999) 1397–1406.

81. S. Virtanen, W.J. Tobler, in: P. Schmuki, D.J. Lockwood, Y. Ogata, H.S. Isaacs (Eds.). Pits and Pores: Formation, Properties and Significance for Advanced Materials. PV 2000-25, The Electrochemical Society Proceedings, Pennington, NJ, (2000).

82. Szklarska-Smialowska. Mechanism of pit nucleation by electrical break down of the passive film. Corrosion Science (44) (2002) 1143–1149.

83. P. Schmuki, H. Boehni. Critical factors in localized corrosion. Electrochemical Society. 92 (1992) 170-188.

84. P. Schmuki, H. Boehni. Metastable pitting and semiconductive properties of passive film. J. Electrochem Society. 139 (1992) 1908-1913.

85. M. F. Montemor, A. M. P. Simoes, M. G. S. Ferreria, M. Da Cunha Belo. The role of Mo in the chemical composition and semiconductive behavior of oxide films formed on stainless steel. Corrosion Science 41 (1999) 17-34.

86. R. F. A. Jargelius-Pettersson, B. G. Pound. Examination of the role of molybdenum in passivation of stainless steels using AC impedance spectroscopy. J. Electrochemical Society 145 (1998) 1462-1496.

87. I. Olefjord, B. Brox, U. Jelvestam. Surface composition of stainless steels during anodic dissolution and passivation studied by ESCA. J. Electrochemical Society 145 (1985) 2854-2861.

88. D.D. MacDonald. The Point Defect Model for the Passive State. J. Electrochemical Society 139 (1992) 3434-3449.

89. P. Marcus, Corrosion Mechanisms in Theory and Practice, Marcel Dekker, New York, (2002).

90. I. Olefjord, B. O. Elfström. The composition of the surface during passivation of stainless steels. Corrosion NACE 38 (1982) 46-54.

91. S. Haupt, H.H. Strehblow. A combined surface analytical and electrochemical study of the formation of passive layers on FeCr alloys in 0.5 M H_2SO_4. Corrosion Science 37 (1995) 43-54.

92. P. Schmutz, D. Landolt. In-situ microgravimetric studies of passive alloys: potential sweep and potential step experiments with Fe–25Cr and Fe–17Cr–33Mo in acid and alkaline solution. Corrosion Science 41 (1999) 2143-2163.

93. W. M. Carroll and T. G. Walsh. The influence of pH, temperature and surface pretreatment on the stability of passive films formed on sanicro 28 and 5R60 stainless steels in aqueous chloride solutions. Corrosion Science 29 (1989) 1205-1214.

94. B. Elsener and A. Rossi. Effect of pH on the electrochemical behaviour and passive film composition of stainless steels. Materials Science Forum Vols. 192-194 (1995) 225-236.

95. B. Elsener, D. DeFilippo, and A. Rossi. Modifications of passive films. Edt. P. Marcus, B. Baroux and M. Keddam , EFC publ. No 12, The institute of Materials London, (1994) 6-11.

96. Seifedine Kadry. Corrosion Analysis of Stainless Steel. European Journal of Scientific Research. ISSN 1450-216X Vol.22 No.4 (2008) 508-516.

97. Outokumpu, Corrosion handbook, Outokumpu Stainless Steel Oy, Espoo (2004).

98. K.R. Tretheway, J. Chamberlain, Dissimilar Metal Corrosion, in: Corrosion for students of science and engineering, Longman Group UK Limited (1988).

99. E. Otero Huerta. Corrosión y degradación de materiales. Ed. Síntesis (1997).

100. M. Carboneras. Evaluación de la influencia de la adición de cobre y estaño en la resistencia a la corrosión de aceros inoxidables. PhD Thesis. Universidad Complutense de Madrid. España, (2004).

101. K.R. Tretheway, J. Chamberlain. Environment-sensitive cracking in: Corrosion for students of science and engineering, Longman Group UK Limited (1988).

102. L. Bertolini, M. Gastaldi, T. Pastore, MP. Pedeferri, P. Pedeferri, “Effects of galvanic coupling between carbon steel and stainless steel reinforcement in concrete”, Int.

Conf. on Corrosion and Rehabilitation of Reinforced Concrete Structures, Federal Highway Administration, Orlando (1998) 7–11.

103. Luca Bertolini, Bernhard Elsener, Pietro Pedeferri, Rob Polder. Corrosion of Steel in Concrete. WILEY-VCH Verlag GmbH & Co. KGaA, Weinheim. ISBN: 3-527-30800-8 (2003) 258-267.

104. L. Bertolini, M. Gastadli, M.P. Pedeferri. Stainless steel in concrete. European community, Cost 521 Workshop, Queen University, Belfast (2000) 27-32.

105. G. S. Frankel. Pitting corrosion of metals: A Review of The Critical Factors. J. Electrochemical Society 145 (1998) 2186-2197.

106. Ana Emilse Coy Echevarria. Evaluación de la modificación de elementos (Mo, Mn, Ti) en el comportamiento frente a la corrosión de aceros inoxidables austeníticos. PhD thesis. University of Complutense de Madrid. (2006).

107. H.H. Strehblow. Nucleation and repassivation of corrosion pits for pitting on iron and nickel. Werk. Korros. 27, 792 (1976) and Wileky-VCH Verlag Gmbh, Weinheim. Germany (1976).

108. C. Y. Chao, L. F. Lin, D. D. Macdonald. A point defect model of anodic passive film: I. Film growth kinetics. J. Electochemical society 128 (1981) 1187-1194.

109. D. D. Macdonald. Passivity- the key to our metals-based civilization. Pure Appl. Chem. 71 (1999) 951-978.

110. J.A. Richardson, G.C. Wood. A study of the pitting corrosion of Al by scanning electron microscopy. Corrosion Science 10 (1970) 313-323.

111. N. Sato. A theory for breakdown of anodic oxide films on metals. Electrochimica Acta 16 (1971) 1683-1692.

112. G.O. llevbare, G.T. Burstein. The role of alloyed molybdenum in the inhibition of pitting corrosion in stainless steels. Corrosion Science 43 (2001) 485–513.

113. A. Schneider, D. Kuron, S. Hofman, R. Kirchheim. AES analysis of pits and passive films formed on Fe–Cr, Fe–Mo and Fe–Cr–Mo alloys. Corrosion Science 31 (1990) 191–196.

114. L. Wegrelius, I. Olefjord. Dissolution and passivation of stainless steels exposed to hydrochloric acid. Material Science Forum 195–188 (1995) 347–356.

115. H. Ogawa, H. Omata, I. Itoh, H. Okada. Auger electron spectroscopic and electrochemical analysis of the effect of alloying elements on the passivation behavior of stainless steels. Corrosion 34 (1978) 52–60.

116. K. Sugimoto, Y. Sawada. Role of alloyed molybdenum in austenitic stainless steels in the inhibition of pitting in neutral halide solutions. Corrosion 32 (1976) 347–352.

117. A. Pardo, M. C. Merino, A. E. Coy, F. Viejo, R. Arrabal, E. Matykina. Effect of Mo and Mn additions on the corrosion behavior of AISI 304 and 316 stainless steels in H_2SO_4. Corrosion Sciences 50 (2008) 780-794.

118. L. Wegrelius, F. Falkenberg, I .Olejford. Passivation of Stainless Steels in Hydrochloric Acid. J. Electrochemical Society 146 (1999) 1397-1406.

119. M. C. Alonso, U. Angst, M. Sánchez, K. Yong Ann. Onset of chloride induced reinforcement corrosion. Hand book of concrete durability. Edt., S. –H Kim, and K. Yong Ann. First edition, Middleton Publishing Inc., an imprint of Marina Glim on Media-Korea (2010) 1-48.

120. M. C. Alonso, M. Sánchez. Analysis of the variability of chloride threshold values in the literature. Materials and Corrosion 60 (2009) 631-637.

121. J. Gulikers. Considerations on the reliability of service life predictions using a probabilistic approach. Journal de Physique IV, 136 (2006) 233–241.

122. J. Gulikers. Probabilistic service life modeling of concrete structures: improvement or unrealistic CONSEC'07, Proceedings of the 5th International Conference on

Concrete under Severe Conditions, Environment and Loading, Tours, France (891–902.

123. L. Bertolini, F. Bolzoni. T. Pastore. P. Pedeferri. Behaviour of stainless steels in simulated concrete. British Corrosion Journal 31 (1996) 218-222.

124. M. F. Hurley, J. R. Scully. Threshold chloride concentration of selected corrosion resistance rebars materials compared to carbon steel. NASA Corrosion 62 (2006) 892-904.

125. M. C. García-Alonso, M. L. Escudero, J. M. Miranda, M. I. Vega, F. Capilla, M. J. Correia, M. Salta,A. Bennani, J. A. González. Corrosion behaviour of new stainless steels reinforcing bars embedded in concrete. Cement and Concrete Research, 37, (2007) 1463-1471.

126. M. C. García-Alonso, J. A. González, J. M. Miranda, M. L. Escudero, M. J. Correia, M. Salta, A. Bennani. Corrosion behaviour of innovative stainless steels in mortar. Cement and Concrete Research, 37, (2007) 1562-1569.

127. L. Bertolini. M. Gastaldi. Corrosion resistance of low-nickel duplex stainless steel rebars. Materials and Corrosion 62 (2011) 120-129.

128. B. Sorensen, P.B. Jensen, E. Maahn. The corrosion properties of stainless steel reinforcement, Corrosion of reinforcement in concrete (Edt.) C.L. Page, London, (1990) 601-610.

129. David Trejo, Radhakrishna, G Pillai. Accelerated chloride threshold testing - Part II: Corrosion -Resistant Reinforcement. ACI Materials Journal 101 (2004) 57-64.

130. S. M. Álvarez, A. Bautista, F. Velasco. Corrosion behaviour of corrugated lean duplex stainless steels in simulated concrete pore solutions. Corrosion Science 53 (2011) 1748-1755.

131. A. Bautista, G. Blanco, F. Velasco. Corrosion behaviour of low-nickel austenitic stainless steels reinforcements: A comparative study in simulated pore solutions. Cement and Concrete Research 36 (2006) 1922 – 1930.

132. G. Blanco, A. Bautista, H. Takenouti. EIS study of passivation of austenitic and duplex stainless steels reinforcements in simulated pore solutions. Cement and Concrete Composites 28 (2006) 212–219.

133. A. Bautista, G. Blanco, F. Velasco, M.A. Martínez. Corrosion performance of welded stainless steels reinforcements in simulated pore solutions. Construction and Building Materials 21 (2007) 1267–1276.

134. H. Luo, C.F. Dong, X.G. Li, K. Xiao. Electrochemical behaviour of 2205 duplex stainless steels in alkaline solution with different pH in the presence of chloride. Electrochimica Acta 64 (2012) 211-220.

135. Milan Kouril, Pavel Novak, Martin Bojko. Threshold chloride concentrations for stainless steels activation in concrete pore solutions. Cement and Concrete Research 40 (2010) 431-436.

136. L. Bertolini, M. Gastadli. Corrosion Resistance of Austenitic and low-Nickel duplex stainless steels bars, EUROCOR-Nice (2009).

137. Y. Wu, F. Recio, U. Nürnberger, M. C. Alonso. Stainless steels tendons- New materials and systems for prestressing structure, European Community, Cost 534 Workshops, (2009) 22-36.

138. A. S. Hamada, L. P. Karjalainen, M. C. Somani. Electrochemical corrosion behaviour of novel submicron-grained austenitic stainless steels in an acidic NaCl solution. Materials Science and Engineering A 43 (2006) 211-217.

139. U. Nürnberger. Stainless steels reinforcement – A survey. Otto-Graf-Journal, 16 (2005) 111-158.

140. B. Elsener, D. Addari, S. Coray and A. Rossi. Stainless steel reinforcing bars – reason for their high pitting corrosion resistance. Materials and Corrosion 62 (2011) 111-119.

141. M. C. Alonso, F. J. Recio. Corrosion performance of galvanized and high strength stainless steel tendons, stress corrosion test applicable to new prestressed steels. COST 534 final report of new materials and systems for perstressed concrete structure. 2007.

142. Robert D. Moser. High strength stainless steels for corrosion mitigation in prestressed concrete: Development and evaluation. Doctoral Thesis, School of Civil and Engineering. Georgia Institute of Technology (2011).

143. Robert D. Moser, Preet M. Singh, Lawrence F. Kahn, Kmberly E. Kurtis. Chloride-induced corrosion resistance of high-strength stainless steels in simulated alkaline and carbonated concrete pore solutions. Corrosion Science 57 (2012) 241-253.

144. F. J. Recio. M. C. Alonso. Evaluación del riesgo de corrosión bajo tensión inducida por la generación de picaduras en aceros inoxidables de lata resistencia. Anales de Mecánica de la Fractura 30 (2013) 439-444.

145. C. Fosca, C. Merino, E. Otero, P. Hierro. Metalografía en color de los aceros inoxidables mediante la técnica de ataque coloreado. Rev. Metal. Madrid, 32 (1996) 226-230.

146. Gerardo G. Clemeña. An alternative potentiometric method for determining chloride concrete content in concrete samples from reinforced concrete. Doctoral thesis, Virginia Transportation Research Council. The University of Virginia (2002).

147. ASTM. Standard Test Method for Water-Soluble chloride in mortar and concrete. C 1218/C 1218M – 99 (2008).

148. S.A.M. Refaey F. Taha, T.H.A. Hasanin. Electrochemical behavior of Sn–Ni nanostructured compound in alkaline media and the effect of halide ions. Applied Surface Science 227 (2004) 416–428.

149. Takatoshi Yamamoto, Koji Fushimi, Masahiro Seo, Shiro Tsuri, Tetsuo Adachi, Hiroki Habazaki. Depassivation–repassivation behavior of type-312L stainless steel in NaCl solution investigated by the micro-indentation. Corrosion Science 51 (2009) 1545–1553.

150. S. Joiret, M. Keddam, X.R. Nóvoa, M.C. Pérez, C. Rangel , H. Takenouti. Use of EIS, ring-disk electrode, EQCM and Raman spectroscopy to study the film of oxides formed on iron in 1M NaOH. Cement & Concrete Composites 24 (2002) 7–15.

151. L. Freire, X.R. Nóvoa, G. Pena, V. Vivier. On the corrosion mechanism of AISI 204Cu stainless steel in chlorinated alkaline media. Corrosion Science 50 (2008) 3205-3212.

152. M. Kaneko, H. S. Isaacs. Effects of molybdenum on the pitting of ferritic- and austenitic-stainless steels in bromide and chloride solutions. Corrosion Science 44 (2002) 1825-1834.

153. C. Fosca, C. Merino, E. Otero. Un método para evitar problemas de corrosión por resquicios en los ensayos electroquímicos de corrosión por picaduras. Rev. Metal. Madrid, 32 (1996) 151-159.

154. J. E. B. Randles. Kinetics of rapid electrode reactions. Discussions of the Faraday Society 1 (1947) 11-19.

155. V. M. Salinas-Bravo, R. C. Newman. An alternative method to determine critical pitting temperature of stainless steels in ferric chloride solutions. Corrosion Science 36 (1994) 67-77.

156. D. Buxton. Stainless steel weld attack - electrochemical corrosion testing. The Technical Journal for Industrial Members of TWI 38 (1997) 11-14.

157. N. J. Laycock, R. C. Newman. Localized dissolution kinetics, Salt films and pitting potentials. Corrosion Science 39 (10-11) (1997) 1771-1790.

158. J.A. González, A. Molina, M.L. Escudero, C. Andrade.Errors in the electrochemical evaluation of very small corrosion rates- I. polarization resistance method applied to corrosion of steel in concrete. Corrosion Science 25 (1985) 917-930.

159. L. Callow, J. Richarson, J. Dawson. Corrosion monitoring using polarization resistance measurements: I. Techniques and correlations, and II. Sources of Ecorr. British Corrosion Journal 11 (1976) 123-139.

160. Milton Stern, and Weisert, D. Edward. Experimental observations on the relation between polarization resistance and corrosion rate. Proceedings ASTM 59 (1959) 1280-1290.

161. M. Stern and A. L. Geary. A Theoretical analysis of the shape of polarization resistance curves. J. Electrochemical Society 104 (1957) 56-63.

162. R. G. Kelly, J. R. Scully, D. W. Shoesmith, R. G. Buchheit. Electrochemical Techniques in Corrosion Engineering, Marcel Dekker, Inc. (2002) 45-61.

163. E. Poorqasemi, O. Abootalebi, M. Peikari, F. Haqdar. Investigating accuracy of the Tafel extrapolation method in HCl solutions. Corrosion Science 51 (2009) 1043–1054.

164. Allen J. Bard, Martin Stratmann, Patrick R. Unwin. Encyclopedia of electrochemistry, Volume 3, Instrumentation and Electroanalytical Chemistry, WILEY-VCH, (2003) 196-221.

165. J. R. Macdonald, “Impedance Spectroscopy. Emphasizing solid materials and systems”. Ed. J. R. Macdonald, John Wiley & Sons (1987).

166. D. D. Macdonald, E. Sikora, G. Engelhardt. Characterizing electrochemical systems in the frequency domain. Electrochimica Acta 43 (1998) 87-107.

167. D. D. Macdonald. Reflections on the history of electrochemical impedance spectroscopy. Electrochimica Acta 51 (2006) 1376.

168. D. D. Macdonald, M. C. H. McKubre. Modern Aspects of Electrochemistry 14 (1982) 61-115.

169. P. Agarval, M. E. Orazem, L. H. García-Rubio. Measurement Models for Electrochemical Impedance Spectroscopy: I. Demonstration of Applicability. J. Electrochemical Society 139 (1992) 1917-1927.

170. D. D. Macdonald, M. Urquidi-Macdonald. Application of Kramers-Kronig Transforms in the Analysis of Electrochemical Systems: I. Polarization Resistance. J. Electrochemical Society 132 (1985) 2316-2319.

171. M. Urquidi-Macdonald, S. Real, D. D. Macdonald. Application of Kramers-Kronig Transforms in the Analysis of Electrochemical Impedance Data: II. Transformations in the Complex Plane. J. Electrochemical Society 133 (1986) 2018-2024.

172. Mark E. Orazem, Bernard Tribollet, Electrochemical impedance spectroscopy, John Wiley & Sons, Inc., Hoboken, New Jersey. (2008).

173. F. El-Taib Heakal, A. A. Ghoneim, A. M. Fekry. Stability of spontaneous passive films on high strength Mo-containing stainless steels in aqueous solutions. Journal of Applied Electrochemistry 37 (2007) 405-413.

174. M. Keddam, H. Takenouti, X. R. Novoa, C. Andrade, C. Alonso. Impedance measurements in cement past. Cement and Concrete Research 27 (1997) 1191-1201.

175. M. Pourbaix, Atlas of electrochemical equilibrium in aqueous solution, Pergamon Press, Oxford (1968).

176. Iva Betova, Martin Bojinov, Timo Laitinen, Kari Makela, Pekka Pohjanne, Timo Saario. The transpassive dissolution mechanism of highly alloyed stainless steels: I. Experimental results and modelling procedure. Corrosion Science 44 (2002) 2675-2697.

177. A. M. Shams El-Din. L. Wang, T. M. H. Saber. Behaviour of high strength molybdenum containing stainless steels in Arabian Gulf water. Part 1: Oxide film thickening. British Corrosion Journal 29 (1994) 58-66

178. Joong-Do Kim, Su LL Pyun. Effects of electrolyte composition and applied potential on the repassivation kinetics of pure aluminum. Electrochimica Acta 40 (1995) 1863-1869.

179. Joong-Do Kim, Su LL Pyun. The effects of applied potential and chloride ion on the repassivation kinetics of pure iron. Corrosion Science 38 (1996) 1093-1102.

180. Jae-Bong Lee. Effects of alloying elements, Cr, Mo and N on repassivation characteristics of stainless steels using the abrading electrode technique. Material Chemistry and Physics 99 (2006) 224-234.

181. C. Alonso, C. Andrade, M. Izquierdo, X. R. Nóvoa, M. C. Pérez. Effect of protective oxide scales in macrogalvanic behaviour of concrete reinforcement. Corrosion Science 40 (1998) 1379.

182. M. Sánchez, J. Gregorio, C. Alonso, J. J. García-Jareño, H. Takenouti, F. Vicente. Electrochemical impedance spectroscopy for studying passive layers on steel rebars immersed in alkaline solutions simulating concrete pores. Electrochimica Acta 52 (2007) 7634-7641.

183. P. Schmuki, S. Virtanen, H. S. Isaacs. In situ XANES investigation of Fe2O3/Cr2O3 artificial passive films. Oxide Films, Eds. K. R. Herbert, R. S. Lillard, B. R. MacDougall. Electrochemical Society INK, New Jersy, USA (2000) 1-11.

184. K. Sugimoto, M. Son, N. Akao, and N. Hara. Electrochemical Properties of Fe2O3-Cr2O3-MoO2 Artificial Passivation Films in HCl Solutions. Oxide Films, Eds. K. R. Herbert, R. S. Lillard, B. R. MacDougall. Electrochemical Society INK, New Jersy, USA (2000) 1-11.

185. Lone Lindbaek Skovbjerg. Reduction of hexavalent chromium by green rust sulphate: determination of end product and reduction mechanism. Master thesis, Geological Institute, University of Copenhagen (2005).

186. Ludovic Legrand, Alaaeddine El Figuigui, Florence Mercier, Annie Chausse. Reduction of aqueous chromate by Fe(II)/Fe(III) carbonate green reust: Kinetic and mechanism study. Environmental Science and Technology 38 (2004) 4587-4595.

187. A. Rossi, R. Tulifero, B. Elsener. Surface analytical and electrochemical study on the role of adsorbed chloride ions in corrosion of stainless steels. Material and Corrosion 52 (2001) 175-180.

188. G. Totten, M. Howes, T. Inoue. Hand book of residual stress and deformation of steel. ASM international, ISBN: 0-87170-729 (2002) 148-149.

189. S. Y. Qian, N. Chagnon, Evaluation of reinforcement in repaired concrete. 9th International Conference and Exhibition, Structural Faults and Repair, London, UK, (2001) 1-12.

190. E. M. Gutman, Mechanochemistry of solid surfaces, World Scientific Publishing. Co. Pte. Ltd. (1994). 95-107 and 301-308.

191. Luca Bertolini, Maddalena Carsana, Piertro Pedeferri. Corrosion behaviour of steel in concrete in the presence of stray current. Corrosion Science 49 (2007) 1056-1068.

192. P. Pohjanne, L. Carén, T. Hakkarainen, P. Kinnunen. A method to predict pitting corrosion of stainless steels in evaporative conditions. J. Constructional Steel Research 64 (2008) 1325-1331.

193. L. Freire, M.J. Carmezim, M.G.S. Ferreira, M.F. Montemor. The electrochemical behaviour of stainless steel AISI 304 in alkaline solutions with different pH in presence of chloride. Electrochimica Acta 56 (2011) 5280-5289.

194. B. Díaz, L. Freire, X.R. Nóvoa, M.C. Pérez, Electrochemical behaviour of high strength steel wires in the presence of chloride. Electorchimica Acta 54 (2009) 5190-5198.

195. B. Díaz, S. Joiret, M. Keddam, X.R. Nóvoa. M.C. Pérez, H. Takenouti. Passivity of iron in red mud´s water solution. Electrochimica Acta 49 (2004) 3039-3048.

196. A. Seghiouer, J. Chevalet, A. Barhoun, F. Lantelme. Electrochemical oxidation of nickel in alkaline solutions: a voltammetric study and modelling, Journal of Electroanalytical Chemistry 442 (1998) 113–123.

197. Yong Liu, Wanzhi Wei, Xiaoying Liu, Xiandong Zeng, Yonghong Li, Shenglian Luo. Direct electrodeposition of the DNA-Ni2+ complex onto a glassy carbon electrode for sensing methanol in alkaline medium. Microchim Acta. 168 (2010) 135–140.

198. A. Rossi, G. Puddu, B. Elsener, in: Corrosion of reinforcement in concrete (Ed.), M. Raupach, B. Elsener, R. Polder, J. Mietz, EFC Publication Nr. 38, Woodhead Publishing, Cambridge UK and CRC Press, New York, (2007) 44-51.

199. S. Coray. High strength stainless steel for structural concrete – electro- chemical and surface analytical investigation. Master Thesis, ETH Zurich and Universita` di Cagliari 2009.

200. B. Elsener, D. Addari, S. Coray, A. Rossi. Nickel-free stainless steel in alkaline media – electrochemistry and surface chemistry. Electrochimica Acta 56 (2011) 4489-4497.

201. A.Igual Muñoz, J. García Antón, J.L. Guiñón, V. Pérez Herranz. Inhibition effect of chromate on the passivation and pitting corrosion of a duplex stainless steel in LiBr solutions using electrochemical techniques. Corrosion Science 49 (2007) 3200-3225.

202. N. Ebrahimi, M.H. Moayed, A. Davoodi. Critical pitting temperature dependence of 2205 duplex stainless steel on dichromate ion concentration in chloride medium. Corrosion Science 53 (2011) 1278-1287.

203. R.J. Brigham, E.W. Tozer. Temperature as a pitting criterion, Corrosion 29 (1973) 33-36.

204. R.J. Brigham, E.W. Tozer, Effect of alloying additions on the pitting resistance of 18% chromium austenitic stainless steels. Corrosion 30 (1974), 161-166.

205. C. Vautrin-UI, A. Taleb, J. Stafiej. Mesoscopic modelling of corrosion phenomena: coupling between electrochemical and mechanical processes, analysis of the deviation from the Faraday law. Electrochimica Acta 52 (2007) 5368–5376.

206. H.X. Guo, B.T. Lu, J.L. Luo, Non-Faraday material loss in flowing corrosive solution. Electrochimica Acta 51 (2006) 5341–5348.

207. Zhicao Feng, Xuequn Cheng , Chaofang Dong, Lin Xu, Xiaogang Li. Passivity of 316L stainless steel in borate buffer solution studied by Mott–Schottky analysis, atomic absorption spectrometry and X-ray photoelectron spectroscopy. Corrosion Science 52 (2010) 3646–3653.

208. B. Gideon, L. Ward, G. Biddle. Duplex stainless steel welds and their susceptibility to intergranular corrosion. J. Minerals & Materials Characterization & Engineering 7 (2008) 247-263.

209. Jia Ging, Y.M. Jiang, B. Deng, J.L. Xu, J.P. Hu, Jin Li. Evaluation of intergranular corrosion susceptibility of UNS S31803 duplex stainless steel with optimized double loop electrochemical potentiokinetic reactivation method. Electrochimica Acta 55 (2010) 5077-5083.

210. P. Merino, X.R. Nóvoa, G. Pena, E. Porto, L. Espada. Intergranular corrosion susceptibility of austenitic-ferritic duplex stainless steel: Application of potentioklinetic reactive tests. Material Science and Technology 9 (1993) 168-171.

211. L. Freire, X.R. Nóvoa, M.F. Montemor, M.J. Carmezim, Study of passive films formed on mild steel in alkaline media by the application of anodic potential. Materials Chemistry and Physics 114 (2009) 962-972.

212. B.E. Conway, Electrochemical Supercapacitors, Scientific Fundamentals and Technological Applications, Kluwer Academic Publishers, New York, USA, 1999, (Chapter 10).